DREKI PDRA Project Report

Heriot-Watt University

Evaluating the Structural Evolution and Hydrocarbon Prospectivity of the Jan Mayen (DREKI) area, offshore NE Iceland

PDRA: Dr. Georgina Heldreich

Supervisors: Prof. John Underhill, Dr. Rachel Jamieson & Prof. Andy Bell

Sponsored by Orkustofnun, The National Energy Authority of Iceland

Seismic Data provided by Spectrum & Norwegian Petroleum Directorate

ORKUSTOFNUN
National Energy Authority

NORWEGIAN PETROLEUM DIRECTORATE

Spectrum
MULTI-CLIENT · SEISMIC IMAGING

This report and the work presented herein is dedicated to the memory of Dr. Þórarinn S. Arnarson, Orkustofnun, for initiating this project and for his support and advice.

Table of Contents

List of Figures

List of Tables

Executive summary

The Jan Mayen Microcontinent (JMMC) is a continental fragment/ sliver that rifted off the East Greenland margin during the Oligocene and is situated offshore northeast Iceland within the Norwegian-Greenland Sea. The JMMC is a structural entity 400 – 450 km long and varies in width from 100 km in the north and 310 km in the south. The northern part of the JMMC is characterised by the main Jan Mayen Ridge, which is a single bathymetric, north-south trending submarine feature with a prominent flat top. Whereas, the southern part is characterised by the fragmentation of the main ridge into a series of smaller isolated bathymetric ridges; collectively forming the Southern Ridge Complex (SRC), which widens southwards.

Prior to North Atlantic opening and onset of sea-floor spreading in the Palaeocene-Eocene, the JMMC was situated between the Mid Norway margin (southern Vøring Basin and Møre Basin) and East Greenland margin (onshore Jameson Land Basin and offshore Liverpool Land Basin). During initial seafloor spreading along the Ægir Ridge since ~55Ma, the JMMC was still attached to the East Greenland margin. However, asymmetrical spreading along the Ægir Ridge and plate reorganisation, lead to the progressive westward migration of rifting and a westerly jump in the spreading centre to the proto-Kolbeinsey Ridge between anomaly 21 and 13 (47.3 – 33.1 Ma)

The JMMC is of interest because previous works have thought it may contain potential accumulations of hydrocarbons, largely due to the microcontinent's geological similarity to its surrounding conjugate margins and its potential to contain similar pre-opening Mesozoic source rocks and reservoir units associated with working petroleum systems encountered on the East Greenland and the mid Norway margins.

This study has utilised an integrated multidisciplinary database. Shallow DSDP boreholes and ROV samples were used to provide a lithological/ biostratigraphic constraint, whilst a total of 152 2-D seismic lines of varying vintages were used for horizon and structural interpretation. Gravity and magnetic surveys were used to help delineate crustal domains and potential basinal areas across the study area, with high resolution multibeam bathymetry data across the Dreki area used to better realise the 3-D surface expression of micro-continental fragments in the southern part of the study area. Seismic refraction analysis was also performed in order to delineate potential older stratigraphic sequences that cannot be easily imaged using seismic reflection data alone. Consequently, the aims of this research were to understand the structural and stratigraphic evolution of the JMMC, evaluate the potential petroleum systems that may be present in the area, including hydrocarbon maturation and migration, identify potential trapping styles/mechanisms, and assess their potential risk.

Major faults and surfaces of tectonostratigraphic importance were mapped across the JMMC (based on seismic reflector terminations) to better understand the structural evolution of the area. Analysis of the conjugate margin geological and structural evolution was also fundamental in order to consider the potential source rock, reservoir and seal units that might be present within the JMMC for a potential working petroleum system to occur in this region. The tectono-stratigraphic framework of the JMMC and conjugate margins is published as a synthesis chart aiming to provide a concise overview of the regional tectonic events affecting the margins of the North Atlantic, summarise the Late Palaeozoic to Cenozoic stratigraphy of these margins and speculate on the potential hydrocarbon systems that may operate over the JMMC, specifically. Furthermore, basin and source rock maturity modelling was undertaken with the aim of constraining the potential timings of hydrocarbon generation in relation to structural trap formation.

Potential hydrocarbon leads have been assessed, most of which are structural. For the JMMC to be prospective, requires hydrocarbons to be trapped prior to and survive the uplift inversion events at around 50 – 30 Ma, otherwise there is a strong risk of leakage. Older structures that have survived the uplift event and presently situated at least 1km below the sea bed (not lower than 50°C)), then there is a better chance of a petroleum system working. The reverse fault on the SE margin of the JMR, deeper tilted fault blocks along the western flank of the JMR and sub-basinal areas of the SRC are relatively lower risk potential lead areas to assess further; but additional data should be acquired for this to be evaluated.

1. Introduction

The Jan Mayen Microcontinent (JMMC) (Figure 1.1) is a continental fragment/ sliver that rifted off the East Greenland margin during the Oligocene and is located offshore northeast Iceland within the Norwegian-Greenland Sea. Water depths around the JMMC range from 200 – 2500 m. The main ridge mainly lies within Norwegian waters, but within a collaboration area between Iceland and Norway, whilst the southern tip lies within an area of the Icelandic Continental Shelf (ICS) known as the DREKI area (Figure 1.2) (www.nea.is).

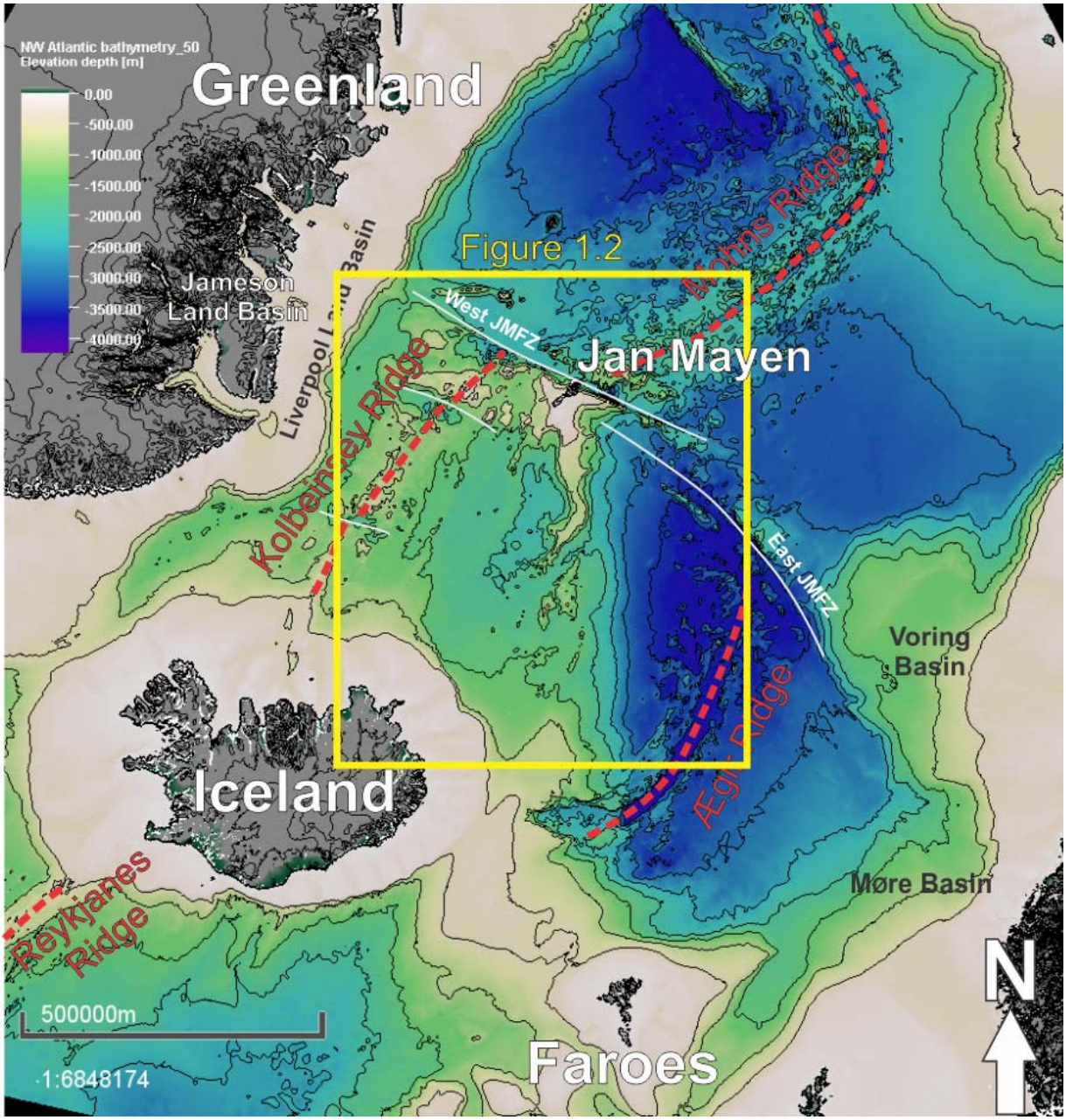

Figure 1.1: NE Atlantic bathymetric map. Jan Mayen study area outlined by yellow box.

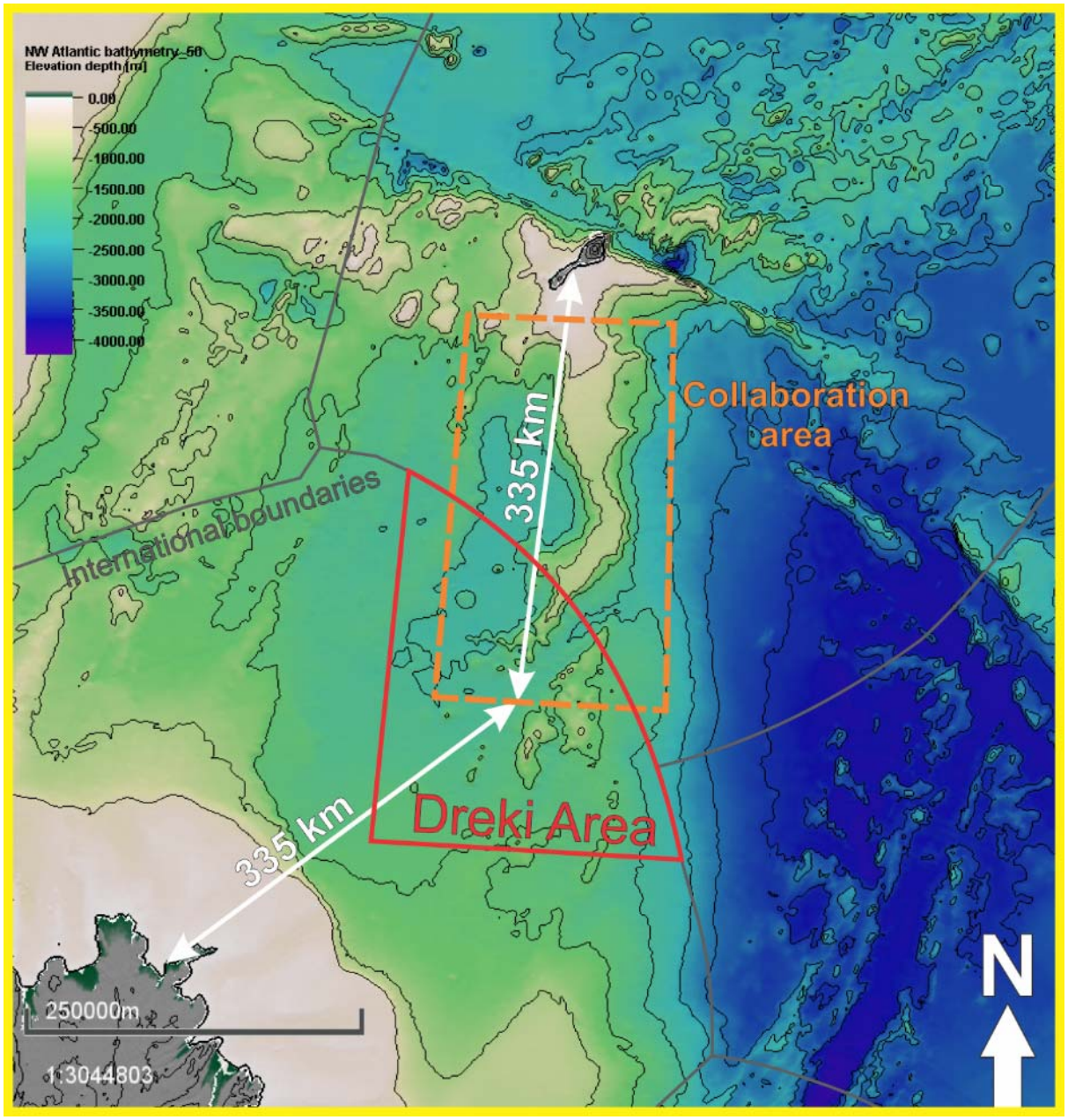

Figure 1.2: Outlines of the Dreki area, Collaboration area and international boundary lines across the JMMC.

The JMMC is a structural entity 400 – 450 km long and varies in width from 100 km in the north and 310 km in the south. It comprises the Jan Mayen Ridge (JMR), the Jan Mayen Basin, Jan Mayen Trough and the Southern Ridge Complex (SRC) (Figure 1.3). The northern part of the JMMC is characterised by the main JMR, which is a single bathymetric, north-south trending submarine feature with a prominent flat top, extending about 400 km southwards from Jan Mayen Island to #69.9°N, where it curves to the SW and ends at ~68.5°N. Whereas the southern part is characterised by the fragmentation of the main ridge into a series of smaller isolated bathymetric ridges, collectively forming the SRC, which widens southwards. The microcontinent is bound on all sides by oceanic crust, although its southern limit is still poorly constrained due to extensive intrusive and extrusive volcanic rocks limiting seismic imaging of the southern area. There is evidence from crustal studies to suggest that the microcontinent itself encompasses a much larger area south towards the east and south-east shelf of Iceland (Figure

1.4 & 1.5) (Leftwich et al 2005; Fedorova et al., 2005; Foulger 2006; Greenhalgh & Kusznir, 2007; Torsvik et al., 2015).

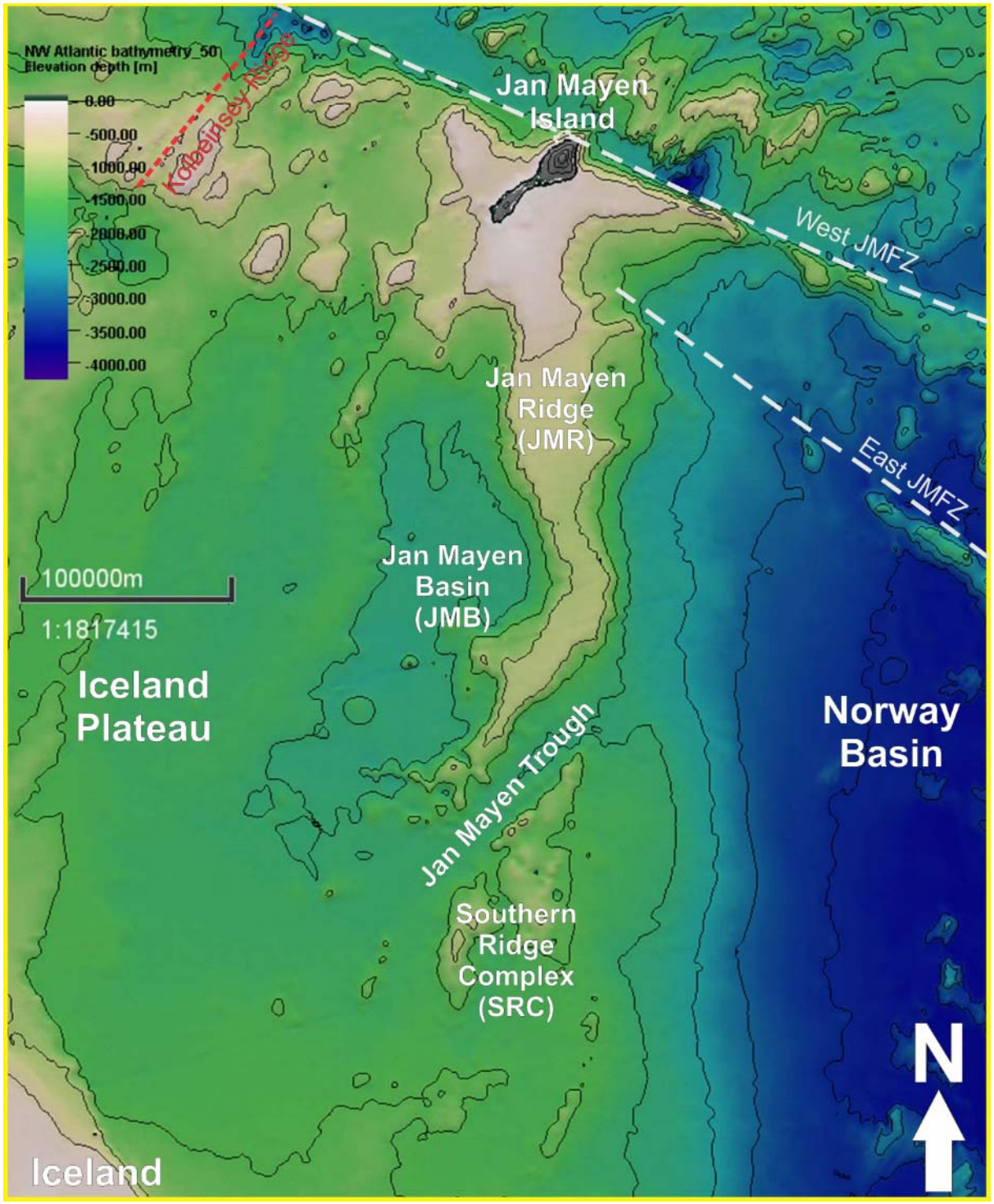

Figure 1.3: Structural domains within the JMMC; main Jan Mayen Ridge (JMR) in the north, the Southern Ridge Complex (SRC) in the south, divided by the NE-SW trending Jan Mayen Trough.

Prior to North Atlantic opening and onset of sea-floor spreading in the Palaeocene-Eocene, the JMMC was situated between the Mid Norway margin (southern Voring Basin and MØre Basin) and East Greenland margin (onshore Jameson Land Basin and offshore Liverpool Land Basin). However, the break-up process and sea-floor spreading history within the North Atlantic has

been complex. Initial sea-floor spreading along the, now extinct, Ægir Ridge continued from anomaly 24 (~55Ma) through to anomaly 7 (~24Ma) (Talwani & Eldholm 1977; Kuvaas & Kodaira, 1997; Scott et al 2005). During this time, the JMMC was still attached to the East Greenland margin and effectively an eastward extension of the Jameson Land and Liverpool Land Basins. However, asymmetrical spreading along the Ægir Ridge and plate reorganisation during Eocene break-up, lead to the progressive westward migration of rifting and the spreading centre towards the proto-Kolbeinsey Ridge between anomaly 21 and 13 (47.3 – 33.1 Ma) (Jung & Vogt, 1997; Gaina et al., 2009; Gernigon et al., 2015). It is likely this plate reorganisation was influenced by the encroaching Iceland Mantle Plume (Larsen, 1988; Muller et al., 2001). This complex, multistage, westward migration of the spreading ridge during the Oligocene caused internal structural segmentation of the microcontinent (forming the Southern Ridge Complex). Simultaneous extension along the Ægir and proto-Kolbeinsey Ridges continued until extinction of the Ægir Ridge at anomaly 7 (~24 Ma) (Gernigon et al., 2015). Opening and formation of oceanic crust along the newly formed Kolbeinsey Ridge finally resulted in the complete separation of the JMMC from the East Greenland margin at around anomaly 6 (~22 – 21 ma ago) (Gernigon et al., 2015). Continued opening along the present day NE Atlantic spreading ridge configuration has resulted in the JMMC being isolated in the middle of the North Atlantic surrounded by oceanic crust.

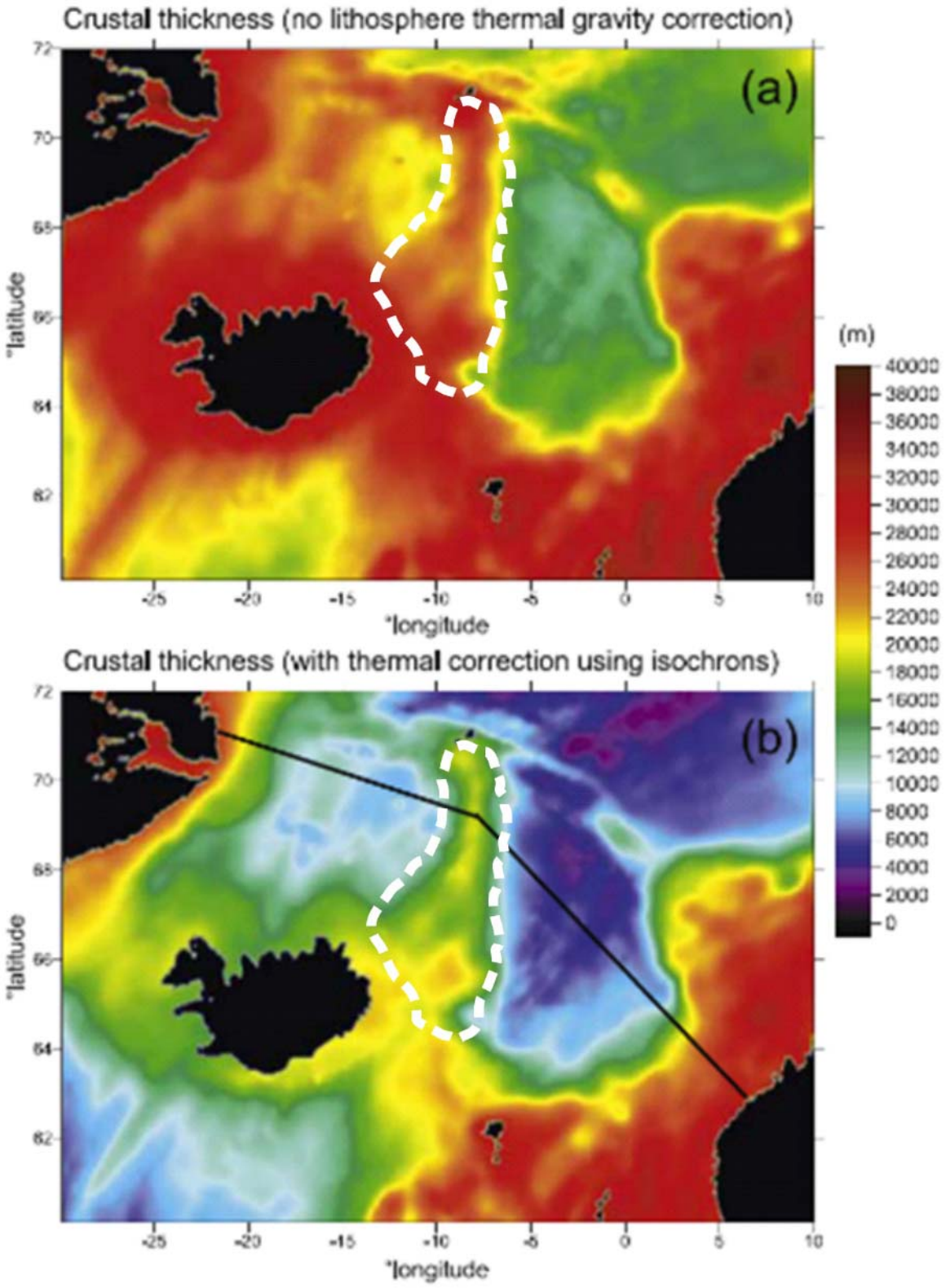

Figure 1.4: Crustal thickness predicted by gravity inversion from Greenhalgh and Kusznir (2007).

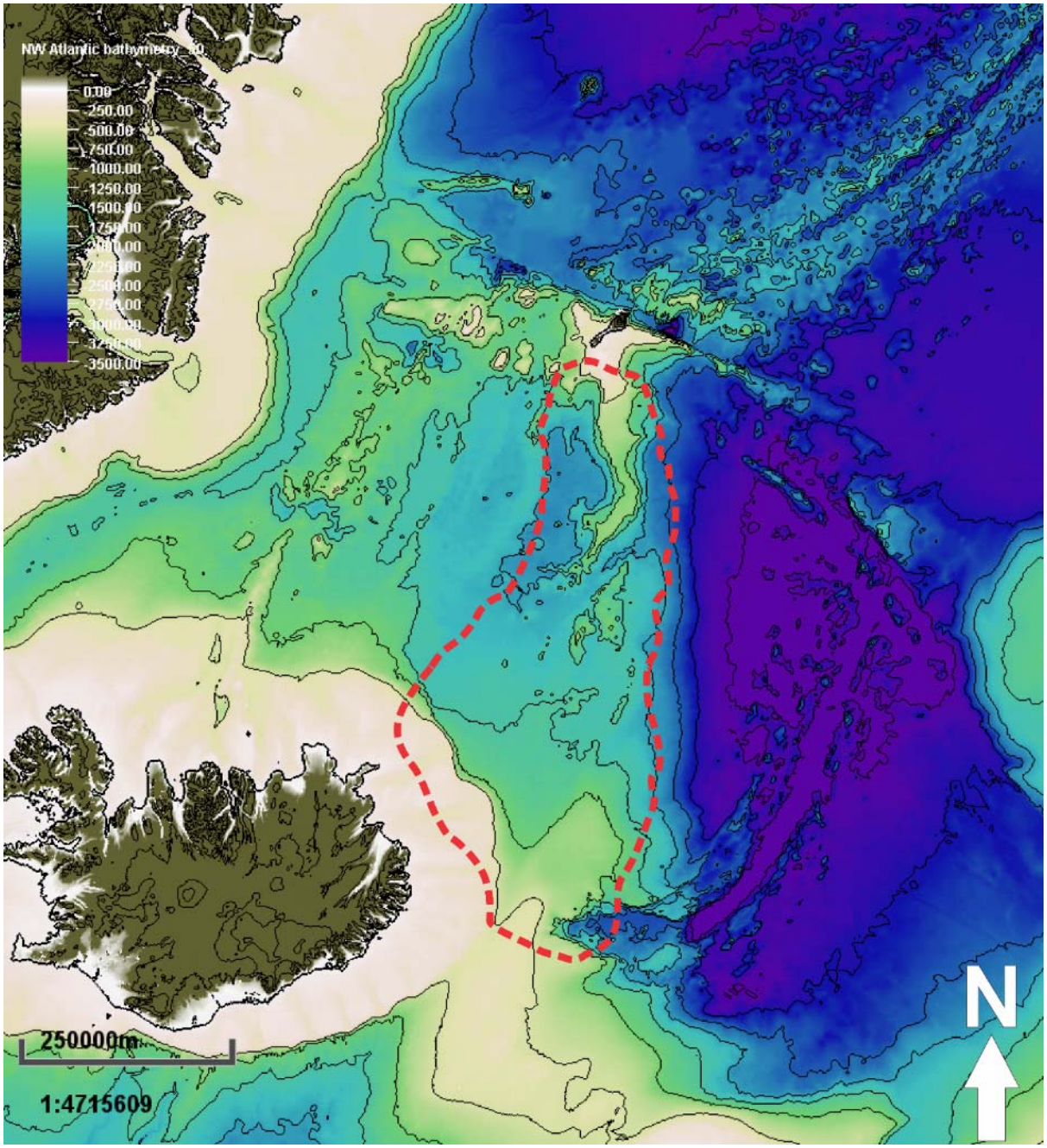

Figure 1.5: Inferred extent of the greater JMMC in relation to Greenhalgh and Kusznir, 2007 study outlined by red dashed polygon (modified from Gernigon et al., 2015).

Shallow DSPD cores and seismic refraction studies over the JMMC identify a large thickness of sediments with velocities comparable to pre-rift age succession from the conjugate margins. As such the JMMC and DREKI area have been highlighted as being one of the areas of the ICS thought to contain potential accumulations of hydrocarbons, largely due to the microcontinent's geological similarity to its surrounding conjugate margins and may potentially contain similar pre-opening Mesozoic source rocks and reservoir units associated with working petroleum systems encountered on the East Greenland and the mid Norway margins.

The JMMC has been studied since the first DSDP cores were drilled on the main ridge in August-September 1974. Talwani et al (1976) and Hood et al (1976) analysed these borehole core samples for potential hydrocarbon indicators through lithological, biostratigraphical and geochemical studies. The first seismic reflection data were acquired from 1985 onwards with the most recent surveys undertaken in 2012. Seismic refraction data were collected over the JMMC in 1995 and 2000 to better constrain the crustal structure through P-wave velocity modelling (Kodaira et al., 1995; Mjelde et al., 2007/ 2008 a & b; Breivik et al., 2006/2012 & Funck et al., 2017). Gunnarsson et al 1989 produced an initial interpretation of the geology and hydrocarbon potential of the microcontinent, with many studies since then focussing on the structural and stratigraphic evolution and architecture of the JMMC (Kuvaas & Kodaira, 1997; Kodaira et al 1998; Peron-Pindivic et al., 2012 a & b; Peron-Pindivic et al., 2013; Blischke et al., 2017/2019) and wider the implications for understanding the regional plate kinematics during opening of the N. Atlantic (Gaina et al., 2009/ 2017; Gernigon et al., 2015) and microcontinent formation (Peron-Pindivic & Manatschal, 2010).

Despite the increased interest and output of scientific publications in recent years, there is scope for further research focussing on analysing the hydrocarbon prospectivity of the region (utilising the most recent seismic surveys (along with some existing surveys, reprocessed by Spectrum) integrated with stratigraphic insights from recent ROV expeditions), and identifying recommendations for further data acquisition.

The aims of this research are to understand the structural and stratigraphic evolution of the JMMC, evaluate the potential petroleum systems that may be present in the area, including hydrocarbon maturation and migration, identify potential trapping styles/mechanisms, and assess their potential risk. An improved understanding of the structural evolution of microcontinent formation and identifying generic implications for other microcontinents around the world are also key academic outcomes of this research.

2. Regional Geological Setting & Tectonic Evolution

The structural and stratigraphic evolution of the NE Atlantic has been extensively studied by many authors (Ziegler, 1988; Dore et al., 1997; Lundin & Dore, 1997; Dore et al., 1999; Tsikalas et al., 2005; Peron-Pindivic et al., 2013; Stoker et al., 2016). In particular, the evolution of the Norwegian-Greenland Sea has been studied from the perspective of volcanic rifted margins, sea floor spreading regimes and ridge extinction and jumps (Talwani & Eldholm; 1977; Gernigon et al., 2012; 2015; Gaina et al., 2017) to generic understanding of how microcontinental fragments form and evolve using the Jan Mayen Microcontinent as an exemplar (Kuvaas & Kodaira, 1997; Muller et al., 2001; Scott et al., 2005; Gaina et al., 2009; Peron-Pindivic & Manatschal 2010; Peron-Pindivic et al., 2012 a&b).

Figure 2.1 is a synthesis of the tectonostratigraphic evolution of the NE Atlantic with specific regards to the JMMC and its conjugate East Greenland and Mid Norwegian margins.

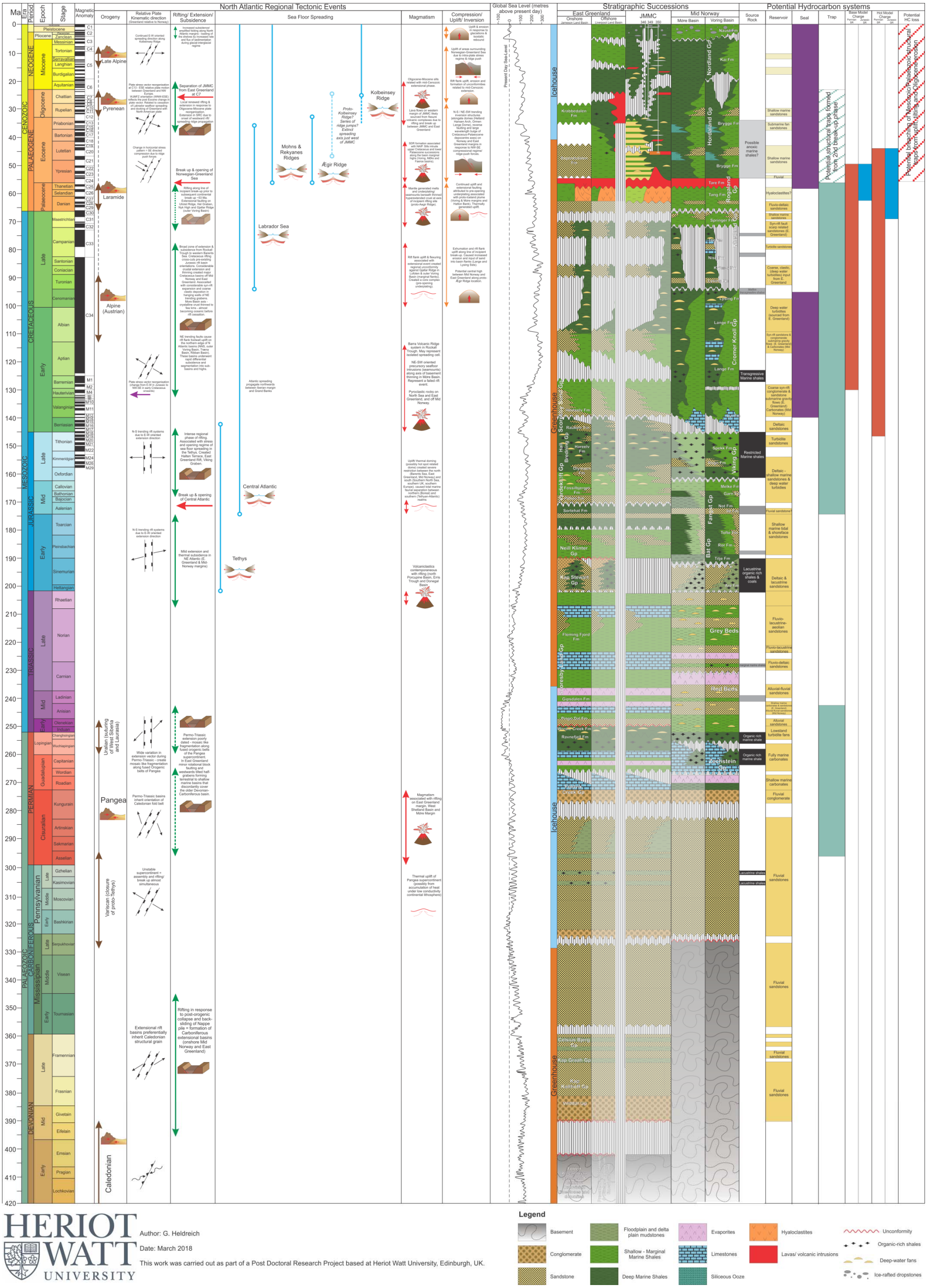

Figure 2.1: Tectonostratigraphic synthesis chart for the JMMC and conjugate East Greenland and Mid Norway Margins. (Note: Potential hydrocarbon systems section based on conjugate margin literature. The source rock "charge" is based on basin and maturity modelling using the JMM pseudowell location from Moore & Pitman (2008) USGS report and present timings of source rock intervals (Upper Permian & Upper Jurassic).

The NE Atlantic margin has undergone a complex geological evolution from collisional events during the Caledonian Orogeny in the Late Silurian and subsequent incorporation into the Late Palaeozoic Pangean supercontinent during the Variscan Orogeny; to a protracted and complicated history of intermittent and mosaic-like extension since the Mesozoic break-up of Pangea, which eventually led to the early Cenozoic opening of the NE Atlantic Ocean (Zeigler 1988; Dore et al., 1999).

Extension began in the form of two separate phases of post-orogenic collapse. The first in the Devonian-Carboniferous after the Caledonian Orogeny, forming molasse basins in Norway (Hossack, 1984) and East Greenland (Dore et al., 1999). The second, during the Late Carboniferous to Early Permian caused by instability shortly following the formation of Pangea during the Variscan Orogeny (Zeigler 1988; Dore et al, 1999). The NE Atlantic subsequently experienced several distinct rifting episodes, each associated with a different extension direction. Figure 2.2 shows the structural evolution and break-up of the North Atlantic through time. Additionally there was a west-NW migration of extensional axes through time as a result of increased mechanical strength of cooler upper mantle material beneath thinned (& necked) continental lithosphere (Dore et al., 1999; Steckler & ten Brink 1986; Brune et al., 2014). Changes in extension direction and a westward migration of rift axes with each successive extensional episode, created a complicated pattern of cross-cutting and overprinting of rift basins along the NE Atlantic margins.

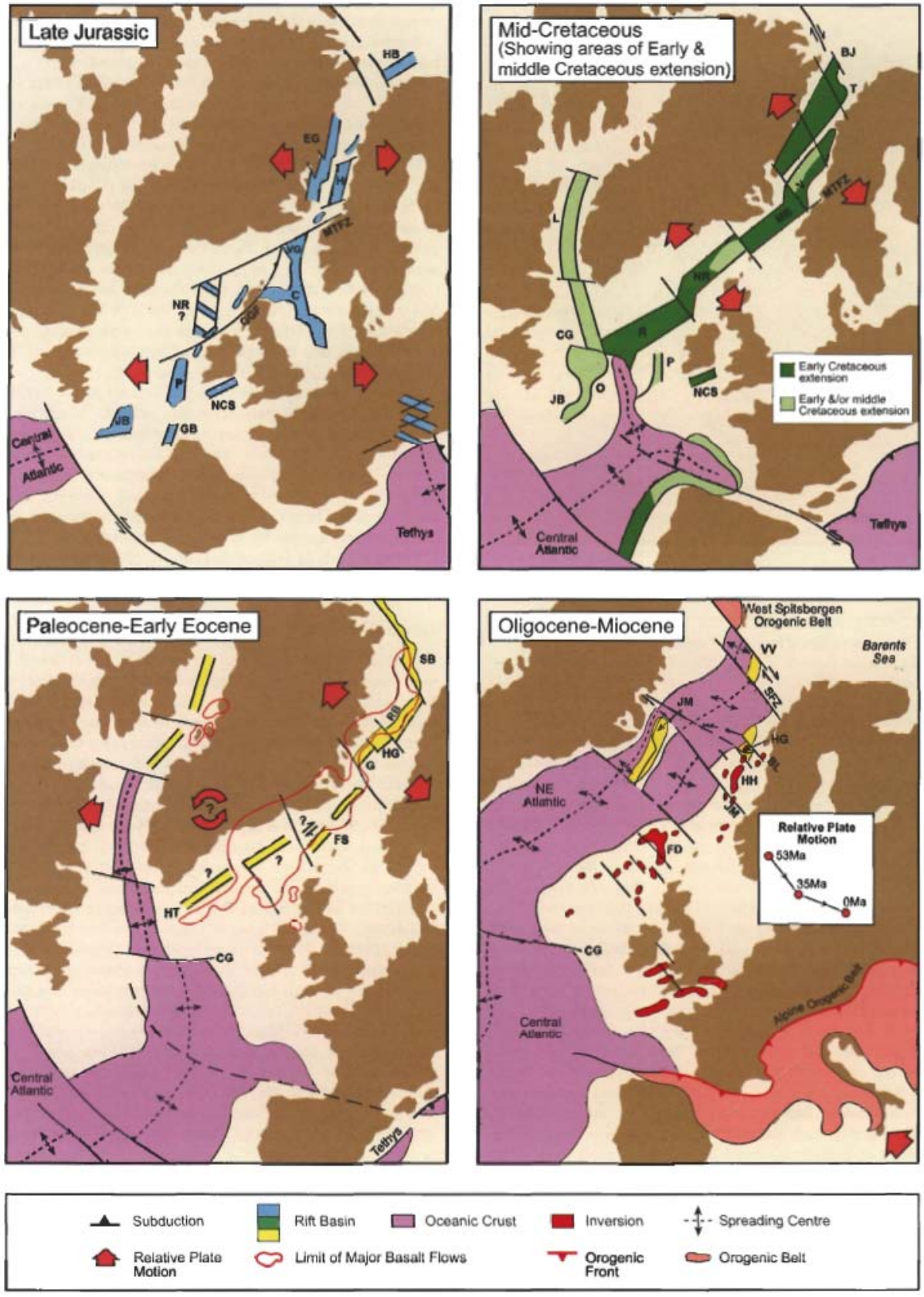

Figure 2.2: Plate reconstructions for the Late Jurassic, Mid-Cretaceous, Palaeocene and Mid-Cenozoic (taken from Dore et al., 1999).

2.1 Permo-Triassic Extension

The first major rifting phase during the Permian and Triassic led to rotational block faulting and formation of tilted half grabens which followed the NE orientation of the basement grain/ Caledonian fold belt. Extension vectors during the Permo-Triassic were varied creating a mosaic-like fragmentation pattern along fused orgenic belts as opposed to a single directed orientation (Dore et al., 1999). These rift basins are typically found lying inboard of younger depocentres on the East Greenland (Stemmerik, 2000) and Mid Norwegian margin, some of which are arranged in a left-stepping en-echelon pattern (Dore et al., 1999). It is likely that these early rift basins are also present beneath the deeper Cretaceous – Cenozoic rift basins to the west (Dore et al., 1999).

2.2 Jurassic Uplift and Extension

The Late Jurassic basins developed largely in response to regional E-W extension, linked to rifting in Central Europe and seafloor spreading in the Tethys, creating broadly N-S trending rift basins such as the East Greenland rift, Halten Terrace, Viking & Central Grabens (Figure 2.2) (Zeigler, 1988; Dore et al., 1997; Lundin & Dore, 1997). However, it is likely that the northern part of the rift system (Barents Sea, Greenland to Norway region) was separate from the southern part (SE Greenland-Faroe-Shetland area southwards) due to the marine faunal provinciality and restriction between the two regions during the mid-Jurassic. It is postulated that the Central North Sea Dome was on of a series of uplifts that extended across NW Europe and created such restriction in the proto NE Atlantic (Underhill & Partington, 1993; Dore et al., 1999). The northern and southern regions of the rift system remained separate entities with a restricted or a completely closed sea-way between the two until the Late Jurassic-Early Cretaceous (Roberts et al., 1999) and the entire NE Atlantic rift system was not fully linked until Mid-Cretaceous (Dore et al., 1999).

2.3 Early Cretaceous (Neocomian) Extension

A second phase of major rifting and extension occurred during the early Cretaceous, however a major change in plate stress vector reorganisation to NW-SE, differentiates this rifting phase from previous extensional phases (Figure 2.2) (Lundin & Dore, 1997). The change in direction was largely linked to cessation of Tethys seafloor spreading and the northward propagation of seafloor spreading in the Central Atlantic (Zeigler 1988). This extension direction was generally maintained through to continental break-up and produced a chain of NE-SW trending extensional basins from the SW Barents Sea to Rockall Trough. The cross-cutting and truncation of pre-existing Jurassic rift basins by NE-SW Cretaceous extension resulted in uplift of the northern margins of these basins in response to rift-flank uplift. Furthermore, significant crustal thinning & hyperextension enabled deep basins to form and exhumation of deep crust and/or mantle (Dore et al., 1999; Peron-Pindivic et al., 2013; Osmundsen & Ebbing, 2008). A chain of seamounts developed within the More Basin which was thinned to a few kilometres, suggesting a nearly successful rift event (Lundin & Dore, 1997; Dore et al., 1999).

2.4 Mid-Cretaceous Extension

Cenomanian extension is most evident on the outer Norwegian margin as a series of regional erosional unconformities in response to rift flank uplift along many basin ridges and terraces (Gjallar Ridge) (Dore et al., 1999). Uplift associated with extension caused an input of coarse clastics into basin flanks, which have been identified as sourced from Precambrian basement exposed in East Greenland (Roberts et al., 1999). This suggests the presence of a central high

along the incipient NE Atlantic rift axis, partially separating the Mid Norwegian depocentres from Cretaceous basins on the East Greenland Shelf (Dore et al., 1999).

2.5 Palaeocene Extension, Magmatism & Break-up

Latest Cretaceous (Maastrichtian) to Palaeocene extension and associated marginal uplift and erosion likely occurred closed to the line of incipient continental break up (Figure 2.2) (Dore et al., 1999). However, evidence of Palaeocene extension and related rift flank uplift is often masked and obscured by Early Tertiary igneous activity. Pre-opening magmatic underplating and volcanic sill and dyke intrusions into continental crust and thick Cretaceous succession on the marginal highs along the Mid Norway basins are related to plume-generated mantle melts into the thinned axis of incipient opening (White & Mckenzie, 1989; Skogseid et al., 1992; White et al., 2008; Mjelde et al., 2009). These marginal highs were later capped by regionally extensive landward flows in the earliest Eocene, composed of subaerial and submarine lava flows forming escarpments and hyaloclastite deltas (Planke et al., 2000; Horni et al., 2016). As such, the magma rich margins are characterised by Seaward Dipping Reflector (SDR) sequences before oceanic crust was formed along the Ægir mid-oceanic Ridge in the Norway basin at chron 24 (~55Ma) (Talwani & Eldholm, 1977; Gaina et al., 2009).

2.6 Intra-Cenozoic Compression

Since the onset of seafloor spreading along the Ægir Ridge in the Early Eocene, previous NW-SE extension was replaced by SE directed compression in response to ridge push forces from the adjacent ocean (Dore et al., 1999). These ridge push forces caused the formation of major compressional inversion domes (Helland Hansen Arch and Orme Lange Dome in the Voring and More Basins, respectively) and folds (in East Greenland) (Figure 2.2) (Price et al., 1997; Dore et al., 1999). Furthermore, since mid-Atlantic opening, the JMMC has been subject to complex multistage rifting and seafloor spreading processes on both sides of the microcontinent (Figure 2.3, 2.4 & 2.5) (Blischke et al., 2017).

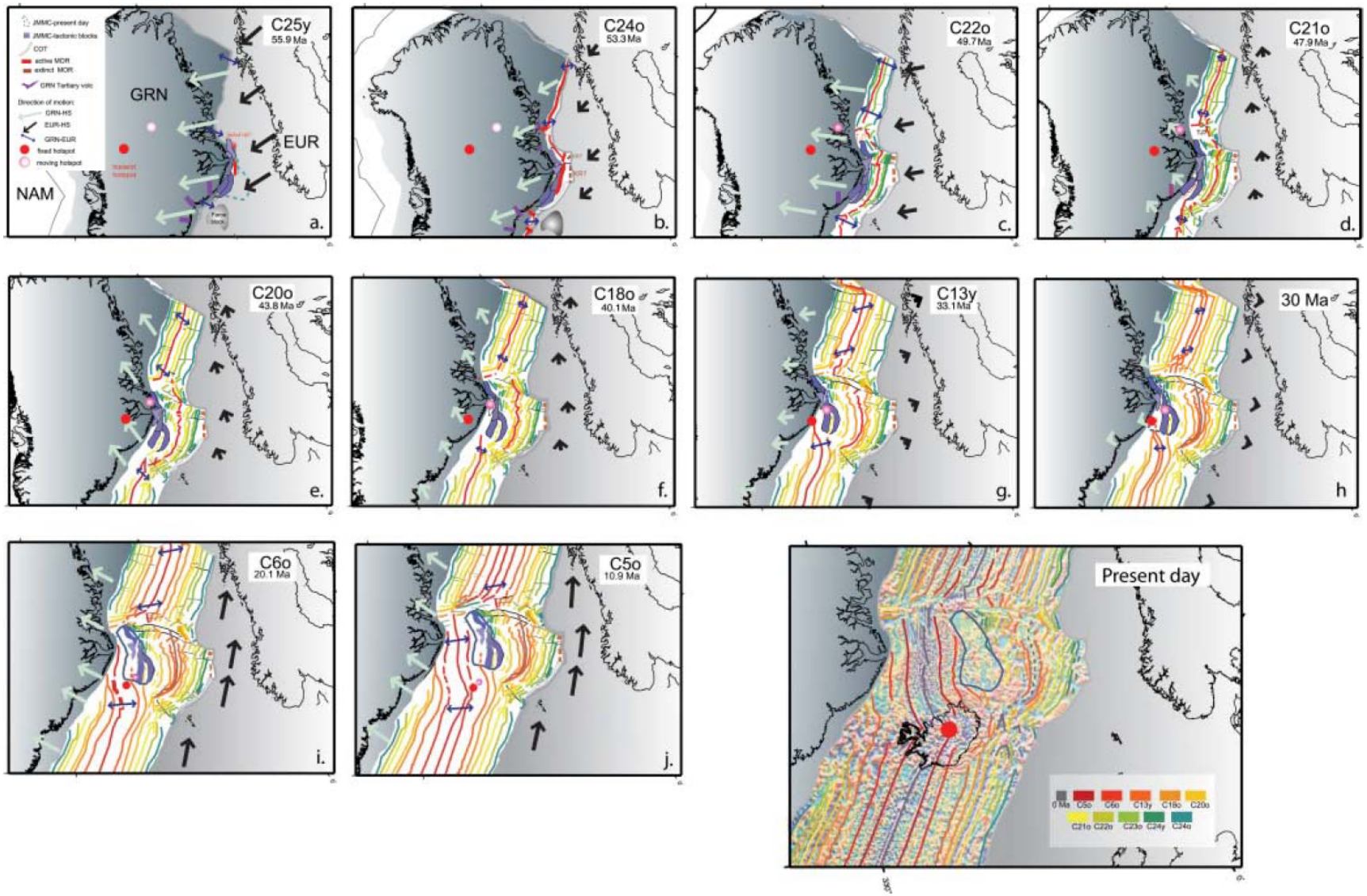

Figure 2.3: Tectonic evolution of the North Atlantic plate boundaries and kinematic evolution of the JMMC from Late Palaeocene to Present (taken from Gaina et al., 2009).

2.7 Mid-Cenozoic Extension

A significant change in spreading rate and direction within the newly formed Norwegian-Greenland Sea (Norway Basin) occurred at Chron 21 (49-47Ma) which resulted in fan-shaped asymmetric spreading along the northern part of the Ægir Ridge (Talwani & Eldholm, 1977; Gernigon et al., 2012/ 2015). Figure 2.4 shows a sketch map of the linked mid-Cenozoic extensional system affecting the North Atlantic. Magnetic anomaly data indicates a 25 Ma time gap between the onset of fan-shaped spreading on the Ægir Ridge and the onset of clear magnetic spreading anomalies between the JMMC and East Greenland at Chron 6 time (23-22.5Ma). A major phase of extensional deformation in at least the southern part of the JMMC is required to compensate for this time gap and counter-balance the fan shaped spreading (widening northwards) along the Ægir Ridge from the Mid Eocene to Late Oligocene (Gernigon et al., 2012).

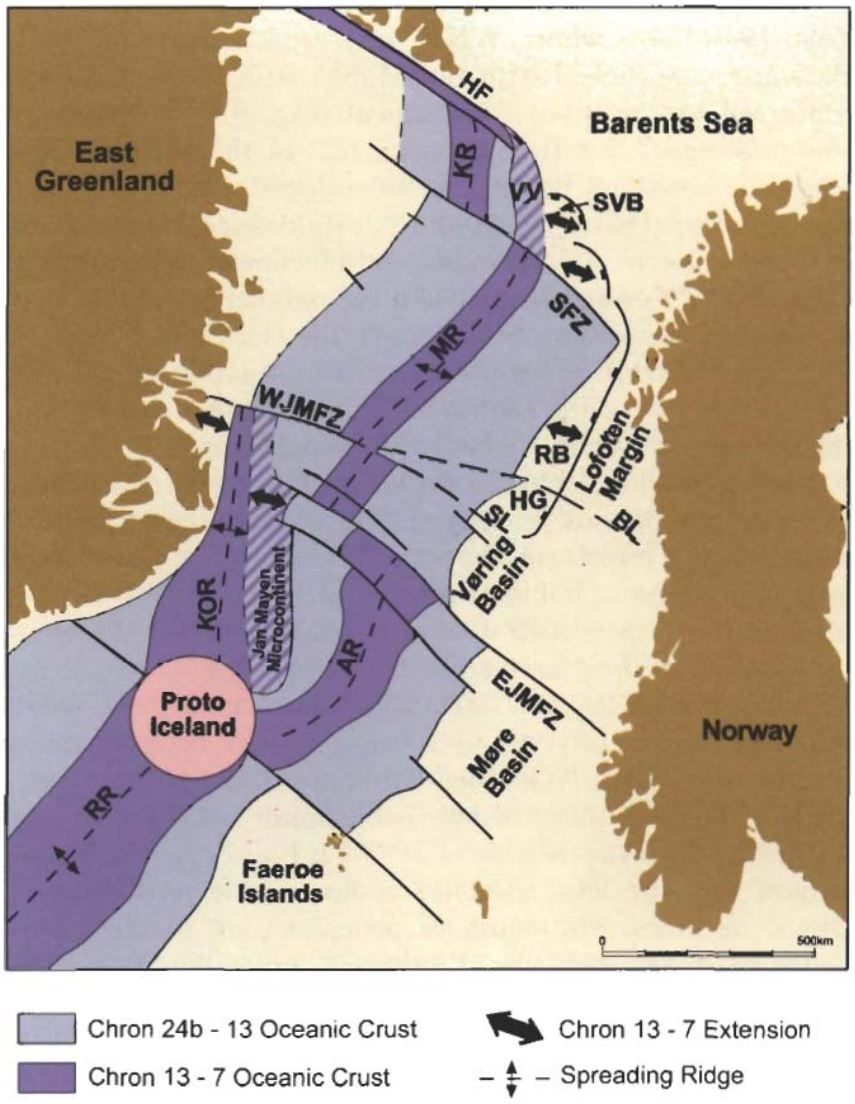

Figure 2.4: Mid-Cenozoic (Oligocene-Miocene) linked extensional system affecting East Greenland, Jan Mayen, the Mid-Norway margin and the western Barents Sea. Plate reconstruction is to chron 7 time (25 Ma) (taken from Dore et al., 1999).

A slowdown in spreading rate along the Labrador Sea and the progressive docking of Greenland with the North American plate caused a major tectonic event in the North Atlantic. The associated plate reorganisation from chron 18 to 13 time (~40 to 35 Ma) resulted in a change in opening direction between Eurasia and North America/Greenland from NNW-SSE to a NW-SE direction which led to the formation of the West Jan Mayen Fracture Zone (Figure 2.5) (Talwani et al., 1977: Gernigon et al., 2015).

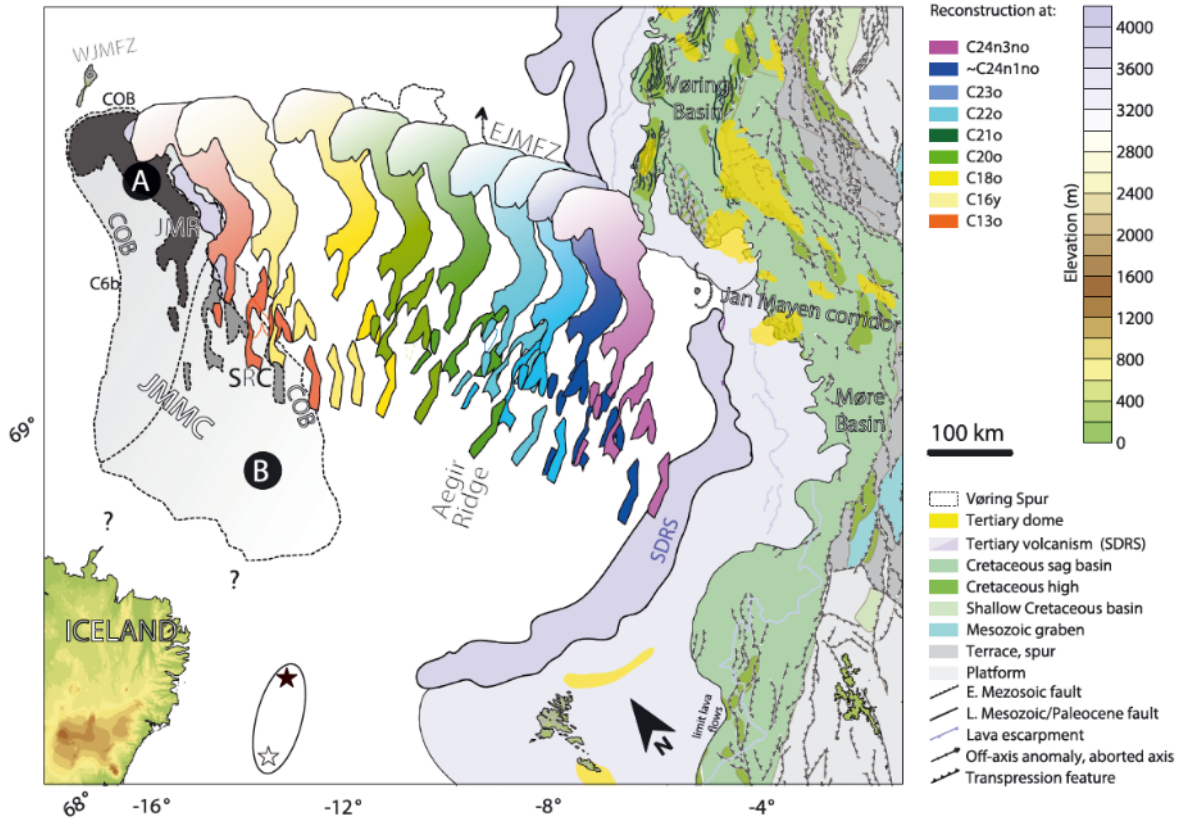

Figure 2.5: Plate reconstruction of the Jan Mayen microcontinent during spreading along the Ægir Ridge (taken from Gernigon et al., 2015).

To accommodate these tectonic changes and spreading rates along the Ægir ridge, it is likely that there was a progressive westward migration of the spreading axis in the form of a series of "westward stepping rift transfer systems" and/or simultaneous spreading along a proto-Kolbeinsey Ridge (Gaina et al., 2009; Gernigon et al., 2012/2015; Blichske et al., 2017). The Jan Mayen Basin and Jan Mayen Trough both developed in response to this extensional phase, whilst the SRC widened to approx. 310km in compensation of the progressive westward jump of spread ridge axes prior to establishment of the Kolbeinsey Ridge (Peron-Pindivic et al., 2012a&b; Blischke et al., 2017). Furthermore rotation and compression along the SE JMMC resulted in the formation of inversion structures along the SE margin of the JMMC until cessation of spreading on the Ægir Ridge (Blischke., et al., 2017). It is also likely that westward (and northward) propagating rifting between the JMMC and East Greenland regional tilting and uplift and the formation of the distinct Oligocene unconformity across the microcontinents ridges (Blischke et al., 2017).

This Mid-Eocene plate reorganisation in the Norway Basin also coincides with compression and dome formation along mid-Norwegian to Rockall-Faroe area, described above (Dore et al., 2008) and the end of post-breakup volcanism in Blosseville Kyst coastal regions of East Greenland and

the sudden influx of clastics sourced from uplifted margin and JMMC (Larsen et al., 2005; Gernigon et al., 2012).

The Ægir Ridge became extinct between chrons 8 & 7 time (25-23 Ma), whilst final separation of the JMMC from East Greenland occurred at chron 6 (21 Ma) when the Kolbeinsey Ridge propagated northward to reach the Western Jan Mayen Fracture Zone (Gaina et al., 2009; Gernigon et al., 2015; Blischke et al., 2017). Continued, normal seafloor spreading along the Kolbeinsey Ridge has caused the JMMC to continue to drift further away from the East Greenland margin to its present day geographical location.

2.8 Neogene Uplift and Erosion

The most severe regional uplift and erosion across the NE Atlantic margins resulted from the encroaching Iceland Plume and Plio-Pleistocene glaciations, which have shaped the current distribution of sea and landmasses. Initial uplift in the Palaeocene and Oligocene/Miocene was tectonic (outlined above) associated with thermally generated uplift along the line of incipient Atlantic rifting and intraplate stresses forming compressional inversion structures, respectively. However, subsequent climatic deterioration caused nucleation of continental scale ice sheets on these earlier elevated areas resulting in increased, rapid erosion and net uplift (of up to 2-3 km on the Norwegian – Barents Sea margin) during each interglacial due to isostatic rebound (Dore et al., 1999). Furthermore, the increased rate and flux of sedimentation from glacial erosion also likely caused loading of the shelves, resulting in induced subsidence and amplified folding along the NE Atlantic passive margins (Lundin & Dore, 2002). These Late Cenozoic regional scale uplift events have had major implications for hydrocarbon prospectivity along the NE Atlantic margins (Dore & Jenson, 1996; Jaspen & Chalmers, 2000; Lundin & Dore, 2002). For the JMMC, aside from the Eocene-Miocene extension, rift-related uplift and compressional tectonic events, the Plio-Pleistocene at least was a period of continued subsidence in response to lithospheric cooling (Blischke et al., 2017).

Known hydrocarbon systems exist within the Jurassic-Cretaceous-Cenozoic successions on the Mid Norway (Voring and Møre Basins) margin and from the Mesozoic succession onshore East Greenland (Jameson Land Basin). Given the regional palaeogeographic palinspastic reconstructions of the NE Atlantic (Figure 2.6), the JMMC would have been situated between the Mid Norway and East Greenland margins, and by inference, likely contains similar pre-Cenozoic stratigraphic successions. The presence of source rocks and reservoir units are likely high from the upper Palaeozoic – Mesozoic stratigraphy. However, key risks for working hydrocarbon systems within the JMMC include charge and trap timing, Eocene basalt emplacement (flood basalts and later volcanic intrusions), and Icelandic mantle plume and tectonic deformation (rifting, inversion and uplift) relating to spreading ridge re-organisation.

55 Ma

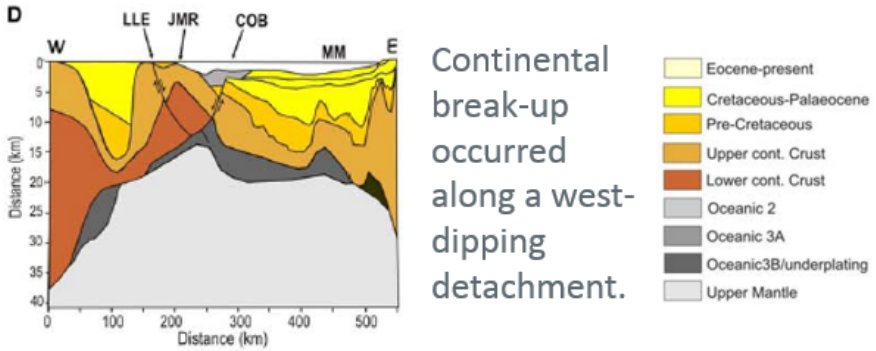

Continental break-up occurred along a west-dipping detachment.

52 Ma

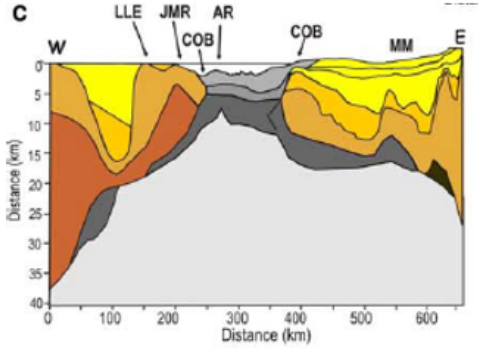

Eocene-Oligocene continental extension in East Greenland was symmetric and concentrated in the lower crustal layer.

25 Ma

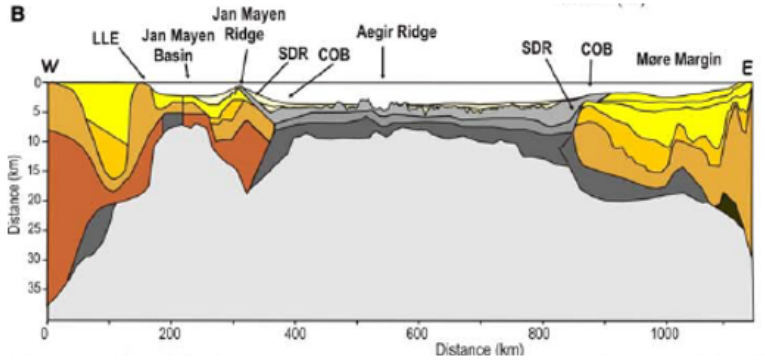

Continued extension rifted off Jan Mayen Ridge from East Greenland margin when Aegir Ridge became extinct – (mid-ocean ridge jump to Kolbeinsey Ridge (Chron 7))

Present

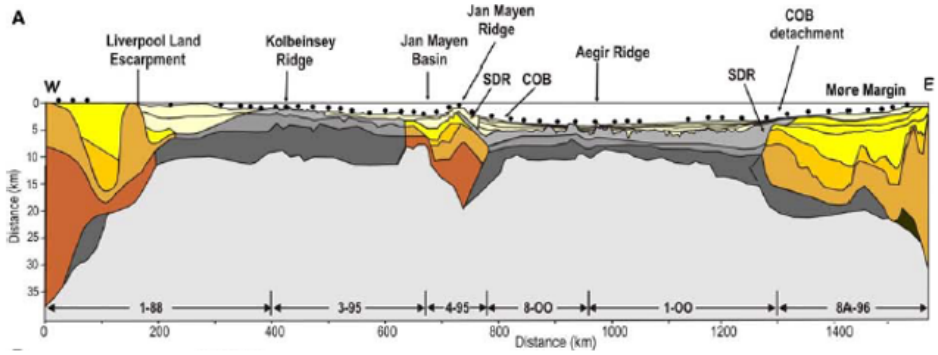

Initial oceanic crustal accretion along Kolbeinsey Ridge was thin (5.5 km). Crustal formation since 23 Ma is ~8 km thick with high magma budget (plume related rifting)

Figure 2.6: Palinspastic Crustal reconstructions across the NE Atlantic margin from Palaeocene-Eocene to Recent (taken from Mjelde et al., 2008).

3. Database

An integrated multidisciplinary database was used for this study (Figure 3.1). Lithological and biostratigraphic data were used from shallow DSDP boreholes and geological samples collected from an ROV expedition by the Norwegian Petroleum Directorate (NPD). A total of 152 2-D seismic lines of varying vintages were used for horizon and structural interpretation. Gravity and magnetic surveys were used to help delineate crustal domains and potential basinal areas across the study area. Furthermore high resolution multibeam bathymetry data across the Dreki area helped to better realise the 3-D surface expression of micro-continental fragments in the southern part of the study area. Table 1 provides an overview of the range of data used for mapping the Jan Mayen Microcontinent.

Data type		Acquisition Date	Coverage/ Areal extent	Additional Information
Wells				
DSDP Leg 38	346	1974	TD in Late Eocene	intersects with line JM-85-07 & NPD-12-121209
	347	1974	TD in Late Eocene	intersects with line NPD-11-110013
	348	1974	TD in Early Miocene	
	349	1974	TD in Late Eocene	intersects with lines JM-85-32; NPD-12-120031; NPD-11-110020; NPD-11-110007
	350	1974	TD in Mid Eocene	intersects with line TGS-ICE-02-103
ODP Leg 151	907A	1993	TD in Early Miocene	
ODP Leg 162	985	1995	TD in late Oligocene	
	987	1995	TD in Late Miocene	
	907C	1995	TD in Early Miocene	
NPD ROV sampling		2011	JMR & SRC	Sampling with gripping arm
		2012	Western flank of JMR & SRC	Sampling with chain saw
Gravimetric		2010 compilation (Olesen et al)	North Atlantic Ocean	
Magnetometric		2010 compilation (Olesen et al)	North Atlantic Ocean	
Multibeam bathymetry		2008	Dreki Area only	
2D Seismic Surveys				
JM-85		1985 (reprocessed 2009)	30 lines	minus 60° constant phase rotated zero-phase negative standard polarity
JM-88		1988 (reprocessed 2009)	14 lines	minus 60° constant phase rotated zero-phase negative standard polarity
IS-JMR-01		2001 (reprocessed 2013)	16 lines	Zero-phase positive standard polarity (American polarity)
TGS-ICE-02		2002	3 lines	Zero-phase positive standard polarity (American polarity)
WI-JMR-08		2008	8 lines	Zero-phase negative standard polarity (European polarity)
NPD 2011		2011	16 lines	Zero-phase negative standard polarity (European polarity)
NPD 2012		2012	65 lines	Zero-phase negative standard polarity (European polarity)

Table 1: Overview of the database available for this research

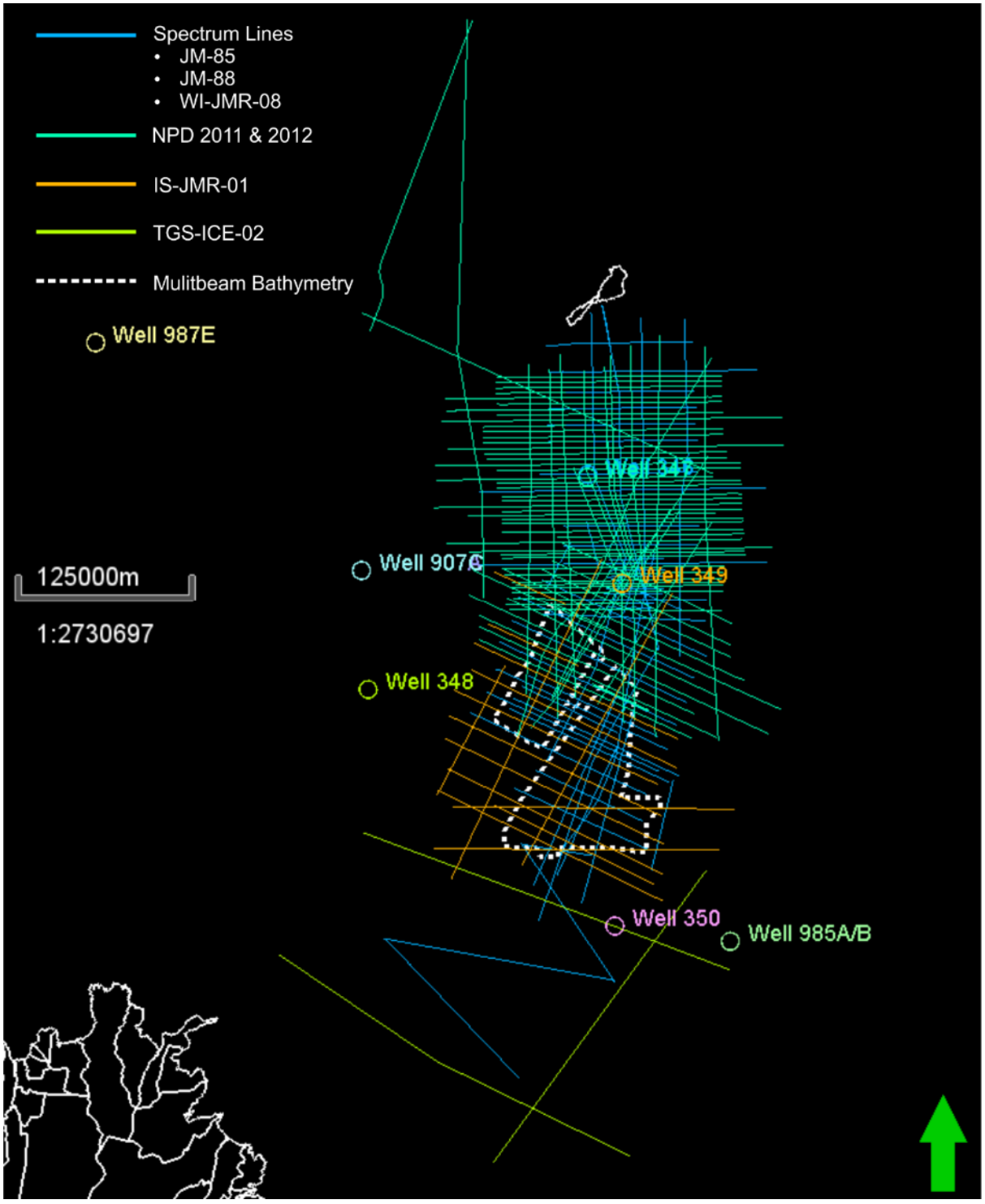

Figure 3.1: Basemap showing well locations, 2D seismic lines (and their respective vintages), and areal extent of multibeam 50x50 m bathymetry data.

4. Interpretation of Data

4.1 Gravity Data

Figure 4.1 shows the free-air gravity map over the study area, with the wider JMMC extent highlighted as a solid white line and individual components of the JMMC, such as the JMR and SRC, outlined in white dashed lines. Strong positive anomalies correspond to the main JMR feature and some of the isolated ridges from the SRC suggesting these areas contain thick crystalline basement at relatively shallow levels. Whereas lower to negative anomalies may indicate basinal areas across the JMMC where the basement is at a relatively lower depth, overlain by a thick sediment pile.

4.2 Magnetic Data

Figure 4.2 shows the magnetic map across the Norwegian-Greenland Sea. The JMMC itself is situated in an area of relatively subdued and negative anomalies corresponding to an area of potential continental crust with associated sedimentary basin successions. The JMMC is surrounded by strong positive and strong negative linear anomalies representing sea-floor spreading anomalies/ chrons from the Ægir Ridge to the east and Kolbeinsey Ridge to the west. As such the magnetic anomalies can help to delineate the geographic extent of the micro-continental crust and Continent-Ocean Transition (COT) around the JMMC. The southern limit of the JMMC remains difficult to ascertain due to a lack of high resolution data and interference of increased volcanic extrusives and intrusives in close proximity to Iceland. Whether this southern-most area contains true oceanic crust, highly extended crust (Mjelde et al., 2007) or a combination of the two (Gaina et al., 2009) remains contentious.

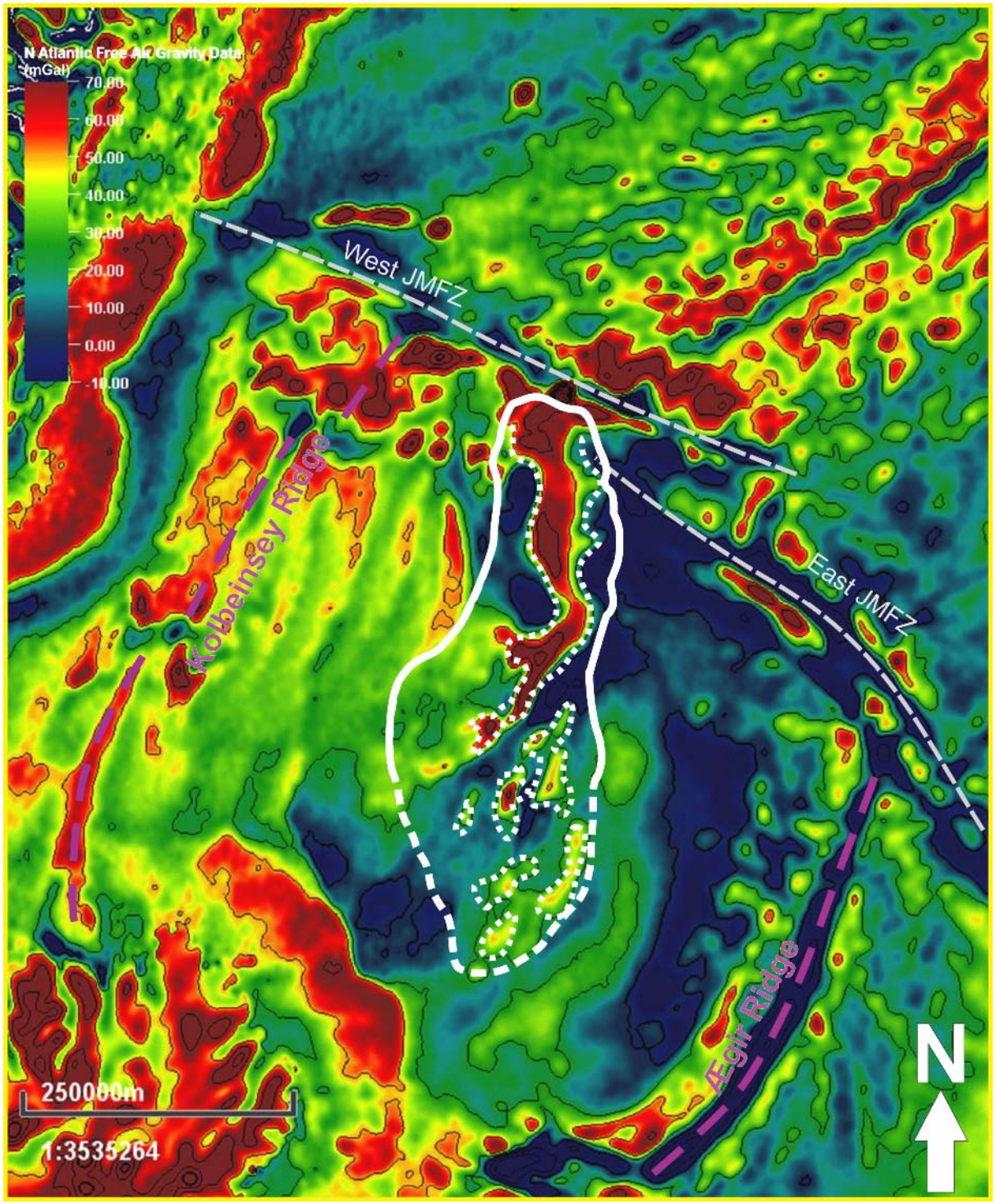

Figure 4.1: Free-Air gravity map over the Norwegian-Greenland Sea. (White solid line suggests the COT around the JMMC. The JMR and SRC are highlighted by the dashed white polygons within the JMMC area).

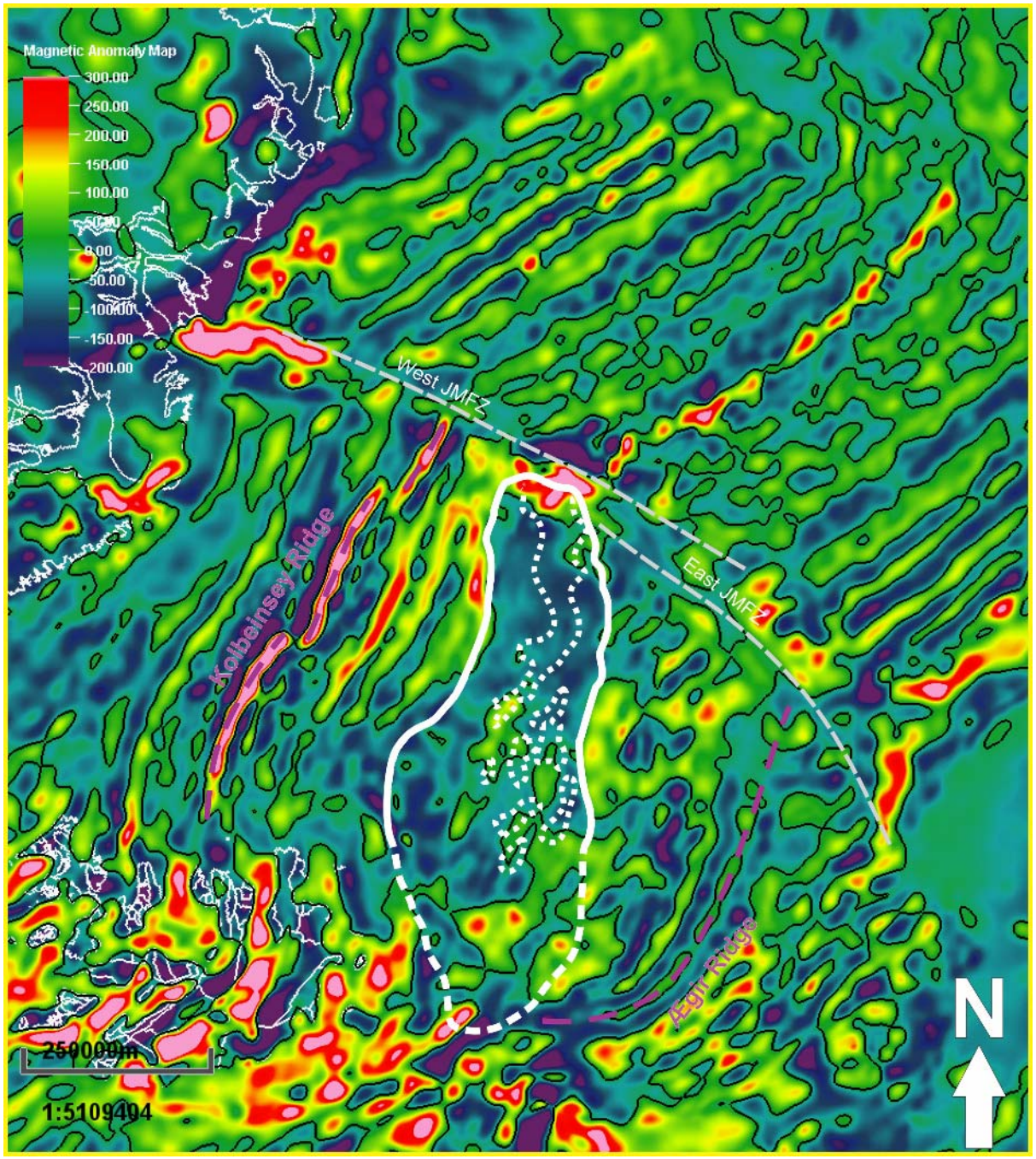

Figure 4.2: Magnetic Anomaly map over the Norwegian-Greenland Sea. (White solid line suggests the COT around the JMMC. The JMR and SRC are highlighted by the dashed white polygons within the JMMC area).

4.3 Well data

A total of eight shallow borehole data were available for this study from DSDP Leg 38 and ODP Legs 151 and 162. DSDP wells 346 to 350 are situated over the JMMC and were most useful for this research to understand the shallow Cenozoic stratigraphy on the main JMR and SRC (Table 2). Well summary sheets were produced for each of these wells in this study, providing a synthesis of the important, relevant information obtained from the well reports, which can be found in Appendix A. Lithostratigraphic and chronostratigraphic summaries have also been produced for each of these wells and can be found in Appendix B.

Four of the DSDP wells, (346, 347, 349 & 350) provided a seismic-well tie for seismic horizon interpretations across the JMR (Figure 4.3) (see Seismic Data section below). The two northern-most boreholes (346 & 347) penetrated 187 m and 190 m subsurface on the eastern edge of the main JMR; whilst well 349 penetrated 320 m subsurface further south-east on the JMR.. Well 350 is situated on and penetrates 388 m of one of the southern-most isolated ridges of the SRC. Site 348 is situated on magnetic anomaly 6 (early Miocene) oceanic crust to the west of the JMR on the Iceland Plateau.

Wells	Water depth (m)	Well penetration (m)	Location on JMMC
346	732	187	northern JMR
347	745	190	northern JMR
348	1763	544	Chron 6 Iceland Plateau
349	915	320	southern JMR
350	1275	388	SRC

Table 2: DSDP Leg 38 wells over the JMMC.

The location of wells 346, 347 and 349 were drilled with the aim of targeting the oldest Cenozoic sedimentary succession (post the Palaeocene-Eocene basalts), due to the regional eastward tilt of the stratigraphy underlying the JMMC (Figures 4.4 & 4.5). However, the oldest succession encountered in all of these wells is Late Eocene, because of unintentional drilling just west of a main westward dipping normal fault (Gunnarsson et al., 1989) (Figure 4.6).

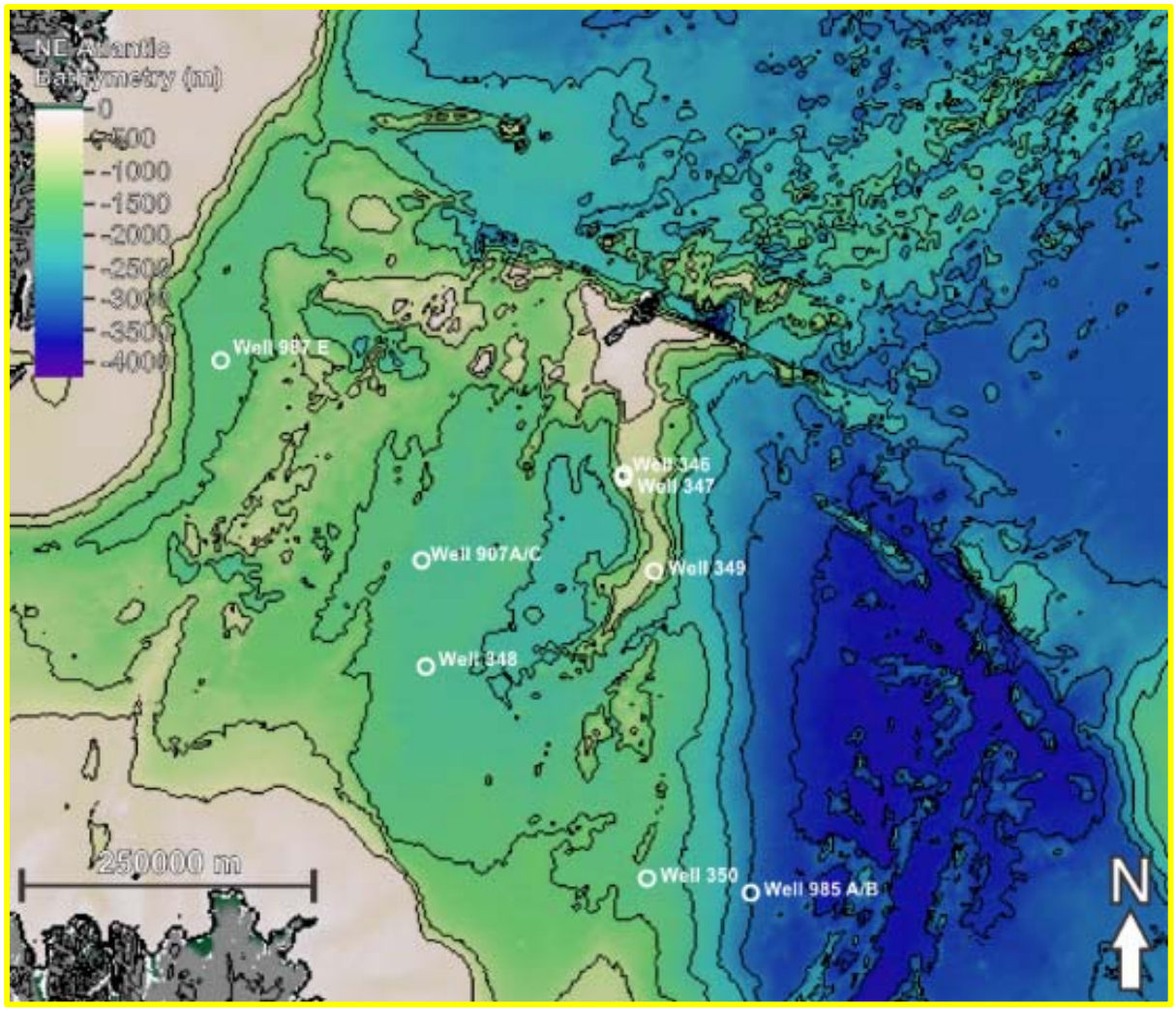

Figure 4.3: Location of DSDP and ODP wells across the JMMC.

The oldest unit is encountered in Well 350, which penetrates Late Eocene age Tholeiitic basalt with a tuff breccia representing the top portion of the igneous basement (Figure 4.6 & 4.7). The overlying unit consists of massive terrigenous mudstone and sandy mudstones, with abundant conglomerate, breccia and sandstone intervals of Oligocene to Late Eocene age. It is interpreted that breccias overlying the basalt, represent slump deposits whilst sandstone intervals represent "proximal" turbidites and gravity flow deposits (Talwani et al., 1976). Clay mineralogy, mica compositions and altered redeposited quartz-biotite schists and gneisses suggest this sediment was sourced from the East Greenland continental margin (Figure 4.7) (Talwani et al., 1976). A distinct unconformity (at a depth of approximately 100 – 120 m below seabed) is present in wells 346, 347, 349 and 350 (Figure 4.7). Sediments below the unconformity are almost entirely terrigenous with only arenaceous foraminifera preserved. The Miocene to Oligocene succession, overlying the unconformity, is dominated by alternating terrigenous claystone and mudstone layers with sandy mud, transitional siliceous and/or glauconitic mud, and persistent volcanic ash layers. The biogenic component also increases markedly in the Miocene sediments from sites 346 & 347. The dominance of fine grained material represents hemipelagic sedimentation, whilst the sandy mudstone units may represent "distal" turbidites within a deeper marine setting, suggesting that the JMMC was located further away from the East Greenland margin receiving only very

fine grained material shed from the continental shelf (Talwani et al, 1976). The Oligocene age unconformity likely marks the time of separation of the Jan Mayen Ridge from East Greenland, represented by the consequent change in lithology and sedimentary regime. The Pleistocene-Pliocene succession is composed of sandy mudstone and nannofossil oozes consistent with representing glacial-marine and interglacial sedimentation along with ice-rafted material (Figure 4.7).

Well 348 located on the Icelandic Plateau records the deposition of mudstones and sandy muds containing mainly cold water fauna of Pleistocene to Miocene-Oligocene age overlying a Tholeiitic basalt of early Miocene age (Figure 4.7) (Talwani et al., 1976; Gunnarrson et al., 1989). The basalt encountered in this well represent the first sea floor spreading anomalies along the Kolbeinsey Ridge (Chron 6) after the sea floor spreading jump associated with plate reorganisation in the Oligocene occurred. The overlying sedimentary succession represents hemipelagic deposition with increasing distance and decreasing sediment input from East Greenland through time (Figure 4.7).

Despite the shallow penetration of these wells in relatively faulted areas on the JMR, seismic to well ties were produced at sites 346, 347, 349 and 350 to at least constrain the uppermost stratigraphy (Figures 4.4 – 4.6). Furthermore, the NPD ROV expeditions in 2011 & 2012 were also undertaken on one of the northern-most ridges of the SRC, providing another location point for calibration between the Cenozoic stratigraphy and seismic horizon interpretation (see ROV section below).

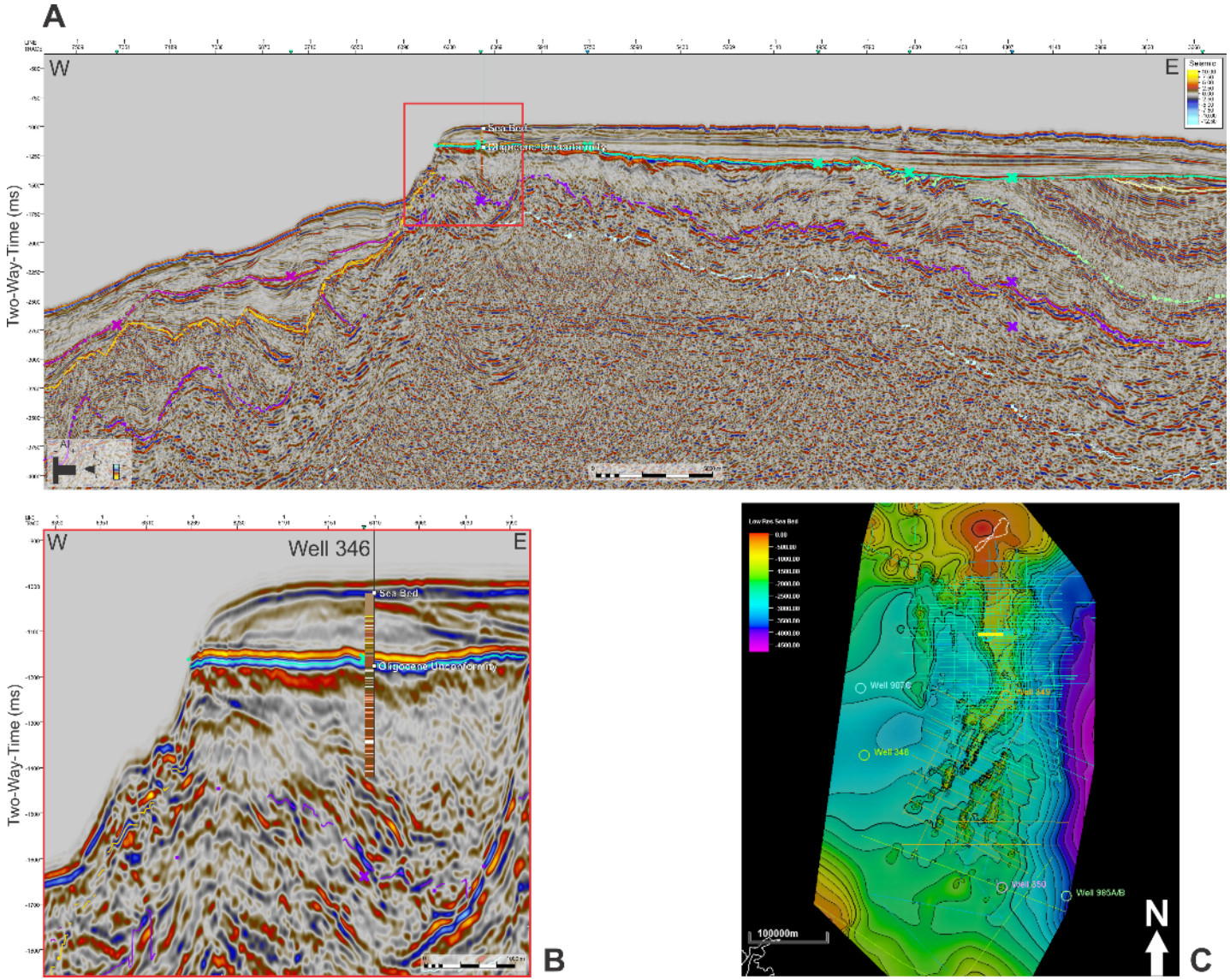

Figure 4.4: Seismic to well tie at well location 346 (and 347) on the western edge of the JMR.

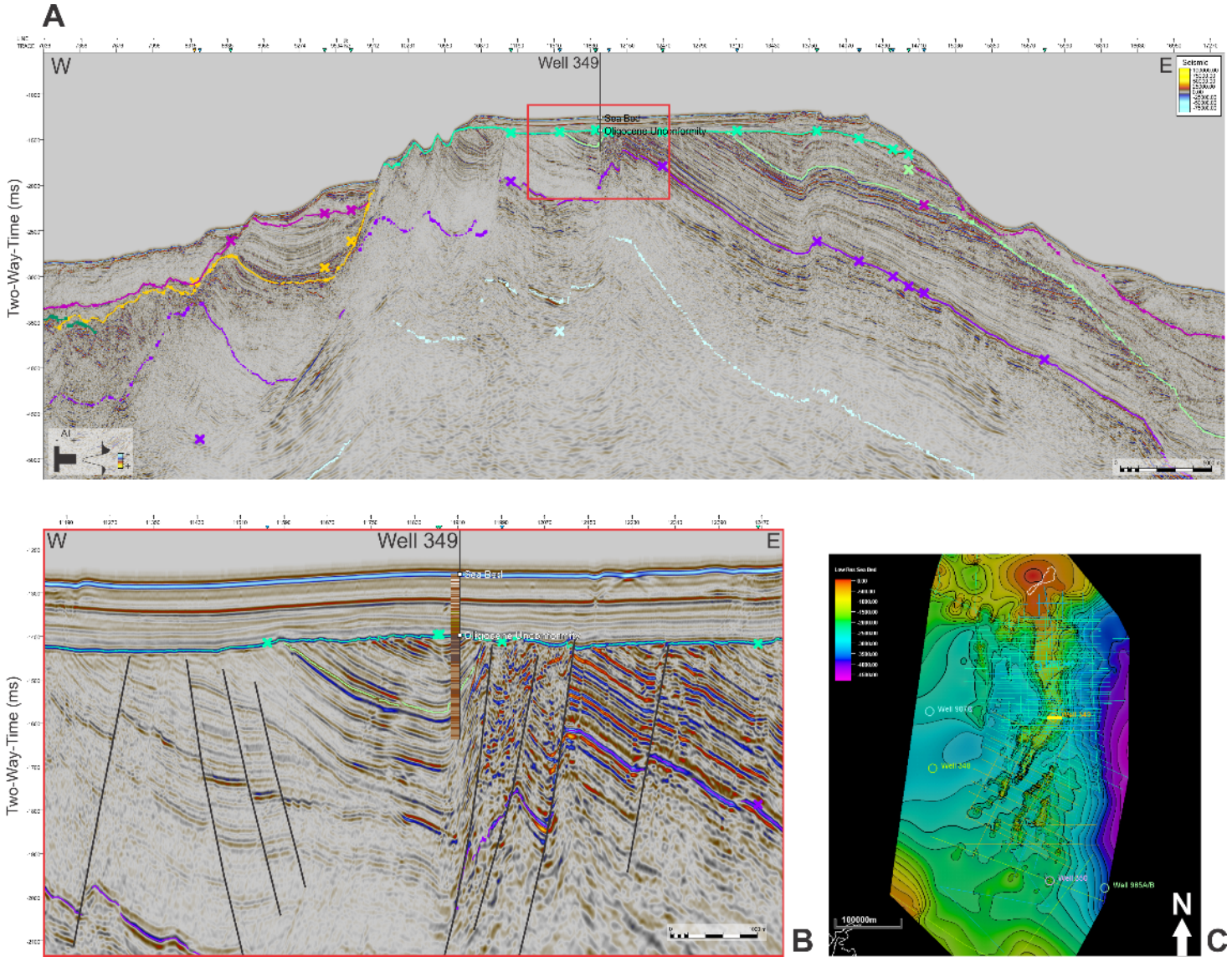

Figure 4.5: Seismic to well tie at well location 349 at the south-eastern edge of the JMR.

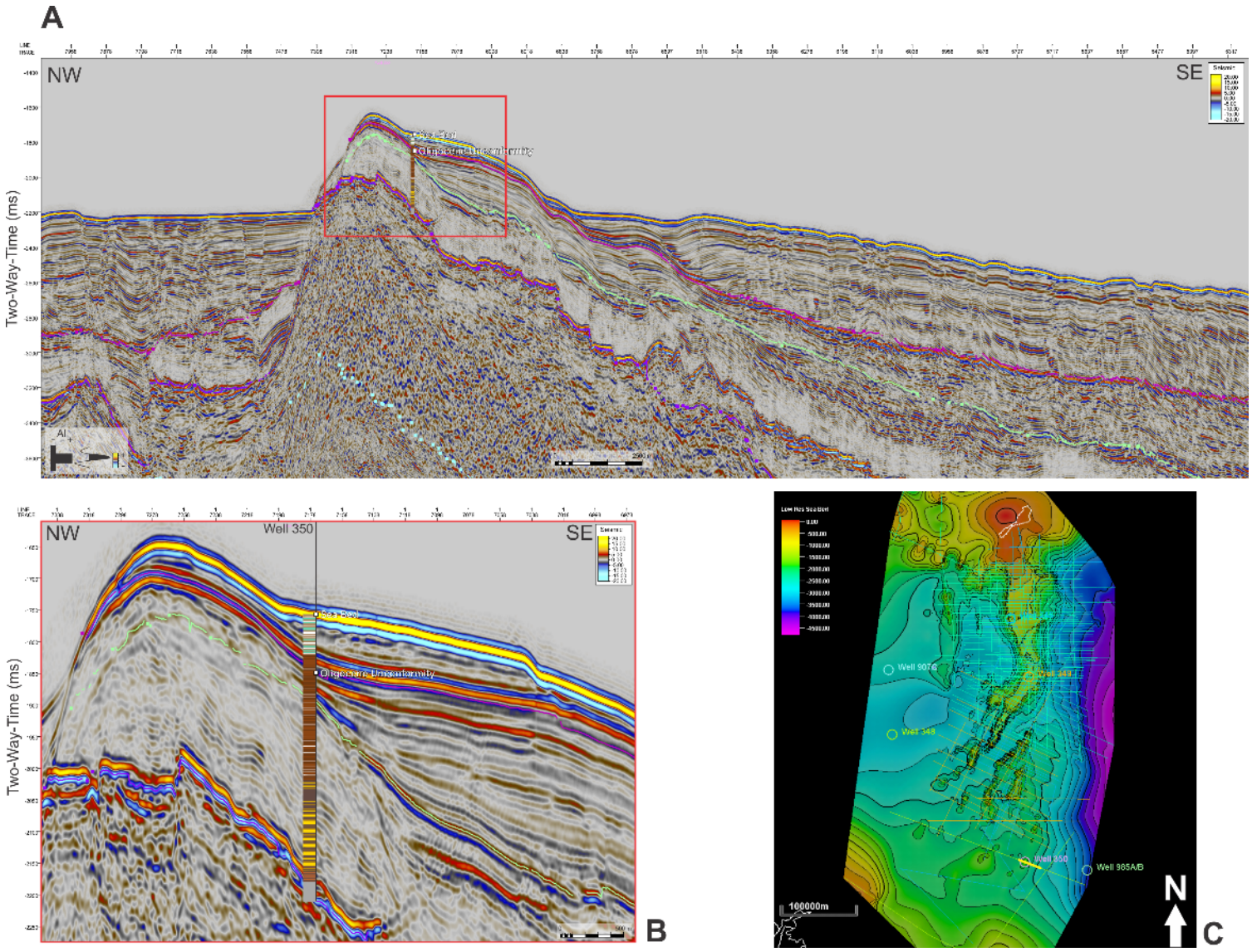

Figure: 4.6: Seismic to well tie at well location 350 on one of the south-eastern most ridges of the SRC.

DSDP Leg 38 well correlation panel across the Jan Mayen Microcontinent

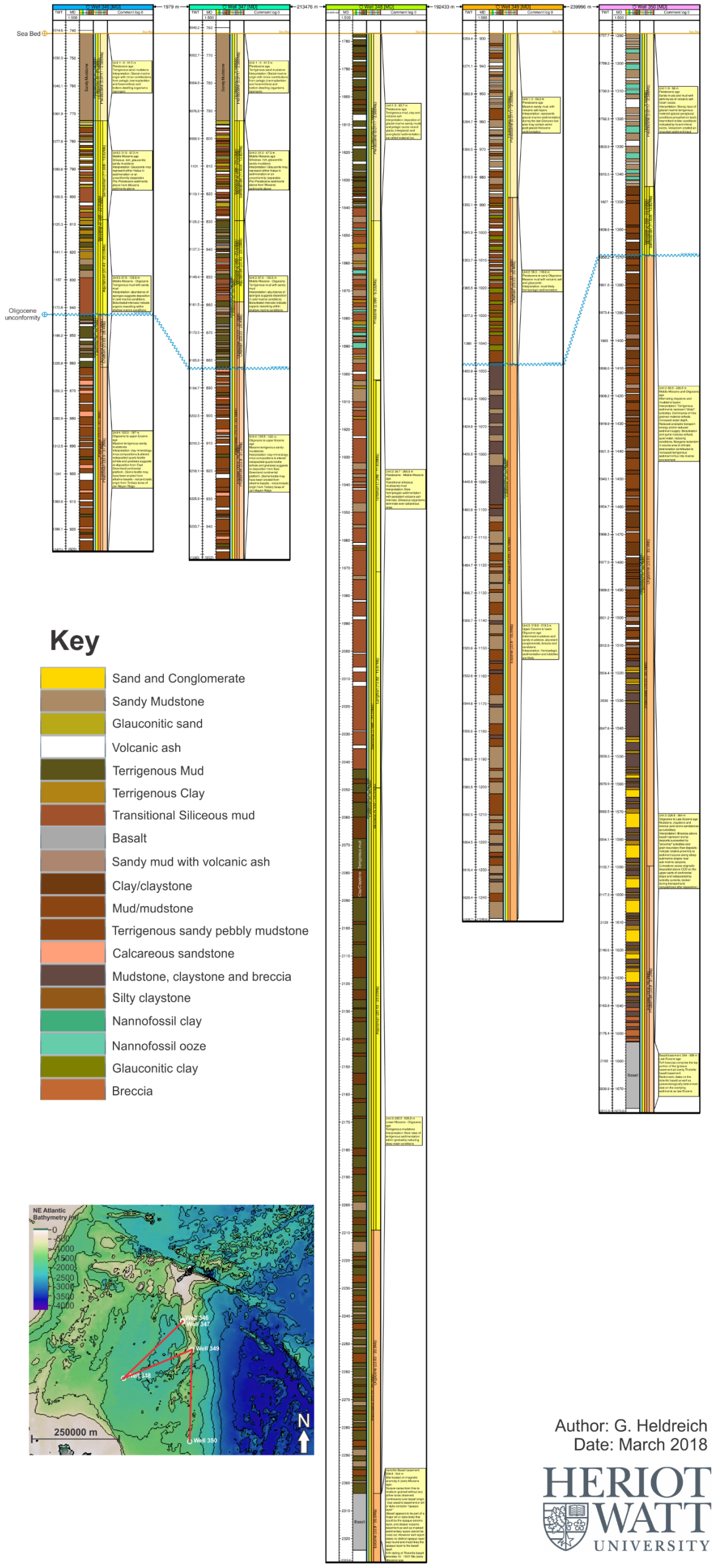

Figure 4.7: DSDP well correlation to show lithological variation within the Pleistocene to Late Eocene sedimentary succession.

4.4 Seafloor Sampling Expeditions

4.4.1 NPD ROV

The NPD conducted rock sampling using a remotely operated vehicle (ROV) at sites predominately along the western flank of the main ridge and isolated ridges of the SRC in 2011 and 2012 (Figure 4.8).

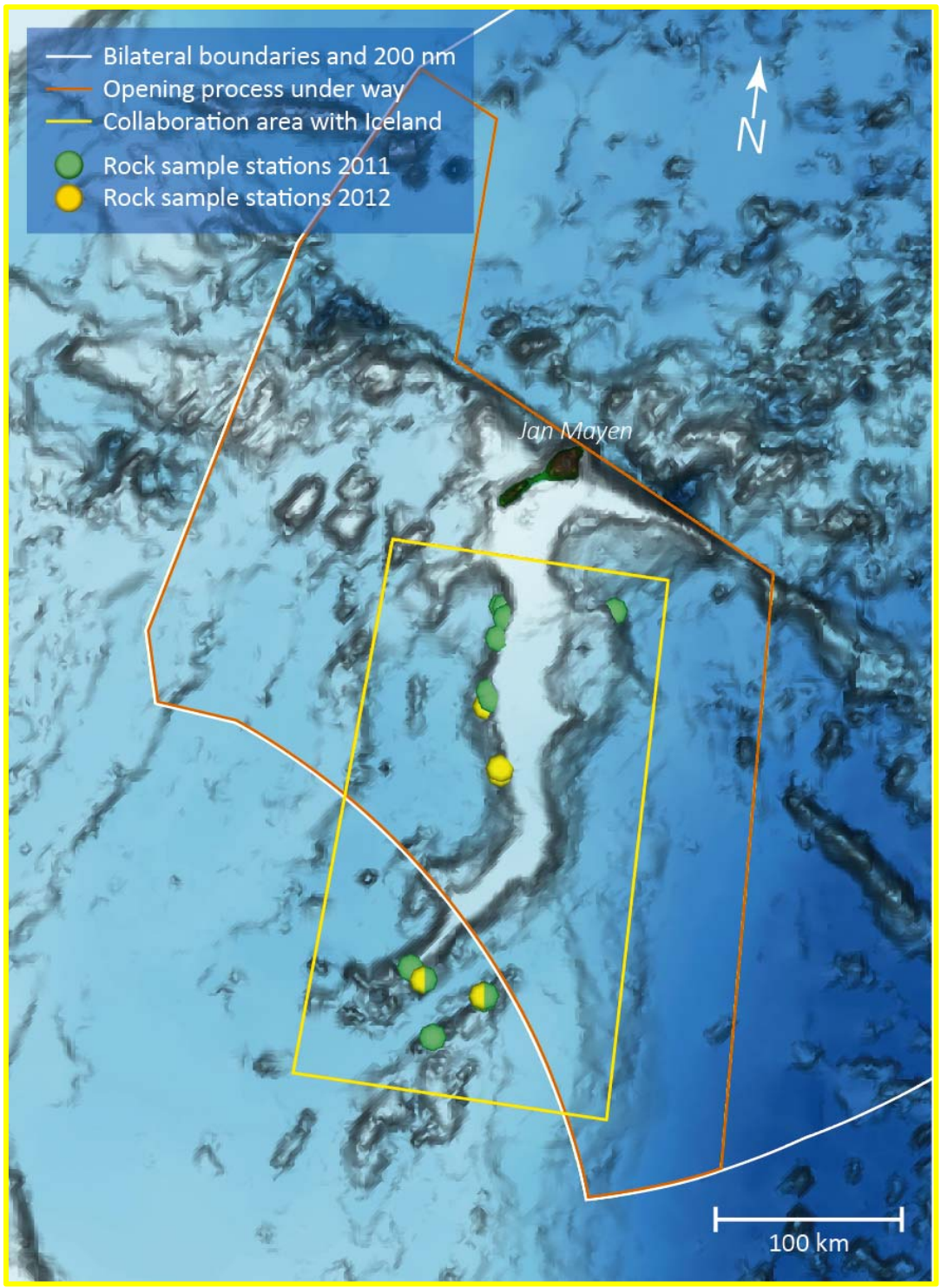

Figure 4.8: NPD ROV sampling locations along the Jan Mayen Ridge and SRC (taken from NPD Resource Report 2013).

Results of the ROV expeditions identify rock samples ranging from Triassic, Jurassic, Cretaceous and Cenozoic. It is thought, however, that only the Cenozoic aged samples represent in-situ geology, whilst Mesozoic aged samples are likely ice-rafted debris from East Greenland. Figure 4.9 provides a constraint on the lithologies present within the Cenozoic stratigraphy of the SRC area and in particular, with regards to enabling a "seafloor outcrop"-to-seismic tie for mapping key surfaces across the JMMC. The Cenozoic samples from these expeditions confirm thick layer of basalt lava, which when tied to seismic data and mapping, is a regionally extensive horizon related to North Atlantic break up and seafloor spreading of Palaeocene-Eocene age (Figure 4.9). Directly overlaying the basalt lava layer are fine grained sediments followed by a quartz-rich sandstone dated as early Eocene. Overlying this quartz rich sandstone later are alternating shales and siltstones dated to the Eocene/early Oligocene (Figure 4.9).

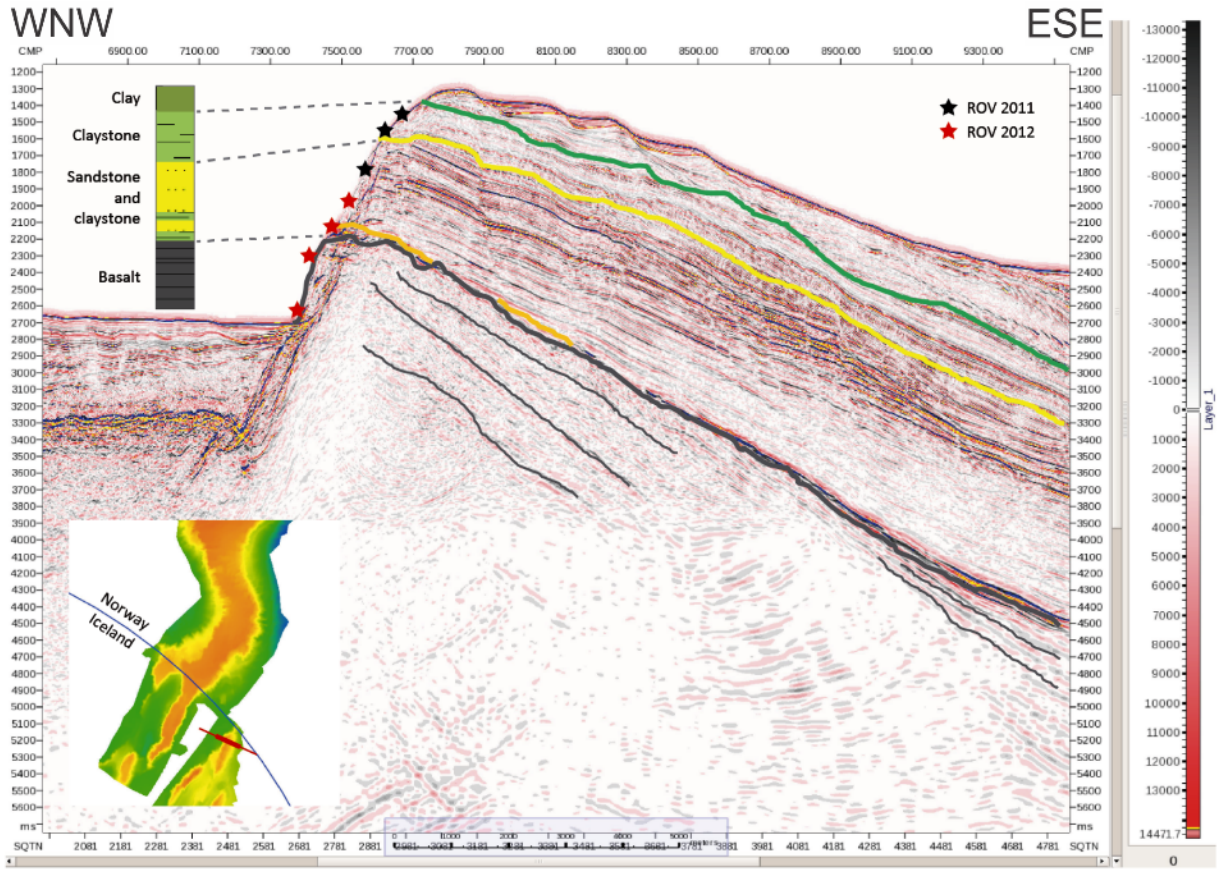

Figure 4.9: Samples acquired from NPD ROV expeditions on one of the eastern most ridges of the SRC (taken from NPD Resource Report 2013).

Lithological information from the NPD ROV seafloor sampling expedition was also used in conjunction with DSDP wells to provide a more complete post-Eocene basalt stratigraphy across the JMMC and provide a secondary tie point for seismic horizon interpretation (Figure 4.9).

4.4.2 VBPR and TGS

Another seafloor sampling expedition on the JMMC SRC was undertaken by Volcanic Basin Petroleum Research (VBPR) and TGS in 2011. Gravity core and dredge samples from this campaign recovered Permo-Triassic, Jurassic, and Cretaceous and middle Eocene age in or "near in-situ" rocks, including break-up igneous rock samples (Figure 4.10) (Polteau et al., 2018). Samples taken in stratigraphic order generated a 1000 m pseudo well along the sampled ridge, providing another pseudo well-to-seismic calibration point for the upper Mesozoic and early Eocene succession. Furthermore, organic geochemical analyses of the recovered sediments, suggests active seepage of Jurassic oil and a working hydrocarbon system within the JMMC (Figure 4.10) (Polteau et al., 2018).

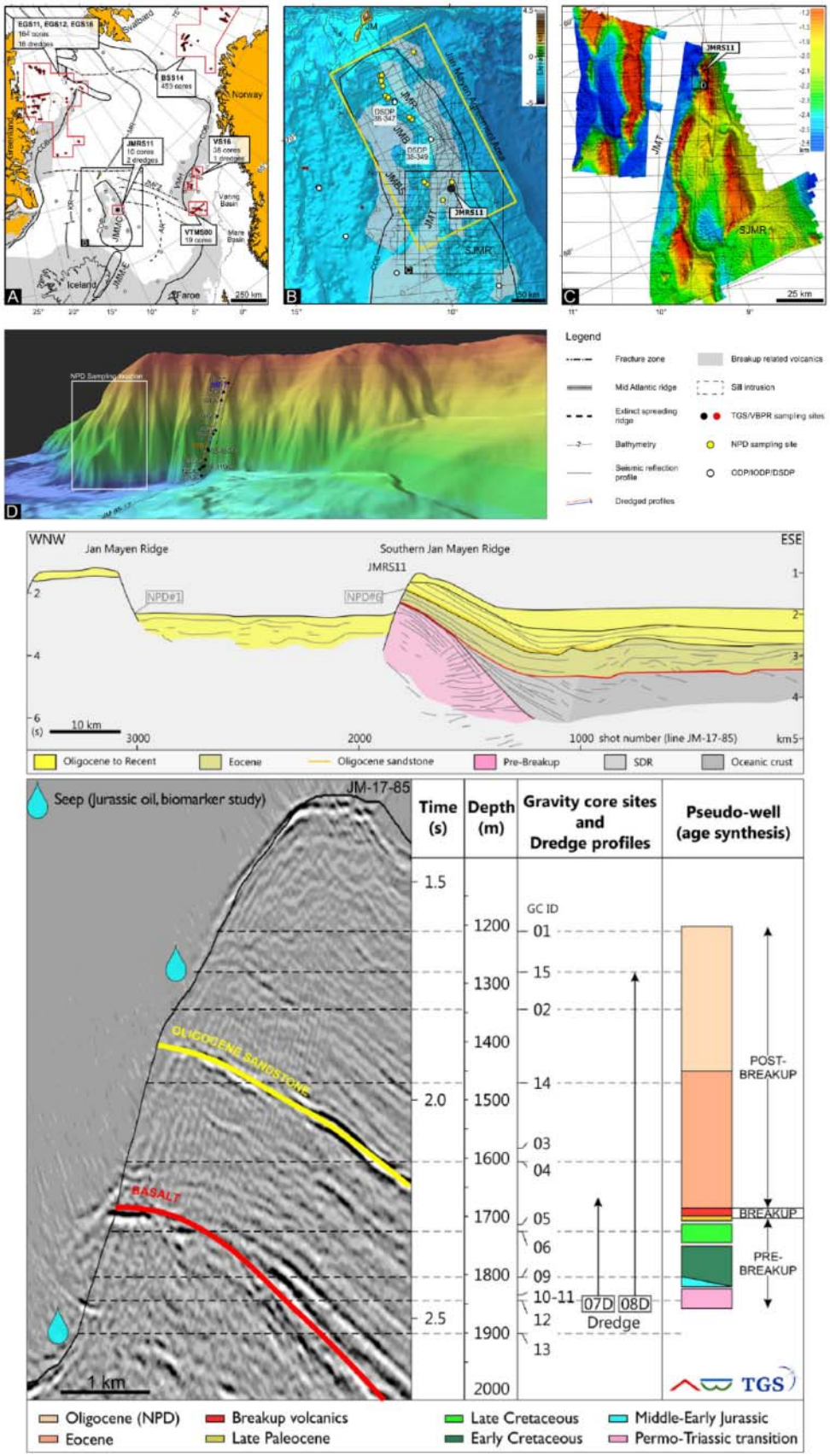

Figure 4.10: Stratigraphic results of the VBPR & TGS seafloor sampling campaign on the SRC, providing a seismic-well tie for horizon interpretations along line JM-85-17 (taken from Polteau et al., 2018).

4.5 Seismic Data

4.5.1 The Structural Style of the JMMC

The passive rifted margins bounding both sides of the JMMC, are markedly different in structural style; creating a distinct structural asymmetry across the microcontinent. As such, different structural domains have been identified across the JMMC based on their respective structural styles (Figure 4.11). Gunnarsson et al., (1989) give a detailed description of the structural style of the JMMC.

The main ridge a flat-topped, asymmetric, bathymetric ridge feature with an eastward tilted eastern margin and a steep faulted western flank (Figure 4.11). The central main ridge was uplifted and eroded during the 2nd rift phase forming the major angular unconformity. Figure 4.12 also shows the horizons that have been mapped as part of this research across the JMMC.

Volcanic sills and lava flows on both margins mask a clear identification of the COB surrounding the JMMC (Figure 4.11 & 4.12). Figure 4.13 shows the areal extent of the igneous domains mapped across the JMMC. Consequently magnetic anomaly data (Figure 4.2) was used in conjunction with seismic reflection and refraction data to delineate a COT zone. The width of the JMMC increases towards the south (observed from the position of oldest magnetic sea floor spreading anomalies on either side of the ridge), as does the bathymetry of ridges, reflecting a southward plunge of the JMMC.

There are also systematic changes in structural style from the main ridge to the SRC (Figures 4.14 – 4.19). This structural diversity across (E-W) and along (N-S) the JMMC is reflected in the tectonic evolution of the NE Atlantic and potentially represents the conjugate structural style of the Mid-Norway and East Greenland margins, respectively (Peron-Pindivic et al., 2012a). As such, the eastern margin is interpreted as a volcanic rifted margin, whilst the western margin is mostly magma-poor (Skogseid & Eldholm, 1987).

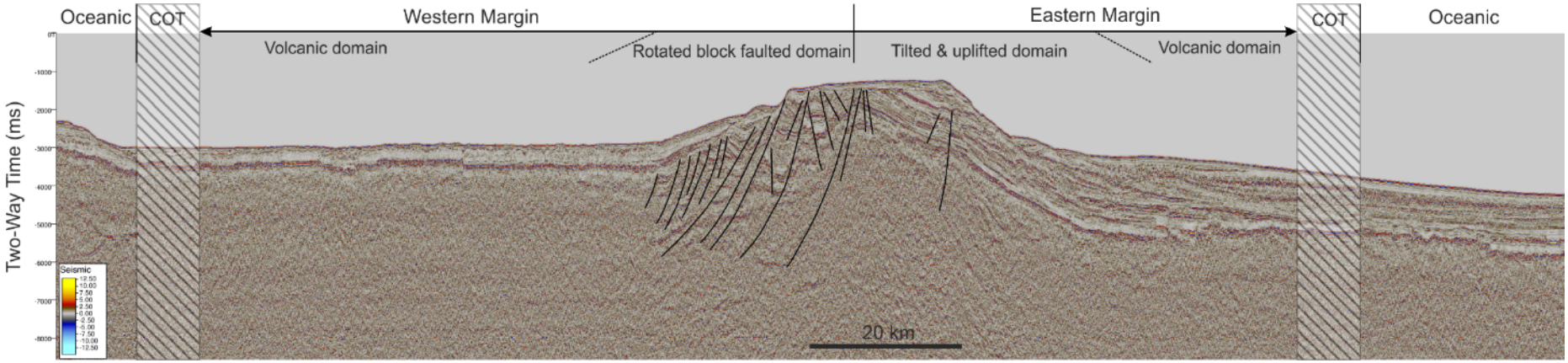

Figure 4.11: Structural style across the JMMC showing clear differences in the eastern and western margins.

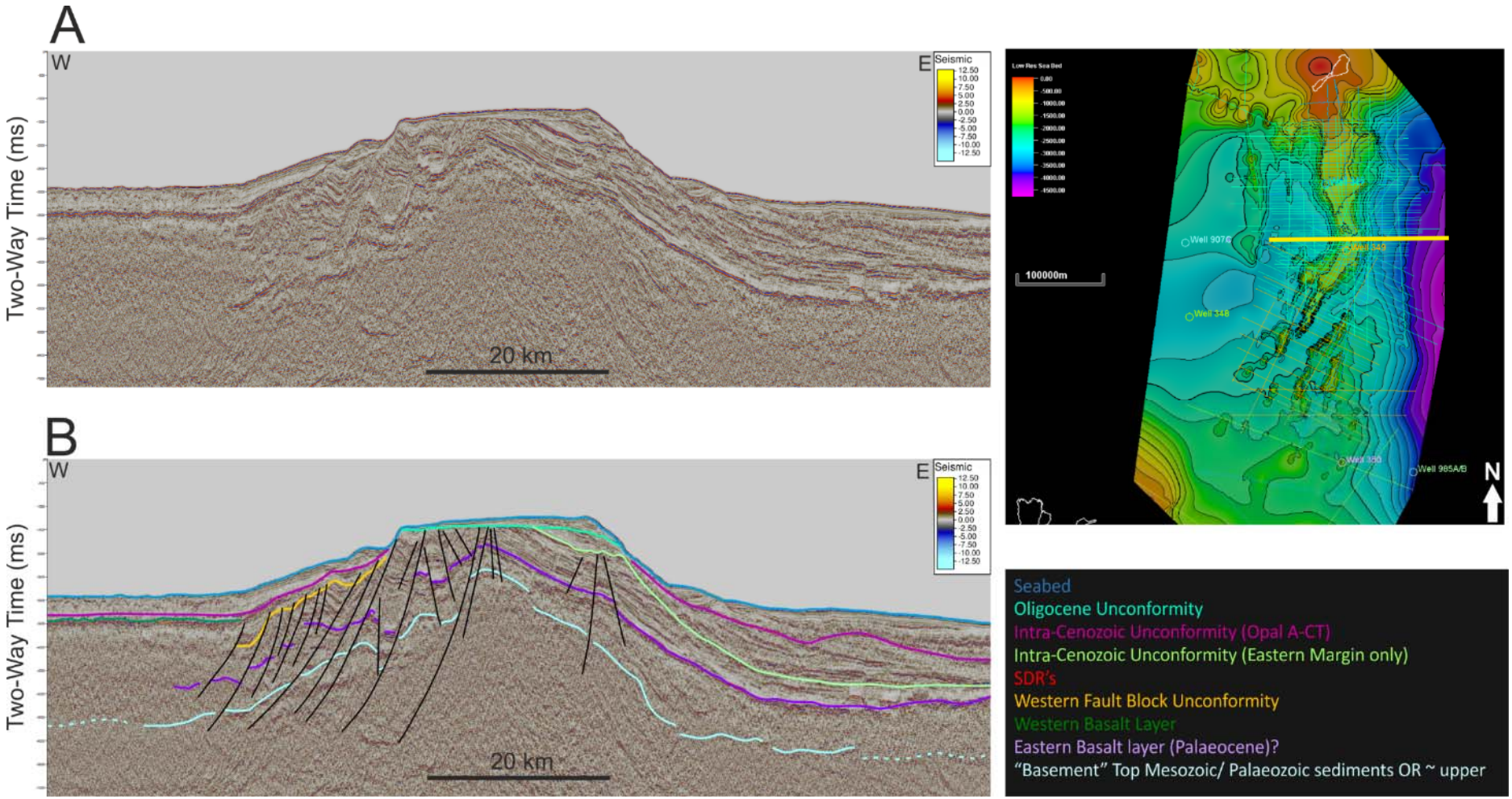

Figure 4.12: Mapped horizons across the JMMC

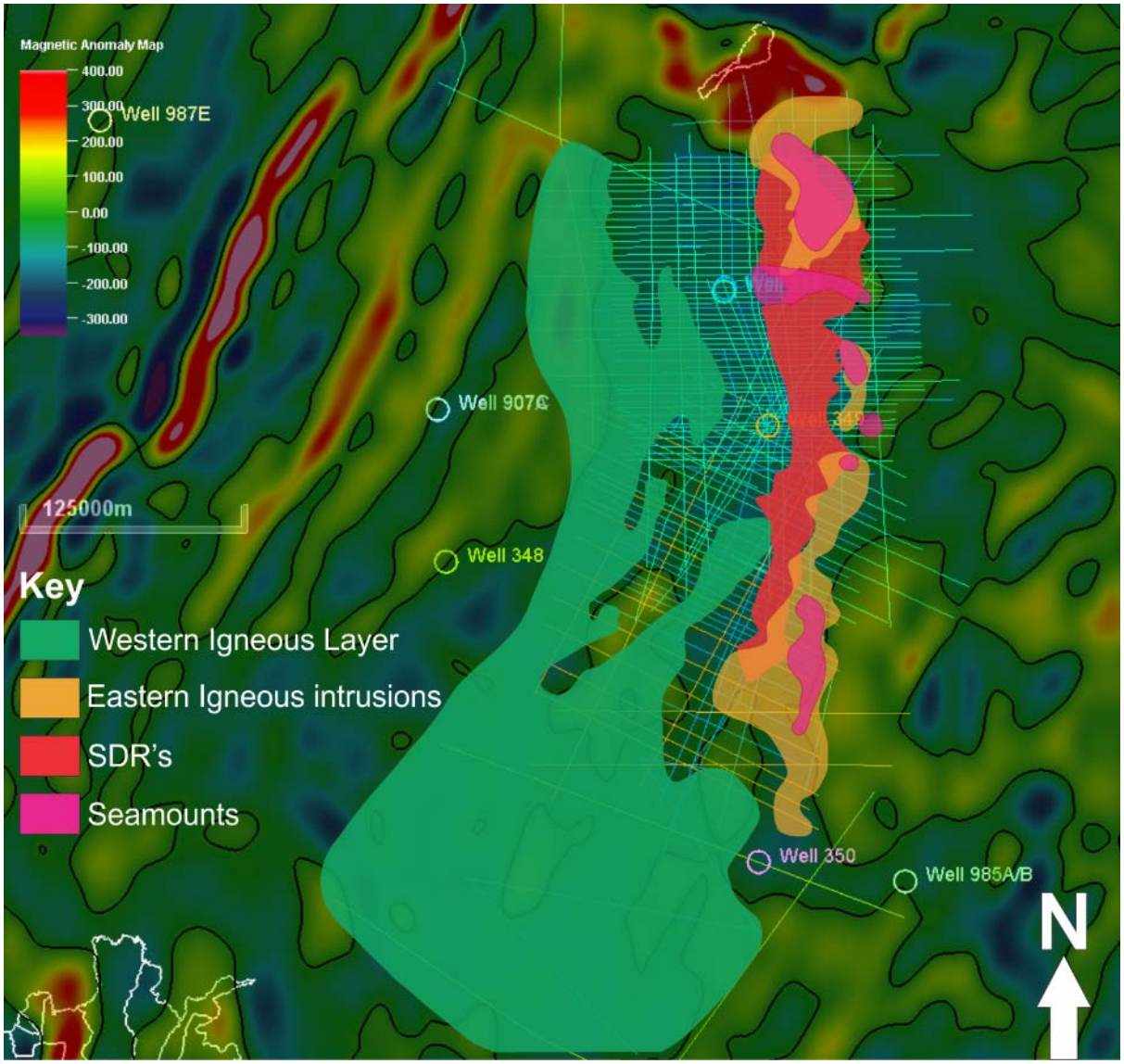

Figure 4.13: Various igneous provinces mapped across the JMMC eastern and western margins.

4.5.1.1 The Eastern Margin

The eastern margin is characterised by strata uniformally dipping/tilted towards the Norway Basin to the East, along with extensive volcanic extrusive and intrusive units with a distinct lack of fault structures associated with the first rift phase (Figure 4.11 & 4.12). The extrusive volcanics are characterised by a bright "to basalt" reflector which overlie pre-opening strata. In places, reflectors below the top basalt horizon show a divergent pattern of seaward-dipping reflectors (SDR's) characteristic of volcanic sequences (Figure 4.11 & 4.12), which thicken towards oceanic crust in the Norway Basin (Gunnarsson et al., 1989; Planke & Alvestad, 1999; Planke et al., 2000). Talwani et al., (1983) provide a detailed description of the volcanic stratigraphy and structure along the JMMC eastern margin.

However, these SDR features are not always well developed in every seismic line across the eastern margin. Lateral variability in reflectivity of the "top basalt" horizon together with numerous intrusions into the overlying sedimentary units make identification of the foot of the

SDR sequence ambiguous (Figure 4.12). Consequently, in places the oceanward thickening wedge of reflectors appear similar to syn-rift sedimentary packages potentially bound to the east by an eastward dipping fault (although again this is obscured by shallower intrusives). Peron-Pindivic et al., (2012a) also acknowledge that the shallow, post-break up intrusions mask identification of the location of the COB and termination of the SDR's and obscure the nature of the underlying basement within the transitional crustal domain. The sill complexes intruded above the main "top basalt" break up unconformity were likely intruded during the Eocene to Early Oligocene associated with tectonic reactivation and the 2nd rifting phase in the Early Oligocene (Figure 4.12).

Peron-Pindivic et al., (2012a) identify enigmatic volcanic edifices on the NE flank of the JMMC, and as such, the true nature and origin of these features are uncertain. However, observations from this research identify that these features align with some of the earliest seafloor spreading anomalies 24A and 24B from the magnetic anomaly data (Figure 4.2), and also lie along strike of potential fracture zones within the Norway Basin which may extend into and offset the northernmost part of the JMMC (Figure 4.1, 4.2 & 4.13) (also see figures 5 and 9 from Blischke et al., 2017). Gunnarsson et al., (1989) interpret this elongate uplifted dome feature as a transverse ridge along trend of a fracture zone, formed as a result of compressional tectonism related to plate reorganisation. However, Gaina et al., (2017) confirm the interpretations by Peron-Pindivic et al. (2012a) and Blischke et al., (2017) that these features represent seamounts associated with continental break-up volcanism. Emplacement of these igneous seamounts likely occurred during and/or after SDR formation. Their location close to fracture zones also suggests that their formation was closely linked to changes in spreading rate and direction along the Ægir Ridge and plate reorganisations between chron 21 to 13 time (47 – 33Ma) (Gaina et al., 2017; Blishcke et al., 2017).

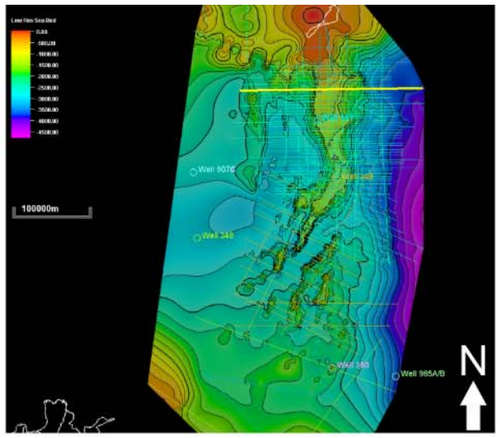

Seabed
Oligocene Unconformity
Intra-Cenozoic Unconformity (Opal A-CT)
Intra-Cenozoic Unconformity (Eastern Margin only)
SDR's
Western Fault Block Unconformity
Western Basalt Layer
Eastern Basalt layer (Palaeocene)?
"Basement" Top Mesozoic/ Palaeozoic sediments OR ~ upper

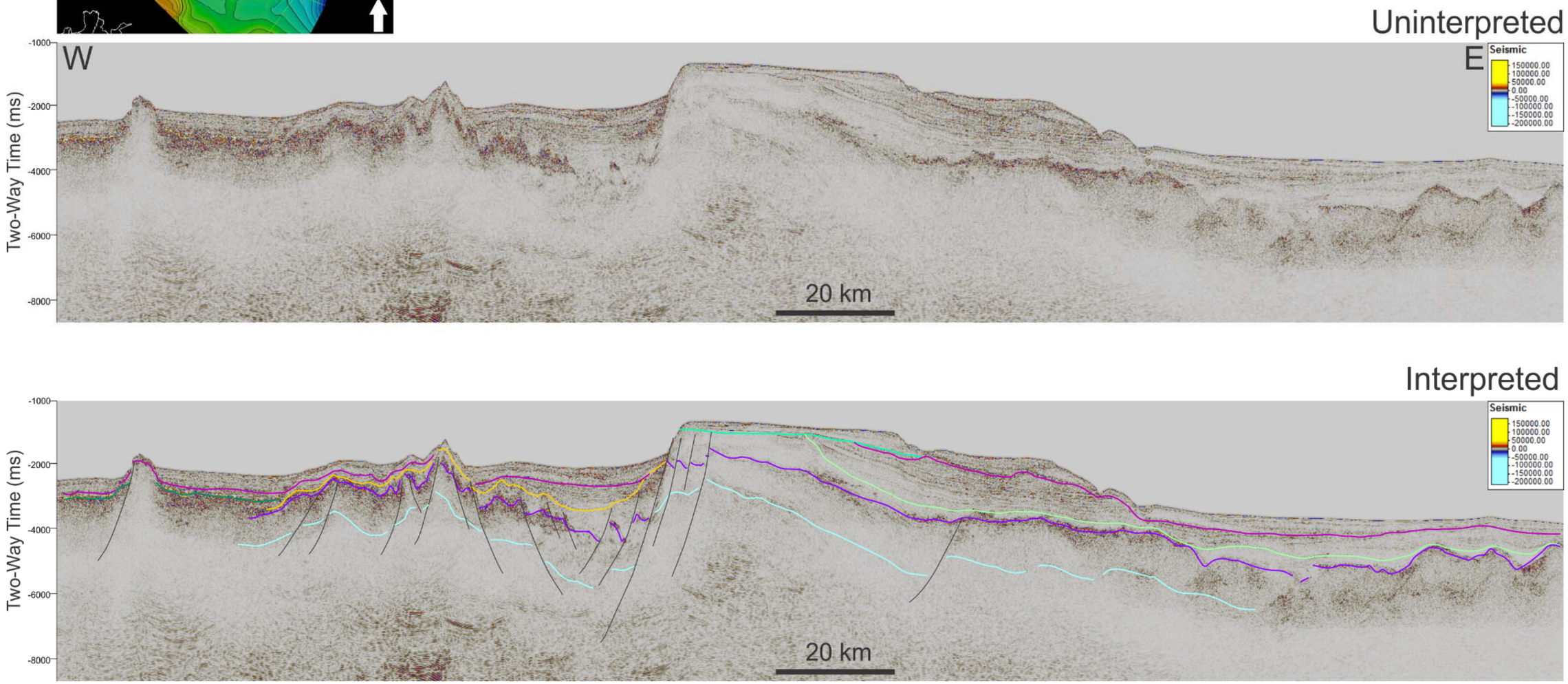

Figure 4.14: Regional cross line from northern part of JMMC (seismic line NPD_1202_120007).

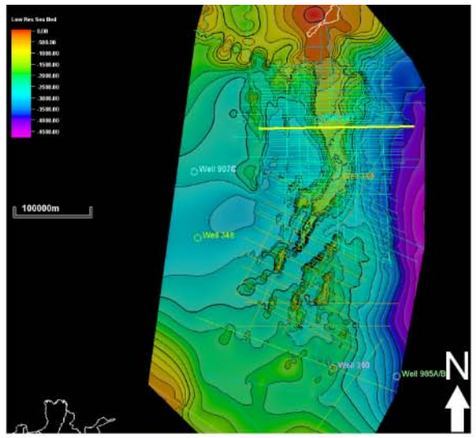

Seabed
Oligocene Unconformity
Intra-Cenozoic Unconformity (Opal A-CT)
Intra-Cenozoic Unconformity (Eastern Margin only)
SDR's
Western Fault Block Unconformity
Western Basalt Layer
Eastern Basalt layer (Palaeocene)?
"Basement" Top Mesozoic/ Palaeozoic sediments OR ~ upper

Uninterpreted

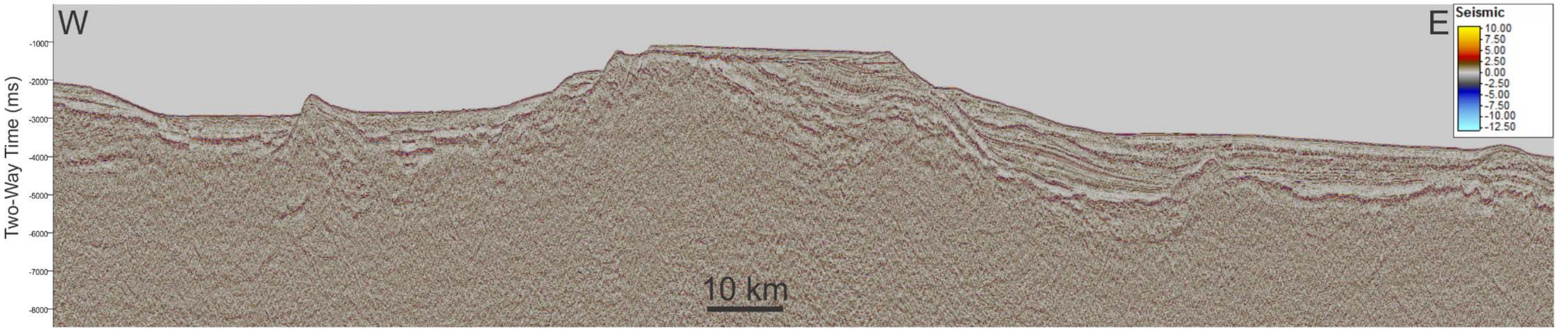

Interpreted

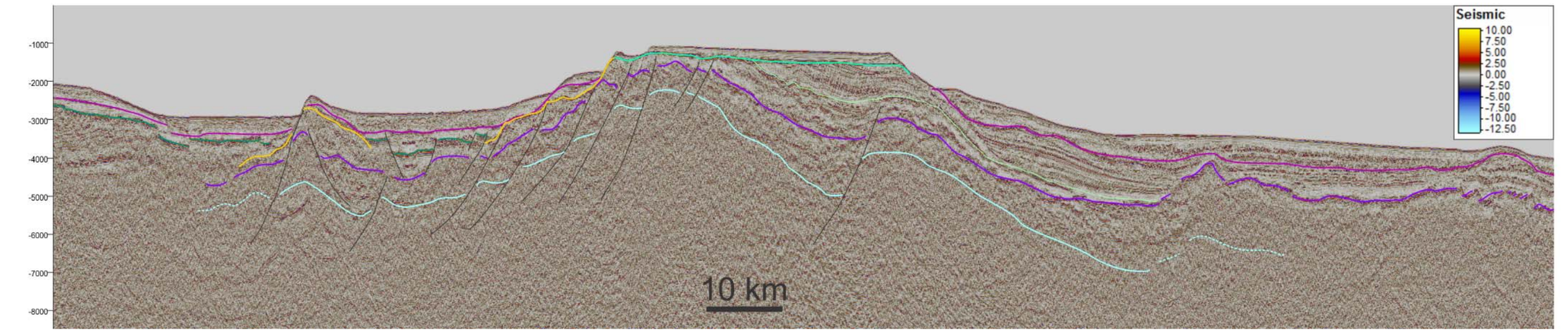

Figure 4.15: Regional cross line from the northern part of the JMMC (seismic line JM-85-08).

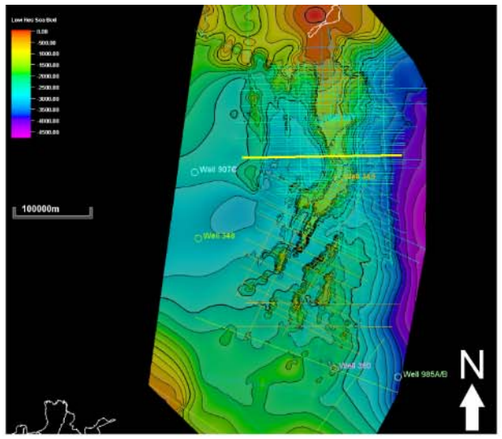

Seabed
Oligocene Unconformity
Intra-Cenozoic Unconformity (Opal A-CT)
Intra-Cenozoic Unconformity (Eastern Margin only)
SDR's
Western Fault Block Unconformity
Western Basalt Layer
Eastern Basalt layer (Palaeocene)?
"Basement" Top Mesozoic/ Palaeozoic sediments OR ~ upper

Uninterpreted

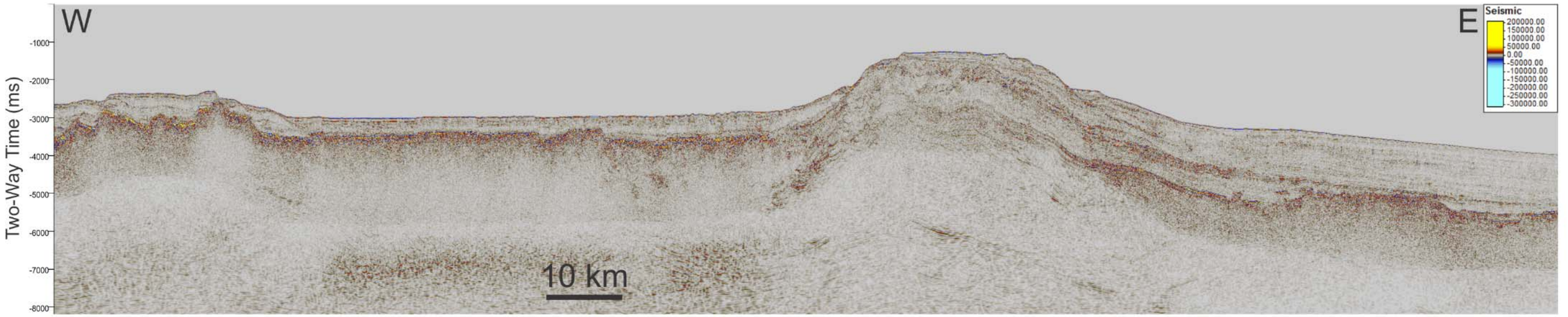

Interpreted

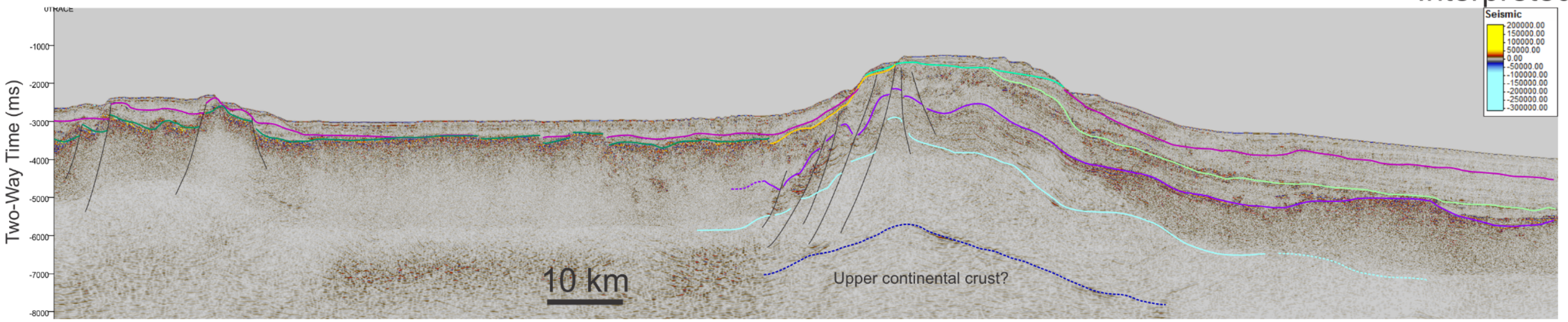

Figure 4.16: Regional cross line from the middle part of the main JMR (seismic line NPD_1202_120025)

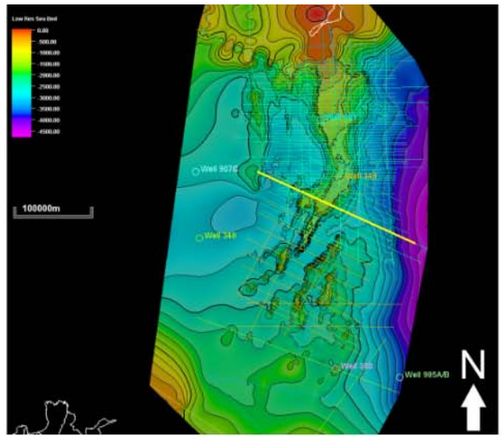

Seabed
Oligocene Unconformity
Intra-Cenozoic Unconformity (Opal A-CT)
Intra-Cenozoic Unconformity (Eastern Margin only)
SDR's
Western Fault Block Unconformity
Western Basalt Layer
Eastern Basalt layer (Palaeocene)?
"Basement" Top Mesozoic/ Palaeozoic sediments OR ~ upper

Uninterpreted

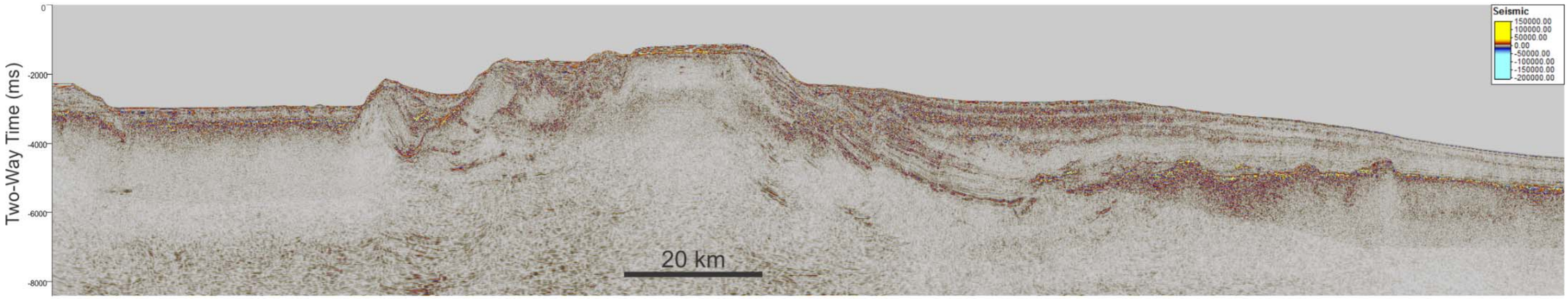

Interpreted

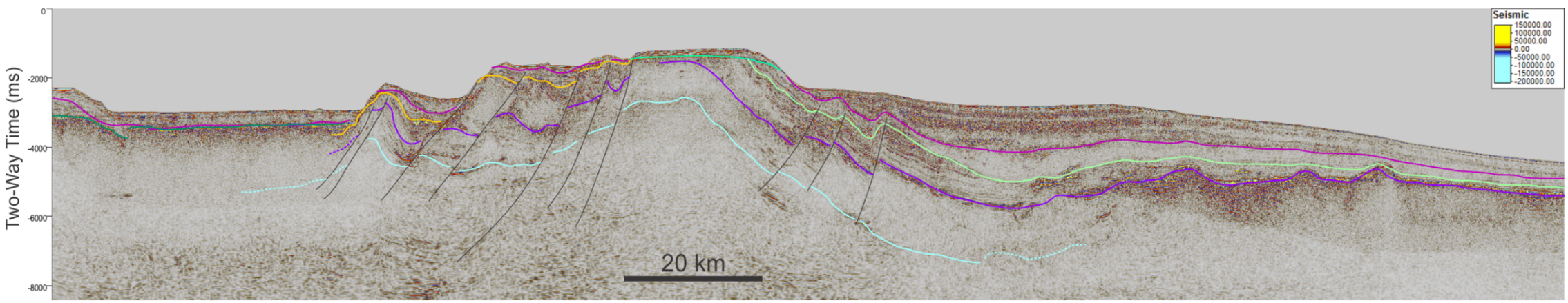

Figure 4.17: Regional cross line from the southern part of the JMR (seismic line JM_11_110003)

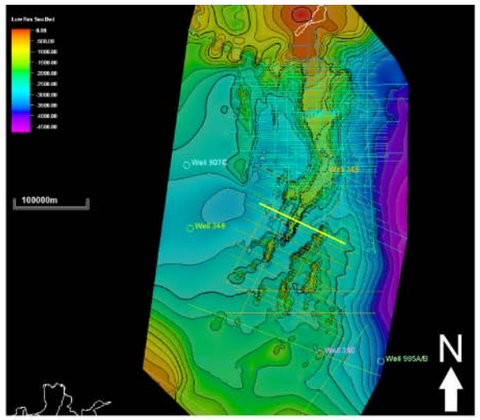

Seabed
Oligocene Unconformity
Intra-Cenozoic Unconformity (Opal A-CT)
Intra-Cenozoic Unconformity (Eastern Margin only)
SDR's
Western Fault Block Unconformity
Western Basalt Layer
Eastern Basalt layer (Palaeocene)?
"Basement" Top Mesozoic/ Palaeozoic sediments OR ~ upper

Uninterpreted

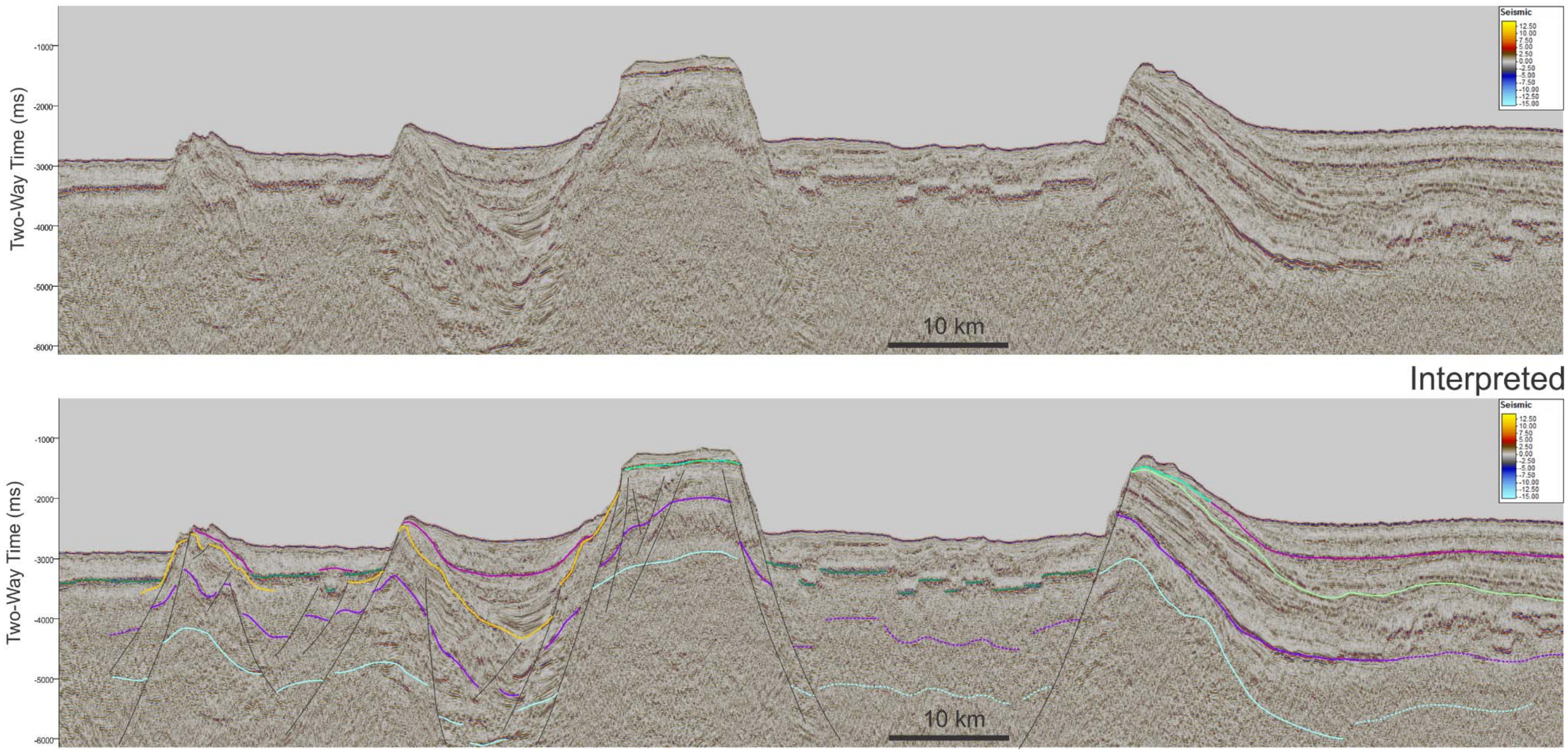

Figure 4.18: Regional cross line from the northern part of the SRC (seismic line JM-85-17).

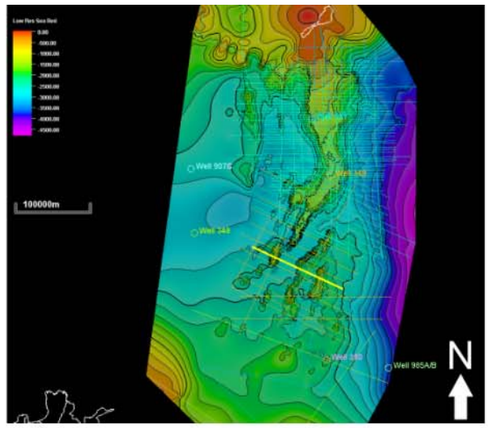

Seabed
Oligocene Unconformity
Intra-Cenozoic Unconformity (Opal A-CT)
Intra-Cenozoic Unconformity (Eastern Margin only)
SDR's
Western Fault Block Unconformity
Western Basalt Layer
Eastern Basalt layer (Palaeocene)?
"Basement" Top Mesozoic/ Palaeozoic sediments OR ~ upper

Uninterpreted

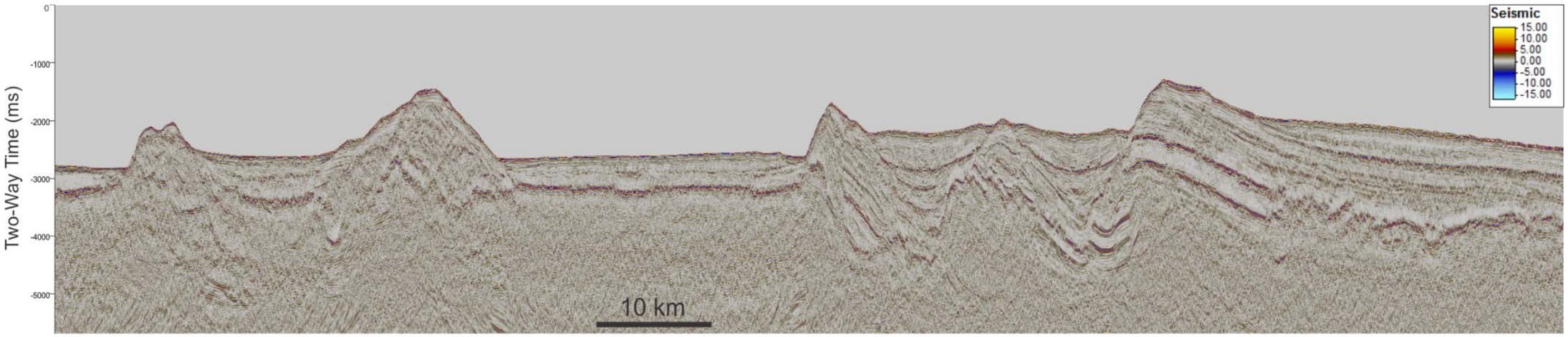

Interpreted

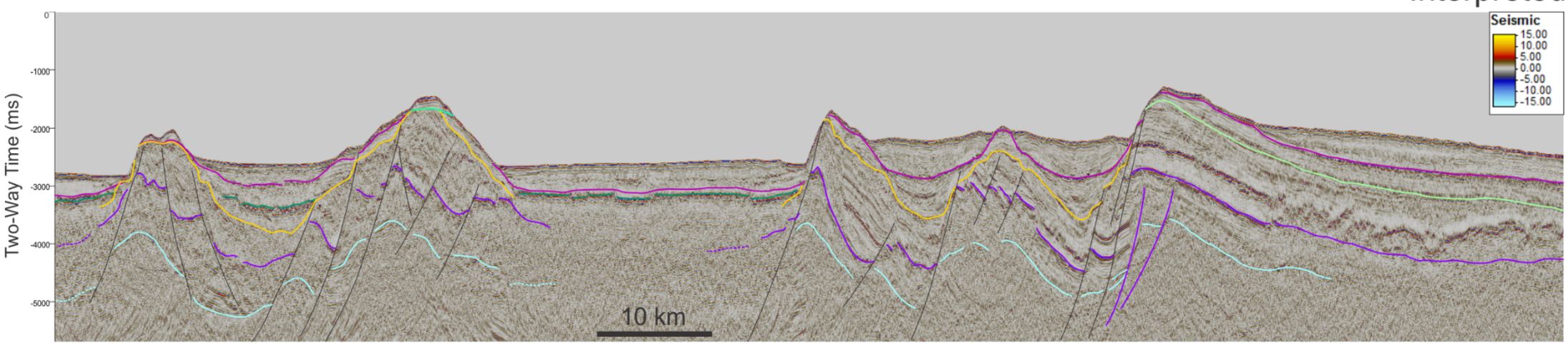

Figure 4.19: Regional cross line from the southern part of the SRC (seismic line JM-85-20).

4.5.1.2 The Western Margin

By comparison, the western flank of the JMR is dominated by a series of deep seated normal-listric faults, which throw and step down towards the west, forming smaller en-echelon extensional terraces (Figure 4.11). This margin resembles a typical block faulted passive margin. The region is bound by a major listric fault zone along strike of the orientation of the JMR, which separates the JMR from the eastward tilted fault blocks to the west.

Seismically opaque reflectors in the JMB mask the transition from continental normal fault blocks to oceanic crust on the Icelandic Plateau (Figure 4.11, 4.14, 4.15, 4.16 & 4.18). They are interpreted as either sills or subaqueous lava flows (Gunnarsson et al., 1989; Peron-Pindivic et al., 2012a). A timing for their emplacement of Late Oligocene to Early Miocene can be inferred indirectly from the lack of tilting or deformation of the volcanic layer and the fact they are observed at approximately the same stratigraphic level across the study area (Peron-Pindivic et al., 2012a). It is therefore likely that volcanic intrusions on the western margin are associated with magmatism at the time of break-up of the JMMC with East Greenland, just prior to seafloor spreading along the Kolbeinsey Ridge at Chron 6 (Peron-Pindivic et al., 2012a).

It is assumed that normal block faulted rift basins may continue to down-step and be present further west beneath the opaque reflector forming a series of smaller rift basins across the JMB (Gunnarsson et al., 1989). However, there is no direct evidence for this from seismic data alone because of the efficient blanketing effect of the shallower basalt layer in these areas. Due to the lack of magnetic anomalies within the JMB, the implication is that the JMB could be underlain by hyperextended continental crust. There are smaller isolated fault blocks that appear stranded within in the JMB, which are surrounded by the shallow western volcanic intrusive reflector and further support the hypothesis that smaller intervening rift basins and tilted fault blocks are present at depth (but cannot currently be imaged) across the JMB (Figures 4.15 & 4.18).

Oceanic crust on the Iceland Plateau, is identified immediately west of the JMB by an east-facing scarp in the NW part of the JMMC where the seismic line coverage crosses the COT in Figure 4.11, 4.15, 4.16 & 4.17). The seismic character of the oceanic crust is not dissimilar to the igneous intrusive/flood basalt to the east covering much of the JMB. It is composed of a suite of layered sub-basement reflectors beneath a smooth, bright reflector, causing an opacity or dimming of overlying reflectors and masking any structural or stratigraphic features below.

Tectonic overprinting

Tectonic overprinting by the second rift phase during the Oligocene can be observed along the entire JMMC in the form of uplift and erosion of the main ridges and reverse faulting (Figure 4.15). Regional uplift, erosion and major peneplanation of the main ridges forming the distinct Oligocene unconformity on the main JMR was likely associated with plate reconfiguration in the Norwegian-Greenland Sea at Chron 13 time (Gaina et al., 2009; Peron-Pindivic et al., 2012a). Reverse faulting on the eastern margin was likely formed in response to reactivation of normal faults during ridge-push forces along the Ægir ridge and later Cenozoic plate reorganisation through a series of ridge jumps and changes in sea-floor spreading direction (Gaina et al., 2009; Gernigon et al., 2012). East-ward rotation of normal fault blocks and syn-rift packages along the western margin and the SRC can also be attributed to overprinting of later phases of tectonic deformation in relation to the separation of JMMC from East Greenland (Figures 4.18 & 4.19). The amount of structural overlap and complexity between the two margins increases southwards towards the SRC.

4.5.2 Structural Mapping

Figure 4.20 shows the fault structure map across the JMMC. Only the major basin bounding faults were mapped using the Palaeocene-Eocene horizon to help identify the faults with significant displacement/ offsets and which were observed on several adjacent seismic lines. Normal and listric faults dominate over the JMR and are most common on the western flanks of the JMMC, which have formed to accommodate the complex extensional phases of North Atlantic rifting during the Cenozoic. The majority of fault planes (listic and normal) dip to the west, with few antithetic faults forming smaller graben structures in the hanging wall (Figures 4.11 to 4.19). Many of these faults propagate through much of the Mesozoic and Cenozoic sedimentary cover and commonly terminate at the Oligocene unconformity surface on the main JMR. There is an abrupt change in the orientation of normal faults coinciding with the prominent bend towards the SW of the main ridge at ~69.3°N (Figure 4.20). North of this point fault patterns trend in a N-S orientation; whereas south of this point, faults are oriented NE-SW.

The southern part of the main ridge widens and bifurcates into a series of smaller ridges of the SRC towards the SW (Figure 4.20). This area is structurally more complex and increasingly affected by magmatic extrusive and intrusive volcanics towards the south. The individual isolated ridges essentially form tilted fault blocks bounded by large scale steep planar - listric faults, creating smaller intervening hanging wall basins (Figures 4.18 & 4.19). Gunnarsson et al., (1989) suggests that the uniform width, rotation and depth to the top of the fault blocks reflects the presence of a near-horizontal ductile shear zone or decollement surfaces at depth over the SRC region. However, in places, the Miocene age volcanic intrusive units inter-finger these isolated continental ridges, acting to mask the underlying structure and stratigraphy, making confident interpretations in this domain challenging. Nevertheless, integration with multi-beam bathymetry and gravity data enable the continental crustal ridges and small scale basins to be inferred.

Some of these normal faults have been reactivated during Cenozoic plate reorganisations. Reverse faults are observed along on the south-eastern margin of the main ridge and along some of the eastern ridges of the SRC (Figure 4.20). The 65 km long NNE trending reverse fault with a near vertical fault plane is the clearest example of reverse structuration (Figure 4.20 C). It is likely that these compressional features formed in response to ridge-push forces during asymmetrical sea floor spreading along the Ægir Ridge from Chron 21 and simultaneous extension in the SRC to accommodate for the associated change in direction and spreading rate. Additionally, it is suggested that extension in the SRC was due to multiple northward ridge propagators of the Reykjanes Ridge and westward migration of rift jumps as spreading migrated from the Ægir to Kolbeinsey Ridge (Scott et al., 2005; Gaina et al., 2009; Gernigon et al., 2012). This extension and widening of the SRC may also account for the compressional reactivation of some of the south-easternmost faults of the isolated ridges (Figure 4.20 C).

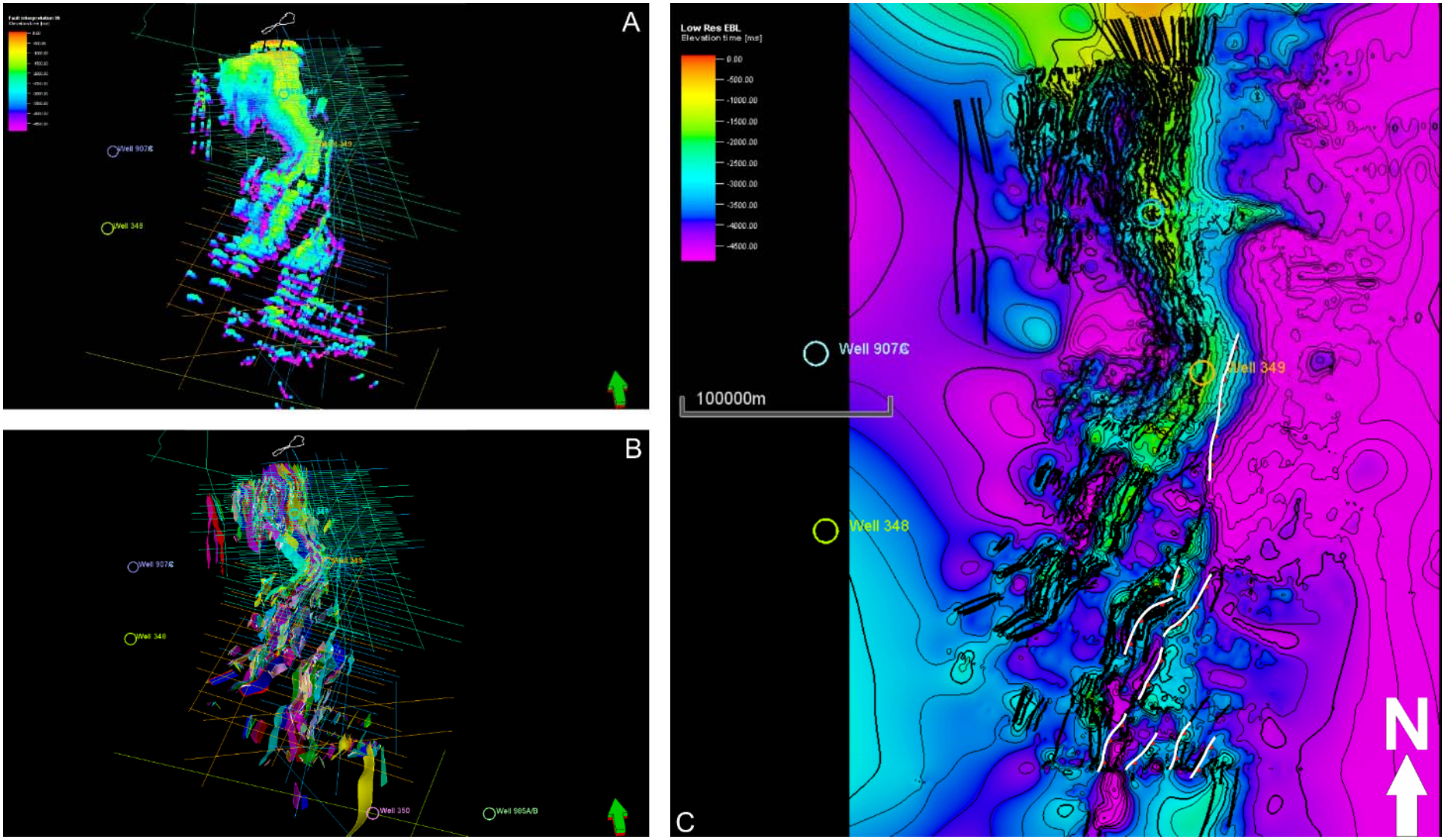

Figure 4.20: Fault structural mapping across of the JMMC. Fault interpretations within the seismic surveys (A) are converted to fault polygons (B) to produce a fault structure map onto the "top basalt surface" (C) (Note that black lines represent normal faults whilst white lines represent reverse fault structure).

4.5.3 Horizon Mapping

The rationale for horizon mapping across the JMMC was to identify surfaces of tectonostratigraphic significance. DSDP well-seismic ties & ROV samples (Figures 4.4 – 4.6, 4.9 & 4.10) provide key constrains of the shallowest stratigraphy at several calibration points. However, due to the shallow penetration of these wells, they were of limited use. Horizon interpretation was made more challenging due to numerous volcanic intrusions masking the underlying stratigraphy. This was particularly problematic in the Jan Mayen Trough and JMB (Figure 4.11 & 4.12). Consequently, confident mapping and correlation of surfaces from east to west across the main ridge and beneath these volcanically intruded domains remains tentative. Uncertainties also remain for stratigraphic correlation across highly faulted domains and between isolated ridges of the SRC with no well calibrations into the deeper stratigraphic succession. Erosional truncation also creates difficulties for confident mapping stratigraphic boundaries. Nevertheless, horizon interpretation based on identifying high level tectonostratigraphic packages, bound by unconformity surfaces (some of which are similar to Gunnarsson et al., 1989 and Peron-Pindivic et al., 2012a) was carried out using seismic facies and reflector termination relationships to correlate across major fault systems of the post-basalt stratigraphy (Figure 4.21). Additionally seismic refraction studies have been utilised to identify the crustal structure of the JMMC and aid interpretations of the deeper stratigraphy and basement (Figure 4.22 – 4.24). Gunnarsson et al., (1989) document a detailed analysis of the seismic stratigraphy present on the JMMC, whilst an even more detailed interpretation of the Cenozoic sedimentary succession has been undertaken by Blischke et al., (2018).

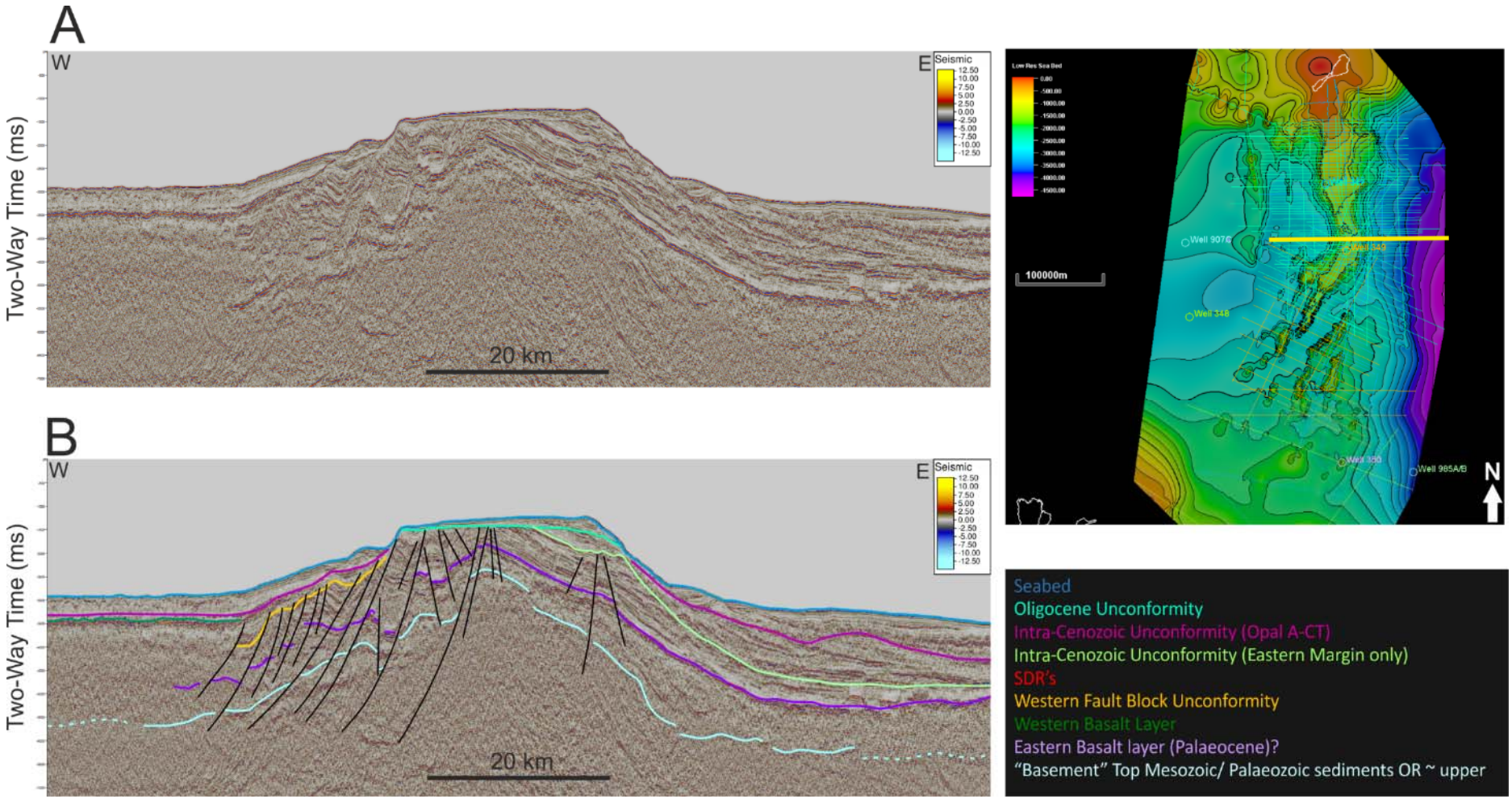

Figure 4.21: Surfaces mapped across the JMMC.

4.5.3.1 Seismic Refraction Studies

Refraction studies across parts of the JMMC were undertaken in 1995 and 2000, and compared to seismic reflection data that lie along the same location to better constrain the crustal structure and configuration of the microcontinent and overlying sedimentary packages based on their respective velocity ranges (Kodaira et al., 1995; Mjelde et al., 2007/2008/2009; Breivik et al., 2012/ 2006; Funck et al., 2017; Peron-Pendivic et al., 2013). The velocities observed from these studies were compared to the conjugate margins where the Palaeozoic-Mesozoic stratigraphy is better constrained.

Figures 4.22 to 4.24 show the correlations and interpretations that can be made between the corresponding seismic refraction and reflection data. Identification of the "basement" top Mesozoic/Palaeozoic horizon can be inferred and used to extend interpretation away from these calibration seismic lines. Furthermore the overlying Cenozoic package in line L8-00 (Breivik et al., 2012) can be subdivided based on the differing velocity structure and offer a coarse framework for correlation from the eastern margin across the main JMR and into the highly faulted western margin (Figure 4.24).

Table 3 documents the velocity ranges from the literature for each seismic package, which were used for basic time-depth conversion of interpreted horizons across the JMMC (see below).

Seismic Packages (P-wave model layers)	OBS model (Kodaira et al., 1998)	OBS model (Breivik et al., 2012)
	Vp (km/s^{-1})	Vp (km/s^{-1})
Cenozoic sediments	2.0-3.5	1.75 - 3.0
Basalt (SDR's & intrusions)	4.0 - 5.0	3.35 - 3.75
Possible Mesozoic	3.9 - 4.7	5.25 - 5.75
Possible Palaeozoic	5.0 - 5.3	5.25 - 5.76
Continental upper crust	5.5 - 6.7	6.0 - 6.60
Continental lower crust	6.7 - 6.8	6.75 - 7.25
Moho		7.5 - 8.0
Oceanic upper crust		3.75 - 5.10
Oceanic middle crust		6.25 - 6.50
Oceanic lower crust		6.75 - 7.0

Table 3: Range of velocities for the different seismic packages modelled from OBS refraction studies (Kodaira et al., 1998 & Breivik et al., 2012).

Velocity layers ranging between 1.70 – 3.5 km/s^{-1} are interpreted as post-break up Cenozoic section (Blischke et al., 2017). A distinct velocity domain of 4.6 – 4.8 km/s^{-1} on the eastern margin corroborates the "SDR" hypothesis here and the high reflectivity volcanic intrusive layers within the post break-up sedimentary section in the JMB have velocity ranges of 4.0 – 5.0 km/s^{-1}. However, the thickness of the volcanic "SDR" package remains untested. The pre-break up sedimentary succession ranges in velocity values of 3.9 – 4.7 km/s^{-1} and 5.0 – 5.7 km/s^{-1} for possible Mesozoic and Palaeozoic intervals, respectively. These velocity ranges correspond well to the Mesozoic – Palaeozoic sections on the conjugate Norwegian shelf (Mjelde et al., 2008/ 2009).

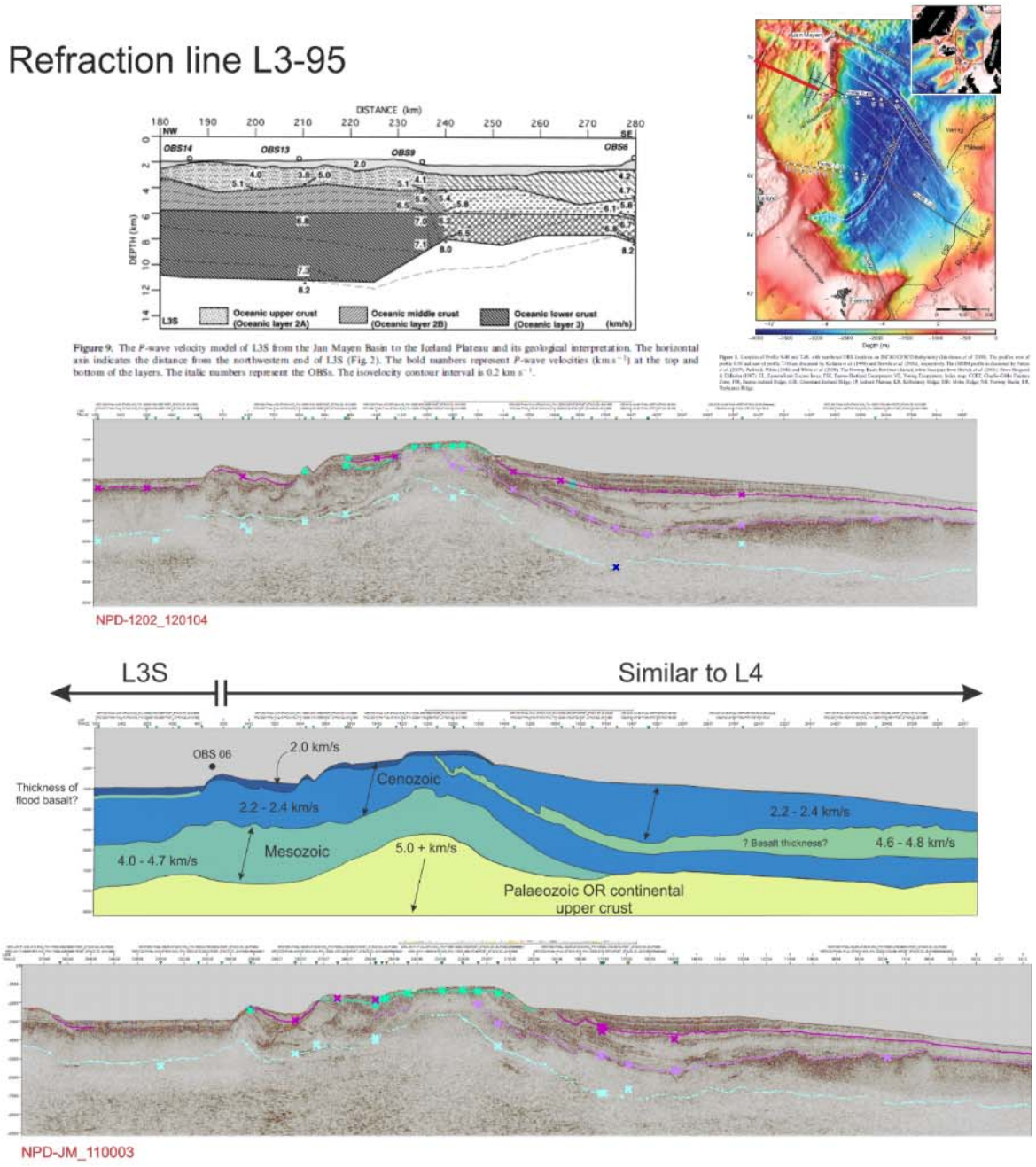

Figure 4.22: Comparison of seismic refraction line L3-95 with seismic reflection lines to help guide horizon interpretation of surfaces below the "top basalt" horizon (from Kodaira et al., 1998).

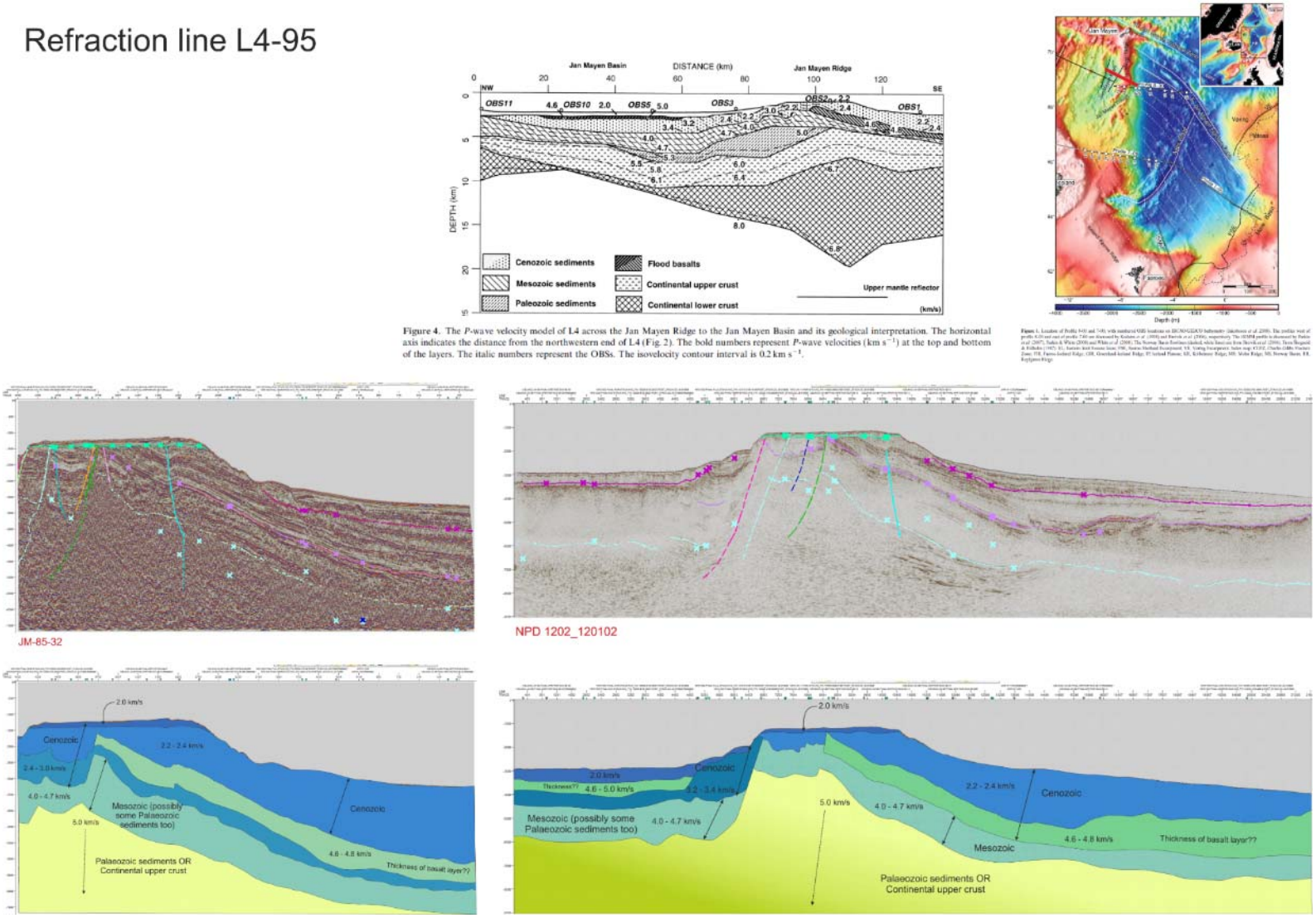

Figure 4. The *P*-wave velocity model of L4 across the Jan Mayen Ridge to the Jan Mayen Basin and its geological interpretation. The horizontal axis indicates the distance from the northwestern end of L4 (Fig. 2). The bold numbers represent *P*-wave velocities (km s^{-1}) at the top and bottom of the layers. The italic numbers represent the OBSs. The isovelocity contour interval is 0.2 km s^{-1}.

Figure 4.23: Comparison of seismic refraction line L4-95 with seismic reflection lines to help guide horizon interpretation of surfaces below the "top basalt" horizon (from Kodaira et al., 1998).

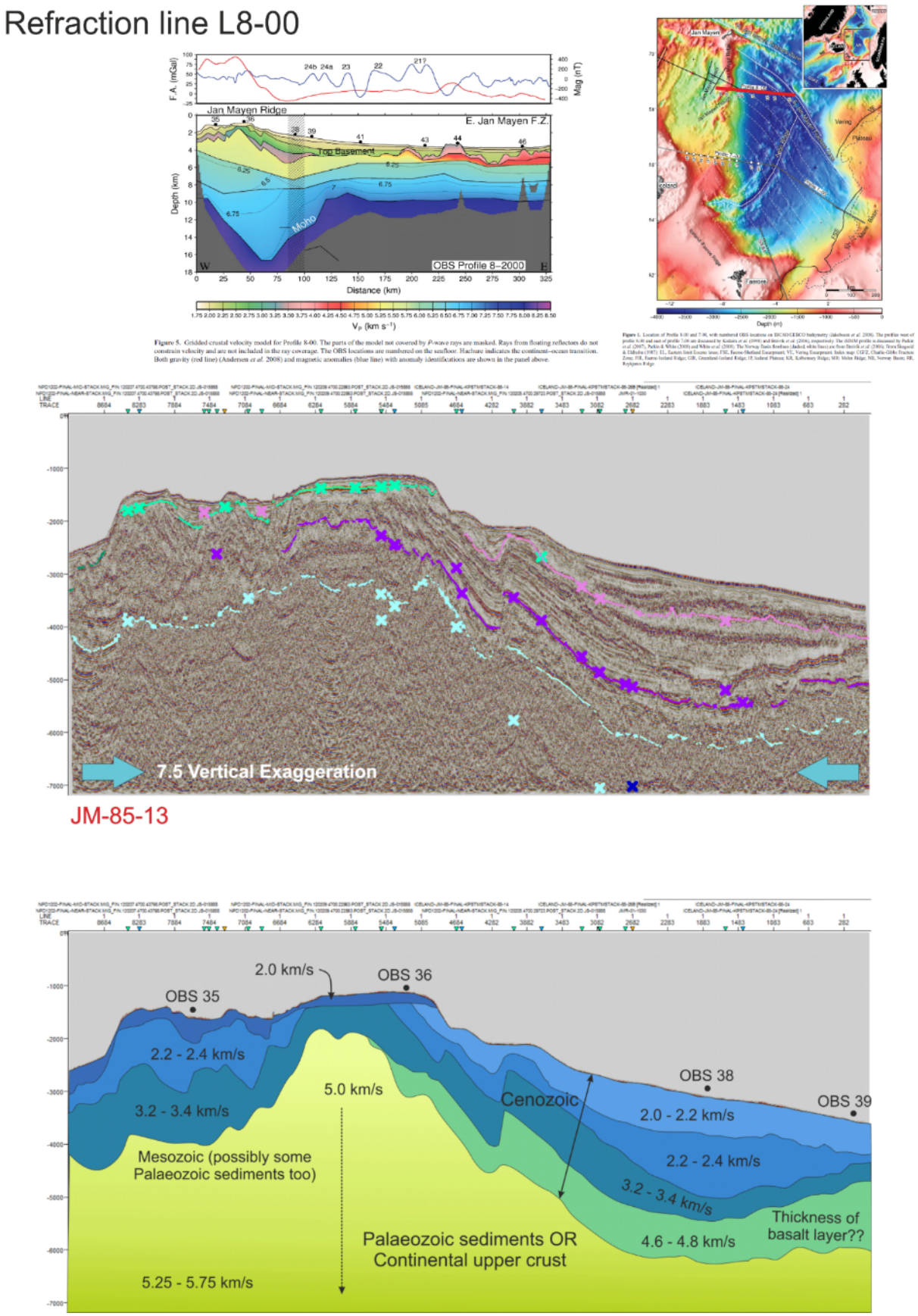

Figure 4.24: Comparison of seismic refraction line L8-00 with seismic reflection lines to help guide horizon interpretation of surfaces below the "top basalt" horizon (from Breivik et al., 2012).

4.5.3.2 TWT Surface Maps

Figures 4.14 to 4.19 Show regional seismic lines across the main JMR and SRC to show the variability in structural configuration (from east to west and north to south) and highlight the main surfaces and unconformities mapped across the JMMC. Figure 4.25 shows the horizon picks used in this research in relation to the major tectono-magmatic events affecting the evolution of the JMMC. The seismic facies of the sedimentary packages between the interpreted horizons are also shown in Figure 4.26.

HERIOT WATT UNIVERSITY

Jan Mayen Tectonostratigraphic horizons in relation to key North Atlantic tectonic events

Author: G. Heldreich
Date: March 2018

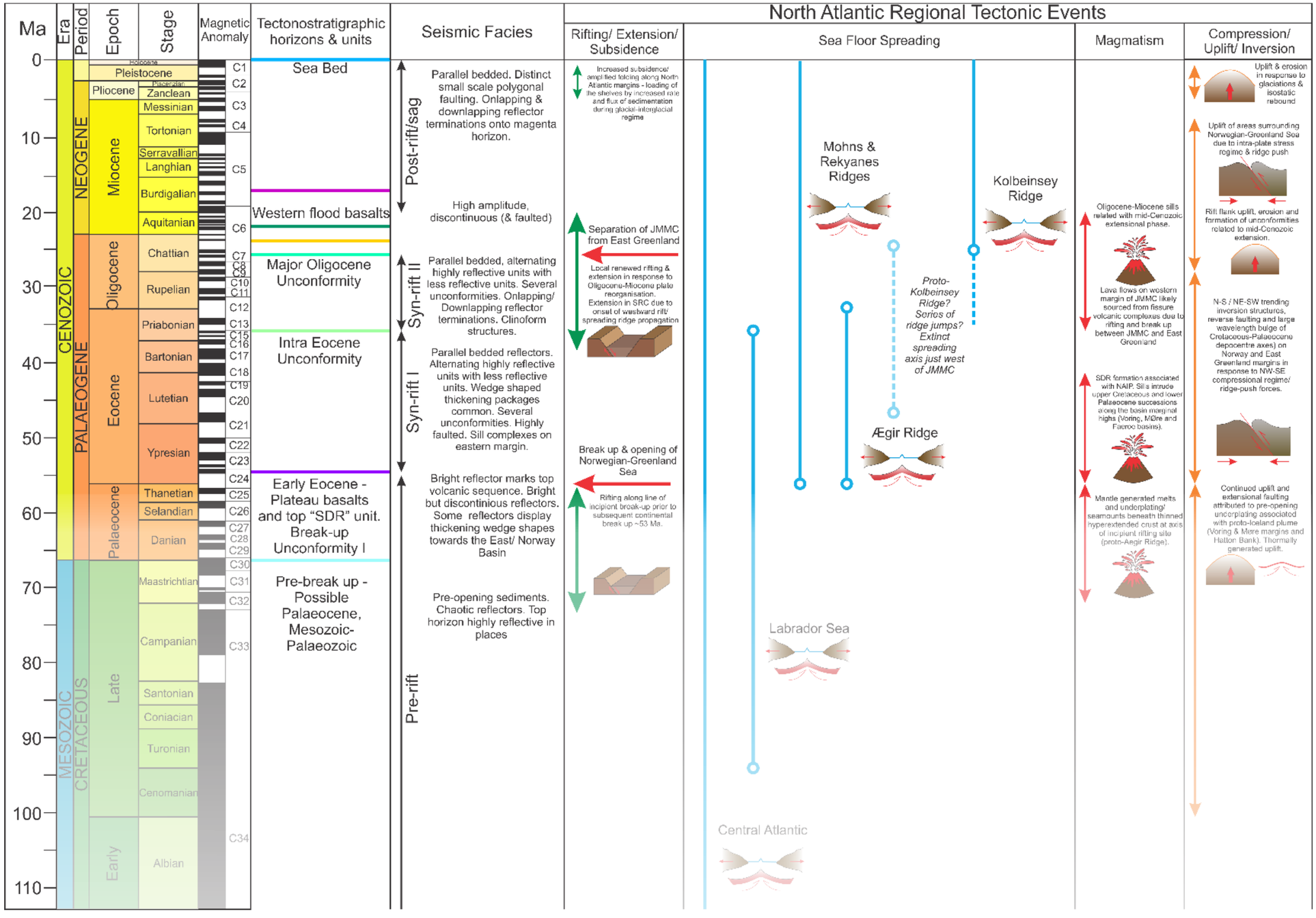

Figure 4.25: Tectonostratigraphic horizons and units interpreted from this research in relation to key North Atlantic tectonic events.

HERIOT WATT UNIVERSITY

Seismic character and facies of tectonostratigraphic horizons and units across the Jan Mayen Microcontinent

Author: G. Heldreich
Date: March 2018

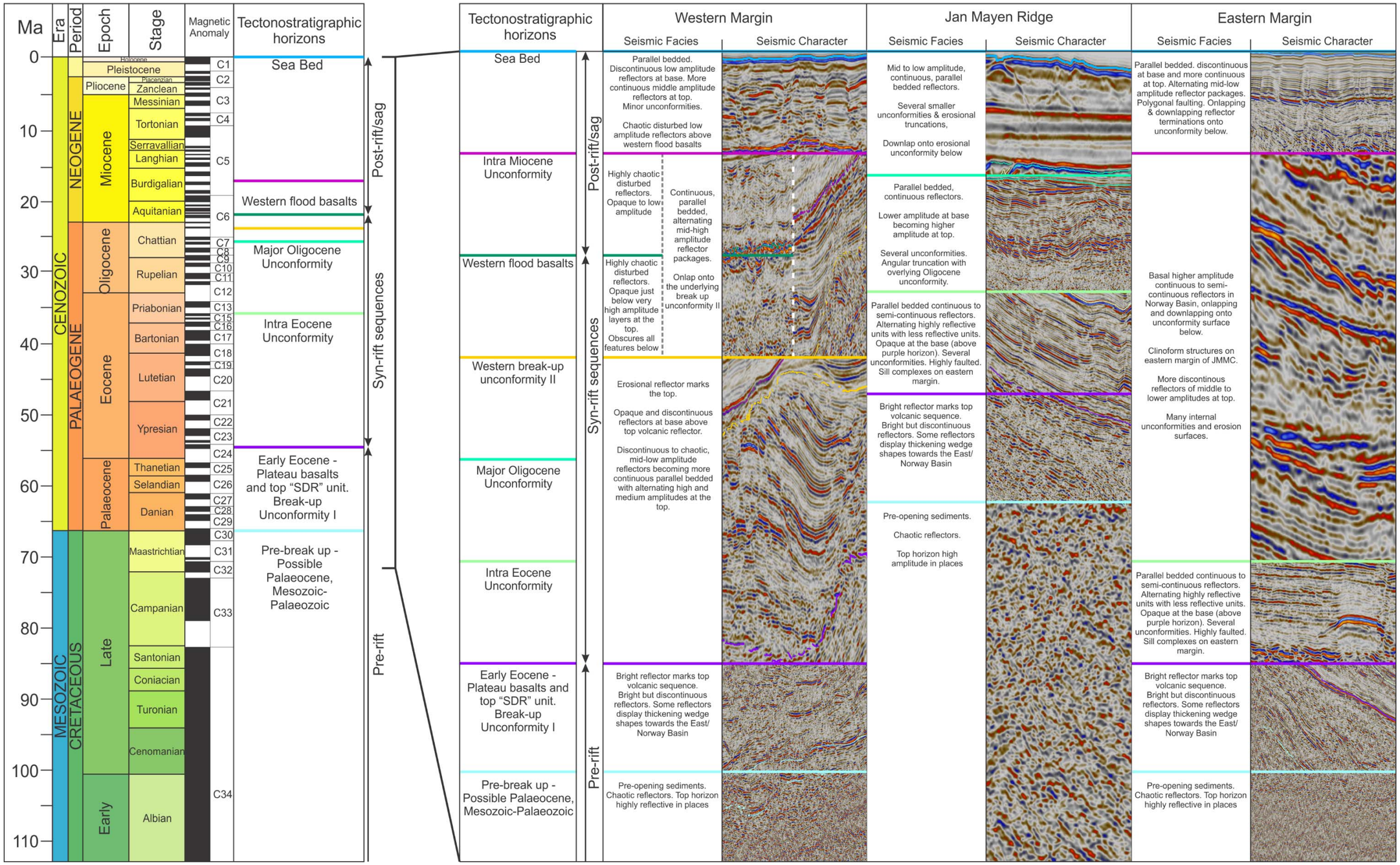

Figure 4.26: Seismic character of tectonostratigraphic horizons and seismic facies of the sedimentary packages they divide.

Pre-break up Section

On some seismic lines a strong bright negative reflector can be observed sporadically across the JMR at a depth range between 6 – 8 s TWT (Figure 4.16). It is possible that this reflector either represents a very shallow Moho due to hyperextension within the microcontinent or the boundary between the upper and lower continental crust. Peron-Pindivic et al., (2012a) infer the overall basement beneath the JMMC reaching a thickness of 12 – 18 km from 3-D gravity inversion modelling. However, Peron-Pindivic & Manatschal (2010) suggest microcontinents ae characterised by >15 km thick crust. Seismic refraction data (see above section) also infer a Moho depth range of 10 – 20 km across the Jan Mayen Ridge. Gunnarsson et al., (1989) identify this strong bright reflector, dipping eastwards from 5 – 6.5 s TWT on cross line JM-85-12 as representing the top of continental basement. Given that the area is likely to contain highly attenuated and heavily intruded crust, constraining the deeper structure and true basement with available data remains enigmatic. As such the occasional deep bright reflector may represent the boundary between upper and lower continental crust (pers. comms Lorcan Kennan).

The turquoise horizon is the deepest interpreted surface and is the most uncertain due to the presence of overlying volcanic sequences and consequent rapid attenuation of the seismic with depth. Where present, the horizon was interpreted as a bright negative reflector above chaotic, non-reflective seismic signal and likely represents the "near top Mesozoic" succession (Figure 4.26). Nevertheless, the horizon was interpreted as accurately as possible across the 2D seismic surveys and the resultant horizon map is shown in Figure 4.27.

The overlying sedimentary package consists of discontinuous to semi-discontinuous reflectors, but is a highly reflective seismic facies unit (Figure 4.26). Along parts of the eastern margin of the ridge, uniform parallel to diverging wedge-like, fairly continuous, high amplitude reflectors may represent SDR sequences as corroborated by high velocity units on seismic refraction data (Kodaira et al., 1998). Gunnarsson et al., (1986) present a detailed account of the seismic volcanic megasequence present on the eastern margin of the JMR. Where present, the better developed wedge shaped areas have been mapped out along the eastern margin as the red reflector (Figure 4.28). Internal reflectors of the wedge feature either pinch out beneath the overlying purple horizon or converge before becoming parallel in an up dip direction. Strike line JM-85-25 clearly shows an erosional unconformity surface depicted by a series of bright semi-continuous reflectors within the turquoise – purple horizon package (Figure 4.29). This likely corresponds to Reflector Brown of Gunnarsson et al., (1989), who interpret this surface as a base Cretaceous unconformity. They also identify an orange reflector marking the upper boundary of the "pre-rift megasequence" and basal boundary of the overlying volcanic break-up package (Gunnarsson et al., 1989); but this surface cannot be traced continuously from east to west across the JMMC and away from a few seismic lines on the SE flank of the JMR. As such, this surface is noted but has not been continuously mapped within the dataset.

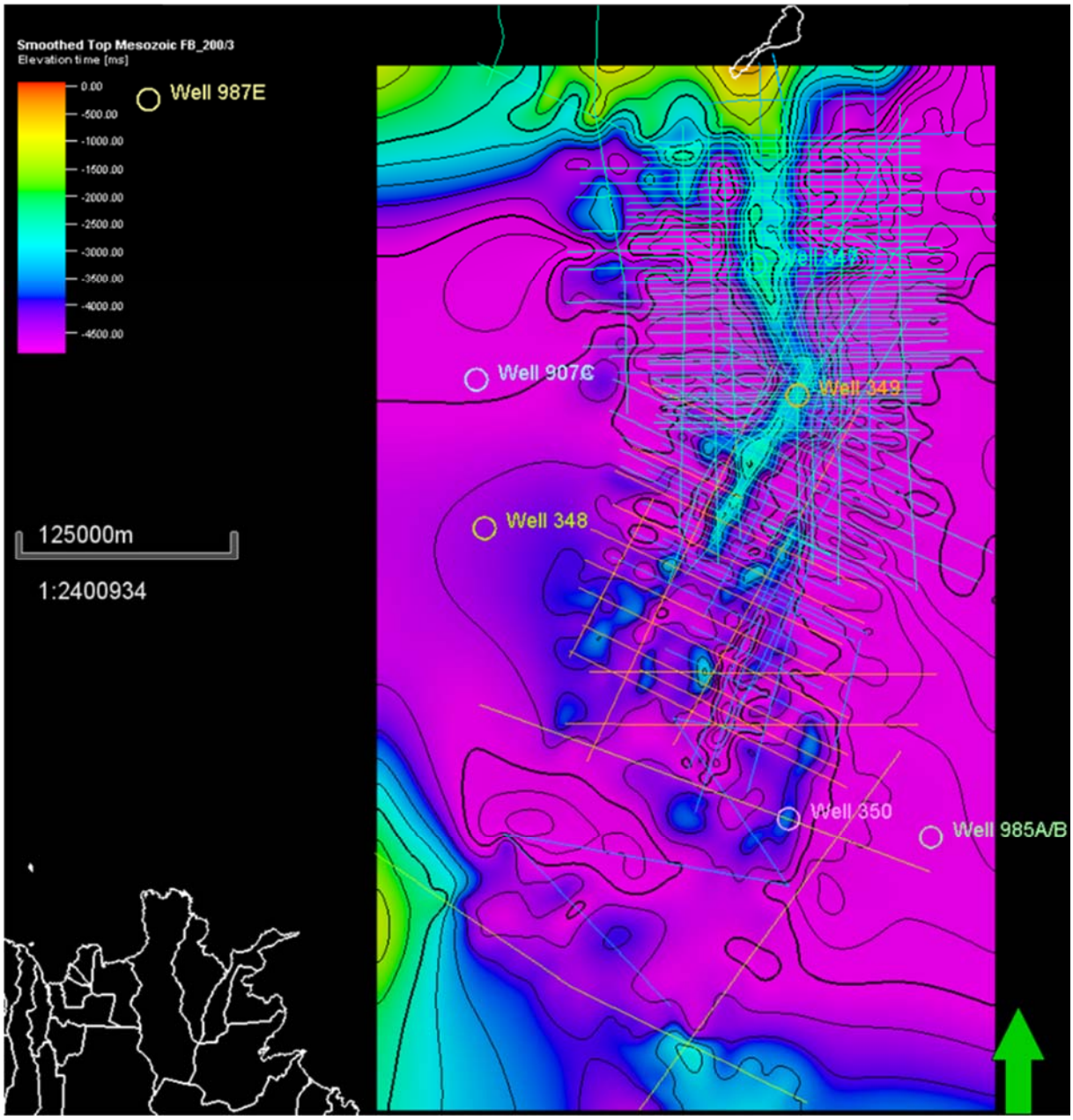

Figure 4.27: TWT map of the turquoise horizon "near Top Mesozoic fault blocks".

However, these wedge-like "SDR" features are not always well developed across the entire eastern margin, and in some areas appear to be bound on their eastern edge by an eastward-tilted, westward dipping normal fault (although this too is obscured by shallower volcanic intrusions above) (Figure 4.30). The "SDR" hypothesis has been assumed to be associated with the extensive volcanic break-up marker, dividing pre-rift successions below and syn- to post-rift sequences above. However, figure 4.30 shows the similarity of these previously interpreted volcanic SDR's as, clearly containing bedded reflectors akin to a classic syn-rift sedimentary wedge forming in the hanging wall of a westward-dipping bounding fault to the east. Furthermore, in some cases deeper reflectors can be observed below the potential syn-rift sedimentary package (Figure 4.30). Analogue studies along the conjugate margin of East Greenland identify pre-break up Palaeocene strata comprising hyaloclastite and pre-break-up turbidite sandstones and fluvial sandstone conglomerate units (Larsen et al., 1999; Henriksen et al., 2009). Therefore, the parallel – diverging bedded units below the top volcanic break-up

unconformity surface (purple horizon) may also contain interbedded volcaniclastic sequences and pre-break up reservoir intervals at depth, potentially forming prospective stratigraphic traps here (Figure 4.30). If these "SDR's" do in fact represent a syn-rift wedge, this has implications for redefining the tectonostratigraphic evolution of the eastern margin of the JMMC suggesting there was an earlier phase of tectonic rifting, enabling pre-break up, syn-rift sedimentation to occur before emplacement of the final break up volcanic flood basalts across the North Atlantic.

The Purple horizon tops this volcanic unit and was mapped as a bright, high amplitude, smooth and continuous negative reflector (Figure 4.26). The surface is the lowermost unconformity observed on the eastern flanks of the main ridge and SRC and corresponds to the purple stratigraphic marker of Gunnarsson et al., (1989) and the JO reflector mapped by Peron-Pindivic et al., (2012a). In places, reflectors below the purple horizon either pinch out and become truncated by this horizon or converge to become parallel beneath it in an up dip direction as a thinner volcanic layer (Figure 4.26 & 4.30). DSDP well 349 and NPD ROV sampling identify this horizon as the top Palaeocene-Eocene plateau basalts and SDR surface, and likely correspond to equivalent aged well developed SDR units on the conjugate Voring and Møre Basin marginal highs (Skogseid & Eldholm, 1987). The eastward continuation of the horizon is obscured by the presence of igneous intrusions, but it has been mapped as merging with true oceanic crust further to the east (Figure 4.21). The surface can be traced westwards to the western margin of the JMMC where is it down-faulted at major boundary faults. Figure 4.31 shows the TWT map for this purple basalt horizon. As such, the purple horizon marks the upper boundary of the igneous (flood basalt and intrusion) megasequence related to the first break-up phase and correlates with the plateau basalts observed on East Greenland in the Blosseville Coast area emplaced between 55 -59 Ma.

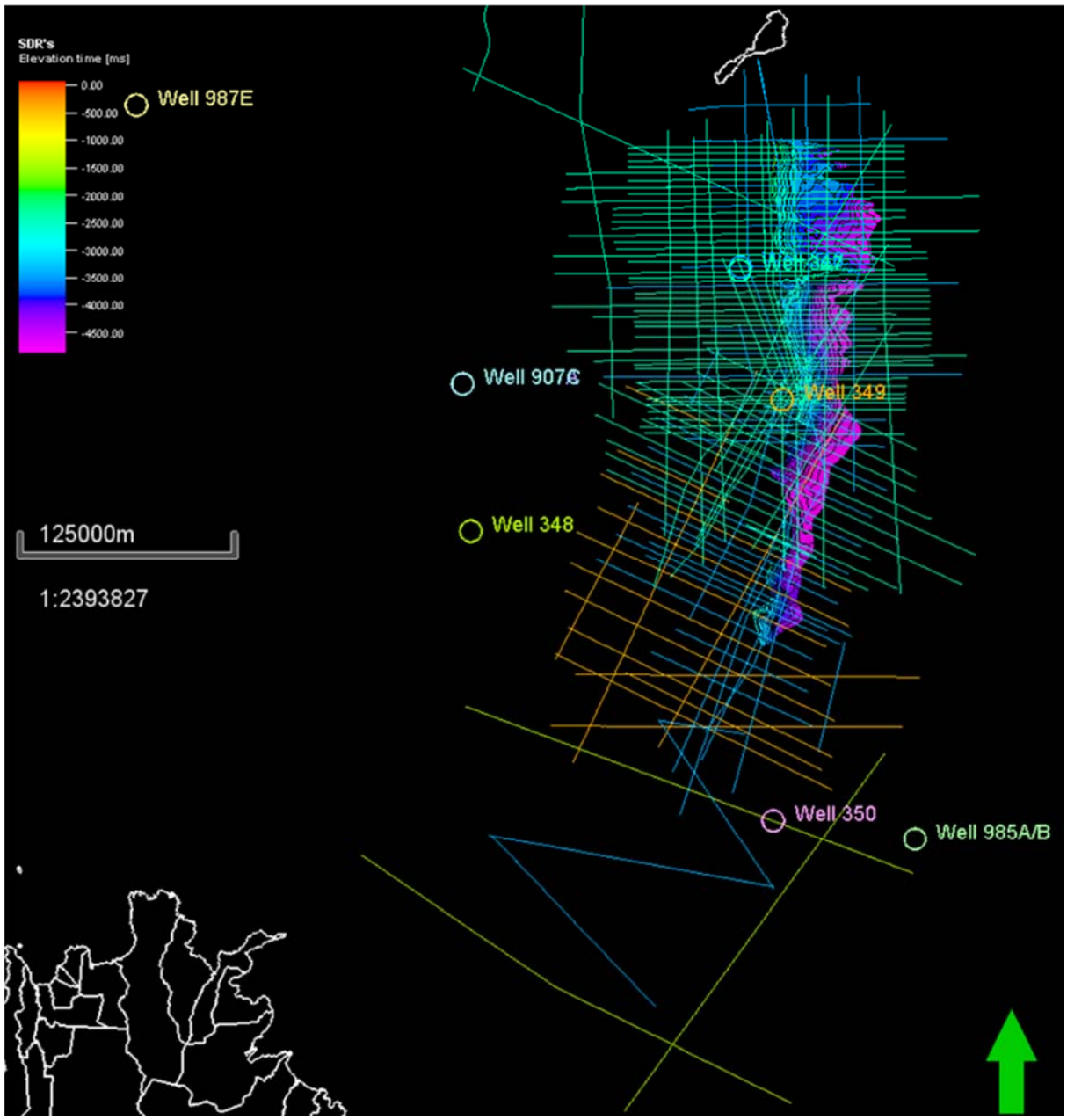

Figure 4.28: TWT map of "SDR" wedges along the eastern margin of the JMMC.

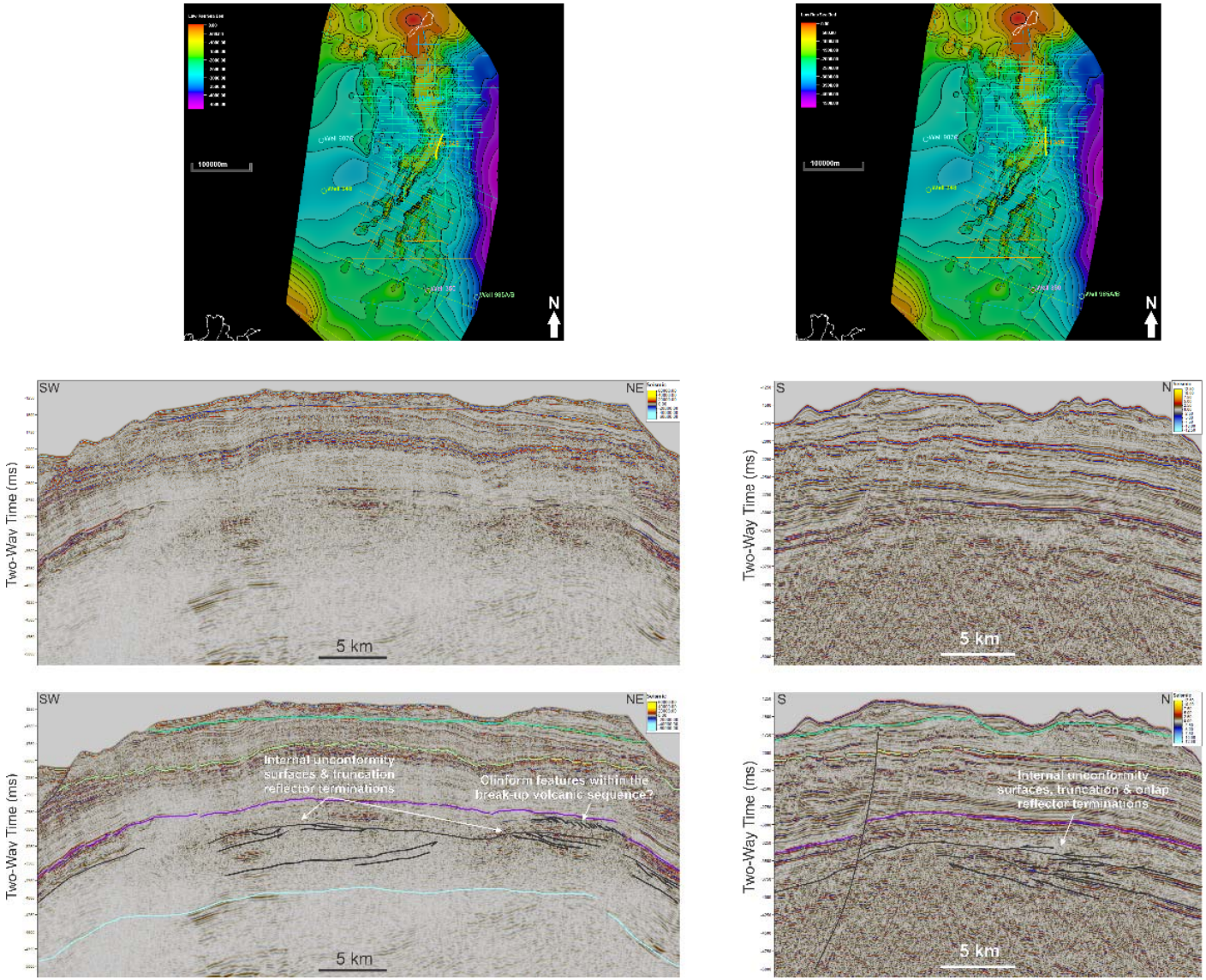

Figure 4.29: Example of potential erosional truncation and unconformities present within the turquoise to purple unit.

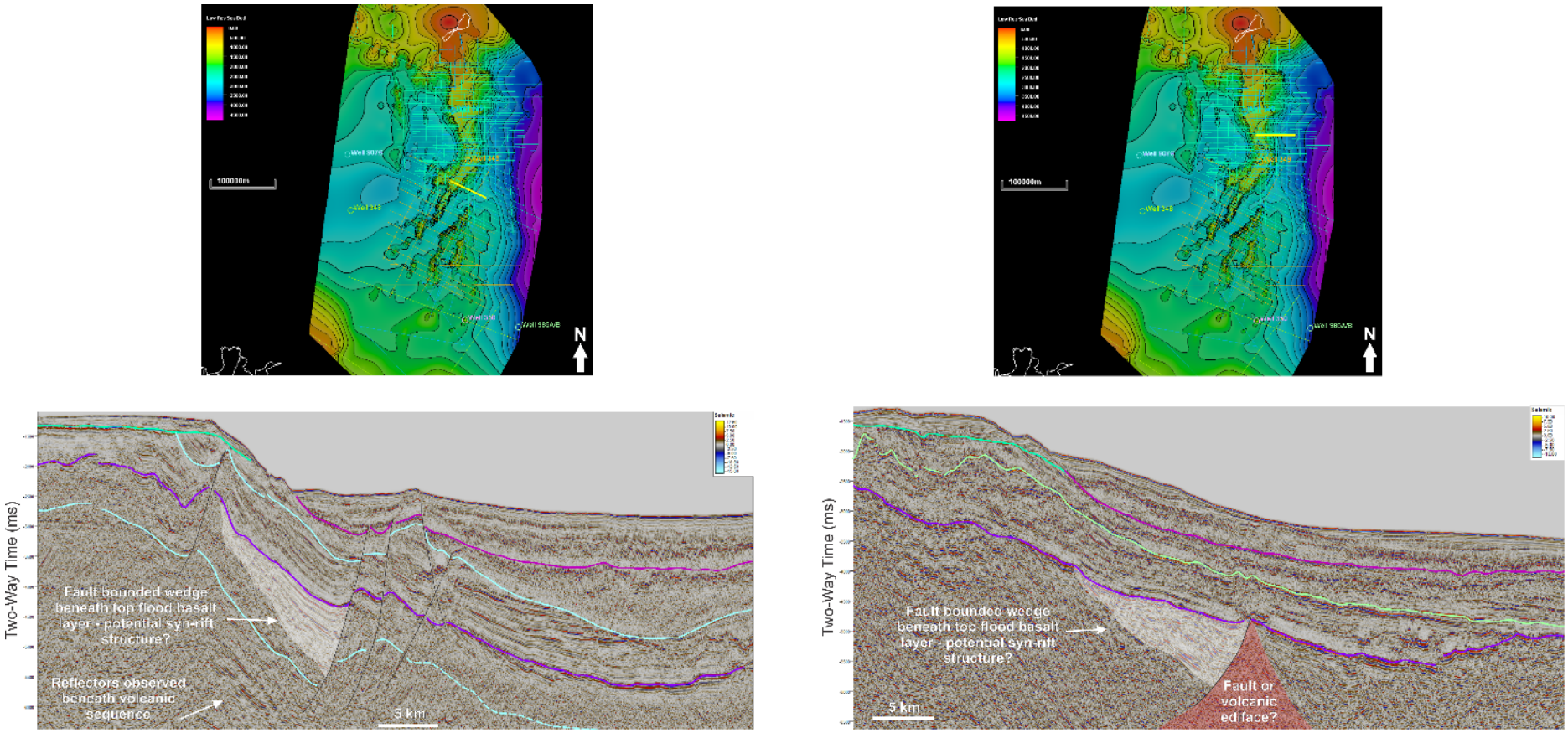

Figure 4.30: Example of areas where "SDR" units appear to look similar to syn-rift wedge structures.

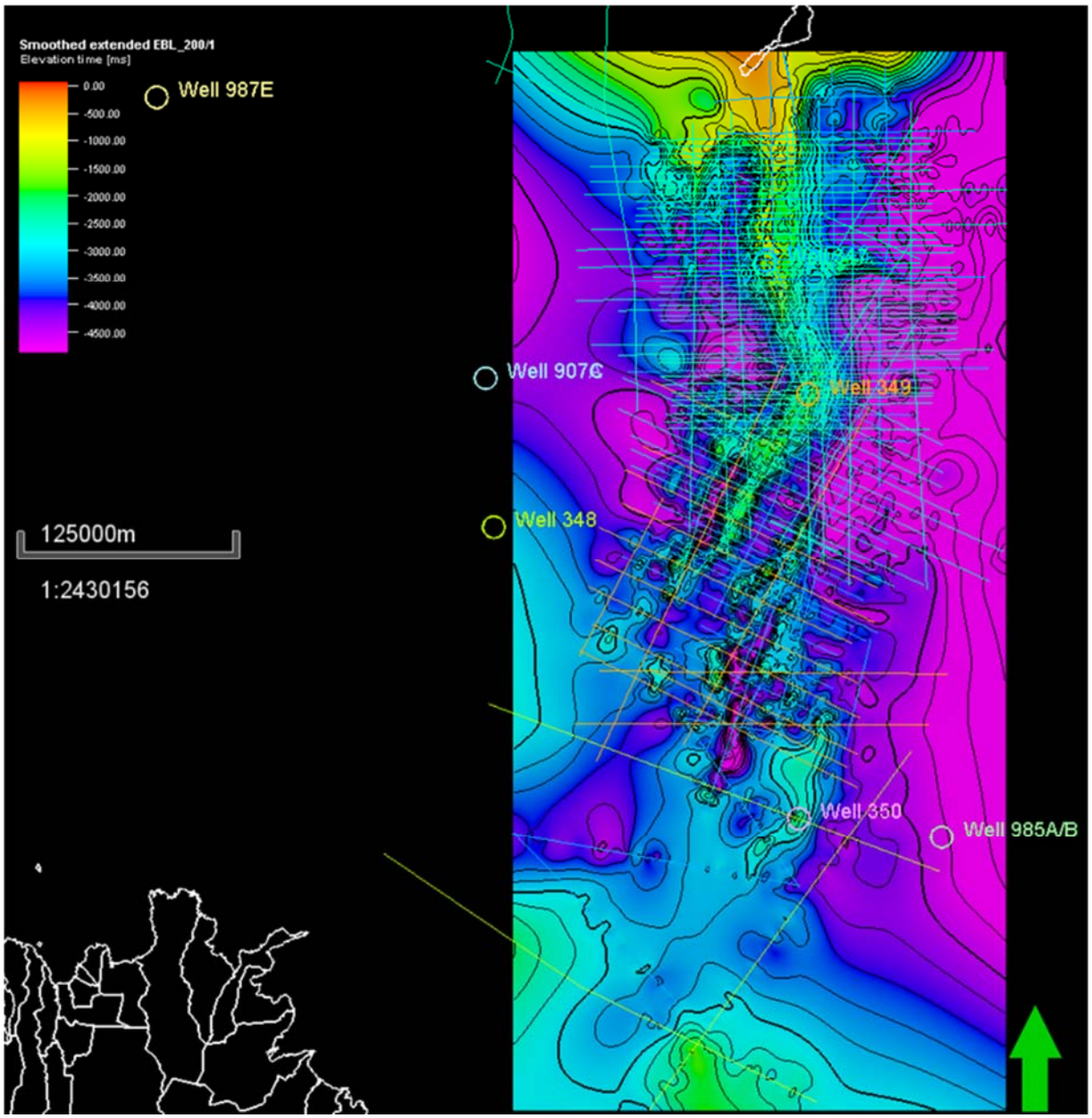

Figure 4.31: TWT map of the Palaeocene-Eocene "top basalt" surface (Purple horizon).

Post-break up Section

The sedimentary unit overlying the purple horizon is composed of parallel bedded, sub-continuous, reflections with alternating low and high amplitudes packages (Figure 4.26). The seismic facies directly above the purple horizon is opaque, which was a key criteria for mapping the horizon across faults and between ridges and sub-basins (Figure 4.26). Other minor unconformity surfaces are also present within this sedimentary package. Peron-Pindivic et al., (2012a) and Gunnarsson et al., (1989) map their "red reflector" as a bright, highly reflective erosion surface. On the eastern flank of the main ridge into the Norway Basin and some of the south-easternmost ridges of the SRC, the eastward extent of their "red reflector" surface becomes masked by numerous igneous intrusions which tend to cluster at a similar stratigraphic level (Figure 4.18 & 4.19). These are characterised as short, sub-horizontal, bright reflectors with sharp edges. Commonly, the sedimentary strata above the sill reflectors are uplifted and display a low to opaque amplitude directly above. These igneous intrusions are likely Early to Middle

Eocene based on inference of the relative timing of emplacement and sedimentary unit they intrude (Blischke et al., 2017). Gunnarsson et al., (1989) also interpret this "early drift phase" megasequence package to consist of marine sediments from shelf and slope depositional settings. The shelf setting is present across much of the central and western part of the JMMC characterised by regular, parallel layered reflectors. Whereas the eastern margin composed of gently diverging and converging reflectors and potential clinoform features represent shelf-edge to slope depositional settings (Figure 4.32) (Gunnarsson et al., 1989).

The light green horizon is a prominent erosional unconformity on the eastern margin and has undergone the same deformation and erosional truncation by the flat topped Oligocene Unconformity on the top of the main ridges as the Palaeocene-Eocene top volcanic horizon and turquoise "top Mesozoic" horizon. This surface is mapped as a positive peak and is characterised by truncation of underlying reflectors and onlap of overlying reflectors (especially on the eastern flanks and into the Norway Basin) (Figure 4.26). Figure 4.33 shows the areal extent of this mapped surface.

The seismic facies of the overlying sedimentary package is predominantly characterised by more discontinuous reflectors of generally lower amplitude than the underlying unit (Figure 4.26). Reflector amplitudes are low beneath the JMR and on the eastern flanks and are higher in the Norway Basin, at its base where sub-continuous reflectors directly downlap onto the light green horizon. The discontinuous nature of the reflectors may represent slump and mass flow deposits (Peron-Pindivic et al., (2012a) (Figure 4.34); whilst the sub-continuous reflectors at the base in the Norway Basin could represent basin floor fan facies. Smaller unconformity surfaces are also present within this unit as well as what appear to be clinoform reflector geometries (Line JM-85-11). Smaller scale erosional features identified on the eastern flank could also represent slope channel and/or canyon systems formed by mass flow and turbidity currents (Gunnarsson et al., 1989) (Figure 4.32 & 4.34).

The aqua horizon is the major distinct angular unconformity present as a flat lying peneplanation surface across the top of the JMR (Figure 4.26). It is mapped as a bright negative reflector. It is characterised by erosional truncations of the underlying sedimentary successions (and older unconformity surfaces (light green and purple horizons)). Peron-Pindivic et al., (2012a) identifies this surface as the JA reflector which correlates with parts of the light green reflector mapped in this study. However, due to a lack of age control with other mapped horizons it is unclear whether this horizon links with this or other unconformities along the eastern and western margin such as the yellow, or magenta horizons (described below). Therefore, in this study, the surface has been mapped as an isolated feature (Figure 4.35). DSDP wells 346, 347 and 349 penetrate this unconformity which dates it as mid Oligocene separating late Oligocene sediments above from underlying early Oligocene to Eocene sediments (Talwani et al., 1976). It is interpreted that this major unconformity was formed in response to uplift and subaerial exposure during plate reorganisations in the Norwegian-Greenland Sea and westward migration of the seafloor spreading ridge (Talwani & Eldholm, 1977)

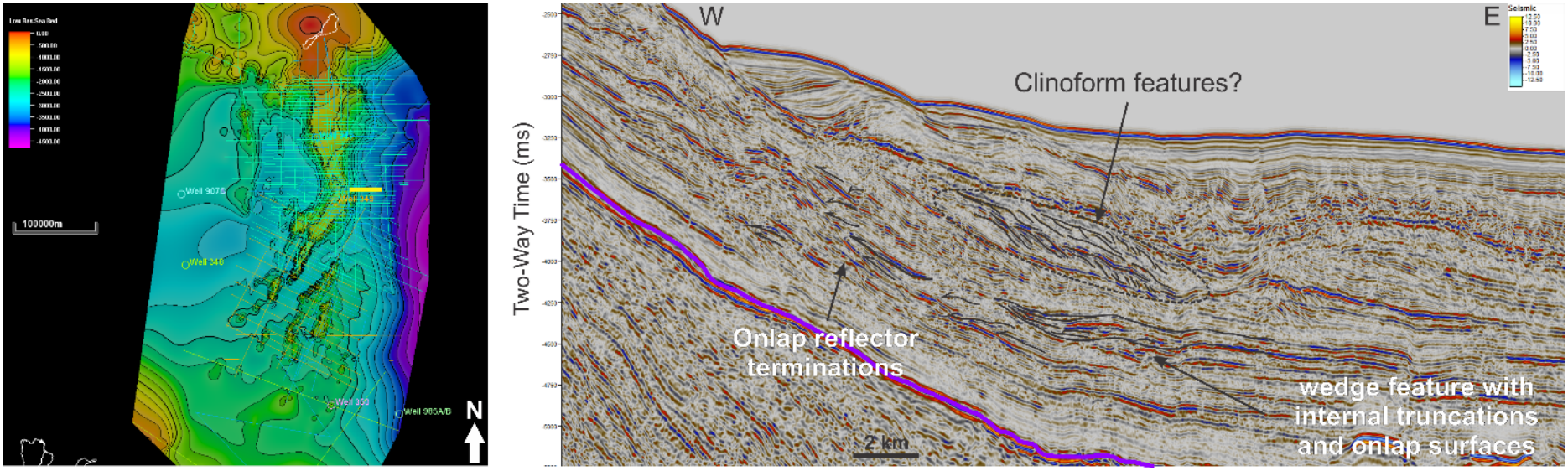

Figure 4.32: Clinoform and erosive channelized features observed from reflector terminations along the eastern margin stratigraphic succession.

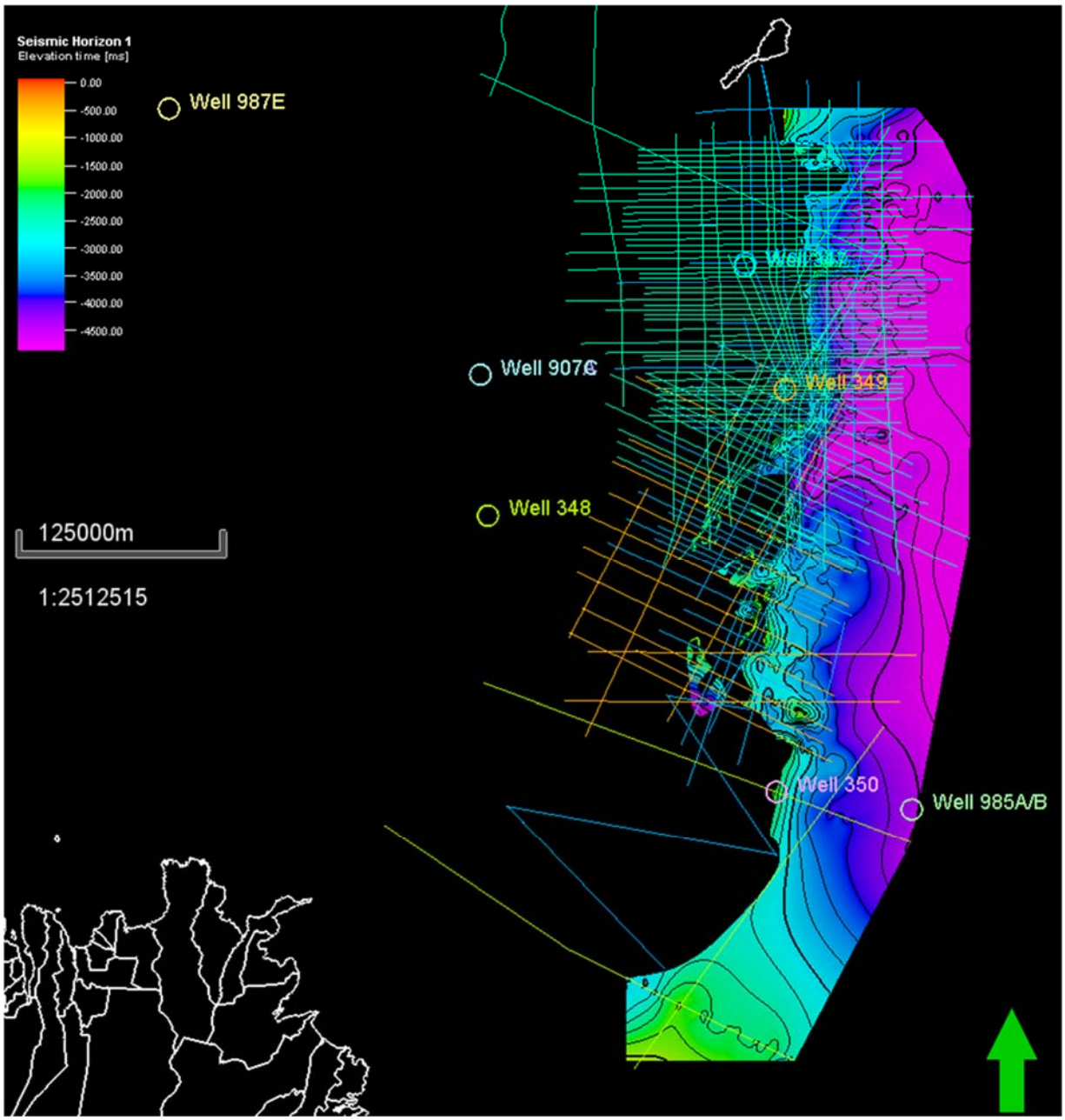

Figure 4.33: TWT map of the intra-Eocene unconformity surface (light green horizon) mapped along the eastern margin of the JMMC.

The yellow horizon is a prominent angular unconformity observed on the western flank and not dissimilar to the main flat-lying Oligocene age unconformity across the top of the JMR. This erosional horizon likely represents the 2nd break-up phase unconformity along the western margin associated with the progressive separation of the JMMC from the East Greenland margin. It may or may not be time equivalent to the main Oligocene unconformity and has been mapped as either a time separate individual surface or combined with the main Oligocene unconformity (Figure 4.36). It is mapped as a negative, bright reflector truncating discontinuous to chaotic, mid-low amplitude reflectors below and onlapped by continuous parallel-bedded mid-high amplitude reflectors above (Figure 4.26).

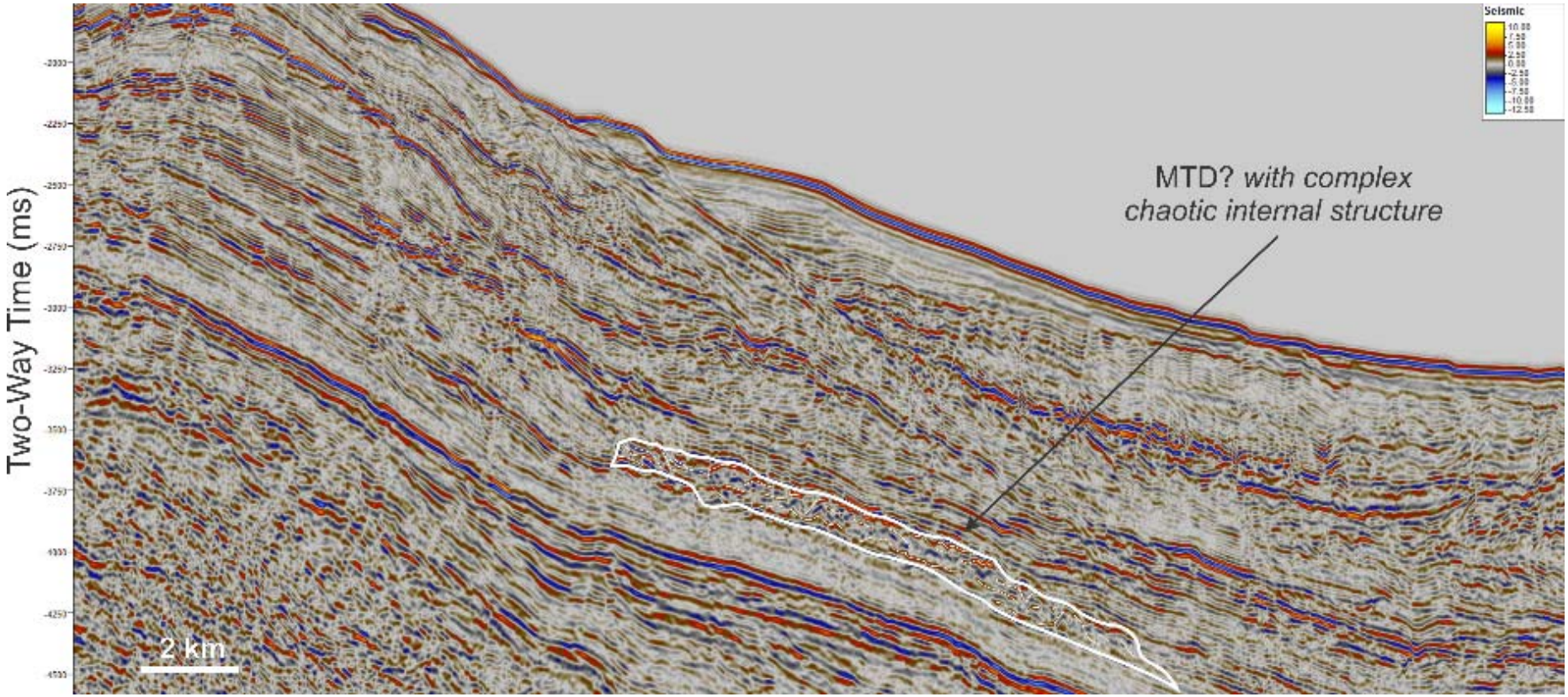

Figure 4.34: Example of potential mass transport deposits along eastern margin stratigraphy.

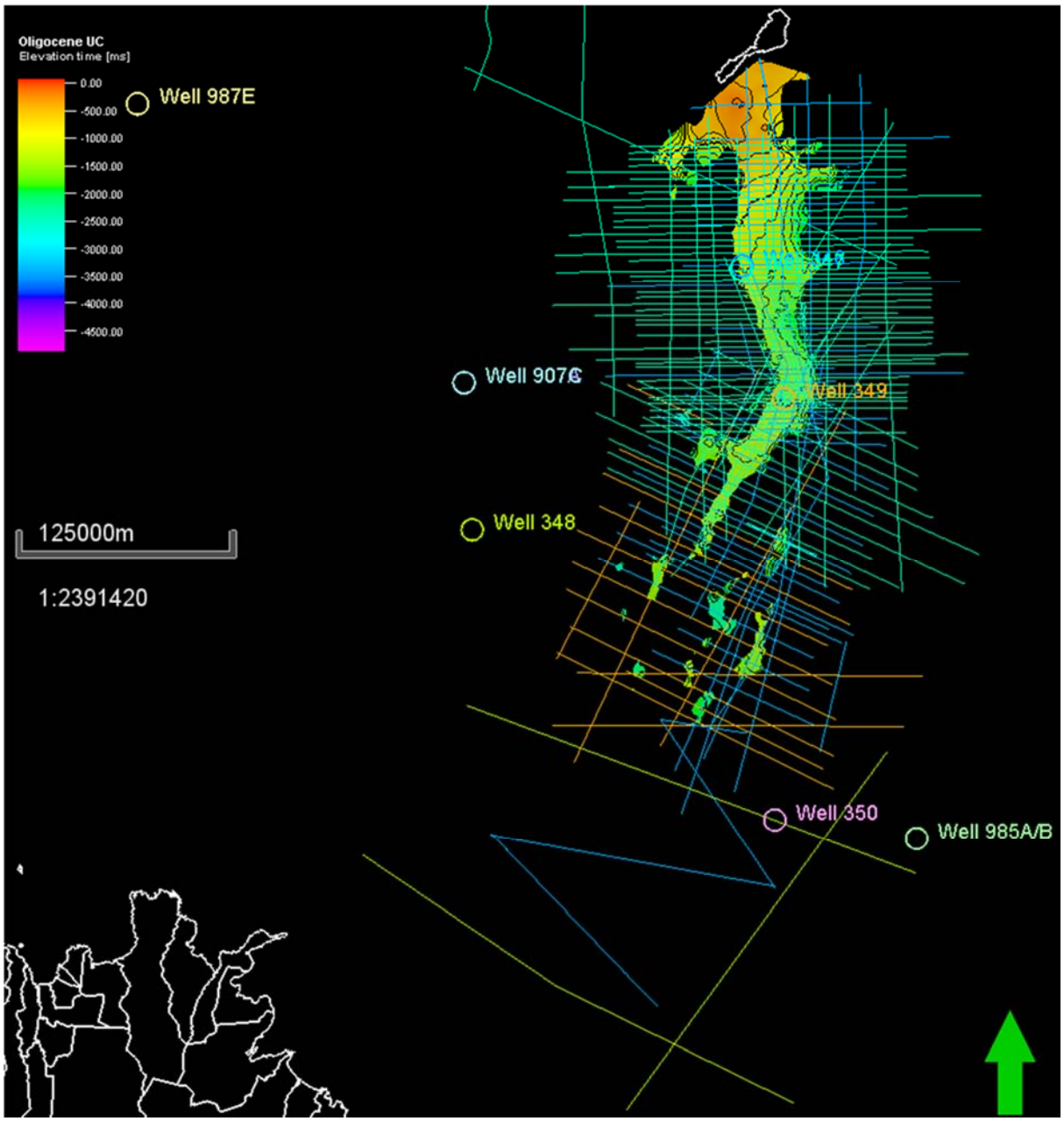

Figure 4.35: TWT map of Oligocene unconformity surface.

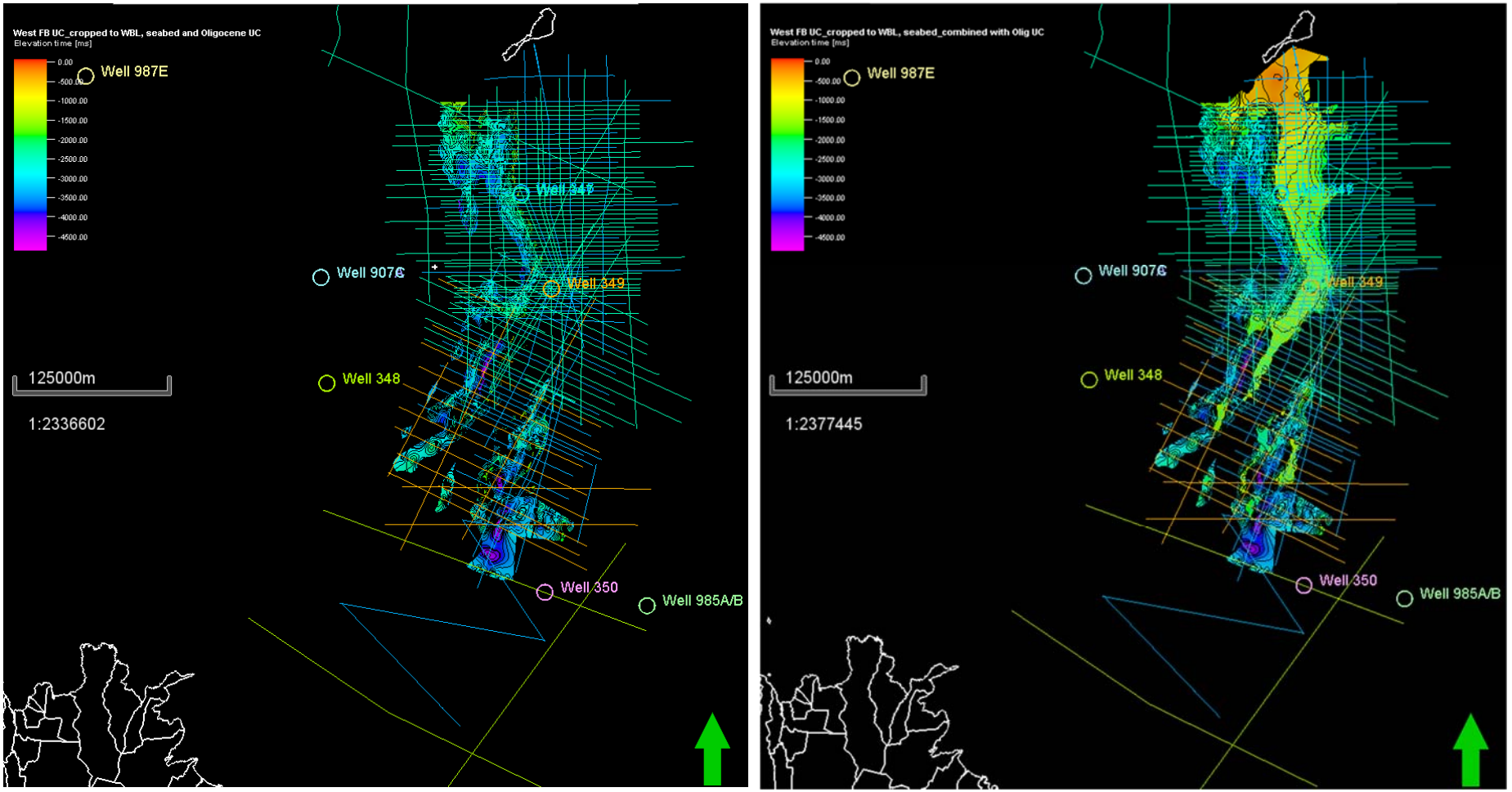

Figure 4.36: TWT map of the western fault block unconformity (yellow horizon). The figure on the right shows this surface combined with the Oligocene unconformity surface along the main JMR.

The overlying sedimentary unit is dominated by continuous, parallel bedded, mid-high amplitude reflectors appearing to onlap the underlying yellow break up unconformity (Figure 4.26). The sedimentary package exhibits large thickness variations infilling the rift basins and half grabens on the western margin (probably as a result of differential subsidence and syn-tectonic sedimentation). Gunnarsson et al., (1989) interpret these sediments to be shed from the uplifted local highs and main ridge and deposited as stratified fan complexes filling in grabens and half grabens on the western margin, and mass flow complexes down the eastern slope along the eastern margin (Figure 4.32 & 4.34).

The dark green horizon is an extensive, highly irregular, discontinuous, flat lying, bright series of reflectors observed along the western margin of the JMMC, the top of which is mapped as a negative reflector. Figure 4.37 highlights the areal extent of this surface. It also appears to be cut by high angle planar faults with very small displacement in many areas of the JMB. This horizon appears at a similar stratigraphic level across most of the JMB, Jan Mayen Trough and western parts of the SRC and small sill features can also be observed beneath the top mapped surface. The horizon creates an opaque zone below masking the identification of deeper stratigraphy and structure across these domains. Due to this masking effect, the southern limit of the Jan Mayen Basin is indiscernible and consequently it is likely that this reflector merges with true oceanic crust towards the south and southwest. The eastern boundary of the reflector is easily observed as a sharp edge that terminates abruptly at the basin plain and against the raised relief of the faulted western flank of the JMMC. There also appears to be saucer-like features beneath the highly irregular top surface which may represent individual sills and feeder dykes (see Figure 4.38 (eastern part on JM-85-11)). On some seismic lines, continuation of sedimentary layers and listric-planar westerly dipping faults can occasionally be observed beneath the horizon's eastern edge. This implies that the westward stepping/dipping fault complex along the western flank of the JMMC may continue westward across the JMB as inferred by Blischke et al., (2011; 2014) & Peron-Pindivic et al., (2012). Corresponding to a higher velocity layer from refraction studies across the western margin of the JMMC and JMB, the surface/ layer likely represents regionally extensive composite sheets of flat lying lava flows and sill complexes 270 – 470 m thick, emplaced within the post-rift basin fill sequence during the Late Oligocene to Early Miocene (28 – 22 Ma) (Gunnarsson et al., 1989; Blishcke et al., 2017). The extensive, consistently horizontal nature within a narrow depth range of this igneous complex contrasts with the morphology of the discordant sills along the eastern margin, suggesting a different emplacement method/setting. Comparison with the morphology of continuous, tabular sheet flood basalts from other volcanic rifted margins (Nelson et al., 2009; Jerram et al., 2009), also advocates an alternative explanation for emplacement of this igneous body. Gunnarsson et al., (1989) proposes emplacement at or just below seafloor where the pressure gradient is steepest enabling the magma pressure to suddenly fall below the prevailing hydrostatic/lithostratigraphic pressure. Miles and Cartwright's (2010) study of the Vigra Sill complex in the Møre Basin is highly analogous to the morphology of the dark green horizon, suggesting this igneous body formed from a series of amalgamated, composite lobate lava sheets and associated feeder sill complexes emplaced intrusively at shallow depths (Figure 4.38).

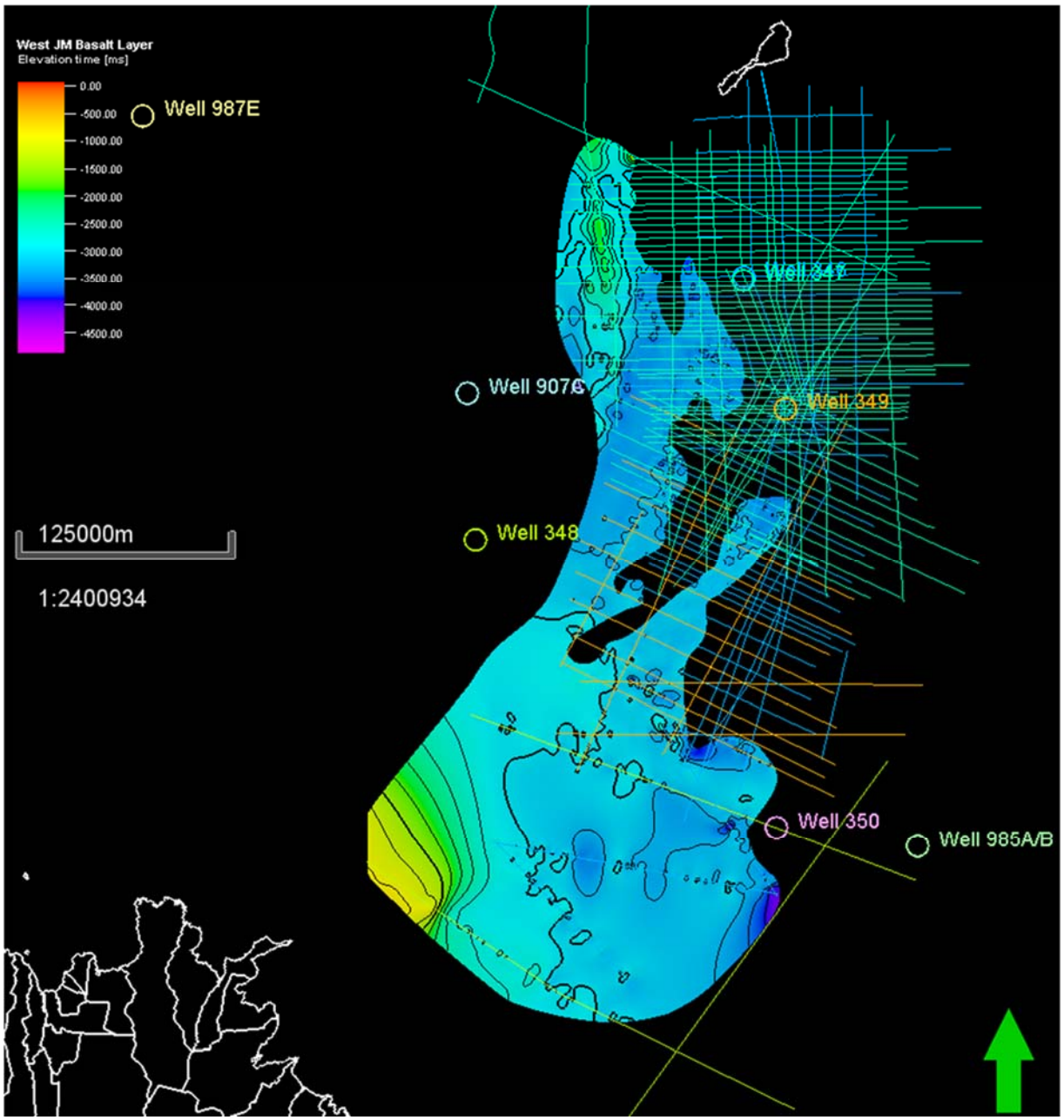

Figure 4.37: TWT map of the western basalt layer (green horizon) occurring within the JMB, Jan Mayen Trough and Iceland Plateau to the south.

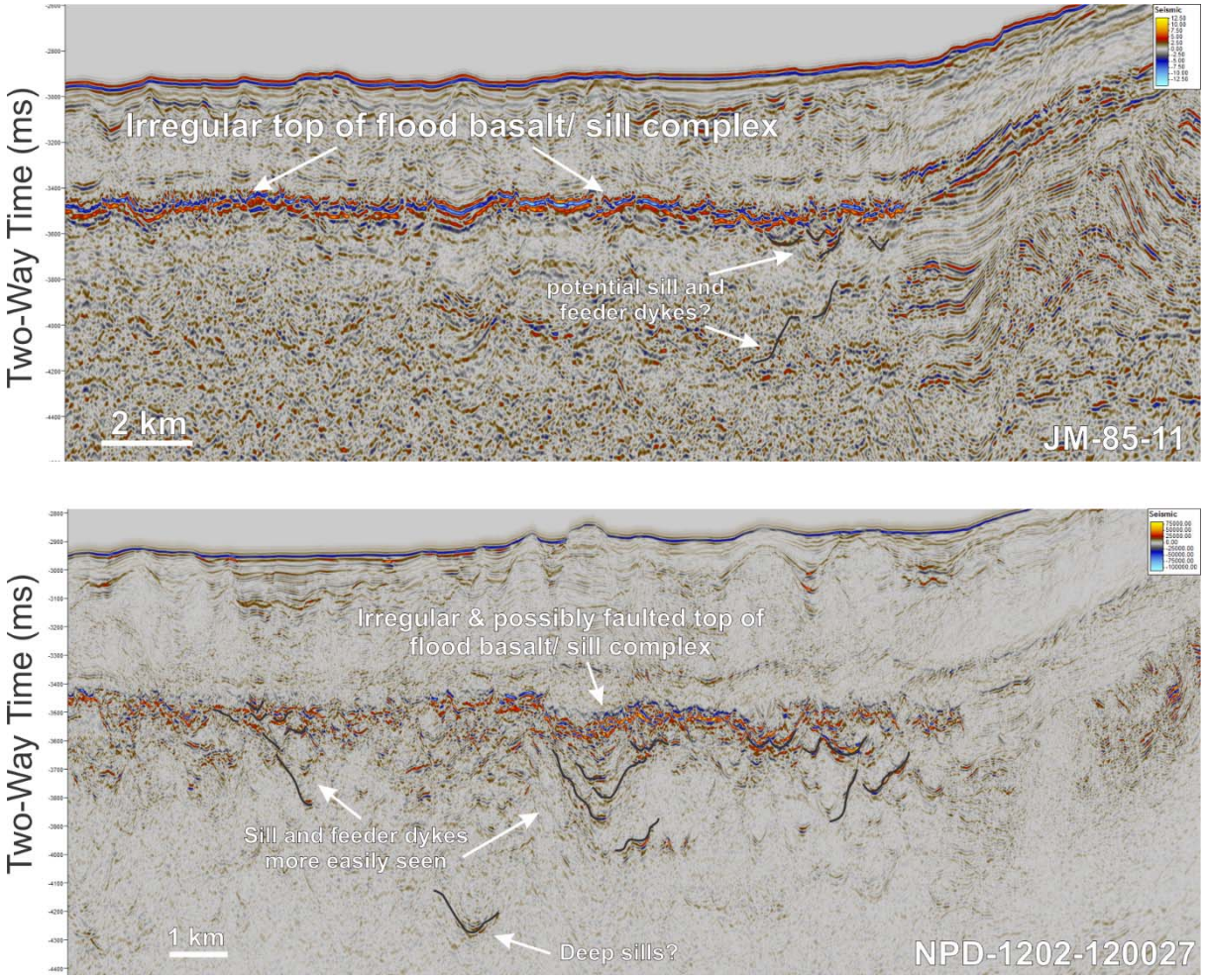

Figure 4.38: Example of irregular topography of the western intrusive sheet (green horizon) likely composed of composite lava flows and sill and feeder dyke complexes.

The magenta horizon is mapped as a bright negative reflector having a similar overlying seismic character on both the eastern and western margins of the JMMC. It is another major unconformity surface based on seismic facies and reflector terminations above and below the horizon. This surface may or may not be time equivalent to the main Oligocene unconformity surface along the top of the main ridge. Figures 4.39 show these two scenarios. In parts of the JMB and Norway Basin this horizon appears to show similarities to a fossilised Opal A to C/T boundary. This is due to its distinctive high amplitude negative reflector, having the same polarity as the seafloor and in some parts, appears to cross-cut the Neogene stratigraphic successions at a consistently similar depth range below the seabed (especially in the Norway Basin) (Figure 4.40). Berndt et al., (2004) also identify extensive diagenetic related Bottom Simulating Reflectors (BSR's) within the conjugate Mid-Norwegian Voring Plateau within the Cenozoic succession. Peron-Pindivic et al., (2012a) infer that the JA reflector is diachronous and corresponds to the magenta horizon in this study which represents an example of an Opal A to C/T transition. In the eastern part of the JMB, this horizon typically lies approx. 50 – 100 ms TWT above the igneous dark green horizon. However, in central and western parts of the JMB, these two horizons commonly merge.

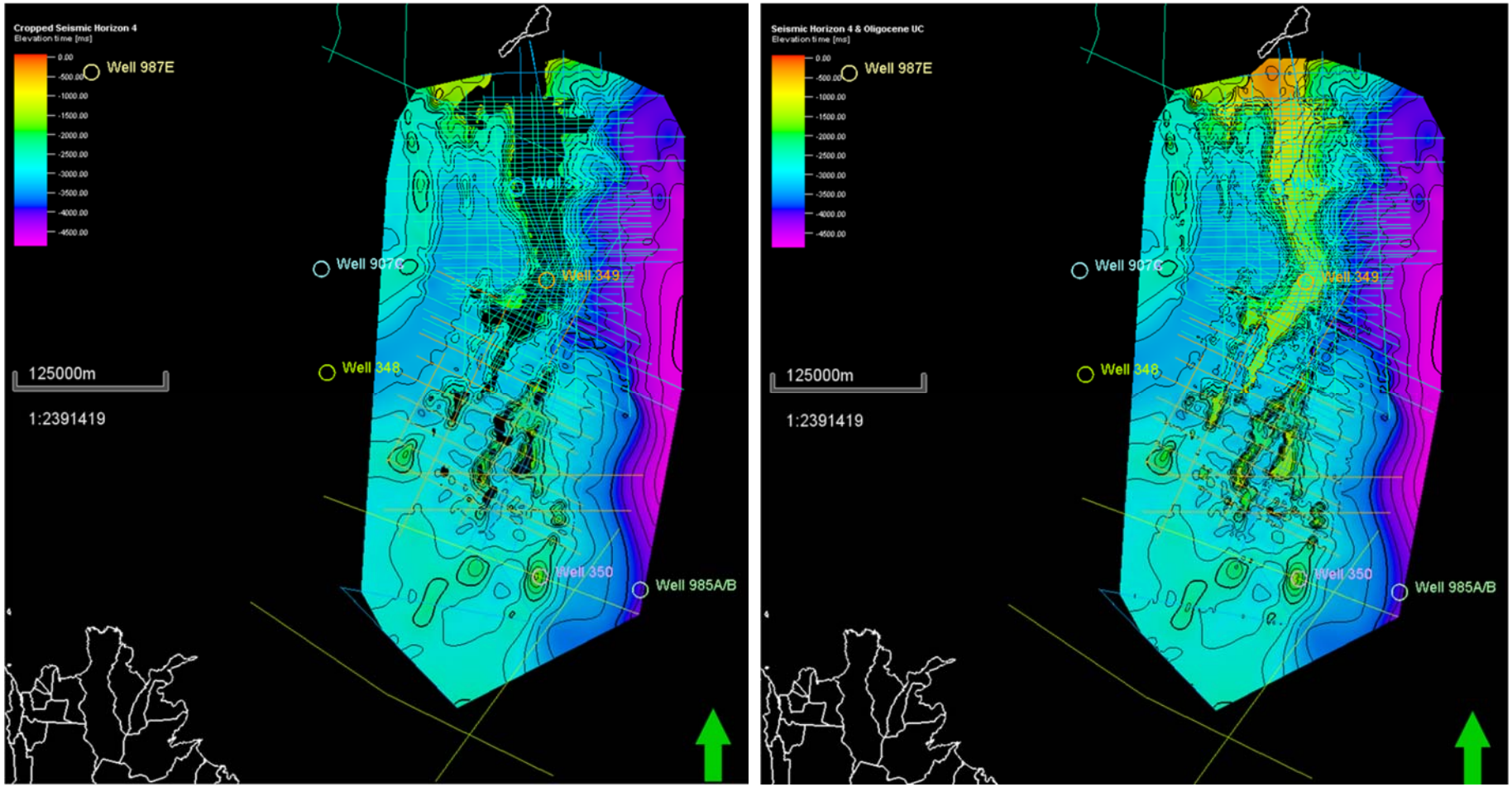

Figure 4.39: TWT of the magenta intra-Neogene unconformity surface. The map of the right shows this horizon combined with the Oligocene unconformity surface.

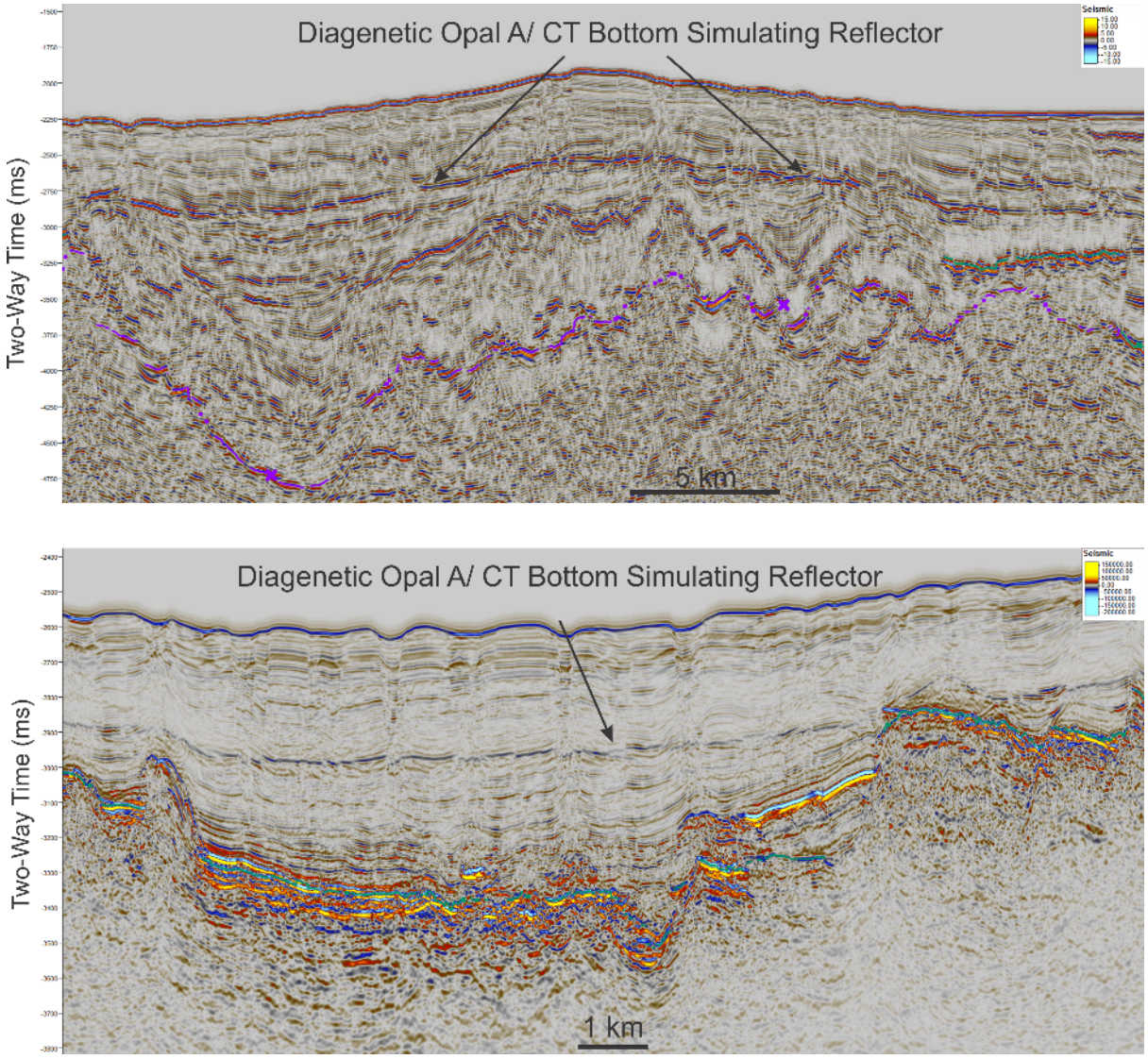

Figure 4.40: Examples of the diagenetic BSR observed within the Neogene stratigraphic succession.

The overlying shallowest unit is characterised by low to medium amplitude reflections (Figure 4.26). On the eastern margin and Norway Basin the seismic facies consists of a basal unit of highly discontinuous medium amplitude reflections with numerous polygonal faulting (Figure 4.26 & 4.41). The upper unit is composed of semi-continuous to continuous parallel bedded reflectors of medium to low amplitude (Figure 4.26). There are also numerous minor unconformities within this sedimentary package. On the western margin, the seismic facies is similar to the uppermost part along the eastern margin, and pinches out up dip towards the main JMR. However, this facies is chaotic and of low amplitude above the magenta/dark green horizon in the JMB, becoming semi-continuous just below the sea bed. Gunnarsson et al., (1989) suggests that the sediments in this megasequence were derived from the slopes of the main JMR (potentially explained by the steepness and consequently unstable nature of the slopes). The lowermost chaotic – discontinuous seismic facies may reflect mass transport and slope deposits, whilst the more continuous parallel bedded nature of the reflectors of the uppermost facies may reflect pelagic sedimentation (Gunnarsson et al., 1989). This youngest sediment package is also observed to have been affected and cut by deep-sea currents flowing axially along strike of the eastern flanks of the JMR, where potential contourite/ sediment wave features can be observed in cross section (Figure 4.42).

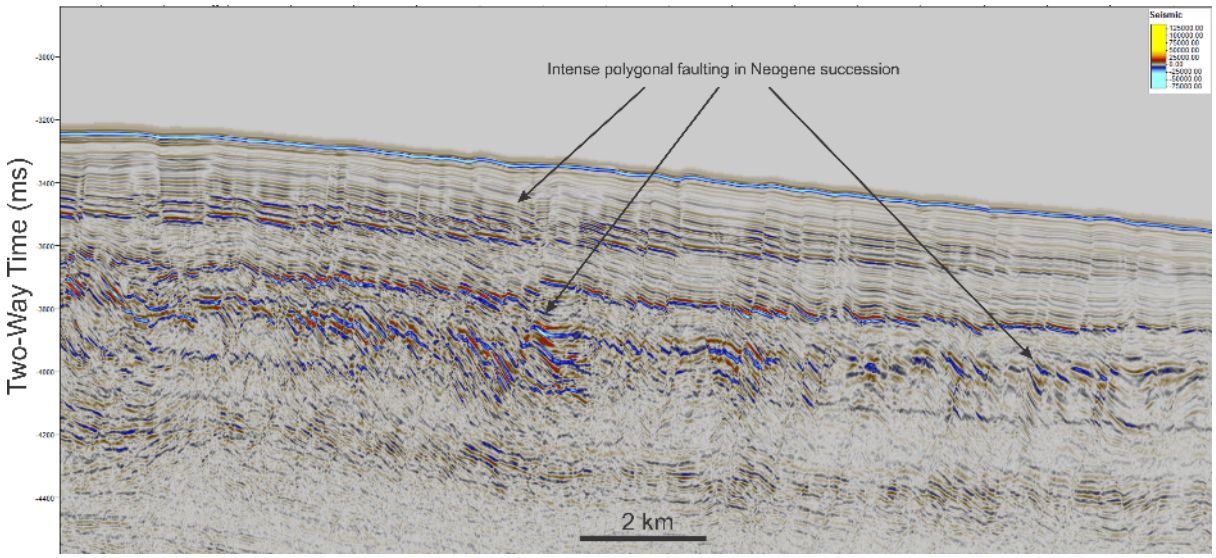

Figure 4.41: Examples of intense polygonal faulting observed in the Neogene succession (commonly above the magenta horizon) along both eastern and western margins of the JMMC.

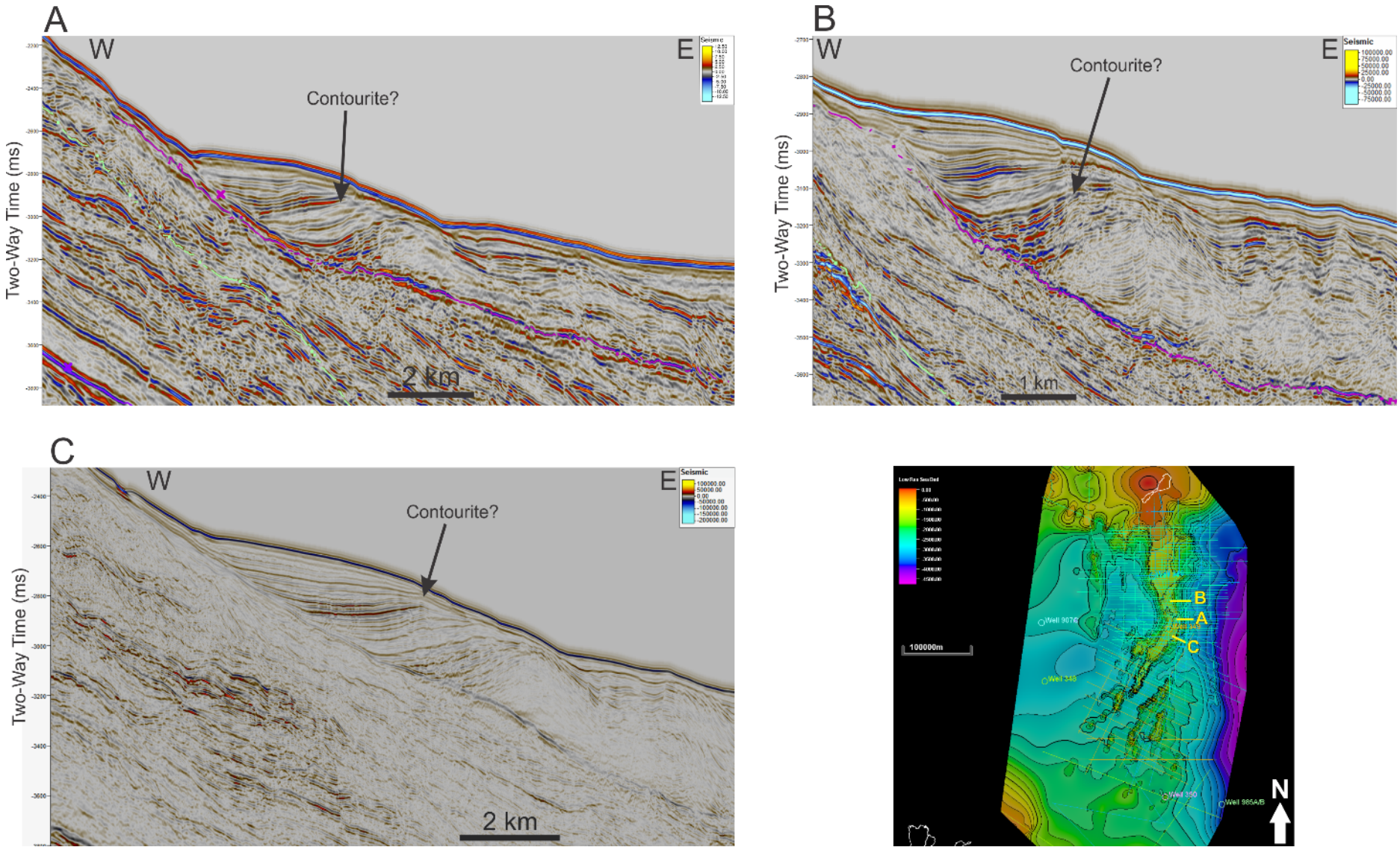

Figure 4.42: Examples of sediment wave features/contourites formed from strong bottom currents flowing along the eastern edge of the JMR.

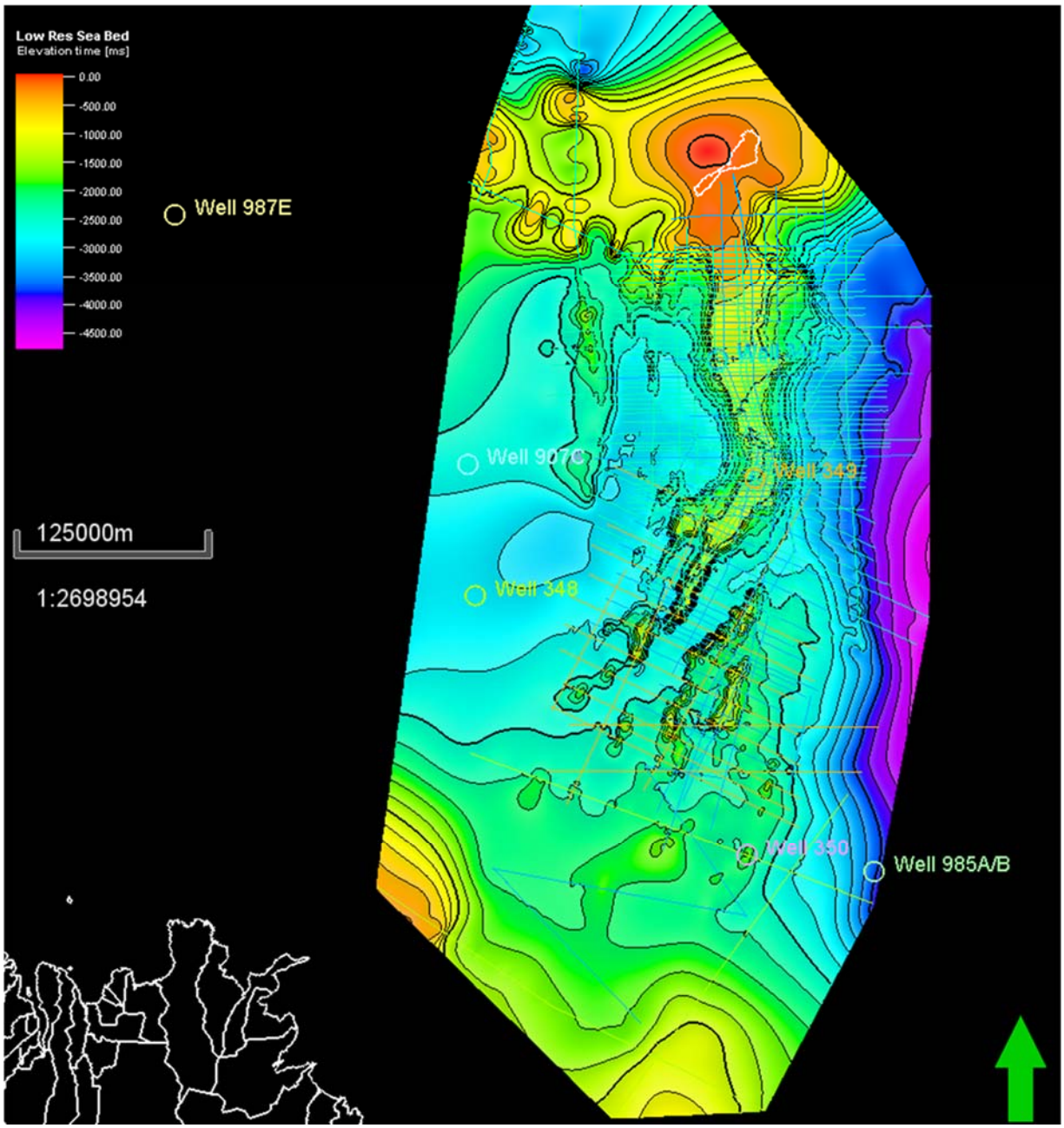

Figure 4.43: TWT Sea bed bathymetry map of the JMMC highlighting the main JMR which segments into a series of isolated ridges in the south.

Figure 4.43 shows the sea bed bathymetry map of the area clearly highlighting the surface expression of the structural domains of the JMMC.

4.5.3.3 Depth-Converted Surface Maps

A simple depth conversion was performed on the interpreted surfaces that could be mapped across the entire JMMC using the interval velocity ranges from seismic refraction studies (Table 4). Average, slow and fast velocity models were constructed to assess the impacts on the resulting depth converted surfaces. There were unappreciable differences, so the average depth converted surfaces are presented here (Figures 4.44 to 4.47).

Surfaces	Interval Velocities (km/s)		
	Slow Model	Average Model	Fast Model
Datum (0 m)			
	1.5	1.5	1.5
Sea Bed			
	2.0	2.2	2.4
Intra Miocene Unconformity			
	3.2	3.3	3.4
Palaeocene-Eocene Volcanic. Break-up unconformity I			
	4.0	4.35	4.8
Pre break-up "Top Mesozoic"			

Table 4: Interval velocities used for depth conversion. Slow, average and fast basic velocity models were created from published ranges of interval velocities (form Kodiara et al., 1995; Mjelde et al., 2007, 2008; Breivik et al., 2006, 2012; Peron-Pindivic et al., 2013; Funck et al., 2017).

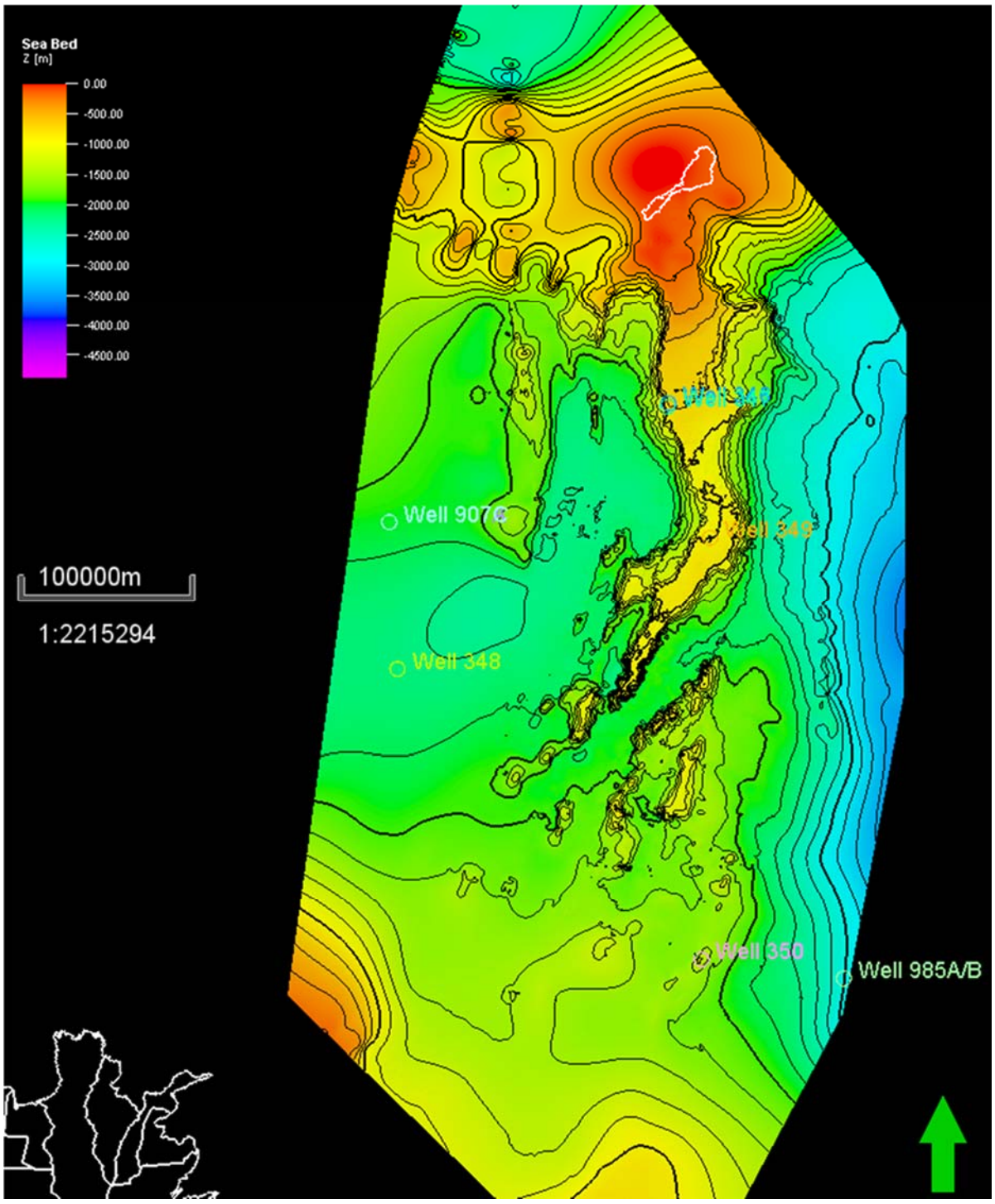

Figure 4.44: Depth map of the sea bed bathymetry (from average velocity model).

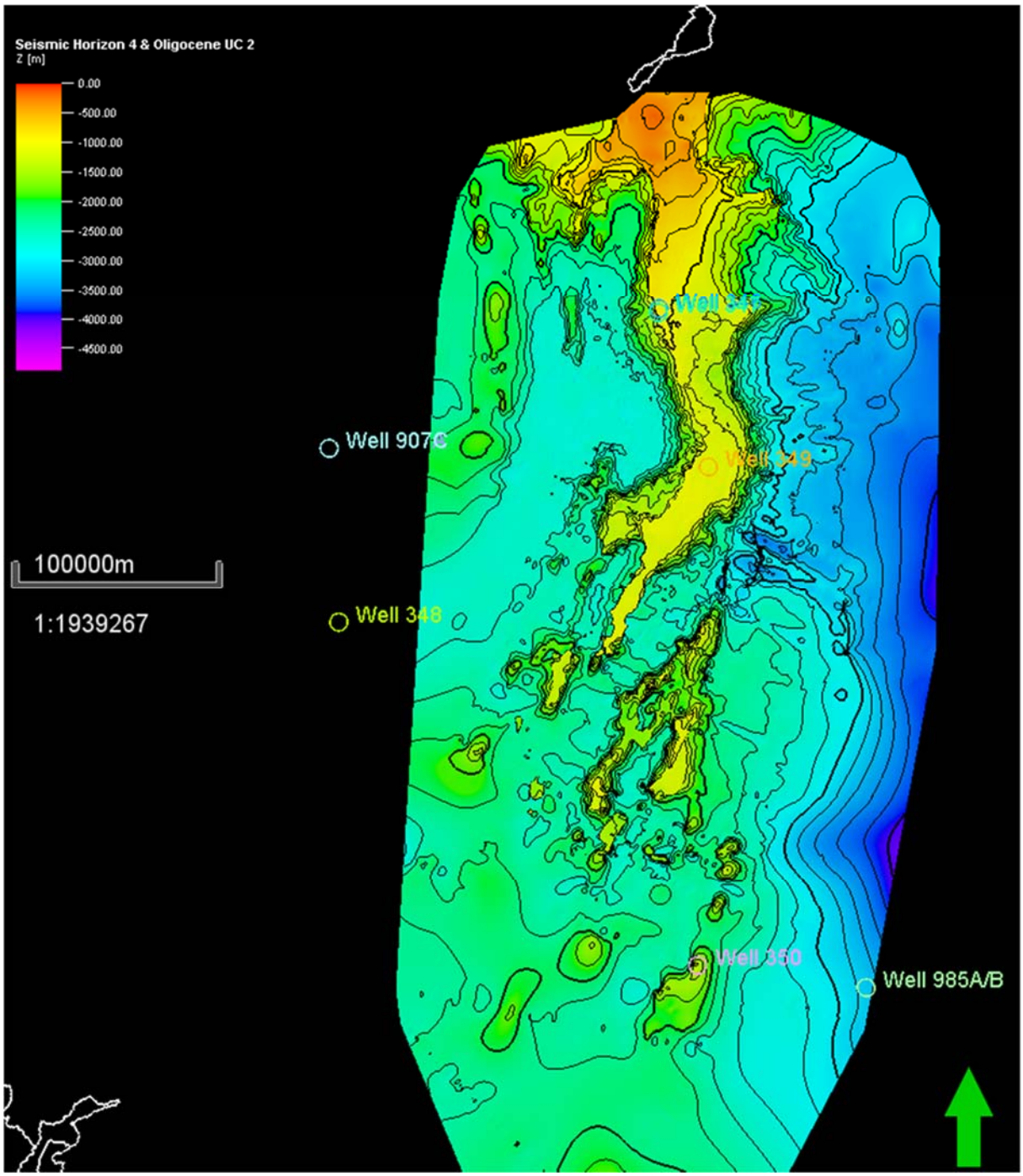

Figure 4.45: Depth map of the Intra-Neogene Unconformity/ Opal A-CT boundary combined with the Oligocene UC (from average velocity model).

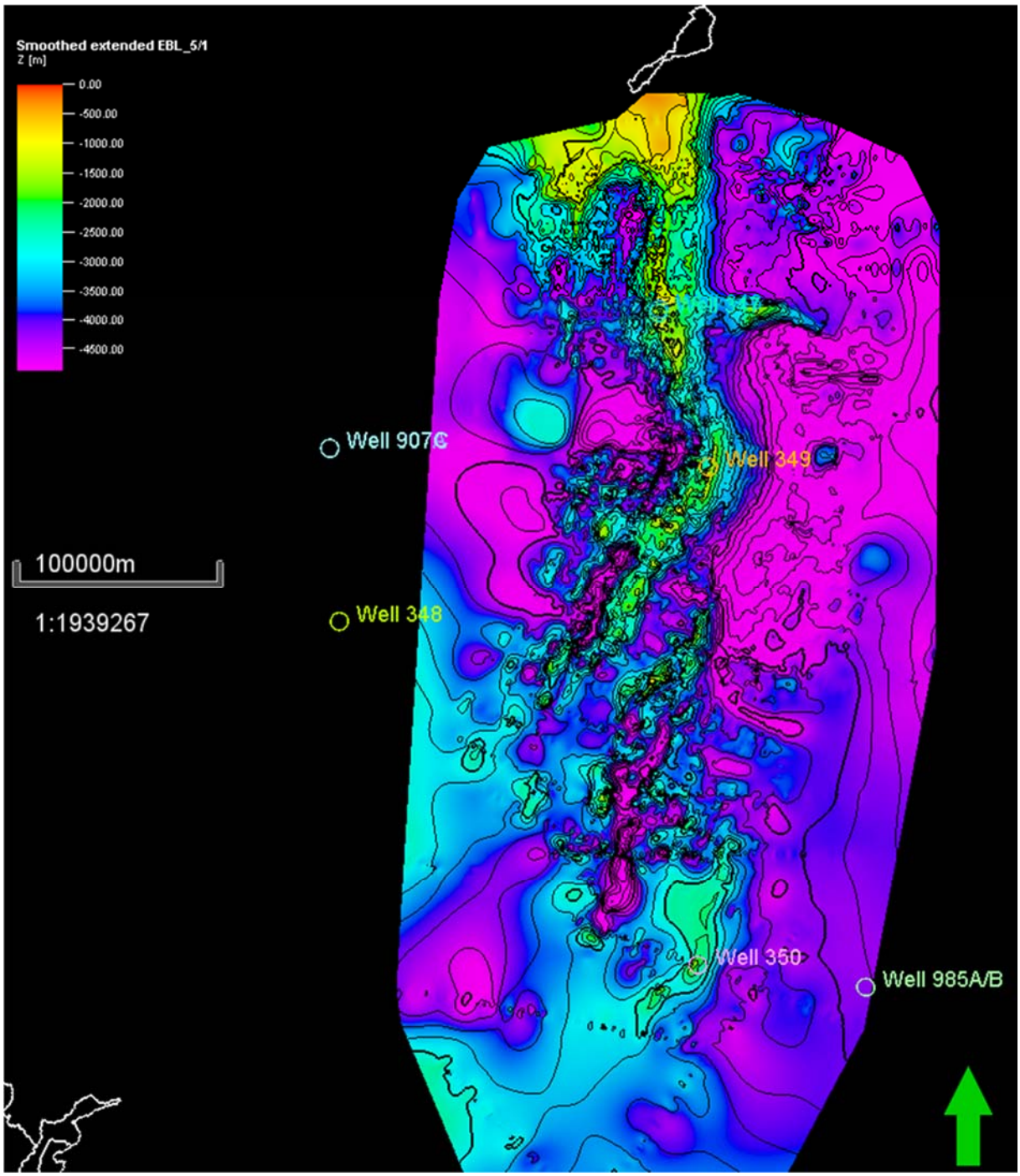

Figure 4.46: Depth map of the Palaeocene-Eocene "top basalt" layer (from average velocity model).

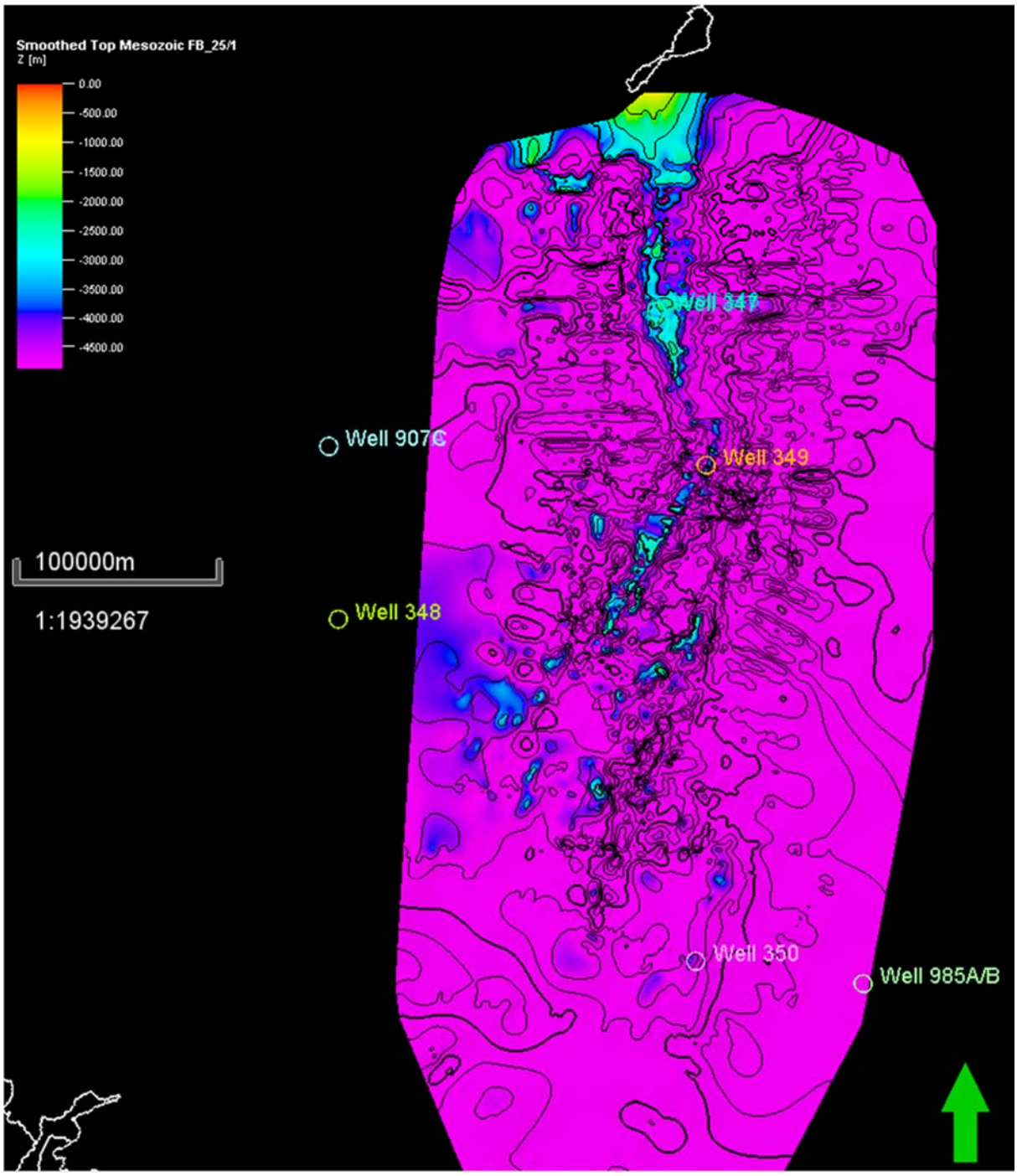

Figure 4.47: Depth map of the near "Top Mesozoic" fault blocks (from average velocity model).

4.5.3.3 Isopach Maps

Thickness maps were created between the surfaces which could be mapped across the entire JMMC, which include the seabed, the top volcanic Palaeocene-Eocene break up unconformity I and near "top Mesozoic".

Total Sedimentary Thickness Map

The thickness map of the total sedimentary succession across the JMMC can only be estimated from the approximate "top Mesozoic" surface as and deeper horizons cannot currently be interpreted from the seismic data. As such, this is a conservative estimate and it is likely that deeper units of Mesozoic to Late Palaeozoic sediments that might be present would consequently create a map of greater overall thickness. Figure 4.48 shows the thickest sediment areas along the eastern margin and into the Norway Basin. A shallowing of the sedimentary succession along the main ridges likely reflects the overall eastward tilting of the JMMC prior to Eocene-Oligocene uplift, erosion and peneplanation in response to seafloor spreading ridge jumps, rifting and second break-up along the western margin. The most complete sedimentary successions will likely be present along the eastern margin and hanging walls of steep westerly dipping planar/ listric faults bounding the isolated ridges of the SRC.

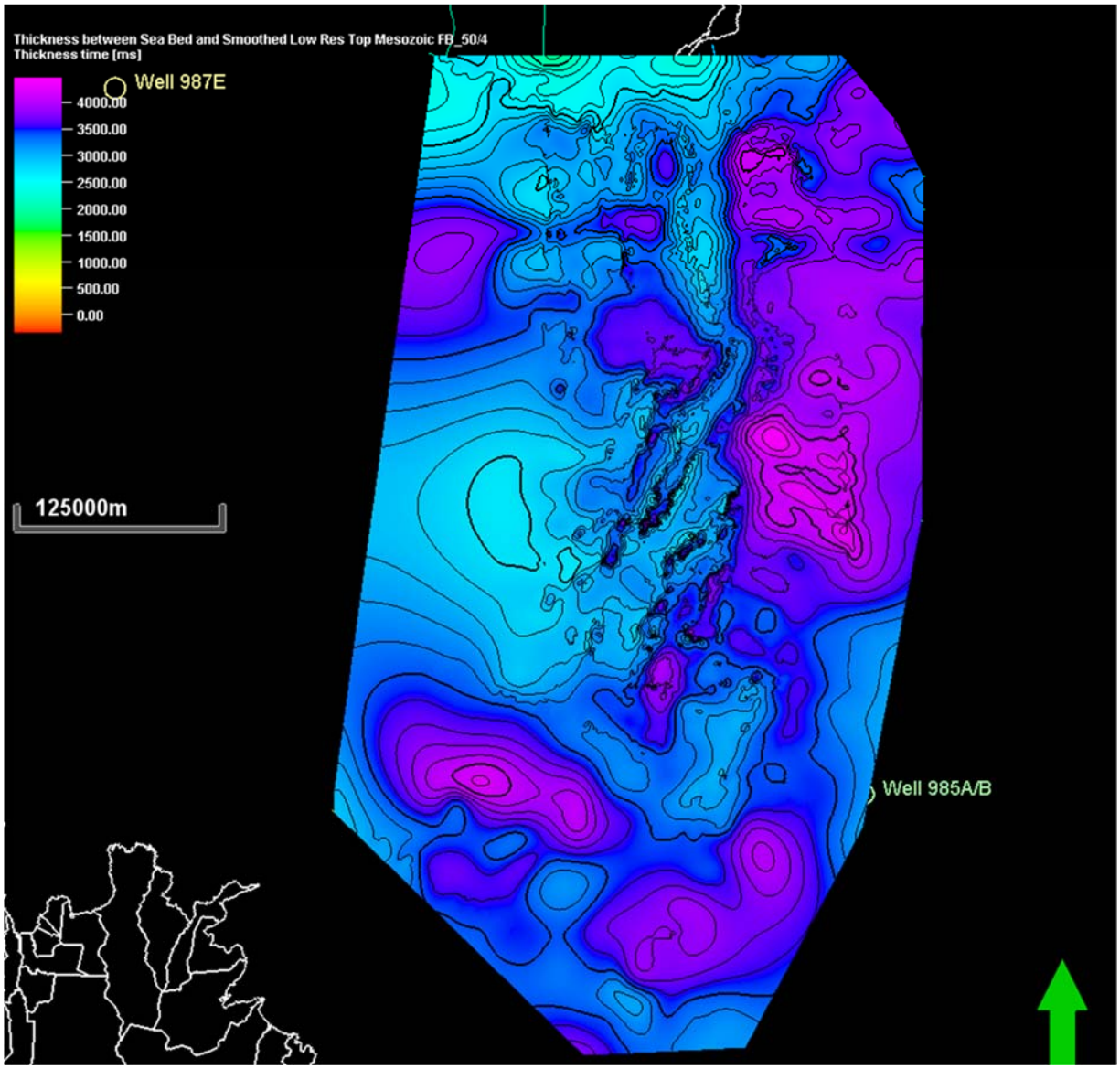

Figure 4.48: Isopach map of total mapped sedimentary cover across the JMMC.

Mesozoic-Palaeogene Thickness Map

The thickness map between the top Palaeocene-Eocene volcanic break-up unconformity I and potential "top Mesozoic" horizon shows an approximate uniform distribution across the JMMC

(Figure 4.49). This is to be expected for an interval representing a "pre-opening" sedimentary package just prior to continental break-up. Where there are some thickness variabilities, it is likely that these have arisen as a result of inaccurate horizon picks due to volcanic obscurities. There appears to be some thickening into the Norway basin, which could be due to the thickening wedge of volcanic extrusive and intrusive units eastward into the Norway Basin towards the Ægir Ridge.

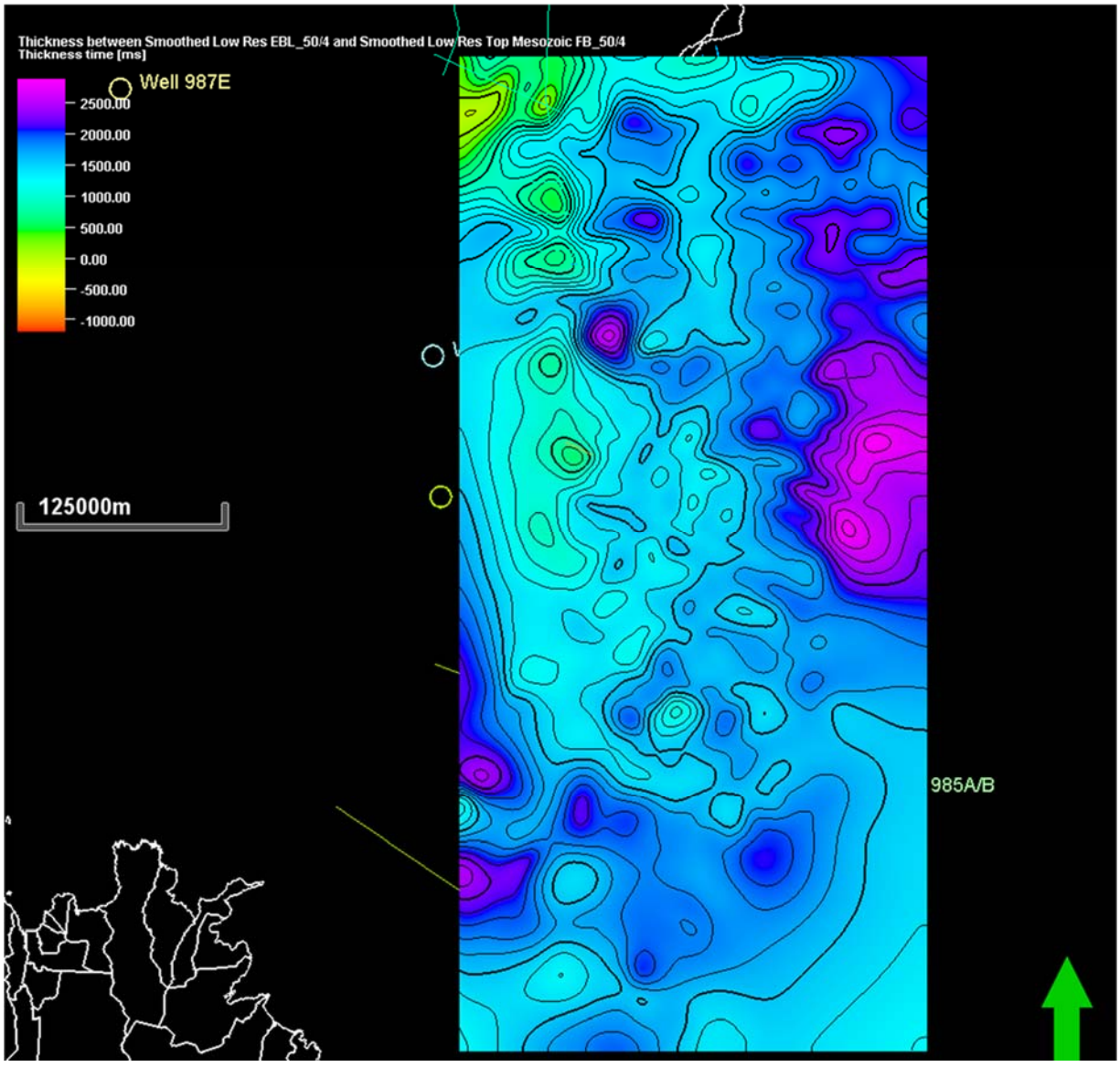

Figure 4.49: Isopach map between the near "Top Mesozoic" fault blocks and the Palaeocene-Eocene basalt layer.

Post break-up Cenozoic Thickness Map

Figure 4.50 shows the post-break up sedimentary unit to be thickest along the eastern margin of the JMMC and between the intervening ridges of the SRC, but has been eroded along the highest parts of the ridges. Blishcke et al., (2017) identify the post-break up stratigraphic thickness to range from 0 to 4200 m along the eastern margin of the JMR.

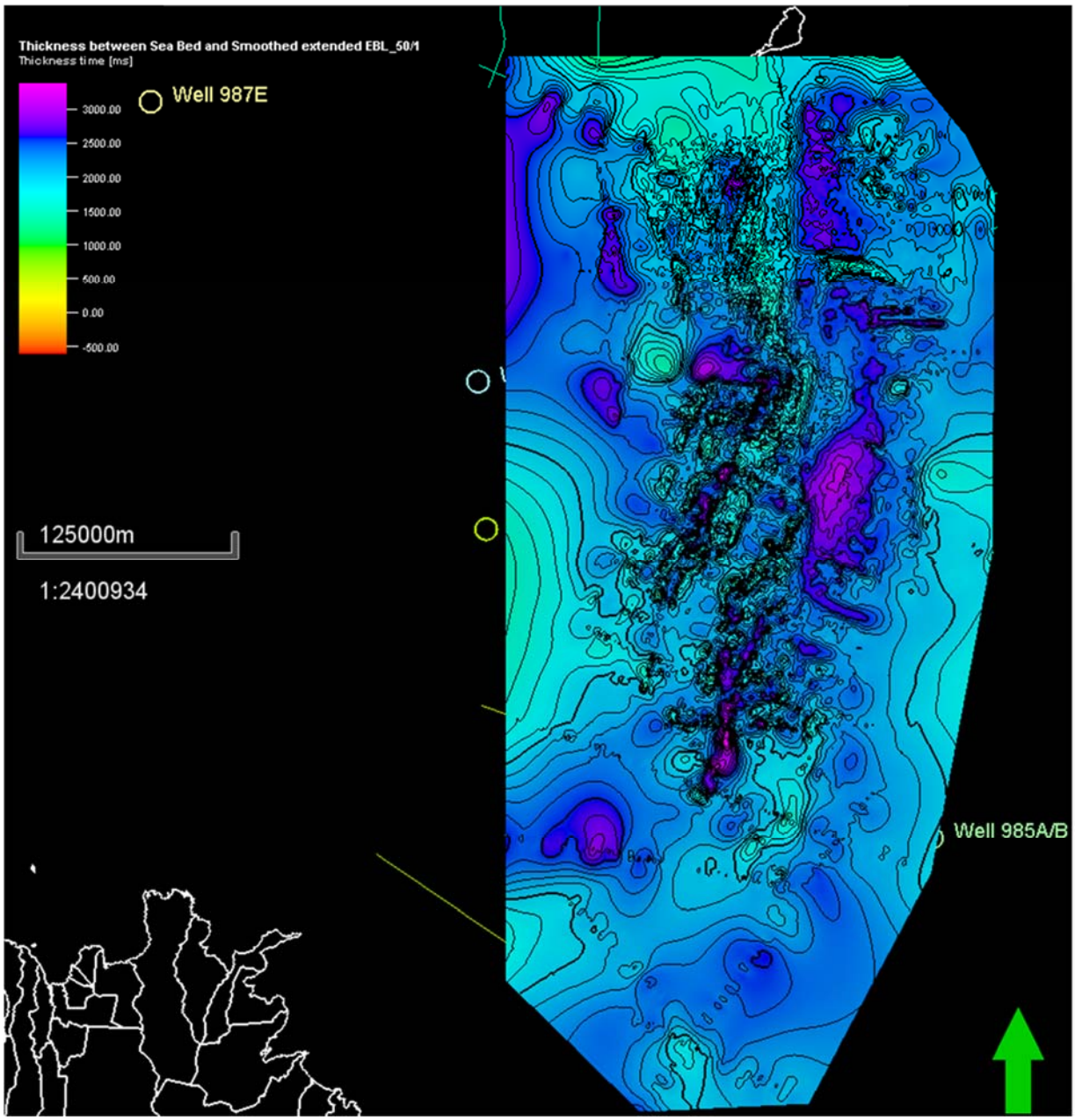

Figure 4.50: Isopach map between the Palaeocene-Eocene basalt layer and sea bed - Cenozoic sedimentary cover (Eocene to Present).

4.6 Seep Studies

A synthetic aperture radar imaging (SAR) seep study was undertaken in 2009 by Fugro NPA in search for natural oil seepage in the Dreki area (Jonsdottir & Valdimarsson, 2009). However, their study did not confirm the existence of natural oil seepage due to the presence of herring fishing ships and associated fish oil pollution in the area during the period of observation, obscuring the identification of natural seep patterns on the sea surface.

5. Conjugate margins

The tectono-stratigraphic diagram shown in Figure 2.1 synthesises the stratigraphic successions and main tectonic phases of the two conjugate margins to the JMMC; the East Greenland onshore Jameson Land Basin and offshore Liverpool Land Basin to the west and the Mid Norway Voring and More Basins to the east. Given the plate reconstructions and palaeogeographical maps of the NE Atlantic throughout the late Palaeozoic to Mesozoic (Figures 2.2, 2.3, 2.4, 2.5 & 2.6), it is likely that at least parts of the JMMC contain a similar pre-opening stratigraphy to its conjugates. Consequently, Figure 2.1 speculates on the upper Palaeozoic – Mesozoic stratigraphic succession that might be present, and most importantly the potential source-reservoir units that could be present within the JMMC.

5.1 East Greenland

The onshore geology of the East Greenland margin has been extensively studied by Larsen, (1980); Surlyk, (1980); Surlyk et al., (1981); Larsen, (1990); Stemmerik et al., (1997), (1998); Price & Whitham (1997); Surlyk & Ineson (2003) and Haman et al., (2005).

5.1.1 Jameson Land Basin

The onshore Jameson Land Basin is a N-S trending, coast parallel graben which formed in response to post-Caledonian extensional faulting and subsidence during the Devonian-Carboniferous, which continued into the Cretaceous (Figure 5.1).

Devonian continental sediments unconformably overlie Ordovician and older deformed basement. Important phases of block faulting and rifting took place during Early and Late Carboniferous and Late Permian. Syn-rift sedimentation, composed of continental fluvial sandstones and Upper Carboniferous type I-II (highly oil-prone to oil-prone) lacustrine shales (which are restricted in lateral extent) infilled fault bounded troughs.

Regional subsidence in the Late Permian over much of the NE Atlantic led to an extensive marine connection between Jameson Land Basin and the Barents Sea and European Zechstein Basin (Stemmerik, 2000). As such, the Permain Foldvik Creek Group records the development from fluvial basal conglomerate to shallow-marine carbonates and hypersaline evaporates. The carbonates form potential reservoir facies (Henriksen et al., 2009). The Upper Permian- Lower Triassic succession is dominated by deep marine organic rich type II source rock shales of the Ravenfjeld Fm, reflecting continued subsidence and transgression (Stoker et al., 2017). Continued rifting and rotational block faulting in the Triassic led to the deposition of the Scoresby Land Group reflecting of an upwards shallowing succession from marine shales and sandy turbidites to shoreface and coastal plain sandstones (forming potential reservoir units) and mudstones. The succession gradually transitions upwards into fine-grained floodplain, freshwater and saline lacustrine and Aeolian deposits of Mid to Late Triassic.

The latest Triassic to Mid-Jurassic was characterised by thermal subsidence whilst the main Mesozoic phase of rifting initiated in the Middle Jurassic, reaching a climax in the Late Jurassic forming strongly tilted fault blocks and waned in the Early Cretaceous. The Kap Stewart Group was deposited in the Rhaetian – Sinemurian, consisting of organic rich lacustrine type I-II source rocks (highly oil-prone to oil-prone) and deltaic reservoir sandstones (Henriksen et al., 2009). Marine transgression during the Pleisbachian – Early Bajocian lead to the deposition of alternating shoreface – restricted tidal embayment mudstones and sandstones of the Neill Klinter Group and potential shallow marine reservoir sandstones of the Vardekløft Group (Stoker et al.,

2017; Henriksen et al., 2009). Continued rifting and marine transgression during maximum sea level in the Upper Jurassic resulted in the deposition of the black organic-rich source rock marine shales (Kimmeridgian equivalent) and mass flow turbiditie (potential reservoir) sandstones of the Hareelv Fm. The Upper Jurassic marine shales are mainly gas-prone onshore, but likely oil-prone source rocks on the continental shelf to the east (Liverpool Land Basin) (Dam & Christiansen, 1990; Hamann et al., 2005). The uppermost Jurassic – Cretaceous transition is represented by the sandy shelf-edge deltaic sandstones of the Raukelv Fm and coarse grained sandstones of the Scoresby Sund Group which could act as reservoir units.

Further extensional faulting occurred in the Cretaceous where deep basins continued to develop, but rifting waned by the Hauterivian. The marginal – shallow marine Scoresby Sund Group is unconformably overlain by alternating basinal mudstones and gravity-flow sandstones (with reservoir potential) of the Hesteelv Fm (Stoker et al., 2017).

Plateau basalts cover an extensive area on the East Greenland margin, resting on Mesozoic sediments in the east and Caledonian-Precambrian gneisses in the west. Over the eastern margin of the Jameson Land Basin, early Tertiary basic sills and dykes intrude into the Mesozoic stratigraphy and reflect episodes of magmatism linked to continental break-up of the NE Atlantic from Late Palaeocene to Oligocene.

5.1.2 Liverpool Land Basin

In the inner part of the Liverpool Land Basin contains a large prograding wedge of Cenozoic sediments up to 6km thick, which was sourced from the mouth of the present day Scoresby Sund area, unconformably overlying a block-faulted Upper Palaeozoic-Mesozoic sedimentary sequence (Figure 5.1). In the outer part of the basin, a Neogene and Plio-Pleistocene succession overlies oceanic crust which formed along the 2nd break-up phase of the Norwegian-Greenland Sea from Chron 6 (late Oligocene or older) (Figure 5.1) (Henriksen et al., 2009).

In other offshore areas along the SW Greenland shelf, the Palaeogene succession contains sandy basin floor fans and turbidite channel complexes encased within basinal mudstones that could also be present in the offshore Liverpool Land Basin (and deposited over the JMMC prior to separation from East Greenland), forming potential stratigraphic traps (Larsen et al., 2002). Onshore analogues of the Palaeocene succession in SW Greenland identify submarine fans and channel-levee complexes (Early Paleocene), unconformably overlain by fluvial sandstone and conglomerate successions (Mid-Late Palaeocene) recording sea-level highstand followed by regional uplift and basin-wide erosion, which could be good potential reservoir units (Larsen et al., 1999; Henriksen et al., 2009). The overlying Early Palaeogene volcanic sequence also contains hyaloclastities, tuffs and sediments at its base (Henriksen et al., 2009), of which the hyaloclastites could also possess potentially good reservoir qualities. Furthermore, corroboration of a potential post-basalt/Cenozoic reservoir unit on the JMMC was made by the NPD ROV sampling expedition (see section above). A quartz rich unit and overlying fine grained sediments were identified from the JMMC ridges, which could correspond to the Bopladsdalen Fm and Krabbedalen Fm respectively that outcrop in Kap Dalton area of East Greenland (NPD Resource Report, 2013; Larsen et al., 2002).

Structural and stratigraphic plays are present within onshore and offshore East Greenland basins. The main risk factor in Jameson Land Basin is the effect of Palaeogene and Neogene uplift and tilting which could be up to 2 km or more (Mathieson et al., 1995; Henriksen et al., 2009) and Tertiary volcanism (Haman et al., 2005). However, Haman et al., (2005) suggest that Tertiary

volcanism and later Cenozoic uplift events are unlikely to have severely reduced the prospectivity of the region. Conversely, for the JMMC it is possible that any hydrocarbon systems present will have been affected by higher heat flow regimes during prolonged rifting events of the multi-stage break-up of the NE Atlantic, extrusive and intrusive Tertiary volcanics, and rift-related uplift during separation of the JMMC from the More Margin and later dislocation from the East Greenland Margin.

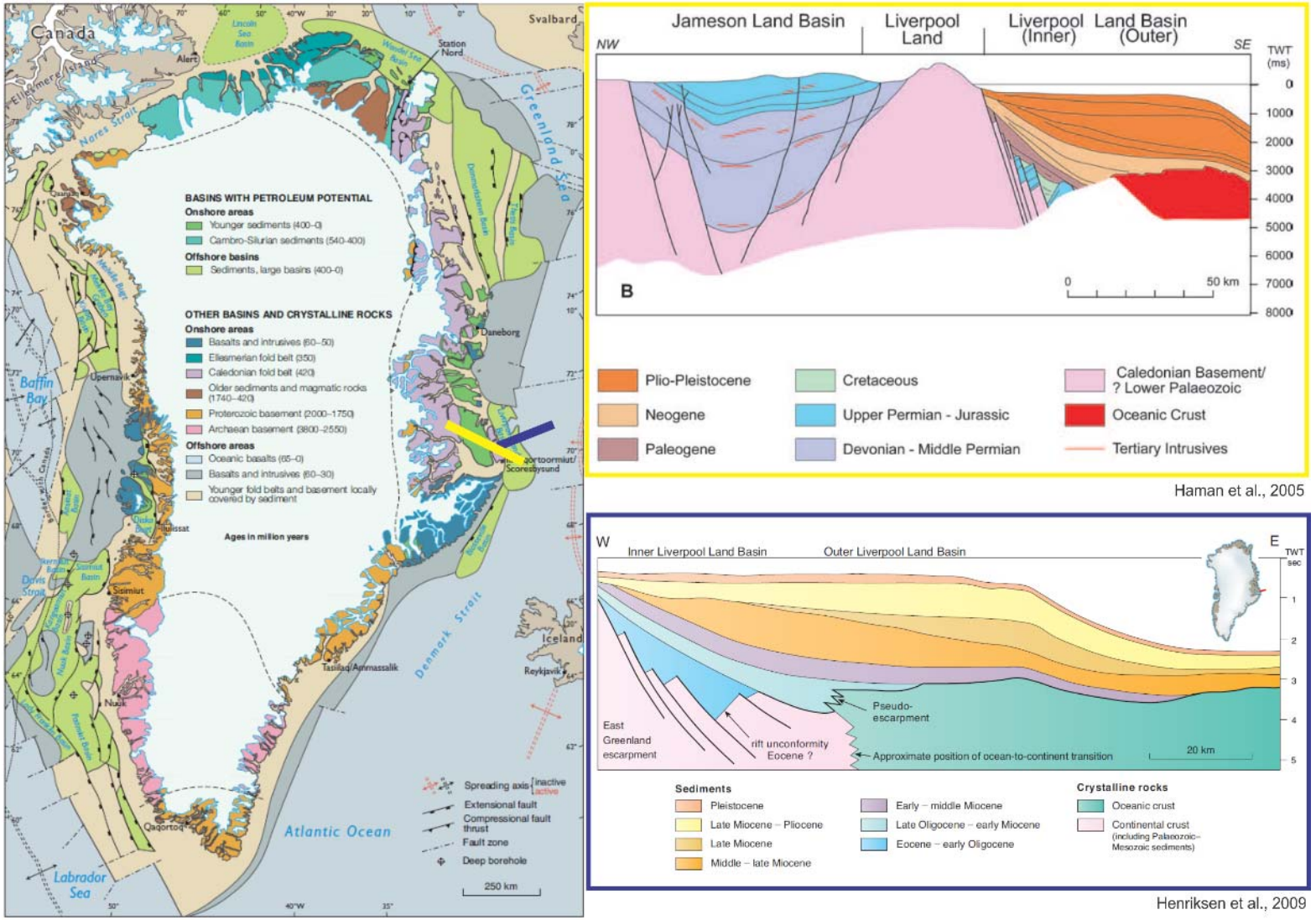

Figure 5.1: East Greenland basin structure and cross sections across the onshore Jameson Land Basin and offshore Liverpool Land Basin (taken from www.geus.dk/uk; Haman et al., 2005 & Henriksen et al., 2009).

5.2 Mid Norway (More Margin)

The volcanic rifted margin offshore Mid-Norway has been extensively studied by Brekke et al., (1999/ 2001); Brekke, (2000); Skogseid et al., (1992/ 2000); Skogseid & Eldholm (1987/1988); Lundin & Dore, (1997); Dore et al., (1997) and Faleide et al., (2010) to name a few.

The Mid- Norwegian margin consists of a continental shelf and slope that vary considerably in width and morphology across the three main segments, Møre, Voring and Lofoten-Vesterålen, from south to north, respectively. It is the Møre Basin and the southern part of the Voring Basin which form the eastern conjugate to the JMMC (Figure 5.2). Both basins are separated by the Jan Mayen Lineament, an onshore extension of the East Jan Mayen Fracture Zone in the Norway Basin, and which marks a sinistral lateral shift of basin axes and flanks (Brekke et al., 1999).

The Møre and Voring Basins are NE-SW trending deep Cretaceous basins composed of sub-basins separated by intrabasinal highs and flanked by palaeo-highs and platforms, formed during the late Mid-Jurassic to Early Cretaceous rifting. The basins dips steeply basinward to the west where crystalline crust thins rapidly from >25 km to <10 km (Figure 5.2)(Faleide et al., 2010).

Late Carboniferous to Permian rifting likely generated block-faulted half graben structures beneath the Trøndelag Platform and Halten Terrace at the inner basin margins. Given the extreme thickness of the Cretaceous stratigraphic succession in these basins, the Carboniferous to Permian stratigraphy is best constrained on the easternmost margins. It is inferred that early syn-rift continental alluvial and fluvial clastics were deposited at this time, which could represent potential reservoir units.

Rifting and rotational block faulting continued into the Permo-Triassic, allowing deposition of shallow water carbonates (dolomites) of the Zechstein Group (Faleide et al., 2010; Stoker et al., 2017). Faulting waned and tectonic subsidence dominated in the Mid-Late Triassic, which recorded a change from arid "red beds", marginal marine evaporites and organic rich shales deposited in isolated sub-basins to be replaced by continental fluvio-lacustrine and alluvial facies deposited under humid conditions "grey beds" to be preserved by the Rhaetian.

Throughout much of the Early-Mid Jurassic, the Mid Norway Margin was subject to uplift and erosion (Brekke et al., 1999; Dore et al., 1999). The Latest Triassic-Early Jurassic Båt Group contains organic rich lacustrine shales, coals and deltaic sandstones of the Åre Fm deposited under lacustrine/lagoonal to shallow marine conditions; which are potentially good source and reservoir intervals and equivalent to the East Greenland Kap Stewart Group. The overlying Fangst Group (Mid-Jurassic) reflects continued deposition of shallow marine-deltaic sandstones and mudstones. However, the influx of sand from the west and north forming the Ile and Garn Fms, suggests the existence of a thermally uplifted hinterland area to the west along the axis of incipient rifting, to allow erosion of transportation of coarse grained sand into the More and Voring Basins during the Middle Jurassic (Brekke et al., 1999; Dore et al., 1999). Larsen (1987); Brekke (1999) and Dore et al., (1999) hypothesise that the areas of the mid Norwegian shelf that were later the deepest part of the basin after subsequent Late Jurassic to early Cretaceous rifting, were the highest elevated areas forming a central land block, restricting marine connectivity between Norway and East Greenland at this time.

The main phase of tectonic rifting on the margin occurred during the Late Jurassic to Early Cretaceous creating highly attenuated crust and a series of tilted half graben sub-basins and structural highs (Brekke et al., 1999). The marine sea-way transgressed large parts of the area and deposition of the Viking Group (late Mid-Jurassic to earliest Cretaceous) during this time was

dominated by open marine conditions, with likely fault-scarp related shallow marine and turbidite sands forming on the terraces and platforms. Organic rich marine shales of the Spekk Group are potentially an excellent source rock interval on the Mid Norwegian margin, corresponding to the "Kimmeridge" and Hareelv Fm equivalents in the North Sea and East Greenland, respectively (Stoker et al., 2017). The upward transition from lacustrine/lagoonal to shallow marine to deep open marine reflects the overall transgressive nature of the Jurassic succession.

Subsequent Cretaceous subsidence was driven by flexure of the basin flanks rather than active faulting enabling in an exceptionally thick Cretaceous succession of mixed clastic to carbonate fine grained sandstones, claystones marls and carbonates of the Cromer Knoll Group to be preserved, infilling much of the structural relief by the Mid-Cretaceous (Faleide et al., 2010). Submarine gravity flows (sandstones and conglomerates) sourced from the elevated platforms on the eastern Voring and Møre Basins, were interbedded with Aptian and Albian transgressive deep organic rich marine shales (Brekke et al., 1999). These deep marine turbidite sandstone and mudstone deposits could form potential stratigraphic traps.

Compressional deformation causing tilting and uplift along the westernmost margin, formation of inversion structures such as the Gjallar Ridge and Nyk and Utgard highs and unconformities in the Voring Basin occurred during the Cenomanian. The Lysing Fm (of the Shetland Group) represent local coarse grained submarine fans eroded from the uplifted western basin margin flanks during the Turonian/Coniacian, which could form good reservoir units (Brekke, 1999/ 2000; Faleide et al., 2010; Stoker et al., 2014). Sediment provenance studies for some of these coarse grained clastic units indicate an East Greenland source from early Cenomanian to early Campanian times (Whitham et al., 2004; Morton et al., 2005). The Møre Basin was tectonically quiescent and underwent thermal subsidence since the Late Cretaceous (Brekke, 2000), during which time maximum regional marine transgression occurred. Organic rich marine shale potential source rock intervals are identified in the uppermost Cenomanian and upper Campanian occurring within the Shetland Group.

Prior to NE Atlantic break-up, the area underwent a period of rifting and thermally generated regional uplift during the Maastrictian to Danian, causing a shallowing of the basins and emergence of the surrounding flanks and platforms. This is reflected in a change to shallow marine mudstones and fluvio-deltaic sandstones of the Rogaland Group; a pattern also observed on the conjugate East Greenland margin during the early Palaeocene (Larsen et al., 1999; Brekke et al., 1999). These Palaeocene deltaic sandstones (likely forming delta-like wedges prograding into the basins from the uplifted surrounding highs and platforms) are of good reservoir quality in the Møre Basin (Brekke et al., 1999).

Large volumes of Palaeocene-Eocene tholeiitic lava flows covered much of the outer margin of the Møre and Voring Basins forming characteristic seaward dipping reflector sequences and sill complexes intruded into the thick Cretaceous succession in central and western parts of the basin margin (Faleide et al., 2010).

Since the Mid Eocene, the Mid-Norwegian margin developed into a passive rifted margin and underwent thermal subsidence giving an increased westward tilt of the whole margin (Brekke, et al., 1999). The Voring Basin experienced compressional tectonism during the Middle Miocene forming domes, erosional hiatuses and reverse faulting; whereas the Møre Basin did not experience any post-Eocene deformation. Consequently, fine grained mudstones, siliceous oozes and minor sandstones of the Hordaland Group and Nordland Group infilled the significant

submarine topography of the Voring Basin but are evenly and continuously distributed across the Møre Basin. Prograding wedges of Plio-Pleistocene sandy/silty mudstones and ice-rafted debris of the Naust Fm are present over much of the Mid-Norwegian shelf, reflecting increased erosion of the mainland from successive glaciations (Brekke et al., 1999; Faleide et al., 2010).

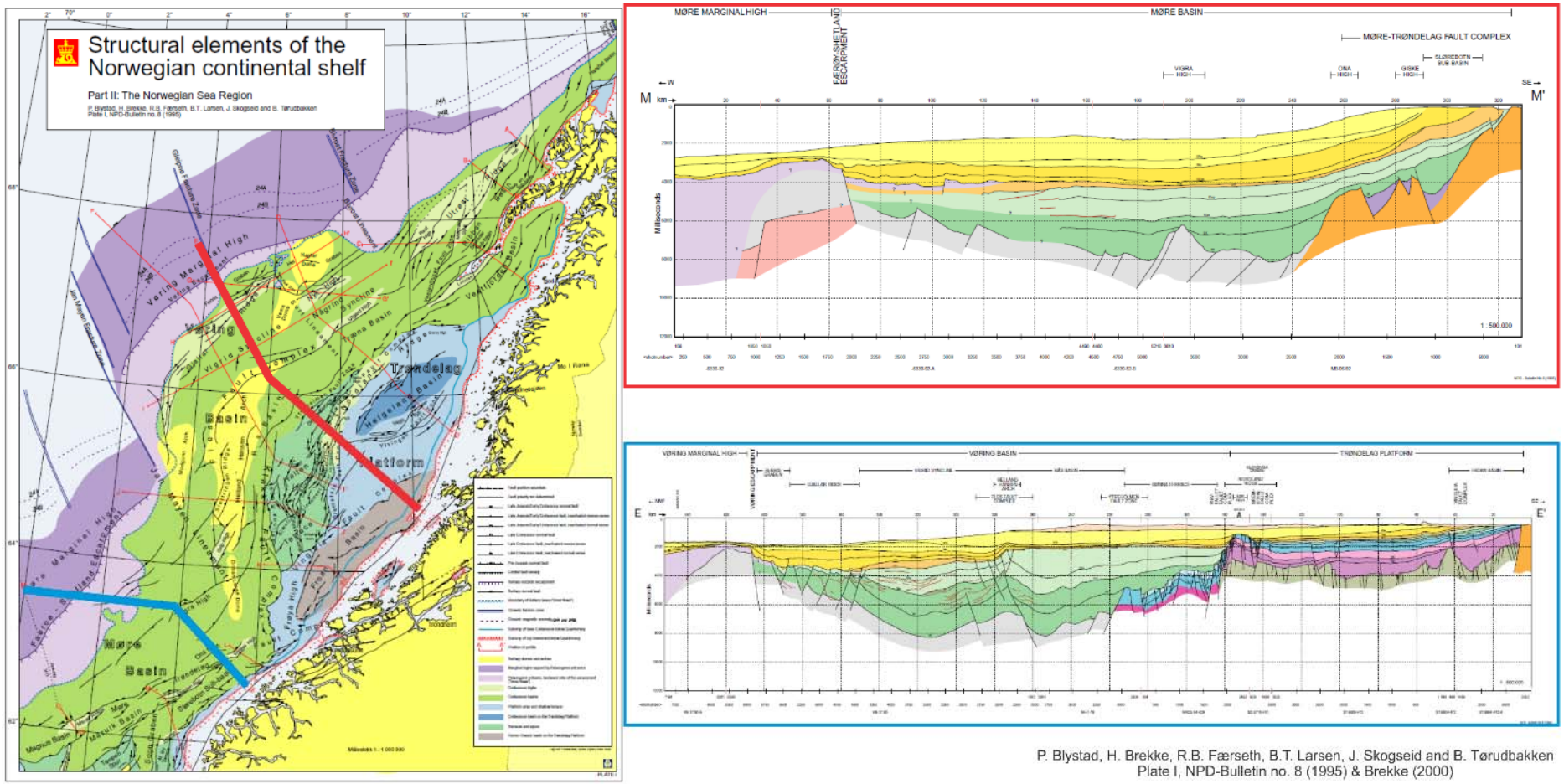

Figure 5.2: Mid Norway basin structure and regional cross section across the Vøring and Møre Basins (taken from NPD Bulletin 8 (1995) & Brekke (2000)).

6. Implications of Basin Modelling for Petroleum Prospectivity

6.1 Heat flow Analysis

Estimates of heat flow through geologic time are required in order to build a basin model; however, due to a lack of direct evidence from wells penetrating the Mesozoic/Palaeozoic succession of the JMMC, ranges of surface heat flow from the Norwegian-Greenland Sea and conjugate margins are used. Gunnarsson et al., 1989 used present heat flow estimates of 85 mW/m^2 on the western flank of the JMR and 65-70 mW/m^2 ontop of the main ridge and eastern margin. They also used two heat flow models (low case of 70 mW/m^2 and high case of 100 mw/m^2) to account for uncertainties in the heat flow history of the JMMC during N. Atlantic break-up. However, both of their models assume a constant heat flow through time. This is not realistic in incorporating the 2 phases of heat pulses associated with Ægir and Kolbeinsey Ridge seafloor spreading events or representing a likely heat flow decay since 25Ma after the JMMC separated from the East Greenland margin.

Comparisons with studies of present day surface heat flow in the Norwegian-Greenland Sea, Mid Norway Margin and East Greenland can help to refine present day heat flow regimes and make geological inferences of past heat flow regimes affecting the evolution of the JMMC. Langseth & Zielinski (1974) and Sundvor et al., (2000) conducted comprehensive studies of the Norwegian-Greenland sea thermal fields. The ranges of surface heat flow for the JMMC and conjugate margins are presented in Table 5.

Author/Study	**Mean heat flow value mW/m^2 (plus standard deviation where present)**						
	East Greenland	JMMC				Mid Norway	
	Continental shelf	Western margin	JMR	SRC	Eastern Margin	More Basin	Voring Basin
Langseth & Zielinksi (1974)	104.6	82.4		76.1	76.9	50.2	58.6
	128.8	79.5			71.5	27.2	41
		87.8			71.5	20.9	86.6
					66.9	25.9	
					71.1	20.5	
						51.8	
						47.3	
						66.9	
Sundvor et al (2000)	70	75	75.2	90	65	50	50
	80	90	90	85	60	55	55
	90	70	65	80	40	52	62
	98	85	75	75	45	45	66
	132	90	70	65	45	40	70
			75	62	70	65	71
			80	65	50	60	
			70		56	55	
					75	52	
						35	

Table 5: Surface heat flow estimates of relevant provinces (JMMC & conjugate margins) across the Norwegian-Greenland Sea.

Figure 6.1 shows a surface heat flow map across the Norwegian-Greenland Sea shows the JMMC situated in an area of values ranging from 75 mW/m^2 on the eastern margin to ~100 mW/m^2 on the western flank of the JMR (Slagstad et al., 2009).

By comparison, surface heat flow estimates on the Mid Norwegian Shelf identify a mean of 58.5 $mW/m^2 \pm 4.40$ mW/m^2 in the Voring Basin and 56.2 ± 6.65 mW/m^2 on the Trondelag Platform (Ritter et al., 2004). Conversely, Sundvor et al., (2000) estimate mean heat flow values of 67.3 ± 12.4 mW/m^2 in the Voring Basin and 51.5 ± 13.9 mW/m^2 in the More Basin.

Modelling of heat flow and hydrocarbon generation through time in the Jameson Land Basin infer a late Cretaceous heat flow at 33.47 mW/m^2, and a slight increase to 41.84 mW/m^2 during 65 – 55Ma (Mathieson et al., 1995). They model tertiary volcanism in as a 2 stage event with an initial heat pulse of 58.57 mW/m^2 at 55Ma, rapidly declining to 43.93 mW/m^2 by 45 – 40Ma. From 40Ma to present day, heat flow was modelled at 41.84 mW/m^2.

Moore and Pitman's (2018) USGS study modelled the JMMC's thermal history using a pre-break up surface heat flow of 60 mW/m^2; 80 mW/m^2 for the period 55 – 20 Ma (combining the 1st and 2nd rift to drift phases), with a monotonic return to 60 mW/m^2 in the present day. However, Scotchman et al., (2006) study of the Faroe Shetland Basin emphasises the importance of incorporating the complexity of elevated heat flows during each individual period of rifting and volcanic activity into the thermal history model.

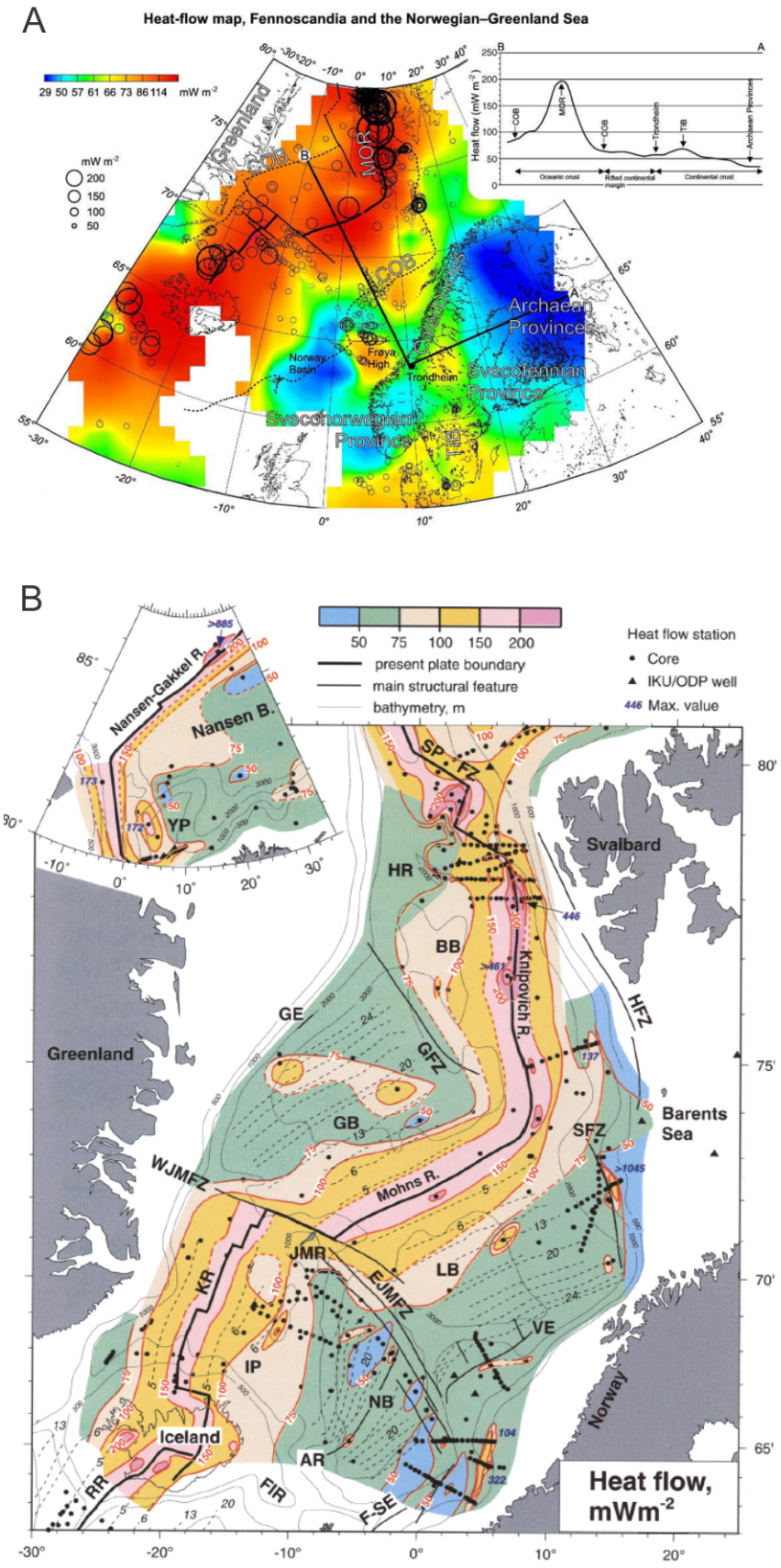

Figure 6.1: Heat flow maps of the Norwegian-Greenland Sea (A is taken from Slagstad et al., (2009); B is taken from Sundvor et al., (2000)).

It is clear from this analysis of heat flow in the area, that there is a large variability in heat flow both across the Norwegian-Greenland Sea from one conjugate margin to the other and also across the published literature (Table 5 & Figure 6.1). However, what can be deduced is that the surface heat flow temperatures used in recent basin modelling studies (and will be used in this research, see section below) fall within the range presented here.

6.2 Basin Modelling

Basin modelling was undertaken using Shell's proprietary BPA-CAULDRON program. However, calibration of the basin model is problematic due to the lack of deeper stratigraphic wells in the region. As such the JMM location of the pseudo-well on the western flank of the Jan Mayen Ridge from Moore and Pitman (2018) USGS professional paper 1824, was used to test and compare the burial graphs and resultant source rock maturity graphs. Burial graphs in figures 6.2 to 6.4 represent the presumed burial history for the JMM location. Figure 6.2 shows the burial curve with sea-level as a datum, whereas figures 6.3 show the same burial graph using the seabed as the datum so a direct comparison can be made with the USGS report.

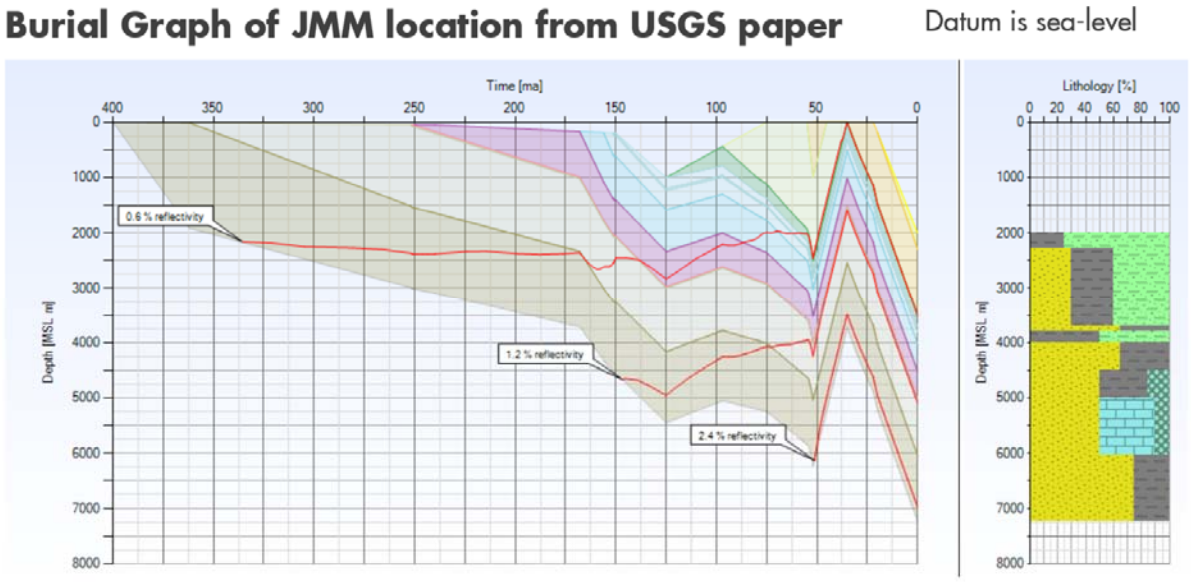

Figure 6.2: Base model burial graph for the JMMC using sea-level as the datum.

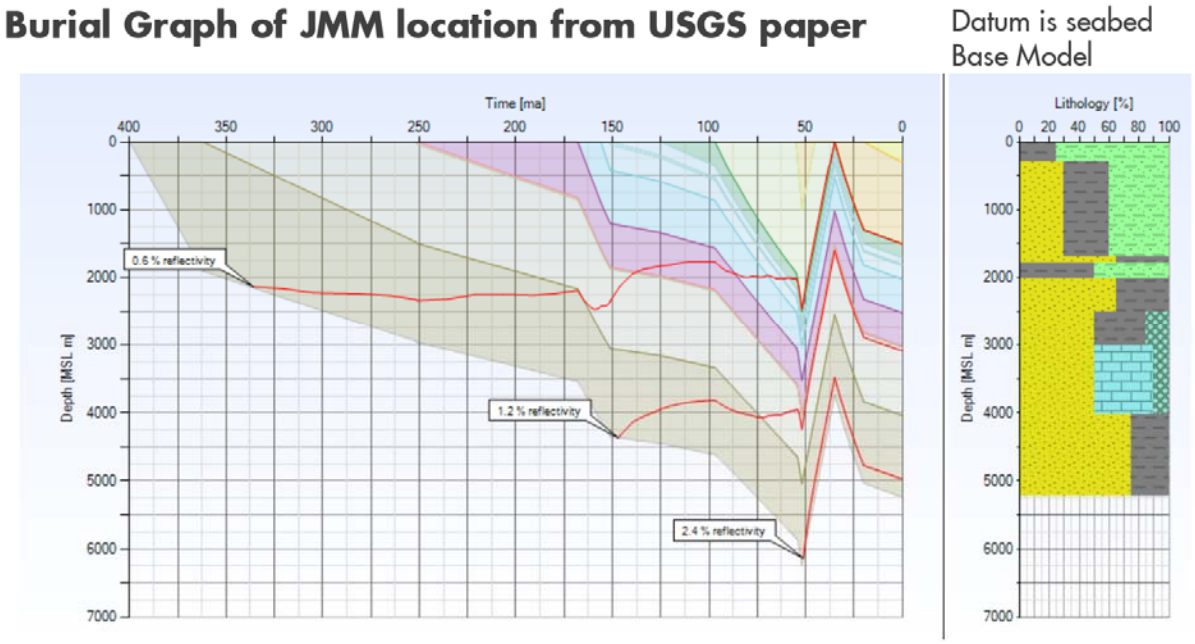

Figure 6.3: Same burial graph as in Figure 6.2, but with seabed as the datum so a direct comparison can be made with Moore and Pitman (2008) study.

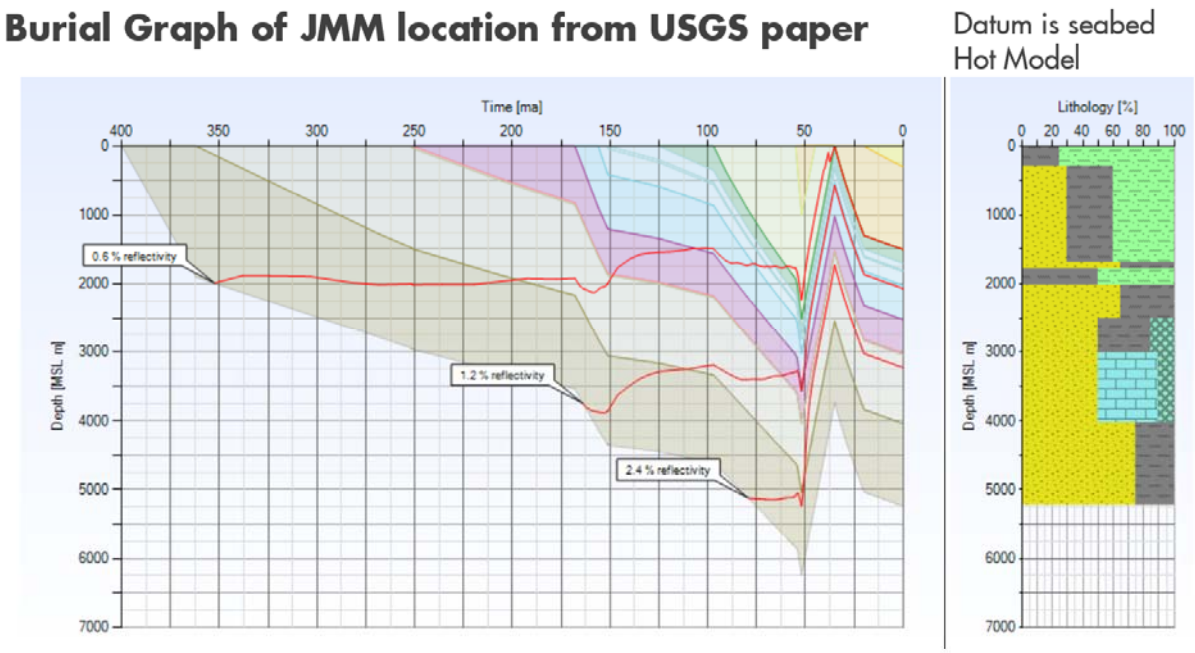

Figure 6.4: Hot model burial graph as in Figure 55, but with seabed as the datum so a direct comparison can be made with Moore and Pitman (2008) study.

Two heat flow scenarios have been used which are in line with the present day heat flow and take allowance of the impacts of rifting and elevated heat flows due to the presence of the Iceland plume (Figures 6.5 & 6.6). The base case is comparable to the USGS model, although it should be noted that the USGS model reports base sediment heat flow which is an input for their model (Figure 6.5). The "hot" case model assumes a higher heat flow regime, both during rifting and also during the Paleogene uplift event associated with the Iceland plume (Figure 6.6).

In BPA-CAULDRON, heat flow is an output of the model, a result of the crustal composition, tectonic history and sedimentation. The heat flow reported here is surface heat flow. In the base case, background surface heat flow is around 55 mW/m^2 rising to 75 mW/m^2 at the height of plume and rifting activity at ~37 Ma (Figure 6.5). A second hot case model was run with a background surface heat flow of around 65 mW/m^2 rising to 105 mW/m^2 at the height of plume and rifting activity (Figure 6.6). These values fall within the range of heat flow values published for the region. An assumption of 2 km uplift at this location at 50 Ma has been made for both base and hot case burial graphs in these models. Gunnarsson et al., (1989) estimate that 1 to 1.5 km of sediments were removed from the main ridge during Eocene-Oligocene uplift and erosion. However, 2 km of eroded missing section has been assumed for these models based on estimates from the East Greenland margin (Mathieson et al., 1995; Hamann et al., 2005; Henriksen et al., 2009).

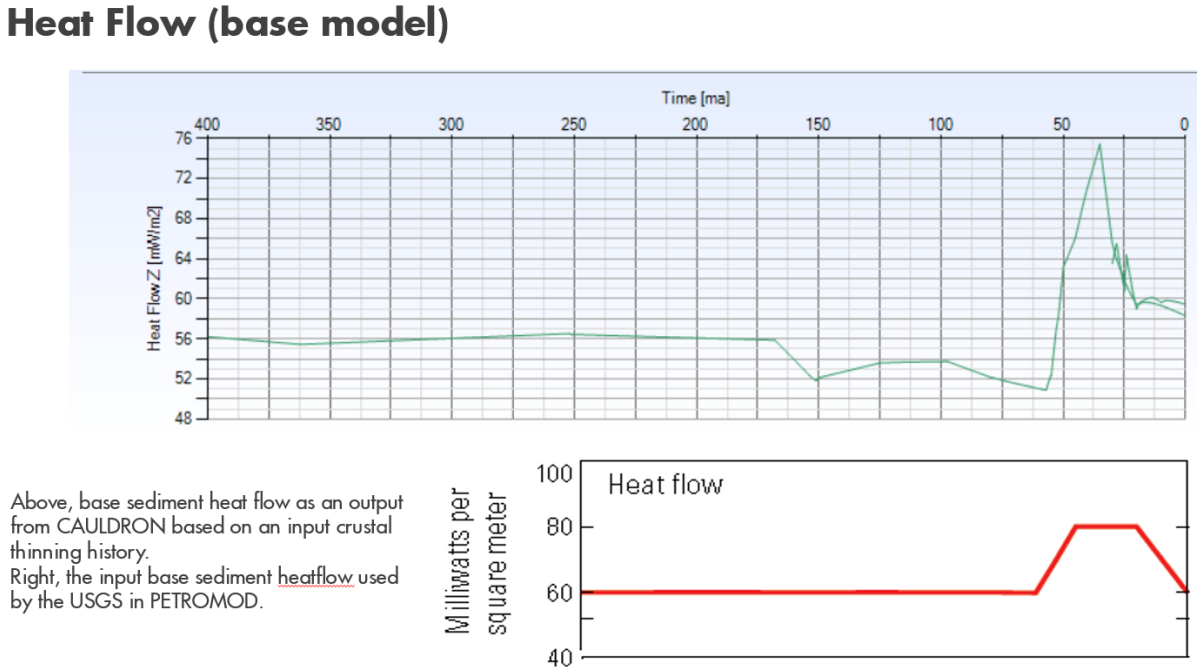

Figure 6.5: Heat flow model for the base case scenario (comparable to the USGS study).

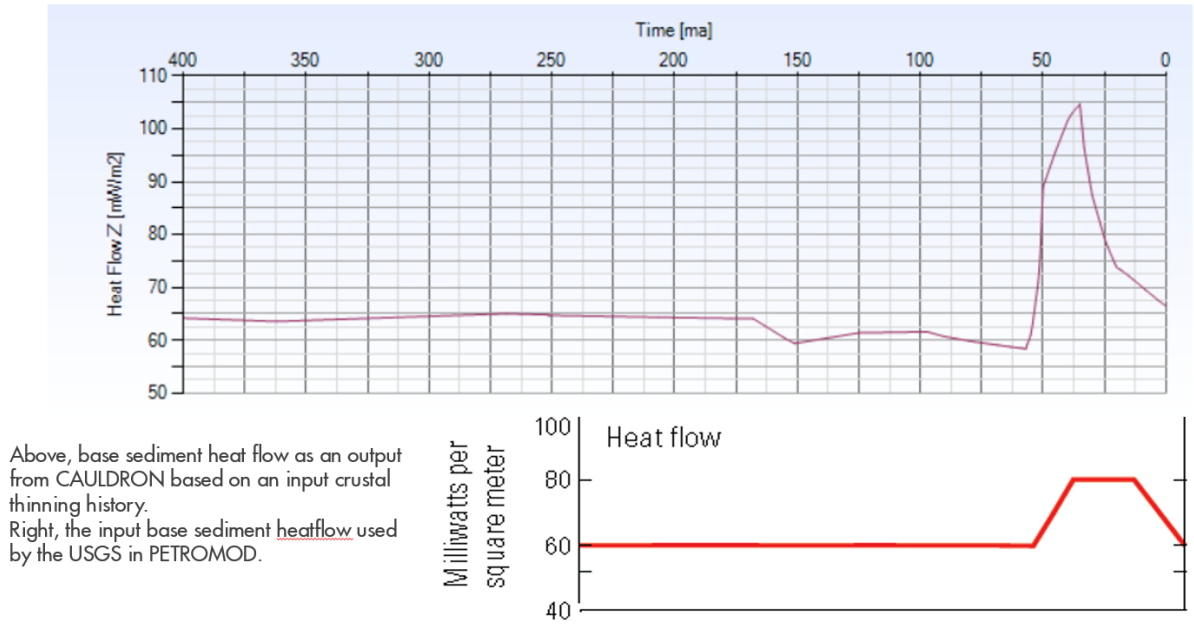

Figure 6.6: Heat flow model for the "Hot" model scenario.

Geochemical studies of DSDP wells over the JMMC found "no occurrences of hydrocarbons encountered at sites 346, 347 and 349" and the low TOC and hydrocarbon pyrolysis values of the samples suggest that it is doubtful that the sediments can be considered potential source rocks (Talwani et al., 1976). Gunnarsson et al., (1989), speculate on the possibility of an Early Eocene organic rich deep marine shale being present and prospective as a source rock in the area based on palaeogeographic reconstructions at that time interval. The entire Tertiary succession has not been fully sampled/drilled and although an Eocene source rock being present cannot be ruled out entirely, it remains hypothetical. Hence a potential Tertiary source rock interval was not considered for basin/ source rock maturity modelling.

Consequently, the models have assumed 2 source rock intervals being present. Both are 20 metres in thickness; one in the Late Jurassic corresponding to the Hareelv Fm from East Greenland and Spekk Fm from Mid Norway, while the second corresponds to the Ravnefjeld Fm (East Greenland) or Zechstein Gp (Mid Norway) in the Late Permian (Figure 2.1). In the base case scenario, both source rocks reach the oil window in terms of maturity, with the Jurassic SR being just mature, by 50 Ma. Both reach maximum maturity prior to the 50 Ma uplift event, with no further increase in maturity after this time (Figure 6.7). In the hot case, the Permian SR reaches the late gas window while the Jurassic SR is fully oil mature by 45 Ma. As with the cooler case, maximum maturity is reached around 45 – 50 Ma and there is no increase after this point in time (Figure 6.8). Temperature profiles for both base and hot model cases show a dramatic decrease in temperatures after the ~50 Ma rifting and plume event when maximum temperature is achieved (Figure 6.7 & 6.8). Moreover, the temperature profiles show an increase in temperature of both the Permian and Jurassic source rocks during the second rift-drift phase separating the JMMC from East Greenland ~37 – 20 Ma. However, the temperatures do not reach or exceed pre-rifting/mantle plume temperatures to turn the source rock kitchen back on again to potentially generate more hydrocarbons (Figure 6.7 & 6.8).

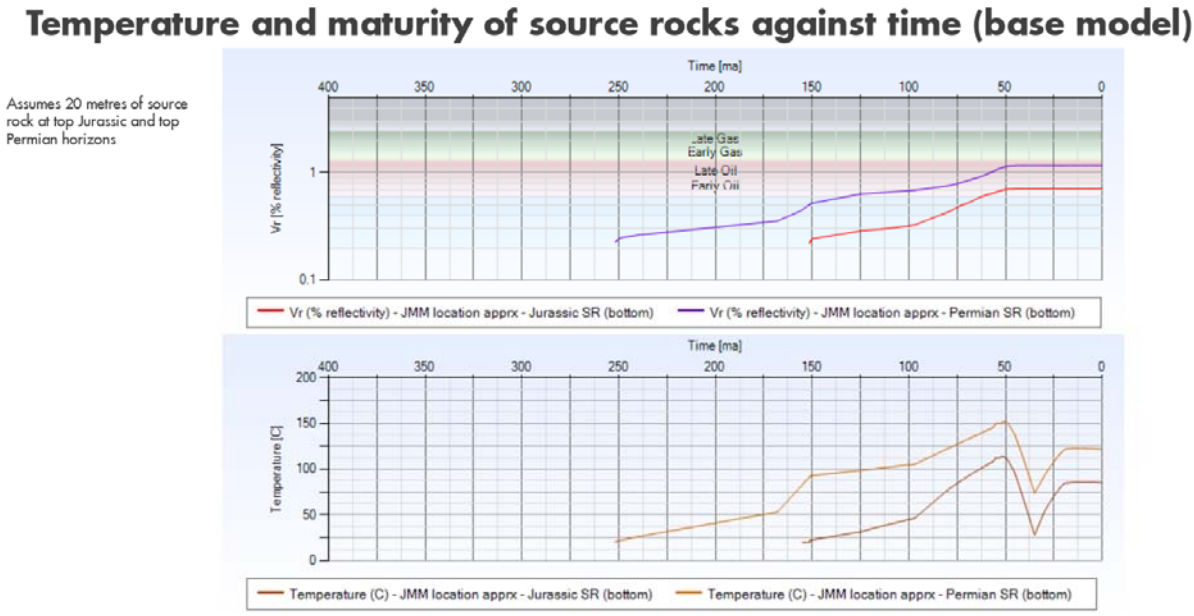

Figure 6.7: Hydrocarbon maturity and temperature graphs under "base case" model heat flow regimes.

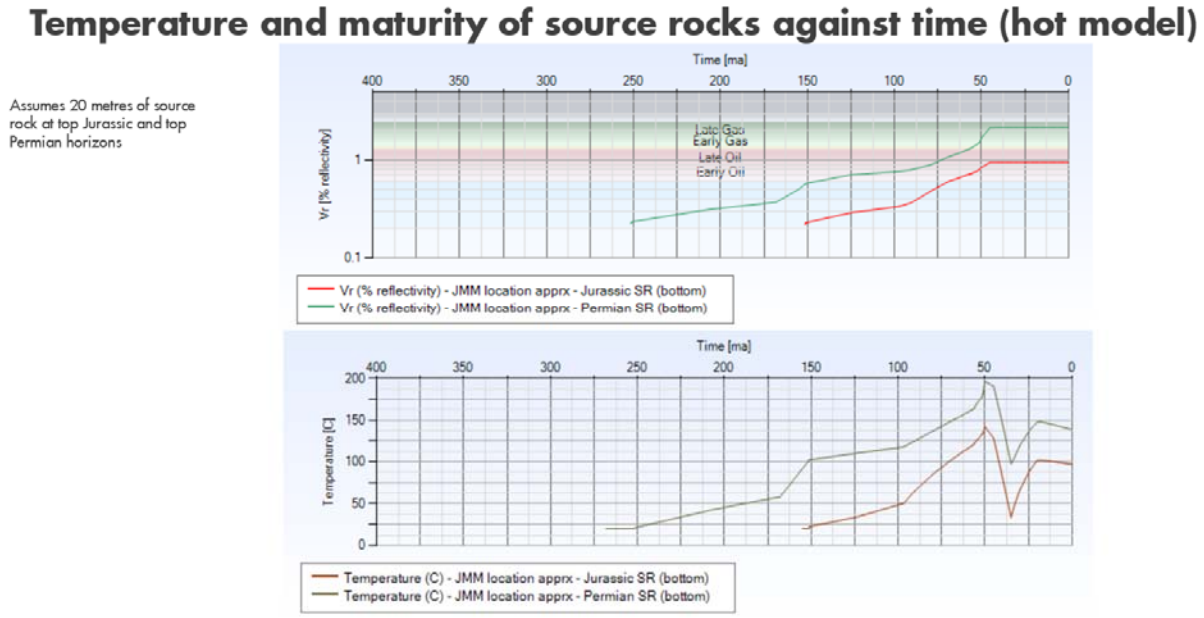

Figure 6.8: Hydrocarbon maturity and temperature graphs under "Hot" model heat flow regimes.

Figures 6.9 – 6.10 show the oil and gas expulsion rates against time with respect to the two basin models. It has been assumed that the marine sources rock consist of Type II kerogen. The thermal histories of the base case would predict significant oil charge from the Permian prior to 50 Ma when the petroleum system is switched off, with marginal to no charge from the Jurassic SR (Figure 6.9). In the hot case, the Permian SR would be almost exhausted for oil by the time of the 50 Ma uplift and rift event while the Jurassic would be a significant source of charge (Figure 6.10). Both Permian and Jurassic source rocks would be significant sources for gas charge in this hot model (Figure 6.10).

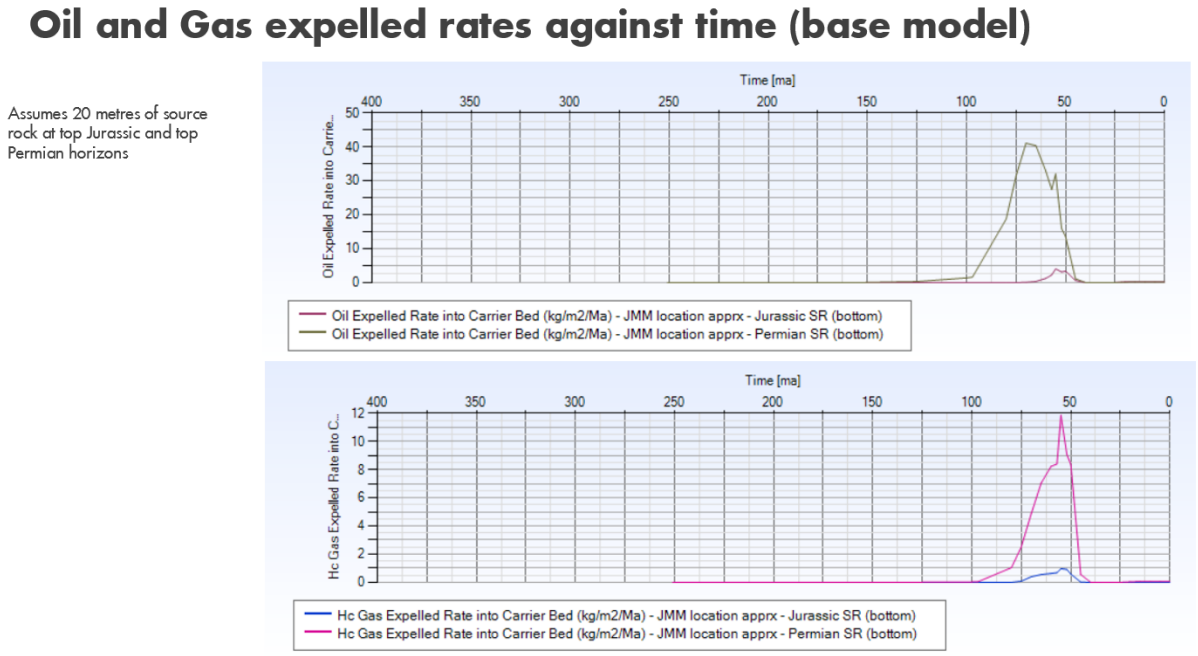

Figure 6.9: Base model oil and gas expulsion rates against time.

Figure 6.10: "Hot model" oil and gas expulsion rates against time.

6.3 Implications

Although the 1D basin model that has been run for the USGS JMM location is relatively poorly constrained, it does give some insights into the possible charge system in the region. Assuming that the stratigraphy underlying the Tertiary volcanics is comparable to the conjugate margins in Norway and East Greenland, the models suggest that the potential for source rock presence is high. While the exact stratigraphic position is uncertain, the modelled horizons of Top Jurassic

and Top Permian allow a range of possible stratigraphic positions to be considered. The missing section and associated erosional unconformity in the Paleogene is also problematic in that the exact amount of missing section is unknown. The two thermal models considered are reasonable for the tectonic setting and in line with regional observations. With all these uncertainties considered, there is a reasonable possibility that the source rocks have reached maturities sufficient for the generation of hydrocarbons. The main issue however, is that charge has all occurred prior to the uplift and erosion events associated with continental break-up and subsequent plate reorganisations.

Table 6 shows a Petroleum Systems chart. This has been developed in conjunction with the tectonostratigraphic synthesis diagram in Figure 2.1, which aims to synthesise the tectonic elements affecting the JMMC and petroleum system (if present) through time and speculate on the timings of maturation/charge vs structuration for the microcontinent.

HERIOT WATT UNIVERSITY

Petroleum Systems Chart for the JMMC

Author: G. Heldreich
Date: March 2018

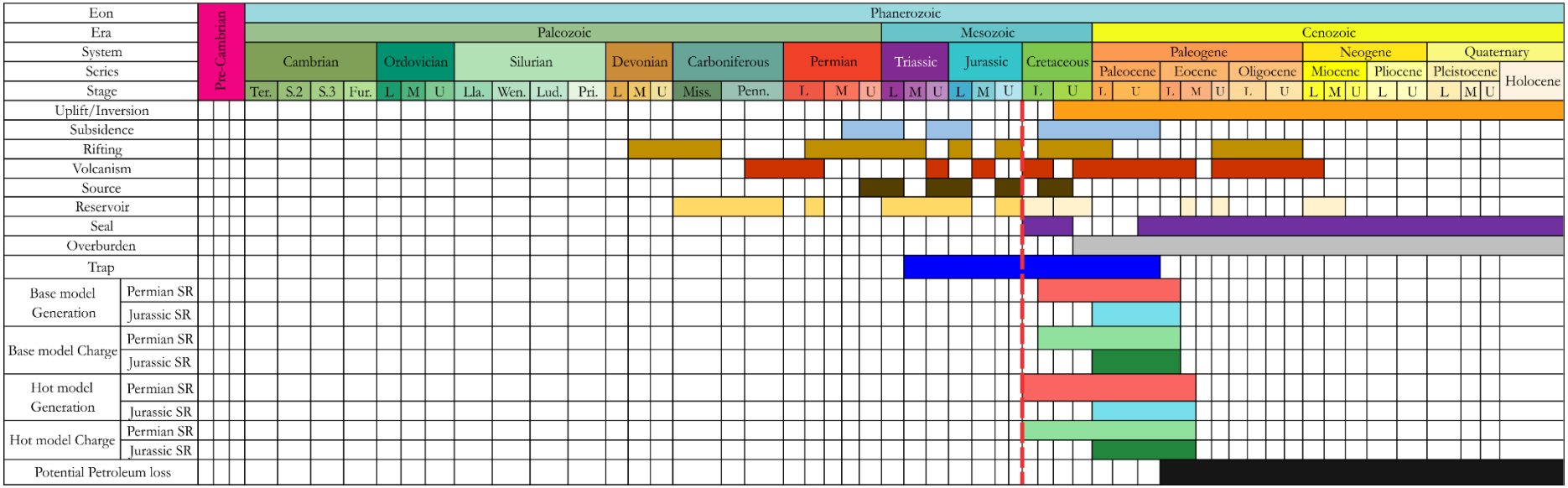

Table 6: Petroleum Systems Chart for the JMMC. Red dashed line marks the earliest critical moment for hydrocarbon generation predicted from basin modelling. (Note: Tectonic events and reservoir, source rock and seal intervals based on synthesis of regional and conjugate margin literature. The source rock "generation" is based on basin and maturity modelling (base and hot models) using the JMM pseudowell location from Moore & Pitman (2008) USGS report and present timings of source rock intervals (Upper Permian & Upper Jurassic)).

Charge prior to a major structural re-organisation event is problematic and any prospect would have high risks for charge. In order to maximise the chances of charge in this region then the following factors would be beneficial. A region where post 50 Ma subsidence and sedimentation exceeds the amount of eroded material at the 50 Ma event would result in a situation where source rocks could generate hydrocarbons after the unconformity. If this is not the case then a reliance on charge prior to 50 Ma being preserved during the uplift and erosional event would be required. Structures would have to be deep below the unconformity surface to be protected from breaching and ideally at depths where biodegradation has not occurred. The structures would also have to be away from any faults that reached the unconformity surface. Decompression of gas saturated fluids on uplift could also lead to breaching of seals, gas-cap creation and spillage during uplift. In total, while the chance of pre-uplift charge being found in old traps cannot be excluded, there is a severe risk that all charge in this part of the basin is palaeo-charge and the chance of palaeo-accumulations surviving the uplift event is low.

7. Discussion & Implications

7.1 Potential Hydrocarbon Traps and Plays

For a hydrocarbon system to work within the JMMC, 7 fundamental criteria must be met; potential source rocks, reservoirs and seals, optimal timing of hydrocarbon charge and migration pathways, trapping mechanisms (either structural, stratigraphic or a combination of both), and the subsequent preservation of any potential accumulations. Based on this research, the likelihood of a mature source rock generating palaeo-charge in the region is high. By analogy with the conjugate margins, the presence of Mesozoic – Late Palaeozoic source rocks and reservoirs is also probable and the extensive Palaeocene basalts likely form an effective seal (away from heavily faulted areas). The main challenges concern the timing of charge vs trap formation, estimating the amount of uplift and erosion that took place during plate reorganisations, and the associated implications of leaking/breaching of previously charged older traps. A further effect of the Eocene/Oligocene uplift and erosion event could be de-gassing of any potentially trapped oil. An understanding of specific heat flow histories for the JMMC is also unknown due to a lack of vitrinite reflectance (VR) data from borehole data. Only analogue VR from the Norway margin and regional heat flow analyses can be used to infer burial histories and potential timings of source rock maturation.

Based on the results of this research, 2 main play intervals are considered and assessed in terms of the potential trap types present within them; the pre-basalt play (Late Palaeozoic/ Mesozoic to Palaeocene) and the Tertiary post-basalt play.

7.1.1 Pre-Basalt Play (Late Palaeozoic/Mesozoic – Palaeocene)

Although there is no direct continuous stratigraphic/lithological constraint below the extensive flood basalts (purple horizon), it is assumed (mostly from seismic refraction studies) that the JMMC contains pre-break up Mesozoic – Late Palaeozoic successions (Figure 2.1). Therefore, by inference from the conjugate margins (namely East Greenland as the JMMC was still attached to this margin during the first break up phase), potential organic rich SR's include, Upper Permian Ravnefjeld Fm, Lower Jurassic Kap Stewart Fm and Upper Jurassic Hareelv Fm equivalents (Figure 2.1). The Upper Permian and Upper Jurassic source rocks have been modelled for

potential maturity accordingly. Although these source rock intervals are only found at shallow depths today on East Greenland, the offshore Liverpool Land area, JMMC (and Norway equivalent) are deeper buried with a greater overburden of basalts and Cenozoic sedimentary sequences, leading to higher temperatures and burial depths for advanced maturation from these potentially excellent shale source rocks. Minor source rock intervals may also be present in the Late Carboniferous and Cretaceous (Figure 2.1). Potential good reservoir intervals include Carboniferous fluvial sandstones, Upper Permian limestones, Triassic fluvio-deltaic sandstones, Jurassic shallow marine sandstones and Cretaceous turbidite sandstones (Figure 2.1). Furthermore, potential good reservoirs exist within the Palaeocene succession. Larsen et al., (1999) identify submarine channel-levee sandstones and fluvial sandstones and conglomerates. The earliest Palaeogene volcanic sequence, also comprise intercalated subaerial basalt flows, hyaloclastites, tuffs and sediments (Henriksen et al., 2009). Hydrocarbon discoveries such as the Rosebank Field and Cambo discovery within the Faroe-Shetland Basin of the Palaeocene-Eocene Flood Basalt Province are key examples of these new types of intra-volcanic play types, consisting of a series of fluvial reservoir siliciclastic sandstones, interbedded with basalt lava flows, hyaloclasties and volcaniclastic sedimentary units (Duncan et al., 2009; Helland-Hansen 2009; Austin et al., 2014; Fielding et al., 2014 & Vosgerau et al., 2016). As, such, the hyaloclastites and volcaniclastic sediments found on the conjugate margins (Henriksen et al., 2009) could also form potential reservoir units within the JMMC, capped by the overlying break-up flood basalts (Figure 2.1).

7.1.1.1 Structural Traps

Large scale bounding normal and listric faults can be observed cross cutting into the pre-basalt succession across the JMR and western flank domains forming large scale titled fault block traps (Figure 4.11, 4.12, 4.20 & 4.21). Due to the lack of clear imaging of seismic reflector geometries in the "pre-basalt succession", it is however, unclear whether these faults were formed during Mesozoic tectonism (known to affect the conjugate margins) or whether they were reactivated or formed primarily by Eocene – Oligocene re-structuration associated with regional plate reorganisation. By analogy with the conjugate margins, it is likely that the JMMC experienced a similar structural history prior to deposition of the break-up basalt in the Palaeocene-Eocene and potentially developed similar structural hydrocarbon traps as seen on the Mid Norway and East Greenland shelves. It is likely that these fault blocks could have been charged by hydrocarbons from Mesozoic source rocks using planar and listric faults as migration pathways. In some cases these major bounding faults do penetrate into the overlying post-basalt succession and reach the seabed or have very little overlying Tertiary cover to act as an effective seal. Where this occurs, these plays are deemed high risk for remigration and leakage of any deeper trapped hydrocarbons. However, where the tilted fault blocks along the western flank are deeper buried and their bounding faults do not penetrate far above the purple and/or yellow western horizons with a thicker overlying Tertiary sequence, these plays could be lower risk.

Similar structural traps are likely to exist within the SRC. Individual "ridges" of the SRC form major tilted fault blocks themselves. However, the major planar and listric bounding faults commonly reach the seabed with little or no sealing sedimentary cover (Figure 4.18 & 4.19). Consequently, it is likely that these faults are a major risk for leakage of any hydrocarbons trapped in either the pre- or post-basalt successions. Nevertheless, these the large scale faults have facilitated the formation of intervening half grabens and sedimentary basins clearly observed in the post-basalt sequence, but are also presumed to exist at depth within the underlying pre-basalt sequence. These potential sub-basins are deeper and possibly experienced

increased temperatures to accelerate hydrocarbon generation sourced from deeper Mesozoic source rock kitchens. As these half grabens cannot be clearly imaged and their presence only based on inference from the overlying structural configuration/expression, the uncertainty remains high here, but the risk would be lower in these structural domains if a petroleum system did exist.

The reverse fault observed along the SE corner of the main JMR is the most favourable candidate for any hydrocarbon traps in the JMMC (Figure 7.1). The structure formed during Eocene-Oligocene ridge push processes and also probably in response to complex compression-extension regimes experienced on the southern margin of the JMMC during westward ridge migration. Figure 7.1 shows a distinct unconformity and termination of reflectors below the top basalt surface against the reverse fault which could enable closures and traps to form here. Gunnarsson et al., (1989) interpret the unconformity surface as the top of a potential fault assisted closure. They identify a potential bright flat-spot at the top of south-east dipping strata, truncated by a potential Cretaceous unconformity and overlain by thin Late Cretaceous to earliest Tertiary sediments (Figure 4.29). However, assessment of the current reprocessed data and new seismic lines across this area, the presence of a flat-spot is very unclear and doubtful (Figure 7.1). The overlying volcanic sequence hampers seismic imaging, making identification of any DHI's highly uncertain. Nevertheless, despite the apparent lack of DHI's, this reverse structure could still be a potentially prospective area on the JMMC.

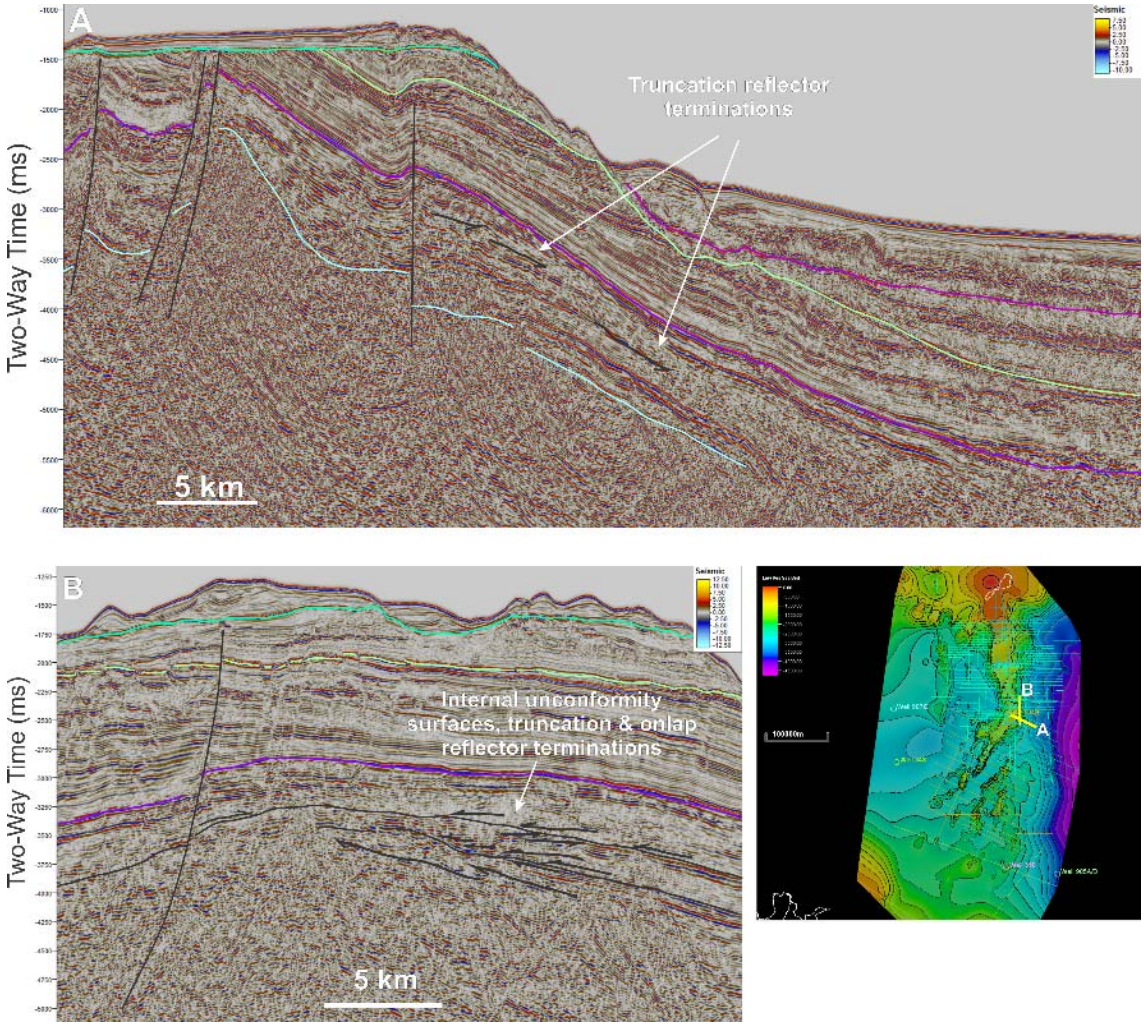

Figure 7.1: Reverse fault along the SE corner of the main JMR highlighting structural configuration of the reverse fault structure and unconformity surface and truncating reflector terminations within the pre-break up succession (Palaeocene – Late Mesozoic).

7.1.1.2 Stratigraphic Traps

Turbidite sandstones, fluvial sandstones and conglomerates and hyaloclastite potential reservoir units which outcrop in the Kangerlussuaq Basin in southern East Greenland are assumed to be present within the JMMC at the time of deposition/ emplacement (Cretaceous – Palaeocene) (Pedersen et al., 1997; Haman et al., 2005; Henriksen et al., 2009). If these reservoirs were charged by underlying Mesozoic – Late Palaeozoic source rocks, the overlying flood basalt sequence could act as an effective seal for these stratigraphic traps. "SDR" wedge features along the eastern margin of the JMR could also contain volcaniclastic reservoir units (and the aforementioned Palaeocene clastic reservoir units at depth) which could pinch out up-dip and become sealed by the overlying basalt layer (Figure 4.30). However, without sampling these SDR features or having a constraint on underlying stratigraphy, this play/trap type remains contentious.

Stratigraphic traps are likely to exist within the Mesozoic – Late Palaeozoic pre-break up succession, by inference of the conjugate margin stratigraphy (Figure 2.1) especially within shallow-deep marine reservoir units encased in mudstones; but these trap types currently cannot be imaged or traced between the spaced 2D grid, to confidently corroborate this hypothesis. As such, without a deep stratigraphic well, this play type remains highly speculative.

7.1.2 Post-Basalt Play (Tertiary)

This interval spans from the top basalt reflector (purple horizon) to the formation of the pink horizon. No direct evidence of good source rocks have been obtained from this interval yet. However, ROV studies have identified a potentially good reservoir unit directly above the basalt succession, corresponding to the Bopladsden Fm on the East Greenland margin. DSDP well studies confirm the Late Eocene to Plio-Pleistocene stratigraphy is dominated by sandy-silty mudstones.

7.1.2.1 Structural Traps

Eastward tilted Tertiary deposits sub-cropping the Oligocene unconformity surface along the JMR, has been proposed as a potential trap by Gunnarsson et al., (1989). However, this assumes that the either the unconformity surface and/or the overlying pelagic Mio-Plio-Pleistocene shales form an effective seal (Figure 4.11, 4.15, 4.16 & 4.17). Normal faults cutting the Tertiary sequence beneath the Oligocene unconformity forming tilted fault block could work as effective hydrocarbon traps if these traps are charged by deeper Mesozoic source rocks utilising the faults as migration pathways. However, these traps too require that the faults do not penetrate the unconformity surface and that this surface and/or the thin overburden form a good seal. Assessment of the seismic data currently available over the main JMR, reveals that in places it appears that the Oligocene unconformity is cut by faults; therefore, making these play types high risk.

Fault blocks occurring in the post-basalt sequence along the western margin of the JMMC, could be more prospective due to the deeper burial of overly sedimentary successions (Figure 7.2). These structural traps could also likely be charged from Mesozoic source rocks with the bounding faults acting as potential migration routes. However, seismic data suggest there is a risk that these normal and listric faults along the western flank transect the overlying stratigraphy above the yellow western unconformity surface and/or even reach the seabed. This situation can be more frequently observed closer to the main JMR, whilst deeper buried fault blocks towards the west have a thicker overlying cover of Tertiary sediments. Therefore, if this play were to work, targeting tilted fault blocks further to the west along the western margin may have a reduced risk.

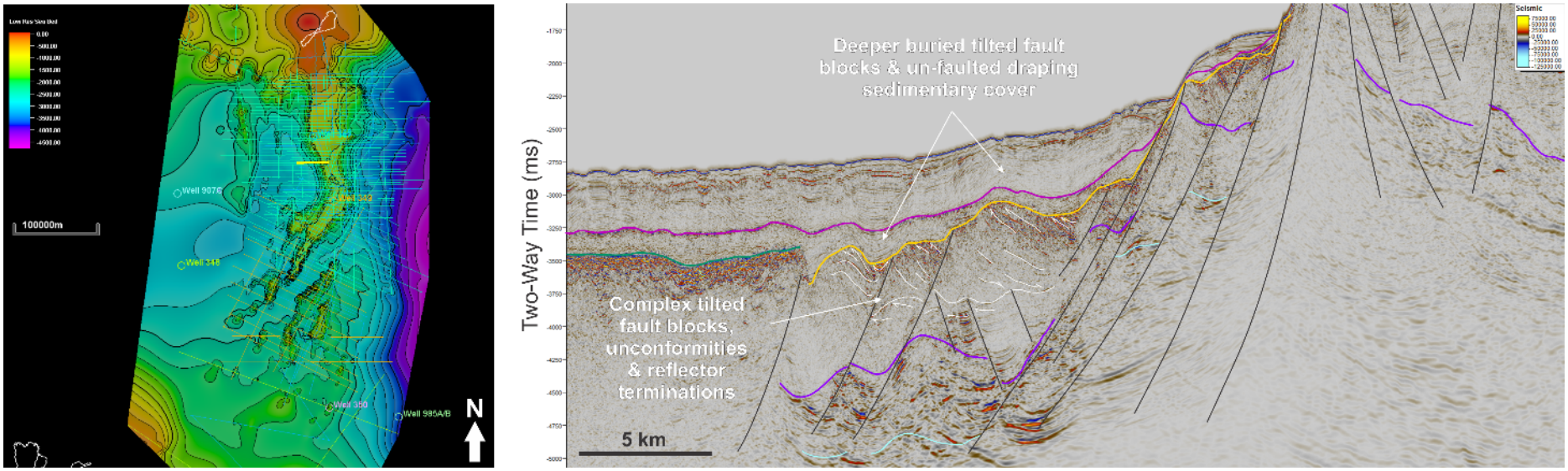

Figure 7.2: Structural configuration of the deeper tilted fault blocks along the western margin of the JMMC.

A similar scenario exists within the SRC in the post-basalt play. Large scale faults planar and listric faults have facilitated the formation of intervening half grabens and sedimentary basins clearly observed in the post-basalt sequence (Figure 7.3). These sub-basins are deeper and possibly charged with hydrocarbons utilising the normal bounding faults as re-migration pathways sourced from deeper Mesozoic traps. In some examples seen in Figure 7.3, there is a thicker cover of Tertiary sediments overlying and appearing to effectively drape the underlying structural topography forming tilted anticline structures. In this case, where the smaller faults do not penetrate into this draping sedimentary cover, these play types could be lower risk with lower uncertainty due to improved seismic imaging within the post-basalt sequence.

The reverse fault along the eastern edge of the JMR could also be a potentially good candidate for a hydrocarbon trap in the post-basalt play (Figure 7.1). This fault was reactivated as a reverse fault after peak hydrocarbon generation and as a result of cross cutting the basalt (purple horizon dividing the two main plays in the area) would likely be an important conduit and migration pathway for any hydrocarbons trapped within deeper, underlying pre-basalt sequences and potentially charge both the pre- and post-basalt plays. A requirement for this structure to work would be for the overlying Oligocene unconformity and thin overburden on top the JMR was an effective seal. For the most part, the current seismic data appears to suggest that the reactivated reverse fault has not penetrated the unconformity surface. However, timing of formation of this structure in relation to peneplanation of the unconformity surface means the risk of any hydrocarbons leaking is high. Even in the worse-case scenario, if the timings of fault and unconformity surface formation is disadvantageous or the reverse fault has breached through the unconformity surface, the reverse fault dome structure might hold some bypass residual volumes in the crests of both the pre- and post-basalt plays (Figure 7.1).

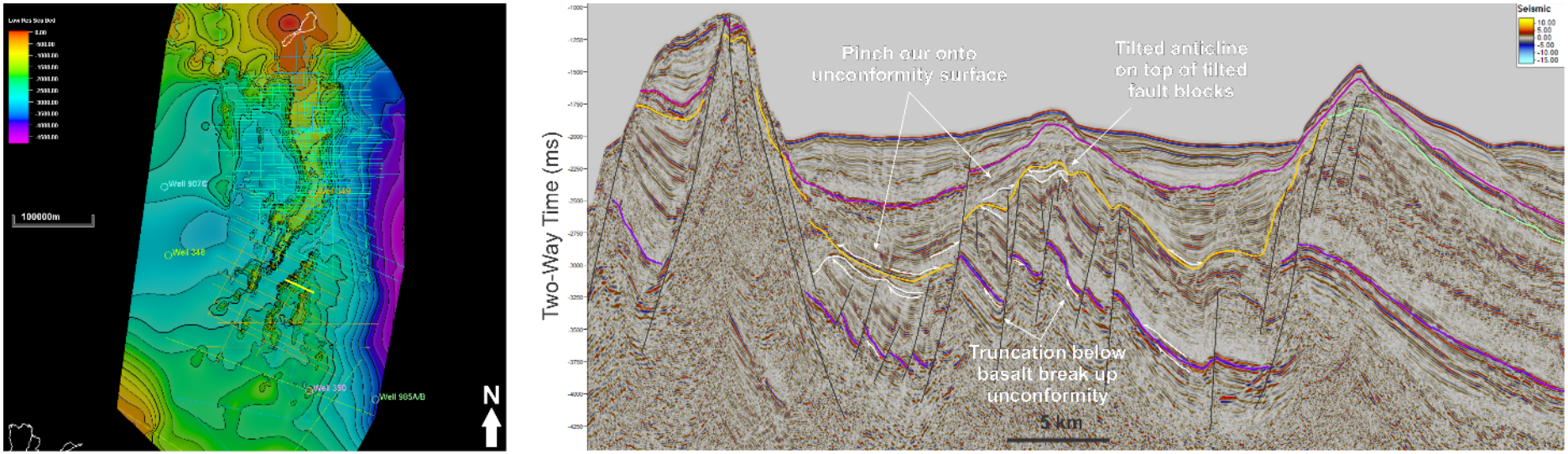

Figure 7.3: Tilted fault blocks draped with overlying Cenozoic cover forming tilted anticline structures and complex internal reflector geometries within the SRC area. Potential charge from deeper Pre-Basalt units using larger faults a migration pathways into shallower structural trapping styles.

7.1.2.2 Stratigraphic Traps

Detailed seismic facies and stratigraphic studies by Peron-Pindivic et al., (2012) and Blischke et al., (2017/ 2019) identify potential turbidite channel features and related lenses and wedges of sedimentary packages which pinch out up dip along the eastern margin of the JMR and into the Norway Basin (Figure 4.32). Potential clinoform features are also observed along the eastern margin of the JMMC. Thus, these traps might include fluvio-deltaic channel sandstone units and/or turbidites and debris flows forming deep marine fan systems surrounded by slope and deep marine shales. These sediments were likely shed off the East Greenland margin (and/or the western parts of the JMMC) in response to rift-flank uplift during initiation of seafloor spreading processes (Blicshke et al., 2019). Such well-defined wedges, which pinch out up dip, may provide effective stratigraphic traps along the eastern slope margin of the JMMC. However, without an understanding of the 3D geometry and potential closure of the wedge/lens stratigraphic features and a constraint on the entire post-Basalt stratigraphy (to ascertain the true lithofacies and reservoir properties of these potential sand bodies and sealing potential of the surrounding mudstone units), this trapping type remains highly uncertain.

Figure 7.4 shows a potential lead map of the most interesting trapping styles which would benefit from further detailed analysis and testing. The reverse fault on the SE margin of the JMR, deeper tilted fault blocks along the western flank of the JMR and sub-basinal areas of the SRC for both the pre- and post-basalt plays are potentially promising structural traps, along with the stratigraphic traps of the post-basalt play on the eastern margin.

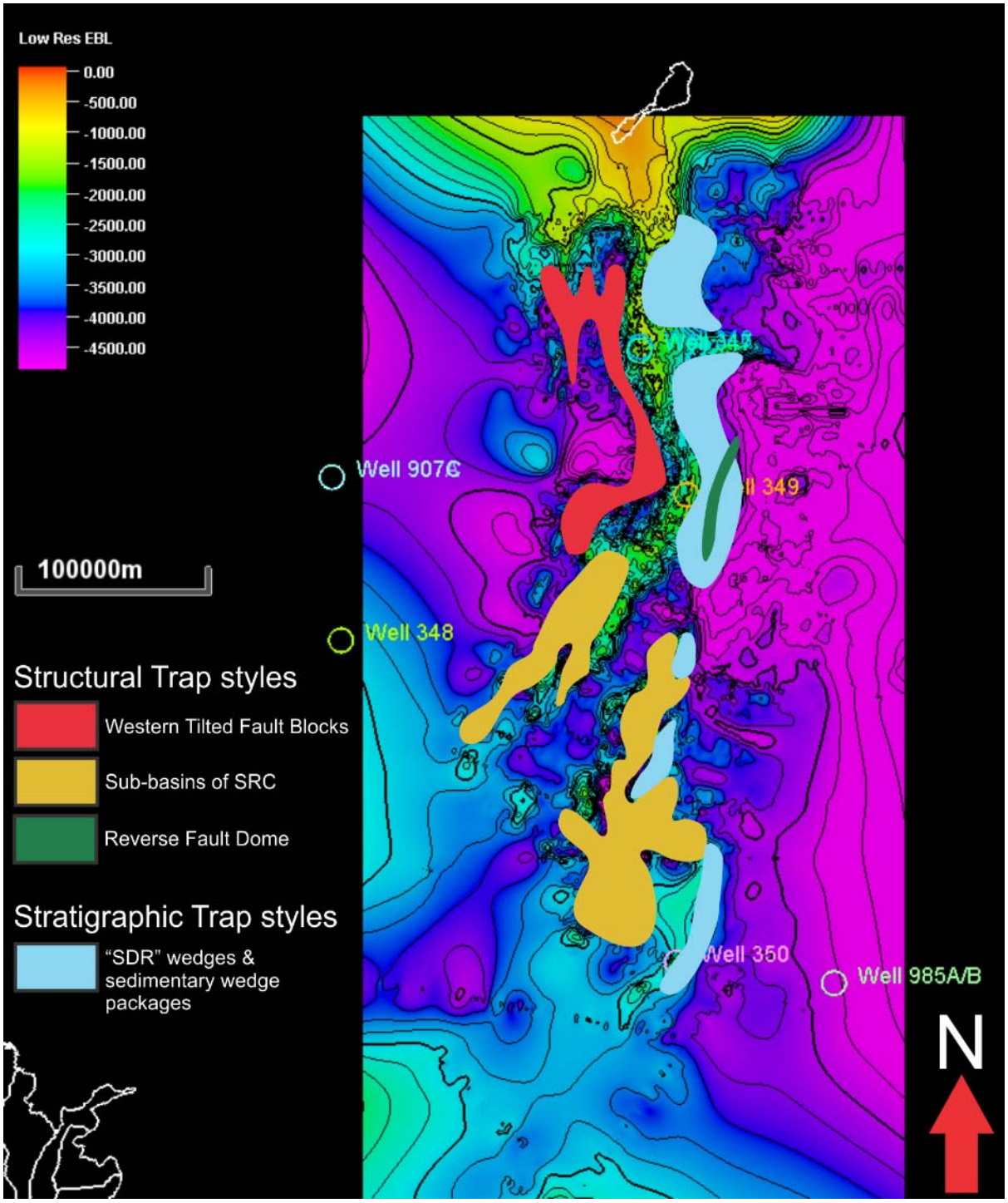

Figure 7.4: Potential lead map highlighting the areal extent of interesting structural and stratigraphic traps for future analysis.

7.1.2.3 Risk Factors for Prospectivity

Figure 7.5 is a risk analysis diagram for the pre- and post-basalt plays and trap types therein. The associated risk and uncertainty level for each trap style is based entirely on qualitative interpretations of the 2D seismic data available for this research. Although it is speculative, it aims to provide an estimate of the confidence level for each potential trap type (based on the interpretations and quality of the data) and identify areas which would benefit from further detailed analysis and/or data coverage.

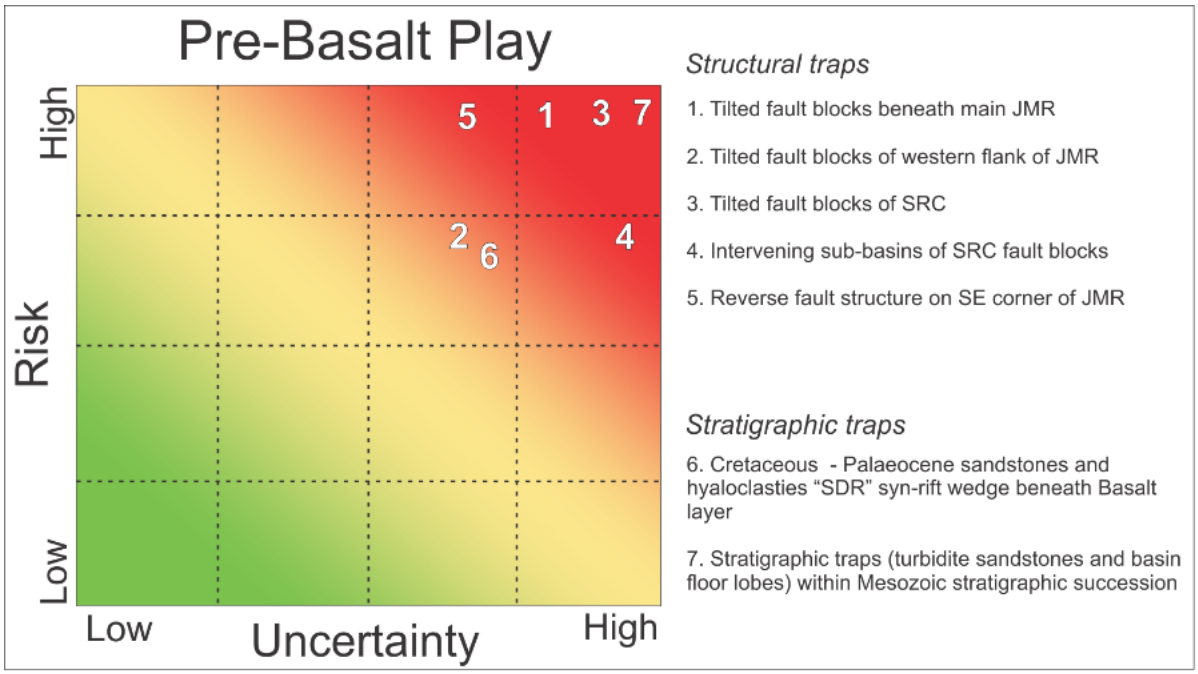

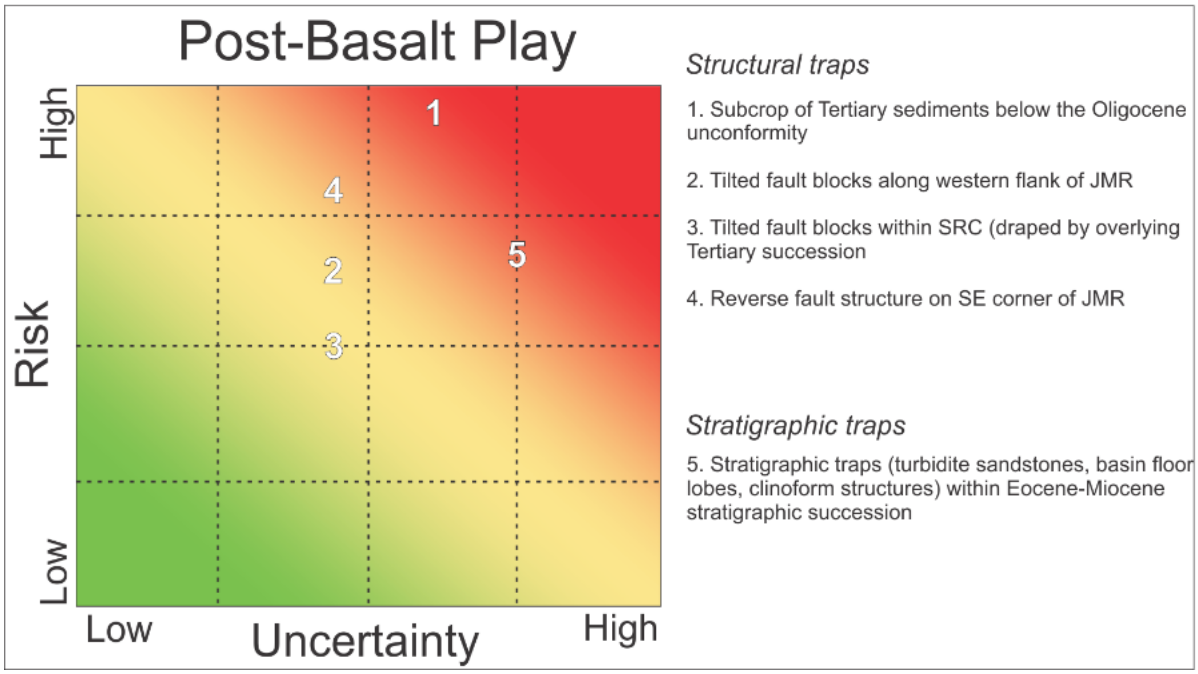

Figure 7.5: Risk Analysis charts for the Pre- and Post-basalt plays based entirely on qualitative seismic interpretation.

Uncertainty with regards to data interpretation is high for the pre-basalt sequence and relatively low for the overlying post-basalt sedimentary succession. The newest NPD 2011/2012 2D seismic survey has enabled some deeper sedimentary reflector sequences to be identified within the pre-basalt sequence. However, future research would benefit from either seismic reprocessing techniques targeting the sub-volcanic sequence and/or new smaller surveys over specific areas of interest which are specifically designed to improve sub-basalt imaging.

As the Pre-basalt sequence is not well imaged, the presence of reservoir and source rock still remain uncertain without a deep stratigraphic test borehole. However, given the palaeo-tectonic/environmental reconstructions of the North Atlantic, it is likely that the JMMC contains similar geological sequences as its conjugate margins which are relatively well constrained.

For the Post-Basalt strata, the presence of reservoir and effective seal units remain untested. The better imaging of this sequence from the existing seismic data suggests lobate/wedge features analogous to stratigraphic trapping styles proven within other working hydrocarbon provinces globally.

Accurate heat flow estimates from the JMMC are unknown. Consequently heat flow ranges for current basin/source rock maturity modelling are derived from surface heat flow estimates or VR ranges from the conjugate margins. Although this is the best that can be done with the available data, it is important to consider that unlike the conjugate margins, the JMMC underwent two separate phases of heat pulses associated with the two rift-drift events and mantle plume within a relatively small sliver of continental crust. Furthermore, the brittle deformation which caused the formation of isolated ridges within the SRC to the south, may have also been subject to locally higher heat flow, compared to the main JMR, in response to increased lithospheric extension and westward migration of the spreading ridge during the Oligocene. Currently these two rifting events are modelled as one single heat flow peak as they occurred within such a short time period. However, without detailed heat flow and VR data from within the JMMC, the effects of these events on a potential hydrocarbon system present remain ambiguous.

The timing of structuration (both potentially pre-break up and during re-structuration in the Oligocene) in relation to timing of peak hydrocarbon generation is the most important risk factor for a hydrocarbon system working within the JMMC. Older structures with palaeo-charge which were not adversely affected by the Oligocene uplift and faulting and are currently at deep enough depths to avoid bio-degradation have a higher chance of being prospective. However, seismic imaging of any potentially deeper structures are hampered by the Palaeocene-Eocene flood basalt. Therefore, the uncertainties and risks for traps with hydrocarbon potential within the JMMC remain high.

The water depths and remote location of the JMMC may also pose significant accessibility issues for any future exploration or drilling activities. Strong sea currents, adverse weather and wave heights, sea and surface temperatures and sea ice are common environmental hazards in the area. Whilst potential deep water geo-hazards include complex and unstable sea beds and deep water drilling hazards.

7.1.3 Concluding Remarks

Results of maturity modelling suggest that it is possible that peak oil/gas generation and expulsion occurred just prior to or coincided with emplacement of the Palaeocene-Eocene basalt seal; whilst the uplift/erosion event and post Oligocene decrease in heat flow caused the hydrocarbon kitchen to shut off. Estimates of present day surface heat flow do not attain as high temperatures as seen during rift related and mantle plume heat pulse during the two phases of break up along the east and west margins of the JMMC. Furthermore, VR estimates for basin and maturity modelling are based on samples from the conjugate Mid Norwegian margin. Although it is beneficial to use these closely analogous estimates of VR, the JMMC is unique in that it has undergone two rift-drift events (with associated heat pulses) within close geographical proximity of each other, compared to the Norway margin that has only undergone one rift-drift event. Without any deep stratigraphic wells to calibrate and refine the basin/maturity models, the effects of these individual tectonic and related heat flow events on a potential hydrocarbon system within the JMMC remain incalculable.

For a hydrocarbon system to work here, it would likely require palaeo-charge into older (Cretaceous or older) structural and/or stratigraphic traps (formed prior to break-up and formation of the flood basalt sequence), that have also not been adversely affected by the later restructuration, uplift and inversion events associated with the spreading ridge migration/jumps in the Oligocene. However, if the regional seal was not in place before potential hydrocarbon generation and charge into reservoirs, then there is a risk that any hydrocarbons could have been lost altogether. Conversely, if the basalt was in place to form an effective seal, yet these structures were affected by later uplift and inversion, any hydrocarbons that leaked would need to have re-migrated into newly formed (Tertiary) structural traps without being lost.

Furthermore, if a reservoir containing hydrocarbons falls to 50-60°C or less, there is also a risk of biodegradation. However, fortuitously for the JMMC, the present day relatively high heat flow (especially along the western margin (see above heat flow section)) may be helping to keep any trapped hydrocarbons from biodegrading. Assuming a decrease in temperature of 35-40°C/km depth from the seabed, reservoirs and traps at a depth of 1 km or less below the seabed could be at high risk of biogenic degradation.

The timing of the uplift event is well constrained, however relative timings on the older structure and stratigraphy is unknown. For the JMMC to be prospective, requires hydrocarbons to trap prior to and survive the uplift inversion events at around 50 – 30 Ma, otherwise there is a strong risk of leakage. Older structures that have survived the uplift event and presently situated far below the unconformity surface (at least 1km below the sea bed (not lower than 50°C)), then there is a better chance of a petroleum system working. The reverse fault on the SE margin of the JMR, deeper tilted fault blocks along the western flank of the JMR and sub-basinal areas of the SRC for both the pre- and post-basalt plays are relatively lower risk potential lead areas to test further for future appraisal.

7.2 Generic Implications for Microcontinents

The JMMC is an excellent example of the range of structural complexity involved with continental rifting and break up, and in particular for volcanic rifted margins. Similarities and comparisons can be drawn with other microcontinents, such as the Seychelles (Plummer & Belle 1995; Plummer et al., 1998; Torsvik et al., 2001; Muller et al., 2001; Collier et al., 2004; Torsvik et al., 2013), Kerguelen Plateau (Benard et al., 2010), East Tasman Plateau (Exon et al., 1997) and Lomonosov Ridge (Moore et al., 2011), which formed under similar geodynamic/plate tectonic processes. Comparably, the Seychelles too was thought to have formed in response to a mantle plume hot spot and also display an asymmetry between its respective margins, with one being considered volcanic and the other non-volcanic.

Microcontinents and outer high areas have long been considered as areas of interest, not just for hydrocarbon prospectivity with regards to the potential of containing continental crust and source rock and reservoir sequences, but also from a plate tectonic geodynamic perspective. The discovery of these crustal blocks/slivers, microcontinents, hyper-extended crust and exhumed continental mantle has led to a paradigm shift in our understanding of the evolution of rifted margins (Peron-Pindivic & Manatschal 2010; Unternehr et al., 2010; Li et al., 2016). It is clear from this study of Jan Mayen, that the rift-drift process is much more complex than previously thought. The evolution of continental rifting involves a series of specific rift process corresponding to sequential phases of stretching, thinning and eventual exhumation of continental lithosphere and formation of new oceanic crust. Furthermore, in the specific case of the JMMC, the impact of the Iceland mantle plume affecting the position of and causing lateral shifts of the seafloor spreading centre through time adds another aspect of complexity to the evolution of the microcontinent. Comparisons of this study with other known microcontinents can be used to better understand these processes and act as case studies to improve our understanding of plate geodynamics.

In addition, the ability to make reasonable assumptions about plate reconstructions of rifted margins can help to better understand the wider regional geology, specific implications of the rift-drift process in these regions and past global circulation patterns. As more potential microcontinents are discovered through basin inversion modelling (e.g. the Comoros and Canary Islands), the need to understand the structural evolution (and related plate tectonic geodynamic implications) and internal stratigraphy preserved within these continental slivers increase.

8. Recommendations for Further Work

2D basin modelling over parts of the JMMC using the latest depth converted surfaces, structural maps and latest improved estimates of heat flow affecting the JMMC would be the next step on from this research. It would also be important to capture the two individual increased heat flow pulses associated with the 2 stages of rifting affecting the JMMC, similar to Scotchman et al., (2006) study of the Faroe Shetland Basin. Increased heat pulse experienced in the Palaeocene-Eocene associated with break-up I along the eastern margin and break up II in the Oligocene along the western margin, respectively would be beneficial to include in a more detailed model to test the potential effects on maturity and charge.

Despite numerous studies since the initial reports from Talwani et al., (1976) and Gunnarsson et al., (1989) on the Jan Mayen Microcontinent, there remains no direct evidence of the existence of a working hydrocarbon system in the area. Although potential play types can be speculated upon from geophysical data, the lack of complete lithological and stratigraphic information from limited boreholes for seismic calibration remains a key uncertainty. As such, a stratigraphic test well is required to gain an accurate assessment of the hydrocarbon potential of the JMMC by deep drilling of the post-basalt (Cenozoic) stratigraphy, and preferably the deeper pre-basalt (potentially Mesozoic – Late Palaeozoic) successions too. This would provide a more robust well – seismic calibration, confirm the presence of a petroleum system, including source rock, reservoir and seal components and enable maturity models to be refined. Potential favourable sites for drilling a deep stratigraphic well would be located in shallower waters on the main ridge highs where the Palaeocene-Eocene basalt layer is shallowest to reach by a drill rig (fig?) and to test if Mesozoic or Palaeozoic strata exists of sufficient thickness and quality. Given the closer spacing, better imaging due to reprocessing and increased coverage of the 2D seismic lines today, new locations either in similar vicinities of the DSPD sites or in more central locations along the main ridge would be advantageous.

The SRC "DREKI" area would benefit from additional seismic acquisition to infill the 2D seismic surveys, or obtain 3D coverage to obtain a more detailed areal extent of various trapping mechanisms that might exist within the sub-basinal areas where buried tilted fault blocks are draped by a younger Tertiary sequence. Also within the SRC area, conducting a more detailed "outcrop" study along the steep ridges to support analogue comparison studies between the JMMC and the conjugate East Greenland margin and Møre Basin for the sub-basalt sequence, would be highly valuable for understanding the Mesozoic successions.

Where current geophysical surveys enable potential structural traps to be postulated, the identification of the inversion structure along the SE corner of the main JMR is of greatest potential to be appraised further by acquisition of a small 3D seismic survey. At the least this could help constrain 3D geometry of the structure and assess it potential for 4 way dip closure on this structure. Although the major risk remains of whether this structure has been charged from a Jurassic/Permian source rock or the process of restructuring and formation of the inversion fold caused re-migration and leakage. In this worst case scenario, the structure could still contain small residual quantities after re-migration along reactivated faults. However, 3D seismic acquisition would enable this hypothesis to be tested further.

Acknowledgements

The Icelandic Government Orkustofnun National Energy Authority Hydrocarbon Research Fund is gratefully acknowledged for sponsoring this research at the Applied Geoscience Unit, Heriot Watt University. Dr Thorarinn Sveinn Arnarson is thanked for his role in setting up the project and providing invaluable support and advice. Spectrum and the Norwegian Petroleum Directorate are gratefully acknowledged for providing 2D seismic data for use within this research. Representatives from Spectrum, Neil Hodgson & Karyna Rodriguez are also thanked for their valuable advice and suggestions for further work. Lorcan Kernnan (Shell Projects & Technology) and other representatives from Shell International are also acknowledged for their invaluable input and suggestions during their biannual visits to the Shell Centre in the Applied Geoscience Unit at Heriot Watt University. I would like to thank past and present, PhD students and post-docs within the Applied Geoscience Unit as well as Anna Clark and Lorna Morrow who have been an important support network throughout the course of this research project. Last, but not least, I would like to extend my greatest gratitude and thanks to Dr Kirstie Wright for her endless support and technical input throughout the course of this research. In particular, a special thanks and acknowledgement goes to her for kindly sharing her detailed Excel templates for tectonostratigraphic synthesis and petroleum systems charts, which took her a lot of time and effort to put together.

References

Blischke, A., Arnarson, T.S., Gunnarsson, K., 2001. The Structural History of the Jan Mayen Micro-Continent (JMMC) and Its Role During the Rift "Jump" Between the Aegir to the Kolbeinsey Ridge. *In AAPG 2001 - The Polar Petroleum Potential Conference & Exhibition, Halifax, Nova Scotia, Canada, August 30-September 2, 2011*, Search and Discovery Article #30198

Blischke, A., Gaina, C., Hopper, J.R., Peron-Pindivic, G., Brandsdottir, B., Guarnieri, P., Erlendsson, Ö. & Gunnarsson., K., 2017. The Jan Mayen Microcontinent: an update of its architecture, structural development and role during the transition from Ægir Ridge to the mid-oceanic Kolbeinsey Ridge. *In: Peron-Pinvidic, G., Hopper, J., Stoker, M.S., Gaina, C., Doornenbal, H., Funck, T. & Arting, U. (eds) The North-East Atlantic Region: A Reappraisal of Crustal Structure, Tectono-Stratigraphy and Magmatic Evolution.* Geological Society, London, Special Publications, **447**, 299 – 337, http://doi.org/10.1144/SP447.5

Blischke, A., Stoker, M.S., Brandsdóttira, B., Hopper, J.R., Peron-Pinvidic, G., Ólavsdóttirf, J., Japsen, P., 2019 The Jan Mayen microcontinent's Cenozoic stratigraphic succession and structural evolution within the NE-Atlantic. Marine and Petroleum Geology, **103**, 702 – 737.

Breivik, A.J., Mjelde, R., Faleide, J.I. & Murai, Y. 2006. Rates of continental breakup magmatism and seafloor spreading in the Norway Basin – Iceland plume interaction. Journal of Geophysical Research, **111**, B07102, doi:10.1029/2005JB004004

Breivik, A.J., Faleide, J.I., Mjelde, R. & Flueh, E.R. 2009. Magma productivity and early seafloor spreading rate correlation on the northern Voring Margin, Norway – constraints on mantle melting. Tectnonophysics, **468**, 206 – 223.

Breivik, A.J., Mjelde, R., Faleide, J.I., Murai, Y., 2012. The eastern Jan Mayen microcontinent volcanic margin. Geophysical Journal International, **188** (3), 798–818.

Brekke, H., Dahlgren, S., Nyland, B., Magnus, C., 1999. The prospectivity of the Vøring and Møre basins on the Norwegian Sea continental margins. *In: Fleet, A.J., Boldy, S.A.R. (Eds.), Petroleum Geology of Northwest Europe: Proceedings of the 5th Conference.* Geological Society, London, 261–274.

Brekke, H., 2000. The tectonic evolution of the Norwegian Sea continental margin with emphasis on the Vøring and Møre basins. *In: Nøttvedt, A. (Ed.), Dynamics of the Norwegian Margin*, Geological Society, London, Special Publications, **167**, 327–378.

Brekke, H., Sjulstad, H.I., Magnus, C. & Williams, R.W. 2001. Sedimentary Environments Offshore Norway - Palaeozoic to Recent. *In: Martinsen., O.J. & Dreyer. T., NPF Special Publication*, **10**, 7-37.

Brune, S., Heine, C., Perez-Gussinye, M. & Sobolev, V., 2014. Rift migration explains continental margin asymmetry and crustal hyper-extension. Nature Communications, DOI:10.1038/ncomms5014

Buck, W.R. 2017. The role of magmatic loads and rift jumps in generating seaward dipping reflectors on volcanic rifted margins. Earth and Planetary Science Letters, **466**, 62 – 69.

Darbyshire, F. A., White, R. S. & Priestley, K. F., 2000. Structure of the crust and uppermost mantle of Iceland from a combined seismic and gravity study, Earth Planetary Science Letters, **181**, 409–428.

Doré, A.G. & Jensen, L.N. 1996. The impact of late Cenozoic uplift and erosion on hydrocarbon exploration: offshore Norway and some other uplifted basins. Global and Planetary Change, **12**, 415 – 436.

Doré, A.G., Lundin, E.R., Birkeland, Ø., Eliassen, P.E. & Jensen, L.N. 1997. The NE Atlantic Margin: Implications for late Mesozoic and Cenozoic events for hydrocarbon Prospectivity. Petroleum Geoscience, **3**, 117 – 131.

Doré, A.G., Lundin, E.R., Jensen, L.N., Birkeland, Ø., Eliassen, P.E., Fichler, C., 1999. Principal tectonic events in the evolution of the northwest European Atlantic margin. *In: Fleet, A.J., Boldy, S.A.R. (Eds.), Petroleum Geology of Northwest Europe: Proceedings of the 5th Conference*, The Geological Society, London. 41–61.

Faleide, J.I., Bjørlykke, K. & Gabrielsen, R.H. 2010. Geology of the Norwegian continental shelf. *In: Bjørlykke, K. (ed.) Petroleum Geoscience: From Sedimentary Environments to Rock Physics*. Springer, New York, 467–499, doi: 10.1007/978-3-642-02332-3_22

Foulger, G. R., Du, Z. & Julian, B. R. 2003, Icelandic-type crust, Geophysical. Journal International, **155**, 567– 590.

Foulger, G. R. (2006), Older crust underlies Iceland, Geophysical Jounral International, **165**, (2), 672 - 676.

Funck, T., Erlendsson, Ö., Geissler, W.H., Gradmann, S., Kimbell, G.S., McDermott, K. & Petersen, U.K. 2017. A review of the NE Atlantic conjugate margins based on seismic refraction data. *In: Peron-Pinvidic, G., Hopper, J., Stoker, M.S., Gaina, C., Doornenbal, H., Funck, T. & Arting, U. (eds) The North-East Atlantic Region: A Reappraisal of Crustal Structure, Tectono- Stratigraphy and Magmatic Evolution*. Geological Society, London, Special Publications, 447, 171 – 205. http://dx.doi.org/10.1144/SP447.9

Gaina, C., Gernigon, L. & Ball, P., 2009. Palaeocene–Recent plate boundaries in the NE Atlantic and the formation of the Jan Mayen microcontinent. Journal of the Geological Society, London, **166**, 601–616, https://doi.org/10.1144/0016-76492008-112

Gaina, C., Nasuti, A., Kimbell, G.S., Blischke, A., 2017a. Break-up and seafloor spreading domains in the NE Atlantic. *In: Peron-Pinvidic, G., Hopper, J., Stoker, M.S., Gaina, C., Doornenbal, H., Funck, T. & Arting, U. (eds) The North-East Atlantic Region: A Reappraisal of Crustal Structure, Tectono-Stratigraphy and Magmatic Evolution*. Geological Society, London, Special Publications, 447, 393 – 417, https://doi.org/10.1144/SP447.12

Gaina, C., Blischke, A., Geissler, W.H., Kimbell, G.S., Erlendsson, Ö., 2017b. Seamounts and oceanic igneous features in the NE Atlantic: a link between plate motions and mantle dynamics. *In: Peron-Pinvidic, G., Hopper, J., Stoker, M.S., Gaina, C., Doornenbal, H., Funck, T. & Arting, U. (eds) The North-East Atlantic Region: A Reappraisal of Crustal Structure, Tectono- Stratigraphy and Magmatic Evolution*. Geological Society, London, Special Publications, **447**, 419 – 442, https://doi.org/10.1144/SP447.6

Geoffroy, L., Burov, E.B. & Werner, P., 2015. Volcanic passive margins: another way to break up continents. Scientific Reports, doi: 10.1038/srep14828

Gernigon, L., Gaina, C., Olesen, O., Ball, P., Peron-Pinvidic, G. & Yamasaki, T. 2012. The Norway Basin revisited: from continental breakup to spreading ridge extinction. Marine and Petroleum Geology, **35**, 1–19.

Gernigon, L., Blischke, A., Nasuti, A. & Sand, M. 2015. Conjugate volcanic rifted margins, seafloor spreading, and microcontinent: insights from new high-resolution aeromagnetic surveys in the Norway Basin. Tectonics, **34,** 907–933.

Greenhalgh, E.E., Kusznir, N.J., 2007. Evidence for thin oceanic crust on the extinct Ægir Ridge, Norwegian Basin, NE Atlantic derived from satellite gravity inversion. Geophysical Research Letters, 34, doi: 10.1029/2007GL029440, 2007

Gudlaugsson, S.T., Gunnarsson, K., Sand, M. & Skogseid, J., 1988. Tectonic and volcanic events at the Jan Mayen ridge microcontinent. *In: Morton, A.C. & Parson, L.M. (eds), Early Tertiary volcanism and the opening of the NE Atlantic*, Geological society Special Publication, **39**, 85 – 93.

Gunnarsson, K., Sand, M. & Gudlaugsson, S.T. 1989. Geology and Hydrocarbon Potential of the Jan Mayen Ridge. Orkustofnun, Reykjavık Report OS-89036 & Norwegian Petroleum Directorate, Stavanger, OD-89-91. 156 pp.

Hamann, N.E., Whittaker, R.C., Stemmerik, L., 2005. Geological development of the Northeast Greenland Shelf. *In: DORÉ, A.G., Vining, B.A. (Eds.), Petroleum Geology: North-West Europe and Global Perspectives - Proceedings of the 6th Petroleum Geology Conference*, 887–902.

Hansen, J., Jerram, D.A., McCaffrey, K. & Passey S.R. 2009. The onset of the North Atlantic Igneous Province in a rifting perspective. Geological Magazine, **143**, (3), 309 – 325.

Henriksen, N., 2008. Geological History of Greenland – Four billion years of Earth evolution. Geological Survey of Denmark and Greenland (GEUS), pp. 272.

Henriksen, N., Higgins, A.K., Kalsbeek, F. and Pulvertaft, T.C.R., 2009. Greenland from Archaean to Quaternary. Geological Survey of Denmark and Greenland Bulletin, **18**, 126 pp..

Hinz, K., 1981. An hypothesis on terrestrial catastrophes wedges of very thick oceanward dipping layers beneath passive continental margins; their origin and palaeo-environmental significance. Geologisches Jahrbuch, E2 3–28.

Hinz, K., Mutter, J.C., Zehnder, C.M. & NGT Study Group. 1987. Symmetric conjugation of continent-ocean boundary structures along the Norwegian and East Greenland Margins. Marine and Petroleum Geology, 4, 166 – 187.

Hinz, K., Eldholm, O., Block, M. & Skogseid, J., 1993. Evolution of the North Atlantic volcanic continental margins. In: Parker, J.R (ed) Petroleum Geology of Northwest Europe: Proceedings of the 4th Conference, The Geological Society, London, 901 – 913.

Hood, A., Castaño, J.R. & Kendrick, J.W. 1976. Petroleum-generating potential and thermal history of DSDP Leg 38 sediments. BRC-EP publication No.685, Shell Development Company, 801 – 803.

Hossack, J.R. 1984. The geometry of listric growth faults in the Devonian basins of Sunnfjord, W Norway. Journal of the Geological Society, 141, 629 – 367. https://doi.org/10.1144/gsjgs.141.4.0629

Jagoutz, O., Muntener, O., Manatschal, G., Rubatto, D., Peron-Pindivic, G., Turrin, B.D. & Villa, I.M. 2007. The rift-drift transition in the North Atlantic: a stuttering start of the MORB machine? Geology, **35**, 12, 1087-1090.

Jaspen, P. & Chalmers, J.A. 2000. Neogene uplift and tectonics around the North Atlantic: overview. Global and Planetary Change, **24**, 165 – 173.

Jolley, D.W. and Morton, A.C., 2007. Understanding basin sedimentary provenance: evidence from allied phytogeographic and heavy mineral analysis of the Palaeocene of the NE Atlantic. Journal of the Geological Society, **164**, (3), 553-563.

Jónsdóttir, I. & Vladimarsson, A.F., 2009. Searching for natural oil seepage in the Dreki area using ENVISAT radar images. Orkustofun report OS-2009/001, 21 pp.

Kodaira, S., Mjelde, R., Gunnarsson, K., Shiobara, H., Shimamura, H., 1998. Structure of the Jan Mayen microcontinent and implications for its evolution. Geophysical Journal International, **132**, 383–400.

Kuvaas, B. & Kodaira, S. 1997. The formation of the Jan Mayen microcontinent: the missing piece in the continental puzzle between the Møre - Vøring Basins and East Greenland. First Break, **15**, 1/12, 239 – 246.

Langseth, M.G. and Zielinski, G.W., 1974. Marine heat flow measurements in the Norwegian-Greenland Sea and in the vicinity of Iceland. *In: Kristjansson (eds) Geodynamics of Iceland and the North Atlantic area*, 277-295.

Larsen, H.C., 1980. Geological perspectives of the East Greenland continental margin. Bulletin of the Geological Society of Denmark, **29**, 77-101.

Larsen, H.C., 1990. The East Greenland Shelf. *In: Grantz, A., Johnson, L. & Sweeney, J.F., (eds), The Arctic Ocean region: Boulder, Colorado, Geological Society of America*, The Geology of North America, **50**, 185-210.

Larsen, M., Hamberg, L., Olaussen, S., Nørgaard-Pedersen, N. and Stemmerik, L., 1999. Basin evolution in southern East Greenland: An outcrop analog for Cretaceous-Paleogene basins on the North Atlantic volcanic margins. AAPG bulletin, **83**, (8), 1236-1261.

Larsen, M., Piasecki, S. and Stemmerik, L., 2002. The post-basaltic Palaeogene and Neogene sediments at Kap Dalton and Savoia Halvø, East Greenland. Geology of Greenland Survey Bulletin, **191**,103-110.

Leftwich, T. E., von Frese, R. R. B., Potts, L. V., Rae Kim, H. R., Roman, D. R., Taylor, P. T. & Barton, M. 2005. Crustal modelling of the North Atlantic from spectrally correlated free-air and terrain gravity. Journal of Geodynamics, **40**, 23–50, doi:10.1016/j.jog.2005.05.001.

Lundin, E.R. & Dore, A.G. 1997. A tectonic model for the Norwegian passive margin with implications for the NE Atlantic: Early Cretaceous to break-up. Journal of the geological Society, London, **154**, 545 – 550.

Lundin, E.R. & Doré, A.G. 2002. Mid-Cenozoic post-breakup deformation in the passive margins boarding the Norwegian-Greenland Sea. Marine and Petroleum Geology, **19**, 79 – 93.

Lundin, E.R., Doré, A.G., 2005. NE Atlantic breakup: a re-examination of the Iceland mantle plume model and the Atlantic–Arctic linkage. *In: Doré, A.G., Vining, B.A. (Eds.), Petroleum Geology: North-West Europe and Global Perspectives. Proceedings of the 6th Petroleum Geology Conference*. 739–754.

Lundin, E.R. & Doré, A.G. 2011. Hyperextension, serpentinization, and weakening: a new paradigm for rifted margin compressional deformation. Geology, **39**, 347–350.

Mathiesen, A., Christiansen, F.G., Bidstrup, T., Marcussen, C., Dam, G., Piasecki, S. and Stemmerik, L., 1995. Modelling of hydrocarbon generation in the Jameson Land basin, East Greenland. First Break, **13** (8), 329-340.

Moore, T.E. and Pitman, J.K., 2018. *Geology and assessment of undiscovered oil and gas resources of the Jan Mayen Microcontinent Province, 2008* (No. 1824-L). US Geological Survey.

Morton, A.C., Whitham, A.G., Fanning, C.M. and Claoué-Long, J., 2005. The role of East Greenland as a source of sediment to the Vøring Basin during the Late Cretaceous. *In: Wandas, B., et al. (eds) Onshore-Offshore relationships on the North Atlantic Margin*. Norwegian Petroleum Society Special Publications,**12**, 83-110.

Mjelde, R., Aurvåg, R., Kodaira, S., Shimamura, H., Gunnarsson, K., Nakanishi, A., Shiobara, H., 2002. Vp/Vs-ratios from the central Kolbeinsey Ridge to the Jan Mayen Basin, North Atlantic; implications for lithology, porosity and present-day stress field. Marine Geophysical Research, **23**, 123–145.

Mjelde, R., Eckhoff, I., Solbakken, S., Kodaira, S., Shimamura, H., Gunnarsson, K., Nakanishi, A., Shiobara, H., 2007. Gravity and S-wave modelling across the Jan Mayen Ridge, North Atlantic; implications for crustal lithology. Marine Geophysical Research, **28**, 27–41.

Mjelde, R., Raum, T., Breivik, A.J. & Faleide, J.I., 2008a. Crustal transect across the North Atlantic. Marine Geophysical Research, **29**, 73 – 87.

Mjelde, R., Breivik, A.J., Raum, T., Mittelstaedt, E., Ito, G., Faleide, J.I., 2008b. Magmatic and tectonic evolution of the North Atlantic. Journal of the Geological Society, **165**, 31–42.

Mjelde, R., Raum, T., Kandilarov, A., Murai, Y., Takanami, T., 2009. Crustal structure and evolution of the outer Møre Margin, NE Atlantic. Tectonophysics, **468**, 224–243.

Müller, R.D., Gaina, C., Roest, W.R. & Hansen, D.L., 2001. A recipe for microcontinent formation, Geology, **29**, 203–206.

Mutter, J.C., Talwani, M., Stoffa, P.L., 1982. Origin of seaward-dipping reflectors in oceanic crust off the Norwegian margin by "subaerial sea-floor spreading". Geology, **10**, 3–12

Mutter, J.C. & Zehnder, C.M. 1988. Deep crustal structure and magmatic processes: the inception of seafloor spreading in the Norwegian-Greenland Sea. *In: Morton, A.C. & Parson, L.M. (eds), Early Tertiary volcanism and the opening of the NE Atlantic*, Geological society Special Publication, **39**, 35 – 48.

Mutter, J.C., Buck, W.R. & Zehnder, C.M. 1988. Convective partial melting: a model for theformation of thick basaltic sequences during the initiation of spreading. Journal of Geophysical Research, **93**, B2, 1031 – 1048.

Myhre, J.C. & Eldholm, O. 1981. Sedimentary and crustal velocities in the Norwegian-Greenland Sea. Journal of Geophysical Researh, **86**, B6, 5012 – 5022.

Myhre, A.M., Eldholm, O. & Sundvor, E., 1984. The Jan Mayen Ridge: Present status, Polar Research., **2**, 47–59.

Norwegian Petroleum Directorate Resource Reports: Petroleum resources on the Norwegian continental shelf 2013 exploration, p 47 – 59.

Olafsson, I. & Gunnarsson, K. 1989. The Jan Mayen Ridge: Velocity Structure from Analysis of Sonobuoy Data. OS-89030/JHD-04. Orkustofnun, Reykjavık.

Olesen, O., Ebbing, J., Lundin, E., Mauring, E., Skilbrei, J.R., Torsvik, T.H., Hansen, E.K., Henningsen, T., Midbøe, P., Sand, M. 2007. An improved tectonic model for the Eocene opening of the Norwegian-Greenland Sea: Use of modern magnetic data. Marine and Petroleum Geology, **24**, 53 – 66.

Olesen, O., Bronner, M., Ebbing, J., Gellein, J., Gernigon, L., Koziel, J., Lauritsen, T., Myklebust, R., Pascal, C., Sand, M., Solheim, D. & Usov, S. 2010. New aeromagnetic and gravity compilations from Norway and adjacent areas: methods and applications. *In: Ving, B.A. & Pickering, S. C. (eds) Petroleum Geology: From Mature Basins to New Frontiers – Proceedings of the 7th Petroleum Geology Conference*, 559–586. doi: 10.1144/0070559

Omosanya, K.O., Harishidayat, D. & Johansen, S.E. 2017. Seismic Interpretation and Characterisation of Igneous Rocks in Jan Mayen Microcontinent, Norwegian-Greenland Sea. AAPG Search and Discovery article #51369.

Osmundsen, P.T., Sommaruga, A., Skilbrei, J.R. & Olesen, O. 2002. Deep structure of the Mid Norway rifted margin. Norwegian Journal of Geology, **82**, 205–224.

Parson, L.M. & the ODP Leg 104 Scientific Party. 1988. Dipping reflector styles in the NE Atlantic Ocean. *In: Morton, A.C. & Parson, L.M. (eds), Early Tertiary volcanism and the opening of the NE Atlantic*, Geological society Special Publication, **39**, 57 – 68.

Paton, D.A., Pindell, J., McDermott, K., Bellingham, P. & Horn, B. 2017. Evolution of seaward dipping reflectors at the onset of oceanic crust formation at volcanic passive margins: insights from the South Atlantic. Geology. **45**, 5, 439 – 442.

Peron-Pinvidic, G. & Manatschal, G., 2010. From microcontinents to extensional allochthons: witnesses of how continents break apart? Petroleum. Geoscience, **16**, 189–197.

Peron-Pinvidic, G., Gernigon, L., Gaina, C. & Ball, P., 2012a. Insights from the Jan Mayen system in the Norwegian-Greenland Sea – I : mapping of a microcontinent, Geophysical Journal International, **191**, 385 - 412, doi: 10.1111/j.1365-246X.2012.05639.x

Peron-Pindivic, G., Gernigon, L., Gaina, C. & Ball, P., 2012b. Insights from the Jan Mayen system in the Norwegian-Greenland Sea – II: Architecture of a microcontinent, Geophysical Journal International., **191**, 413 – 435, doi: 10.1111/j.1365-246X.2012.05639.x

Peron-Pinvidic, G., Manatschal, G., Osmundsen, P.T., 2013. Structural comparison of archetypal Atlantic rifted margins: A review of observations and concepts. Marine & Petroleum Geology, **43** (0), 21–47.

Planke, S., Eldholm, O., 1994. Seismic response and construction of seaward dipping wedges of flood basalts: Voring volcanic margin. Journal of Geophysical Research, **99**, (B5), 9263–9278. https://doi.org/10.1029/94JB00468.

Planke, S., Alvestad, E. & Eldholm, O. 1999. Seismic characteristics of basaltic extrusive and intrusive rocks. The Leading Edge, 18 (3), 342 – 348. http://dx.doi.org/10.1190/1.1438289

Planke, S., Symonds, P.A., Alvestad, E., Skogseid, J., 2000. Seismic volcanostratigraphy of large-volume basaltic extrusive complexes on rifted margins. Journal of Geophysical Research, **105**, (B8), 19335–19351. https://doi.org/10.1029/1999JB900005

Polteau, S., Mazzini, A., Jerram, D.A., Millett, J., Planke, S., Abdelmalak, M.A., Hansen, G., Blischke, A., Mykklebust, R., 2018. The pre-breakup stratigraphy and petroleum system of the Southern Jan Mayen Ridge revealed by seafloor sampling, Tectonophysics. https://doi.org/10.1016/j.tecto.2018.04.016.

Price, S.P. and Whitham, A.G., 1997. Exhumed hydrocarbon traps in East Greenland: analogs for the Lower-Middle Jurassic play of Northwest Europe. AAPG bulletin, **81**, (2), 196-221.

Ritter, U., Zielinski, G.W., Weiss, H.M., Zielinski, R.L. and Sættem, J., 2004. Heat flow in the Vøring Basin, mid-Norwegian shelf. Petroleum Geoscience, **10** (4), 353-365.

Sandstå, N.R. 2016. Searching more in deeper water. Norwegian Continental Shelf, No.1 (2016), 34 – 35.

Schiffer, C., Pearce, A., Phethean, J., Gernigon, L., McCaffrey, K., Petersen, K. D. & Foulger, G. 2018. The Jan Mayen microplate complex and the Wilson Cycle. *In: Wilson, R. W., Houseman, G. A., McCaffrey, K. J. W., Dore, A. G. & Buiter, S. J. H. (eds) Fifty Years of the Wilson Cycle Concept in Plate Tectonics*. Geological Society, London, Special Publications, 470. https://doi.org/10.1144/SP470.2

Scotchman, I.C., Carr, A.D. and Parnell, J., 2006. Hydrocarbon generation modelling in a multiple rifted and volcanic basin: a case study in the Foinaven Sub-basin, Faroe–Shetland Basin, UK Atlantic margin. Scottish Journal of Geology, **42** (1),1-19.

Scott, R.A., Ramsey, L.A., Jones, S.M., Sinclair, S., Pickles, C.S., 2005. Development of the Jan Mayen microcontinent by linked propagation and retreat of spreading ridges. *In: Wandås, B.T.G., Nystuen, J.P., Eide, E., Gradstein, F. (Eds.)*, Onshore–Offshore Relationships on the North Atlantic Margin. Norwegian Petroleum Society, 69–82.

Skogseid, J. & Eldholm, O. 1987. Early Cenozoic crust at the Norwegian continental margin and the conjugate Jan Mayen ridge. Journal of Geophysical Research, **92**, (B11), 11471 – 11491.

Skogseid, J., Planke, S., Faleide, J.I., Pedersen, T., Eldholm, O., Neverdal, F., 2000. NE Atlantic continental rifting and volcanic margin formation. *In: Nøttvedt, A., (eds) Dynamics of the Norwegina Margin*. Geological Society, London, Special Publications, **167** (1), 295–326. https://doi.org/10.1144/GSL.SP.2000.167.01.12

Slagstad, T., Balling, N., Elvebakk, H., Midttømme, K., Olesen, O., Olsen, L. and Pascal, C., 2009. Heat-flow measurements in Late Palaeoproterozoic to Permian geological provinces in south and central Norway and a new heat-flow map of Fennoscandia and the Norwegian–Greenland Sea. Tectonophysics, **473** (3-4), 341-361.

Stemmerik, L., Clausen, O.R., Korstgård, J., Larsen, M., Piasecki, S., Seidler, L., Surlyk, F. and Therkelsen, J., 1997. Petroleum geological investigations in East Greenland: project 'Resources of the sedimentary basins of North and East Greenland'. Geology of Greenland Survey Bulletin, **176**, 29-38.

Stemmerik, L., Dam, G., Noe-Nygaard, N., Piasecki, S. and Surlyk, F., 1998. Sequence stratigraphy of source and reservoir rocks in the Upper Permian and Jurassic of Jameson Land, East Greenland. Geology of Greenland Survey Bulletin, **180**, 43-54.

Stoker, M.S., Stewart, M. et al. 2016. An overview of the Upper Paleozoic–Mesozoic stratigraphy of the NE Atlantic region. *In: Peron-Pinvidic, G., Hopper, J., Stoker, M.S., Gaina, C., Doornenbal, H., Funck, T. & Arting, U. (eds) The North-East Atlantic Region: A Reappraisal of Crustal Structure, Tectono-Stratigraphy and Magmatic Evolution*. Geological Society, London, Special Publications, 447, https://doi.org/10.1144/SP447.2

Sundvor, E., Eldholm, O., Gladczenko, T.P. and Planke, S., 2000. Norwegian-Greenland Sea thermal field. Geological Society, London, Special Publications, **167** (1), 397-410.

Surlyk, F., Clemmensen, L.B. and Larsen, H.C., 1981. Post-Paleozoic evolution of the East Greenland continental margin. Canadian Society of Petroleum Geologists Memoir 7, 611 – 645.

Surlyk, F., 1990. Timing, style and sedimentary evolution of Late Palaeozoic-Mesozoic extensional basins of East Greenland. *In: Hardman, R.F.P. & Brooks, J., (eds) Tectonic Events Responsible for Britain's Oil and Gas Reserves*. The Geological Society, London, Special Publications, **55** (1), 107-125.

Surlyk, F. and Ineson, J.R., 2003. The Jurassic of Denmark and Greenland: key elements in the reconstruction of the North Atlantic Jurassic rift system. Geological Survey of Denmark and Greenland Bulletin, **1**, 9-20.

Talwani, M. & Udintsev, G. 1974, Tectonic Synthesis. IODP deep sea drilling project Leg 38 report, 1213 – 1242.

Talwani, M. & Eldholm, O. 1977. Evolution of the Norwegian-Greenland Sea. Geological Society of America Bulletin, 88, 969 – 999.

Talwani, M., Mutter, J., Eldholm, O. 1981. The initiation of opening of the Norwegian Sea. Oceanol. Acta. 1981. Proceedings 26th International Geological Congress, Geology of continental margins symposium, Paris, July 7-17th. 1980, 23 – 30.

Torsvik, T.H., Amundsen, H.E.F., Trønnes, R.G., Doubrovine, P.V., Gaina, C., Kusznir, N.J., Steinberger, B., Corfu, F., Ashwal, L.D., Griffin, W.L., Werner, S.C., Jamtveit, B., 2015. Continental crust beneath southeast Iceland. Proc. Natl. Acad. Sci. Unit. States Am. 112, 1818–1827, www.pnas.org/cgi/doi/10.1073/pnas.1423099112

Tsikalas, F., Faleide, J.I., Eldholm, O. & Wilson, J., 2005. Late Mesozoic – Cenozoic structural and stratigraphic correlations between the conjugate and mid-Norway and NE Greenland continental margins *In: Dore, A. G. & Vining, B. A. (eds) Petroleum Geology: North-West Europe and Global Perspectives—Proceedings of the 6th Petroleum Geology Conference*, 785–801.

Vosgerau, H., Passey, S., Svennevig, K., Strunck, M.N., Jolley, D.W. 2016. Reservoir architectures of interlava systems: a 3D photogrammetrical study of Eocene cliff sections, Faroe Islands. *In: Bowman, M., Smyth, H. R., Good, T. R., Passey, S. R., Hirst, J. P. P. & Jordan, C. J. (eds) 2016. The Value of Outcrop Studies in Reducing Subsurface Uncertainty and Risk in Hydrocarbon Exploration and Production*. Geological Society, London, Special Publications, 436, 55–73.

Whitham, A.G., Price, S.P., Koraini, A.M. and Kelly, S.R.A., 1999, January. Cretaceous (post-Valanginian) sedimentation and rift events in NE Greenland (71–77 N). *In: Fleet, A.J. & Boldy,*

S.A.R. (eds) Petroleum Geology of Northwest Europe: Proceedings of the 5th Conference, The Geological Society, London, **5**, (1), 325-336.

Whitham, A.G., Morton, A.C. and Fanning, C.M., 2004. Insights into Cretaceous–Palaeogene sediment transport paths and basin evolution in the North Atlantic from a heavy mineral study of sandstones from southern East Greenland. Petroleum Geoscience, **10,** (1), 61-72.

Petroleum Systems chart and Tectonic events chart templates provide by Dr Kirstie Wright using: http://www.stratigraphy.org/index.php/ics-chart-timescale and https://timescalefoundation.org/charts/RGB.pdf

APPENDICIES

APPENDIX A

Well Summary Sheets

- DSDP Leg 38 (1974)
  - Well 346
  - Well 347
  - Well 348
  - Well 349
  - Well 350

- ODP Leg 151 (1993)
  - Well 907 A

- ODP Leg 162 (1995)
  - Well 907 C
  - Well 985 B
  - Well 987 E

DSDP Leg 38- Well 346

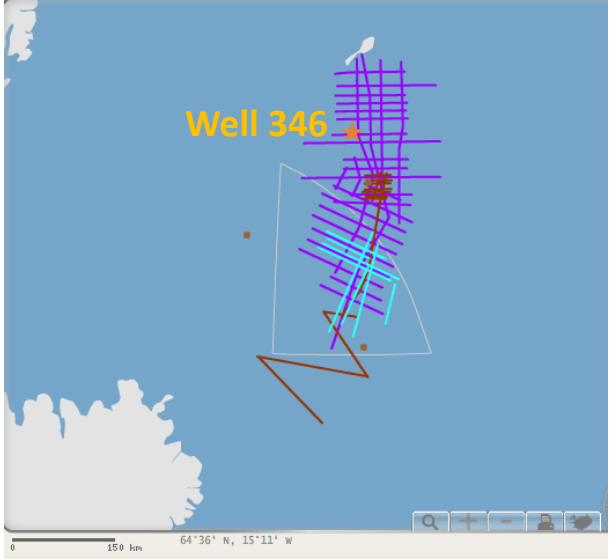

Well Summary
Date: **06/09/1974**
Latitude: **69.8892**
Longitude: **-8.6855**
Water Depth from sea level (m): **732**
Bottom Felt at: **741 meters (drill pipe)**
Well penetration (m): **187**
Physiographic feature: **Ridge**
No. of cores: **20**
Interval cored (m): **187**
Core recovered (m): **119**
Oldest sediment cored depth below sea floor (m): **187**
Oldest sediment age: **Eocene**
Oldest sediment description: **sandy mudstone**
Type of crust: **oceanic**

Holes at Sites 346 and 347 were among a series of holes designed to investigate the Jan Mayen Ridge. Site 346 was designed to reach the acoustic basement and determine its nature and age. When the cores from Site 346 yielded a hard and difficult to penetrate sandstone in which coring times were comparable to coring times in basalt, the question arose whether this sandstone itself represented acoustic basement or whether igneous basement lay further to the west and dipped down at a much steeper angle. If this were the case, it would be impractical to reach igneous basement at Site 346. To settle this point, Site 347 was drilled at the extreme western edge of the Jan Mayen Ridge. This hole could determine whether the sandstone under the unconformity would be encountered or whether igneous basement would be reached under the western flank of Jan Mayen Ridge

Well lithology

Principal Results
Site 346 was located on the Jan Mayen Ridge. Pliocene and Pleistocene sediments extend from the top to a depth of 25.5 meters and consist of terrigenous sandy mud, as well as mud and clay. The middle Miocene sediments consist of sandy mud and biogenic siliceous oozes characterized by a high percentage of sponge spicules. Below the Miocene section is a massive terrigenous sandy mudstone. This unit was quite hard to penetrate, and is almost completely barren of fauna except for arenaceous foraminifera (benthonic), and a few badly preserved calcareous foraminifera.

The hole remained clean throughout during drilling, no hydrocarbon indicators were encountered and the well was abandoned during drilling an unexpectedly dense and compacted material.

AGE	DEPTH SERIES, SUBSERIES (m)		LITHOLOGIC COLUMN	CORE, SECTION, INTERVAL (cm) AND SAMPLE NO. (GIN)	THICKNESS OF SERIES (m)
MIDDLE MIOCENE-PLIOCENE OR PLEISTOCENE TO PLEISTOCENE	10.5	1		2-3, 25-27 (2007)	10.5
	I	2		4-3, 75-77 (2017)	21.5
	31.5				
MIDDLE MIOCENE(?)	39.7	1		5-4, 80-85 (2023)	8.2
	II	2		8-3, 70-72 (2033)	27.8
	67.5				
OLIGOCENE AND MIDDLE MIOCENE(?)	84.0	1		10-1, 29-31 (2024)	16.5
	III	2			36.5
	120.5			13-4, 29-31 (2060)	
EOCENE	120.5	(121.8)		14-1, 19-21 (217) 14-2, 80-82 (218) 14-3, 29-31 (219) 14-5, 27-29 (220) 15-2, 75-77 (221) 15-4, 75-77 (223) 15-5, 75-77 (224) 16-1, 75-77 (225) 16-2, 75-77 (226) 17-1, 75-77 (227) 17-2, 75-77 (228) 17-3, 75-77 (229) 18-2, 93-94 (231) 18-3, 118-120 (232) 19-1, 133-135 (233) 19-2, 58-60 (234) 19-3, 104-106 (235) 19-4, 26-28 (236) 20-1, 86-88 (237) 20-2, 88-90 (238)	59.5
	IV				
	180.0	(187.0)			

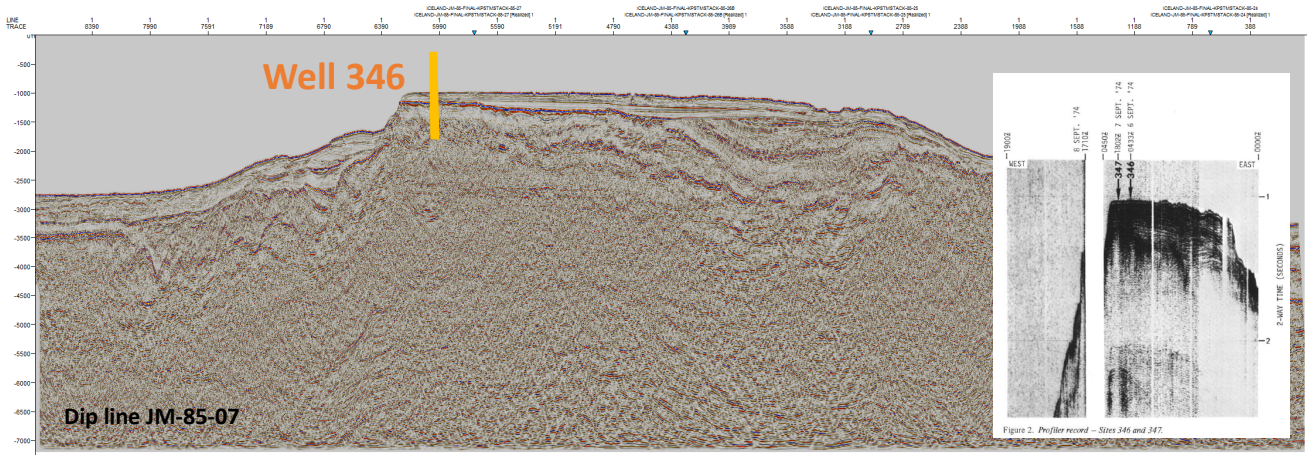

Figure 2. *Profiler record – Sites 346 and 347.*

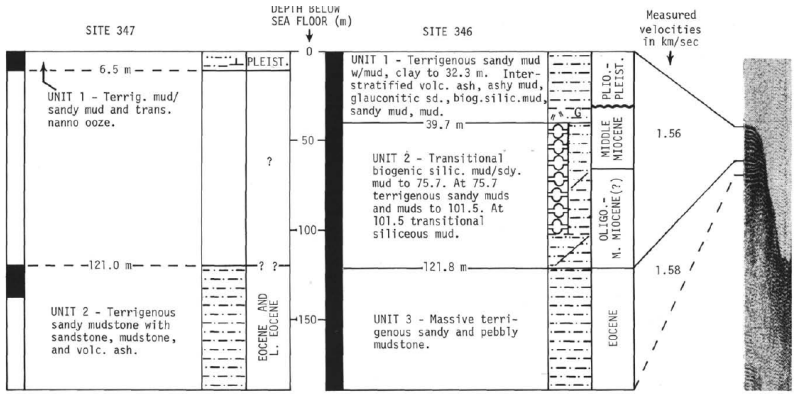

Figure 5. *Lithologic summary and seismic profile, Sites 346, 347.*

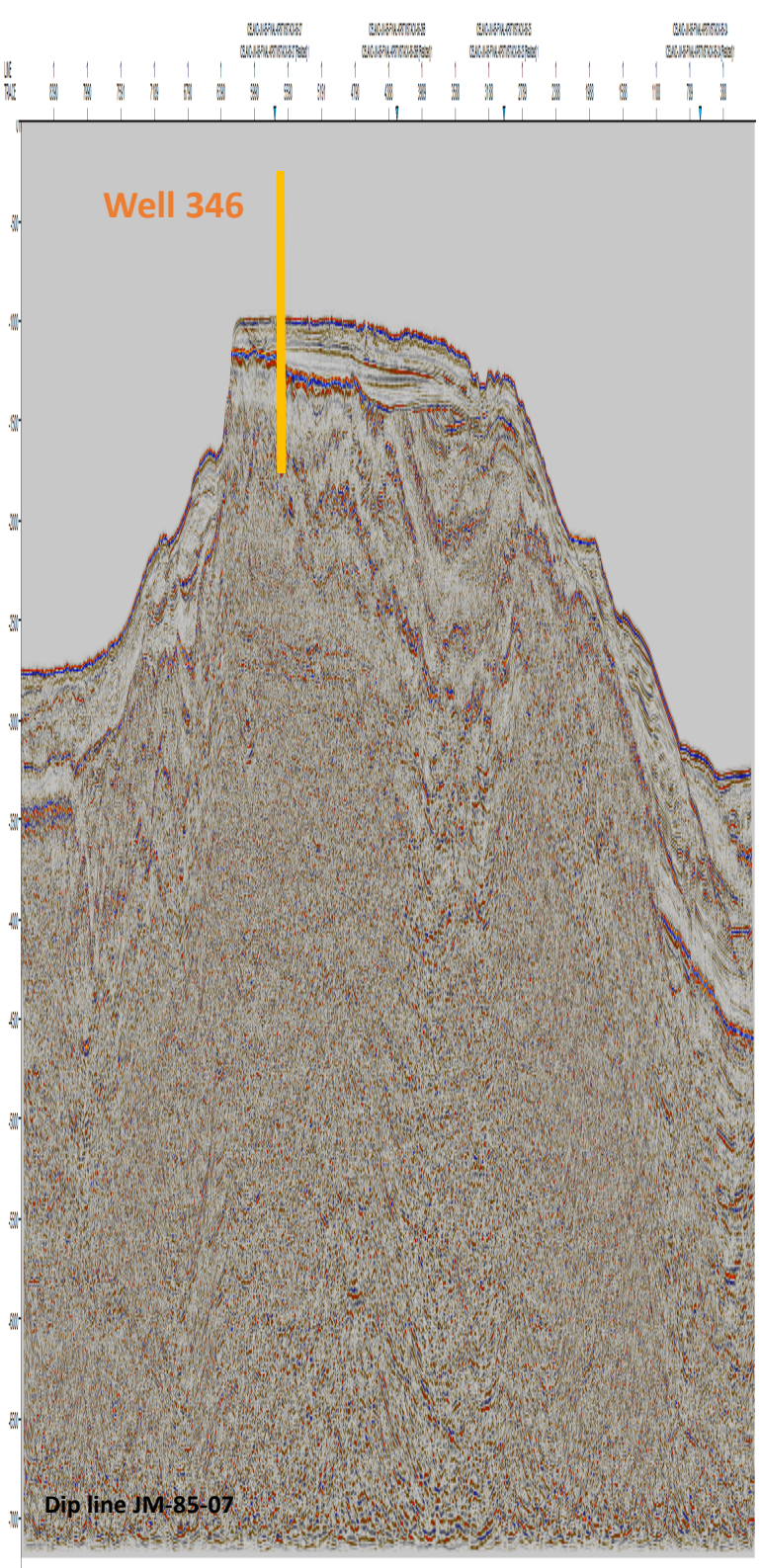

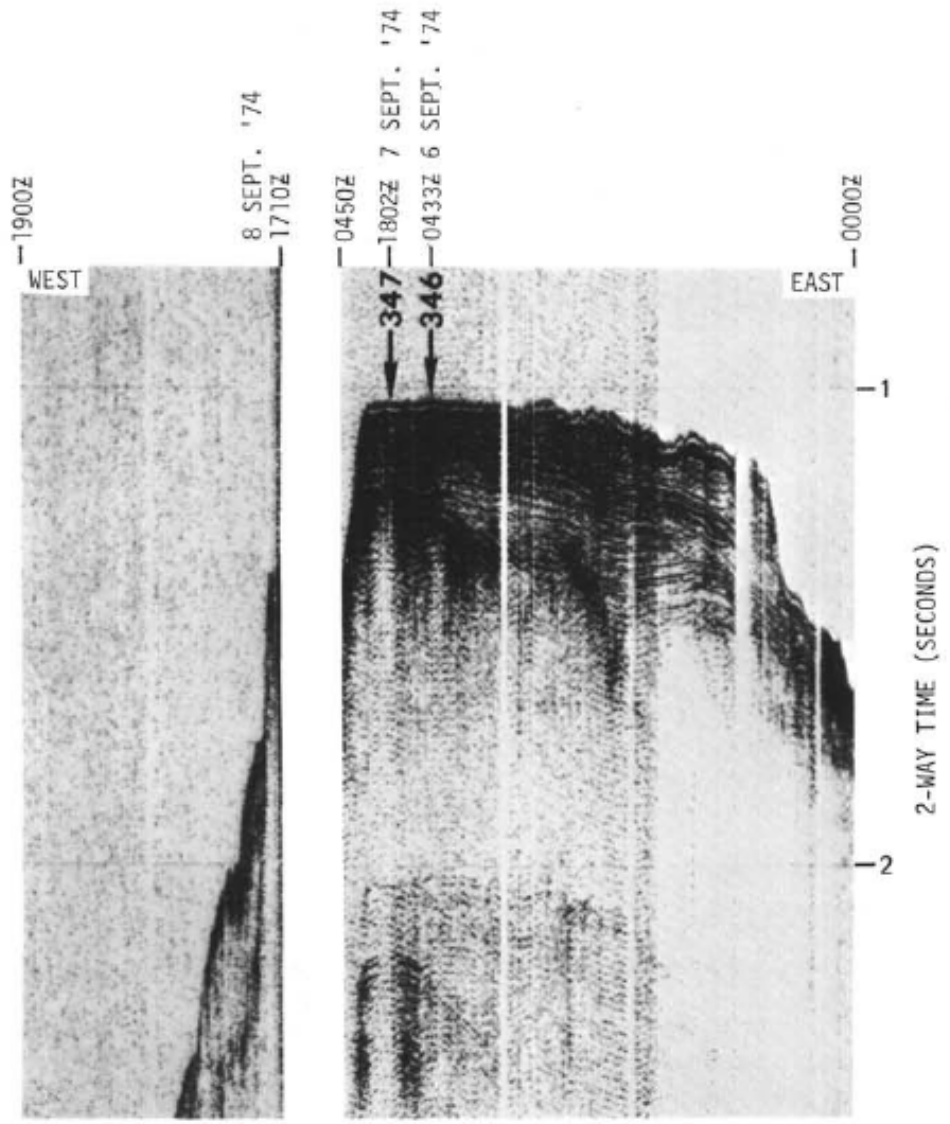

Figure 2. *Profiler record – Sites 346 and 347.*

TABLE 4
Lithologic Summary, Site 346

Unit	Depth (m) and Core Numbers	Age	Significant Characteristics
1A	0-32.3 (1-1 to 4-5, 80) 32.3 m thickness	Pleistocene Pliocene	Terrigenous sandy mud and mud with intermixed sandy muds and muds in lower 1.9 m of unit, of the sediments recovered, 61% is sandy mud, 32% mud, and 7% intermixed sandy mud and mud. The texture consists of 5%-18% sand, 10%-40% silt, and 45%-75% clay
1B	32.3-39.7 (4-5, 80 to 5-4, 18) 7.4 m thickness	Middle	42% transitional siliceous-rich glauconitic sandy mud, and volcanic ash, 10% glauconitic sandy mud and sand, and 8% transitional siliceous mud and sandy mud; transitional siliceous-rich glauconitic sandy muds occur in Core 5, Sections 1 and 3
2A	39.7-63.5 (5-4, 18 to 7, CC) 23.8 m thickness	Middle Miocene	Transitional siliceous sandy muds and muds texture varies from 5%-30% sand, 15%-30% silt, and 50%-55% clay
2B	63.5-75.7 (8-1 to 9.2, 50) 12.2 m thickness	Middle Miocene	Terrigenous mud with sandy mud in Core 9, Section 1 and 0.1 m volcanic ash unit in Core 8, Section 5; texture of the mud is comprised of 15%-20% sand, 30%-40% silt and 30%-55% clay
2C	75.7-101.5 (9-2, 50 to 11, CC) 25.8 m thickness	Middle Miocene	Transitional siliceous mud and minor sandy mud with a texture comprised of 3%-15% sand, 17%-60% silt, 35%-80% clay
2D	101.5-121.8 (12-1 to 14-2, 133) 20.3 m thickness	Oligocene (?)	Terrigenous mud with a texture comprised of 5%-10% sand, 60%-70% silt, 20%-45% clay
3	121.8-187.0 (14-2, 133 to 20, CC) 66.2 m minimum thickness	Eocene (?)	Massive terrigenous sandy and pebbly mudstone that is interrupted by minor amounts of mudstone and calcareous sandstone arranged into graded beds less than 30 cm thick and rare volcanic ash laminae; generally lithified with no coring deformation; extensively bioturbated throughout except for graded turbidite units, which are laminated to very thinly stratified; abundant scattered pebbles of quartz, chert, siltstone, and basalt (?) less than 0.5 cm; worm tubes scattered throughout; locally calcareous and very hard

[a]Core numbers in parentheses.

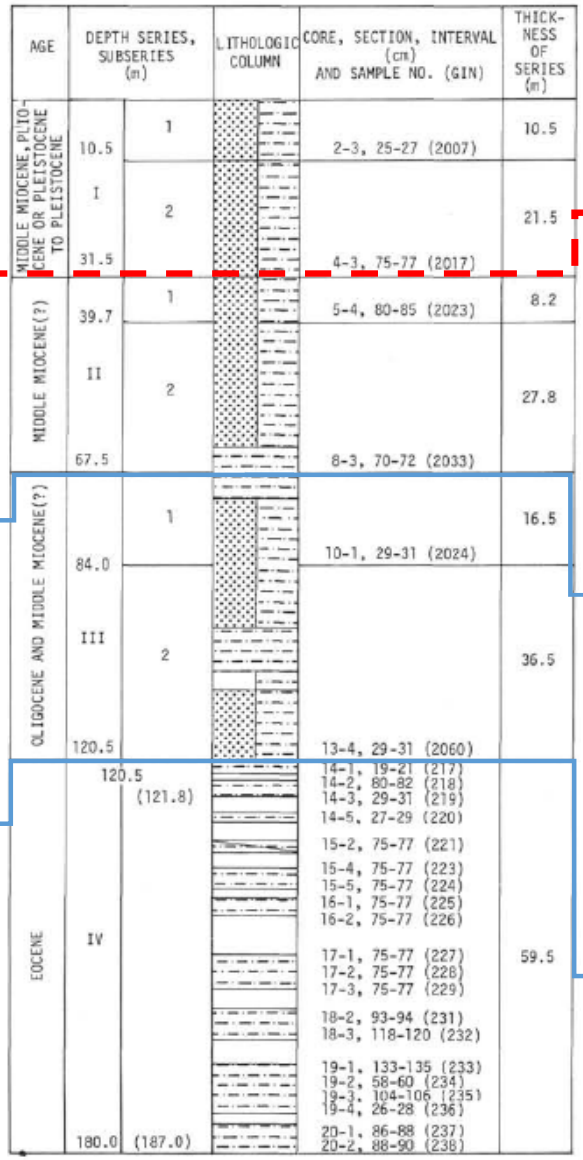

U/C?

Lithology

- Unit 1: 0 – 31.5 m. Pleistocene age, terrigenous sandy mudstone.
  - Yellow-brown in upper part. Grey to olive-grey in lower part.
  - subseries 1-1: dominated by clay sediments & planktonic foraminiferal tests, variously silty & admixture of sand-sized quartz grains and fragments of basalt
  - Subseries 1-2: unsorted sand-clay-silt polymitic sediments. Non-uniformly distributed fragments of different sizes (sand to gravel and pebbles) of various rock types (quartz, feldspar grains, mica, chlorite, fragments of basalt, hornblende biotite schists, granite and limestones also present).
  - Interpretation: glacial-marine origin with minor contributions from pelagic (nannoplankton and foraminifera) and bottom-dwelling organisms (sponges)
- Unit 2: 31.5 – 67.5 m. Middle Miocene age, Siliceous rich, glauconitic sandy mudstone.
  - Upper part consists of interstratified siliceous-rich, glauconitic sandy muds and sands, terrigenous sandy mud, volcanic rich sandy mud, transitional siliceous muds and sandy muds and volcanic ash units.
  - Lower unit consist of massive transitional siliceous sandy muds and muds containing 7-20% sponge spicules and 2 thin volcanic ash bands. Green-grey and soft – firm. Clay-sand-silt containing abundant glauconite. Glauconite grains are larger than most terrigenous clastic particles.
  - Interpretation: Glauconitic sediments may represent either a hiatus in sedimentation or an unconformity (separates Quarternary (Plio-Pleistocene) sediments above (unit 1) from Miocene sediments below.
- Unit 3: 67.5 – 120.5 m. Middle Miocene to lower Miocene/ middle-upper Oligocene age, terrigenous mud with sandy mud
  - Upper part consists of terrigenous clay siltstones with admixture of sand-size particles. Generally massive – poorly stratified, olive grey and greyish olive green. Contains small amount of volcanic ash.
  - Middle part contains transitional siliceous mud and minor sandy mud, olive black and olive grey.
  - Lower part consists of dark olive grey terrigenous mud with carbonaceous detritus, scattered volcanic ash and admixture of silty quartz grains.
  - Interpretation: abundance of sponges suggests deposition in cold marine conditions. Bioturbated intervals indicate organic reworking within shallow marine conditions.
- Unit 4: 120.5 – 187 m. Oligocene – upper Eocene age, massive terrigenous sandy mudstones.
  - Massive extensively bioturbated terrigenous sandy mudstone locally grades into sandstone and mudstone. Hard and lithified. Olive and dark greenish grey to medium and medium dark grey. Rare and thin layers of volcanic ash and locally calcareous. Thin normally graded units represent turbidites which increase in abundance downward within the unit. Dominated by sandy siltstones with rounded clasts of quartz, feldspars, chert, siltstone and basalt fragments.
  - Interpretation: clay mineralogy suggests re-deposition from the continental platform & mica compositions suggest transformation associated with the alteration and re-deposition of ancient quartz-biotite schists and gneisses from Greenland. However a part of the biotite may have been eroded from alkaline basalts (volcaniclastic/volcanogenic origin from Tertiary lavas of Jan Mayen Ridge)

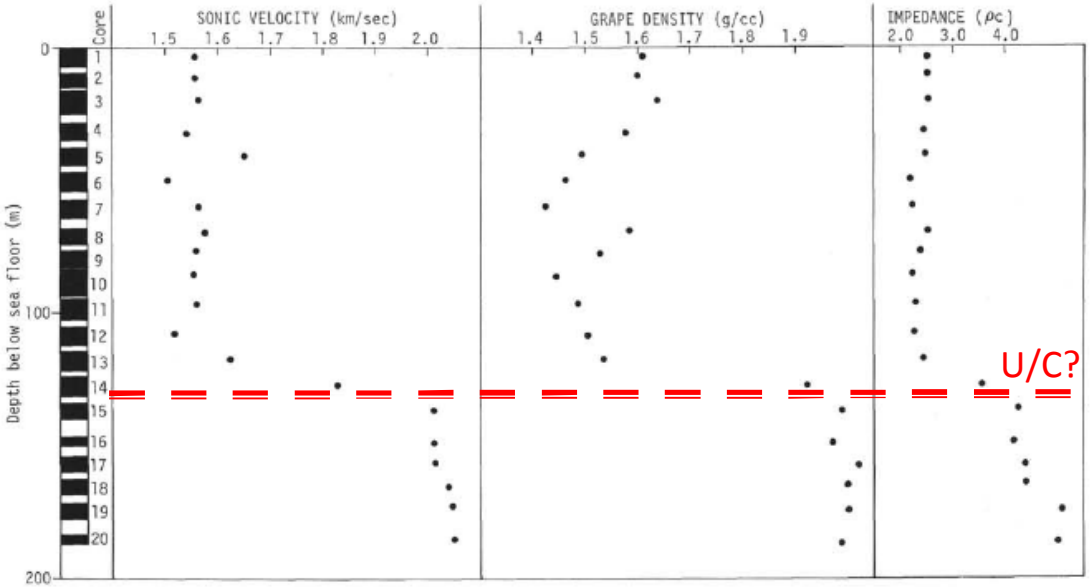

Figure 7. *Density, velocity, impedance, Site 346.*

Physical properties of well 346

- The section is differentiated into two distinct units: (1) a lower high density sediment possessing high (>2.0 km/sec) sonic velocity, and (2) an upper unit with low bulk density and low sonic velocity. The abrupt change in acoustic impedance at Core 14, Section 2, indicates the lower unit is a strong reflector of sound, and would be expected to be visible on seismic profile records. (possibly marks the unconformity surface).
- Cores 5 and 6 show a sonic velocity variation that is not matched by the other parameters. Figure 8 is a plot of bulk density for each core section in the upper unit. Although a greater scatter of points results, five separate subunits can be seen (Table 7).
- The Miocene(?) unit is clearly shown to have high compressive strength, high density and velocity, and high acoustic impedance. It is a significant reflector at 132 meters and should be clearly visible on seismic profiles records = **Unconformity on top of Jan Mayen Ridge?**

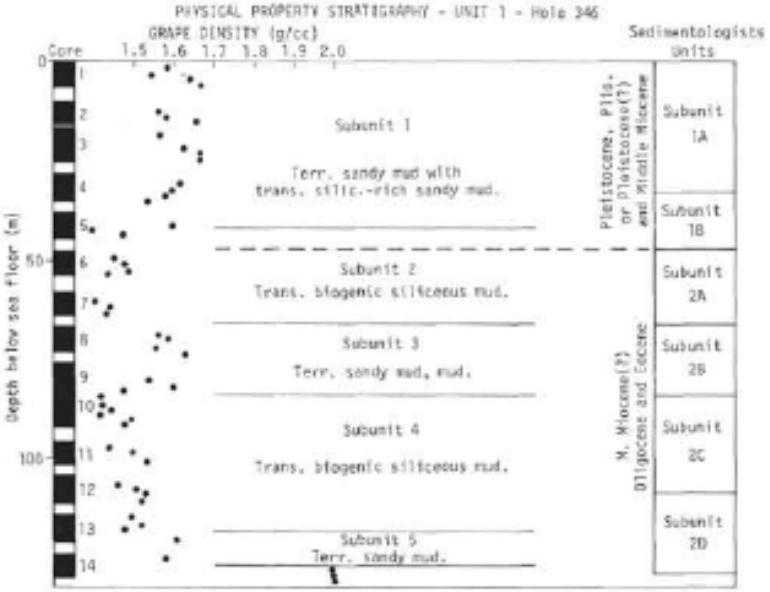

Figure 8. *Density profile – Cores 1-14, Site 346.*

TABLE 7
Sediment Units (Site 346) Based on Physical Properties

Unit 1	
Subunit 1 –	Extending from the surface to Core 5, Section 3 Avg. density – 1.605 g/cc Avg. water content – 35.07% Avg. velocity – 1.565 km/sec
Subunit 2 –	Extending from Core 5, Section 3 to Core 8, Section 2 Avg. density – 1.447 g/cc Avg. water content – 43.83% Avg. velocity – 1.533 km/sec
Subunit 3 –	Extending from Core 8, Section 2 to Core 9, Section 6 Avg. density – 1.580 g/cc Avg. water content – 36.74% Avg. velocity – 1.565 km/sec
Subunit 4 –	Extending from Core 9, Section 6 to Core 13, Section 4 Avg. density – 1.479 g/cc Avg. water content – 38.77% Avg. velocity – 1.564 km/sec
Subunit 5 –	Extending from Core 13, Section 4 to Core 14, Section 2 Avg. density – 1.597 g/cc Avg. water content – 31.75% Avg. velocity – 1.588 km/sec

Biostratigraphy

- "Glacial" sediments (Pliocene to Pleistocene) were recovered in Cores 1 to 3 (0-25.5 m) characterized by left-coiled *Globigerina pachyderma,* few nannofossils, and some cold water radiolarians.
- Ice-rafted material and reworked nannoplankton and pollen are less abundant compared with "glacial" sediments of previous sites. This may indicate that this site was often under permanent ice cover with low organic production, and receiving little ice-rafted material.
- Siliceous microfossils of Cores 4 to 11 (25.5-101.5 m) are generally rare and poorly preserved.
- In Core 5, Section 1 – diatom assemblage of Pliocene age. Core 5, Section 3 to core 11 – middle Miocene age. Therefore hiatus including the upper Miocene age.
- Core 13 = (111 – 120.5m) foraminifera and dinoflagellates indicate Oligocene age.
- Core 14-20 (120.5 – 187m) large foraminifera and dinoflagellates tests give an Eocene age.

DSDP Leg 38 - Well 347

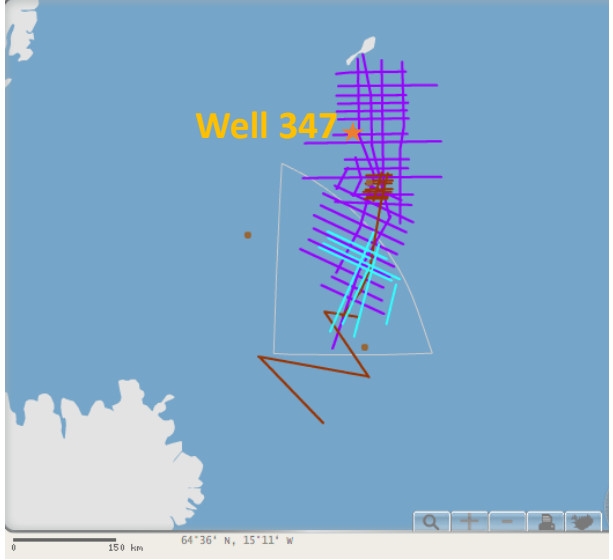

Well Summary

Date: **07/09/1974**
Latitude: **69.8718**
Longitude: **-8.6967**
Water Depth from sea level (m): **745**
Bottom Felt at: **762.0 meters (drill pipe)**
Well penetration (m): **190**
Physiographic feature: **Ridge**
No. of cores: **4**
Interval cored (m): **24**
Core recovered (m): **12.15**
Oldest sediment cored depth below sea floor (m): **190**
Oldest sediment age: **Eocene**
Oldest sediment description: **calcareous mudstone**
Type of crust: **oceanic**

Holes at Sites 346 and 347 were among a series of holes designed to investigate the Jan Mayen Ridge. Site 346 was designed to reach the acoustic basement and determine its nature and age. When the cores from Site 346 yielded a hard and difficult to penetrate sandstone in which coring times were comparable to coring times in basalt, the question arose whether this sandstone itself represented acoustic basement or whether igneous basement lay further to the west and dipped down at a much steeper angle. If this were the case, it would be impractical to reach igneous basement at Site 346. To settle this point, we moved to Site 347 at the extreme western edge of the Jan Mayen Ridge, and drilled another hole. This hole could determine whether we would still run into the sandstone under the unconformity or whether igneous basement would be reached under the western flank of Jan Mayen Ridge

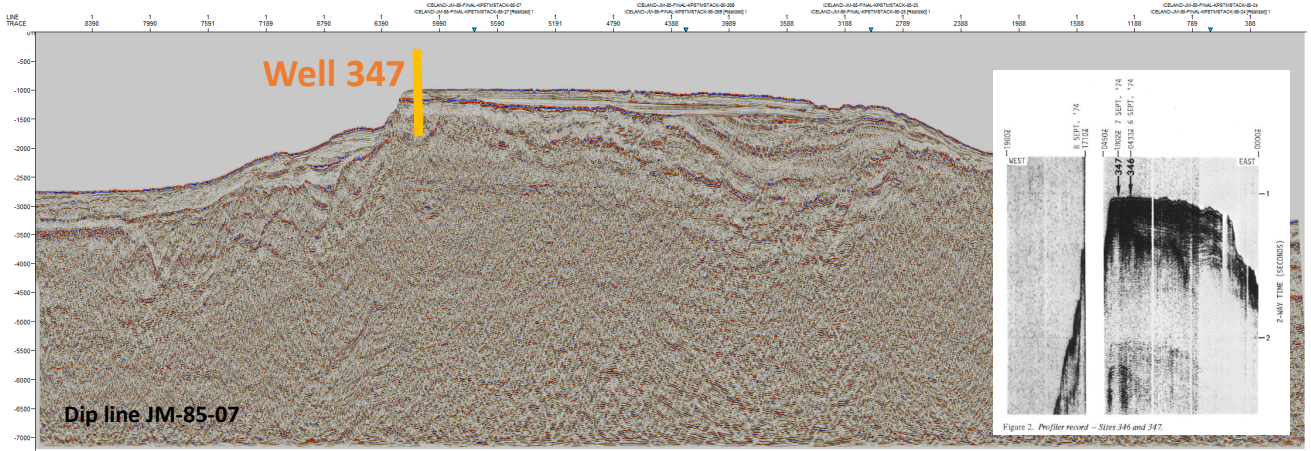

Well lithology

Principal Results

Site 347 was located on the Jan Mayen Ridge about 1 n mi southwest of Site 346, at the edge of the ridge platform. It was hoped that basement would be reached at a shallower depth closer to the edge. The seismic reflection record was unclear near the unconformity at 120 meters, and it was suspected that basement might lie below it. However, even after 190 meters were drilled into Pleistocene and late Eocene sediments, basement was not reached. Since progress was slow and there was no clear indication of when basement might be reached, the hole was terminated.

AGE	DEPTH SERIES, SUBSERIES (m)		LITHOLOGIC COLUMN	CORE, SECTION, INTERVAL (cm) AND SAMPLE NO. (GIN)	THICKNESS OF SERIES (m)
MIDDLE MIOCENE, PLIOCENE OR PLEISTOCENE TO PLEISTOCENE	10.5	1		2-3, 25-27 (2007)	10.5
	I	2		4-3, 75-77 (2017)	21.5
	31.5				
MIDDLE MIOCENE(?)	39.7	1		5-4, 80-85 (2023)	8.2
	II	2		8-3, 70-72 (2033)	27.8
	67.5				
OLIGOCENE AND MIDDLE MIOCENE(?)	84.0	1		10-1, 29-31 (2024)	16.5
	III	2		13-4, 29-31 (2060)	36.5
	120.5				
EOCENE	120.5	(121.8)		14-1, 19-21 (217) 14-2, 80-82 (218) 14-3, 29-31 (219) 14-5, 27-29 (220) 15-2, 75-77 (221) 15-4, 75-77 (223) 15-5, 75-77 (224) 16-1, 75-77 (225) 16-2, 75-77 (226)	
	IV			17-1, 75-77 (227) 17-2, 75-77 (228) 17-3, 75-77 (229) 18-2, 93-94 (231) 18-3, 118-120 (232) 19-1, 133-135 (233) 19-2, 58-60 (234) 19-3, 104-106 (235) 19-4, 26-28 (236) 20-1, 86-88 (237) 20-2, 88-90 (238)	59.5
	180.0	(187.0)			

Because Site 347 was located only a few kilometres from Site 346, and the drilling objective was to reach basement beneath the sedimentary sequence as quickly as possible, little coring was done in the sedimentary sequence. It may generally be assumed that the sequence at Site 347 is similar to Site 346, since both sites lie adjacent to one another on the top of the Jan Mayen Plateau.

Progress while coring in the lower drilled section was slow sue to the compacted and tough nature of the sediments encountered. The hole remained clean throughout, no hydrocarbons were encountered and the well was abandoned accordingly

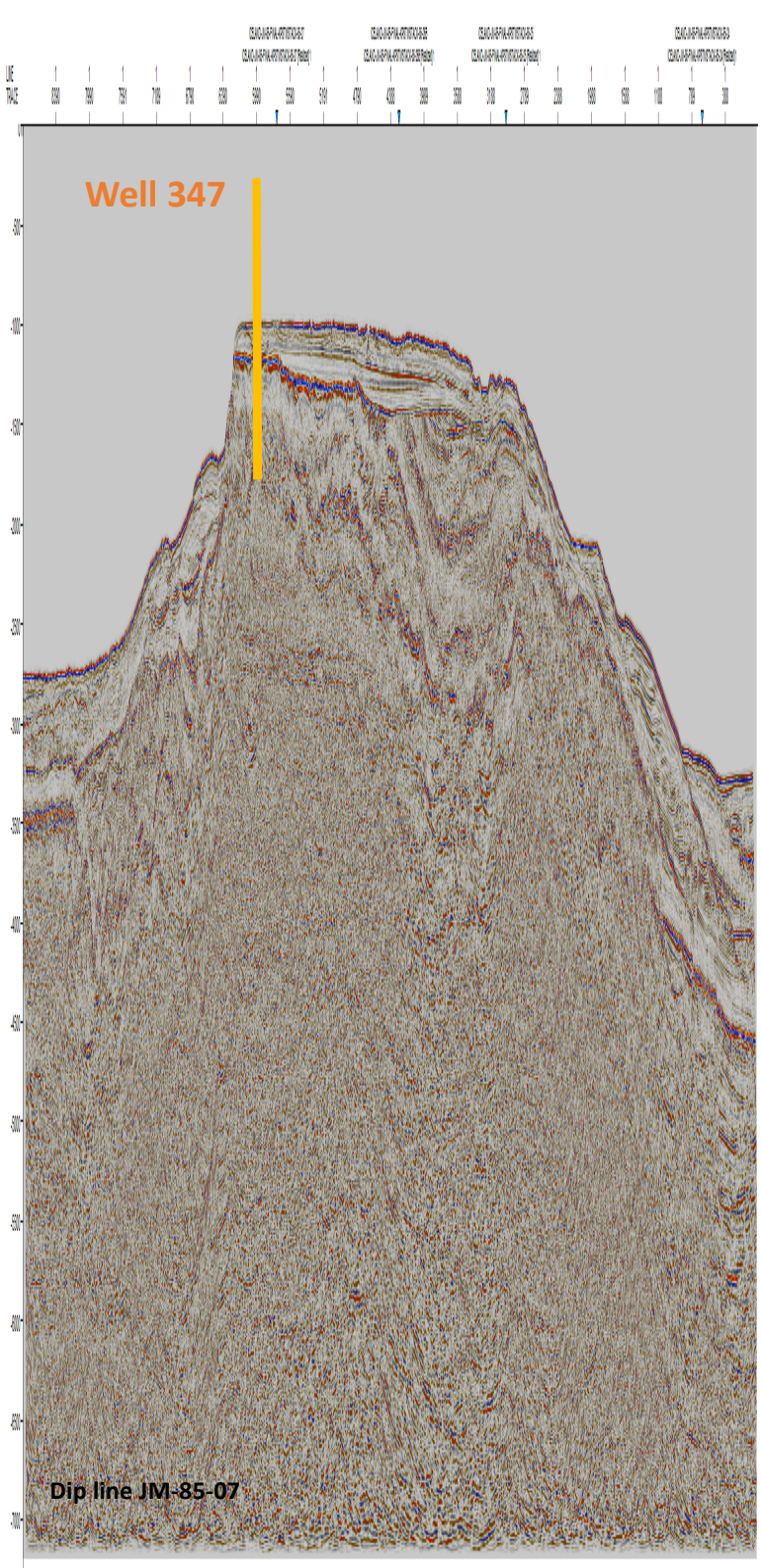

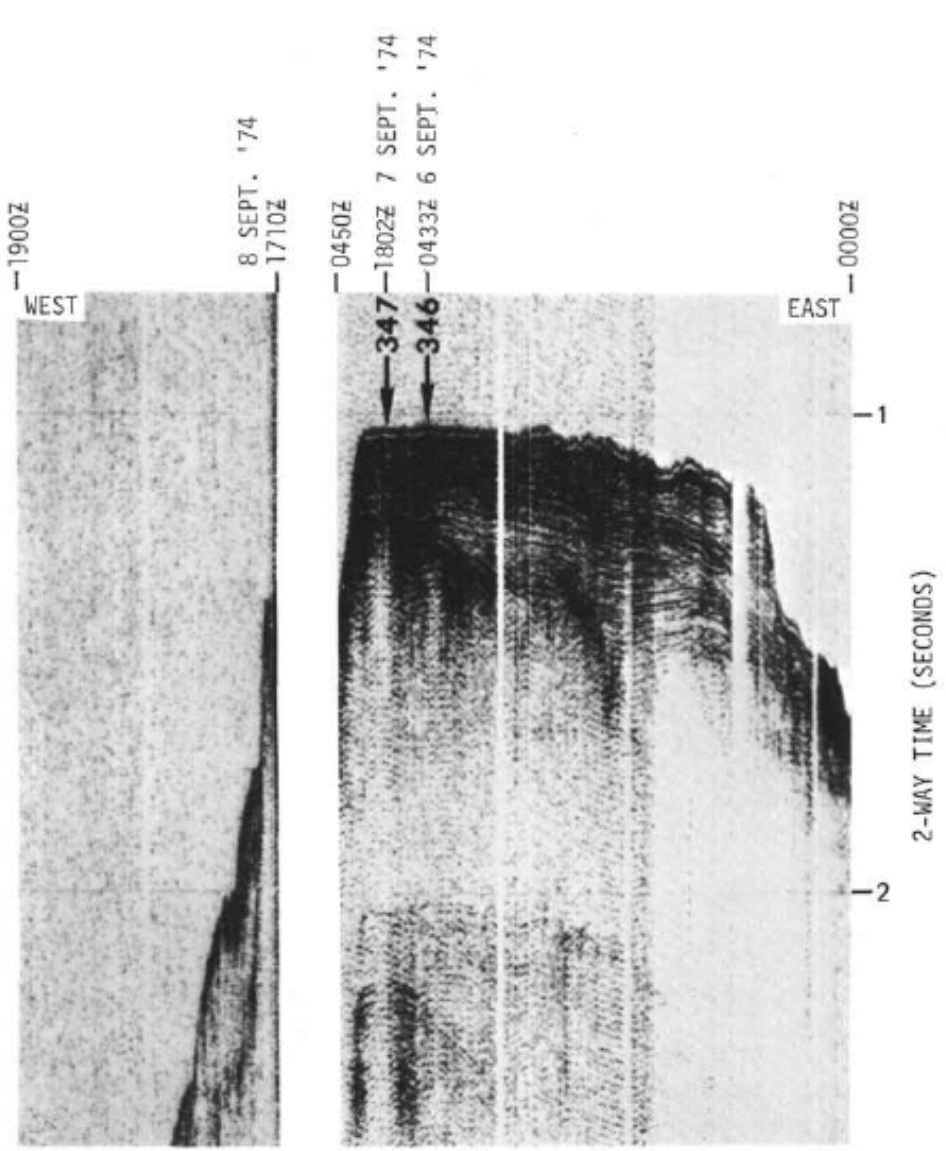

Figure 2. *Profiler record – Sites 346 and 347.*

TABLE 4
Lithologic Summary, Site 346

Unit	Depth (m) and Core Numbers	Age	Significant Characteristics
1A	0-32.3 (1-1 to 4-5, 80) 32.3 m thickness	Pleistocene Pliocene	Terrigenous sandy mud and mud with intermixed sandy muds and muds in lower 1.9 m of unit, of the sediments recovered, 61% is sandy mud, 32% mud, and 7% intermixed sandy mud and mud. The texture consists of 5%-18% sand, 10%-40% silt, and 45%-75% clay
1B	32.3-39.7 (4-5, 80 to 5-4, 18) 7.4 m thickness	Middle	42% transitional siliceous-rich glauconitic sandy mud, and volcanic ash, 10% glauconitic sandy mud and sand, and 8% transitional siliceous mud and sandy mud; transitional siliceous-rich glauconitic sandy muds occur in Core 5, Sections 1 and 3
2A	39.7-63.5 (5-4, 18 to 7, CC) 23.8 m thickness	Middle Miocene	Transitional siliceous sandy muds and muds texture varies from 5%-30% sand, 15%-30% silt, and 50%-55% clay
2B	63.5-75.7 (8-1 to 9.2, 50) 12.2 m thickness	Middle Miocene	Terrigenous mud with sandy mud in Core 9, Section 1 and 0.1 m volcanic ash unit in Core 8, Section 5; texture of the mud is comprised of 15%-20% sand, 30%-40% silt and 30%-55% clay
2C	75.7-101.5 (9-2, 50 to 11, CC) 25.8 m thickness	Middle Miocene	Transitional siliceous mud and minor sandy mud with a texture comprised of 3%-15% sand, 17%-60% silt, 35%-80% clay
2D	101.5-121.8 (12-1 to 14-2, 133) 20.3 m thickness	Oligocene (?)	Terrigenous mud with a texture comprised of 5%-10% sand, 60%-70% silt, 20%-45% clay
3	121.8-187.0 (14-2, 133 to 20, CC) 66.2 m minimum thickness	Eocene (?)	Massive terrigenous sandy and pebbly mudstone that is interrupted by minor amounts of mudstone and calcareous sandstone arranged into graded beds less than 30 cm thick and rare volcanic ash laminae; generally lithified with no coring deformation; extensively bioturbated throughout except for graded turbidite units, which are laminated to very thinly stratified; abundant scattered pebbles of quartz, chert, siltstone, and basalt (?) less than 0.5 cm; worm tubes scattered throughout; locally calcareous and very hard

[a]Core numbers in parentheses.

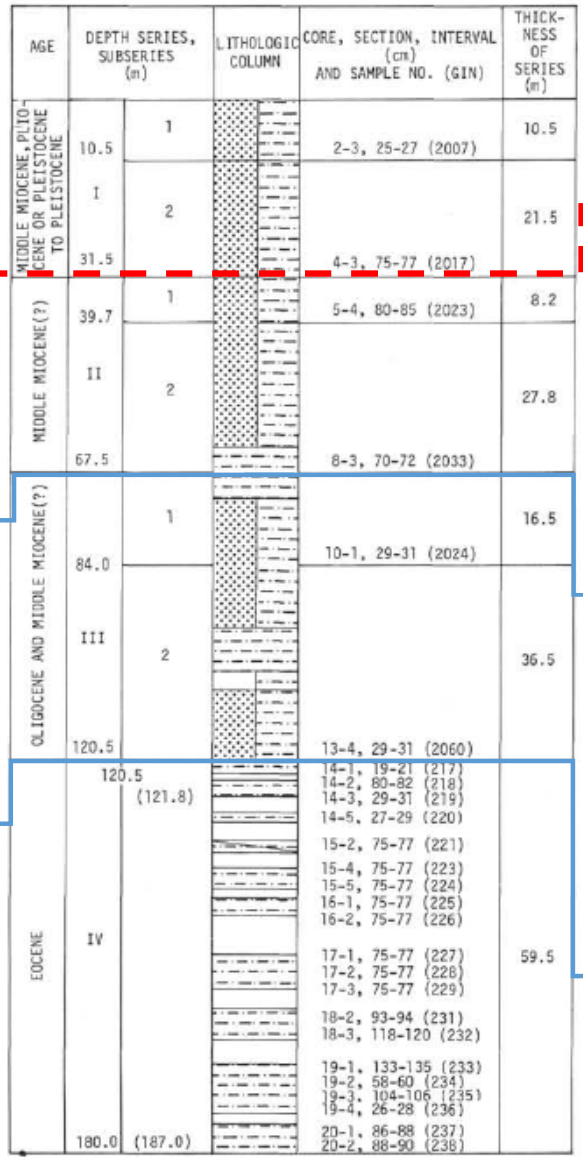

U/C?

Lithology

- Unit 1: 0 – 31.5 m. **Pleistocene age**, terrigenous sandy mudstone.
  - Yellow-brown in upper part. Grey to olive-grey in lower part.
  - subseries 1-1: dominated by clay sediments & planktonic foraminiferal tests, variously silty & admixture of sand-sized quartz grains and fragments of basalt
  - Subseries 1-2: unsorted sand-clay-silt polymitic sediments. Non-uniformly distributed fragments of different sizes (sand to gravel and pebbles) of various rock types (quartz, feldspar grains, mica, chlorite, fragments of basalt, hornblende biotite schists, granite and limestones also present).
  - Interpretation: glacial-marine origin with minor contributions from pelagic (nannoplankton and foraminifera) and bottom-dwelling organisms (sponges)

- Unit 2: 31.5 – 67.5 m. **Middle Miocene age**, Siliceous rich, glauconitic sandy mudstone.
  - Upper part consists of interstratified siliceous-rich, glauconitic sandy muds and sands, terrigenous sandy mud, volcanic rich sandy mud, transitional siliceous muds and sandy muds and volcanic ash units.
  - Lower unit consist of massive transitional siliceous sandy muds and muds containing 7-20% sponge spicules and 2 thin volcanic ash bands. Green-grey and soft – firm. Clay-sand-silt containing abundant glauconite. Glauconite grains are larger than most terrigenous clastic particles.
  - Interpretation: Glauconitic sediments may represent either a hiatus in sedimentation or an unconformity (separates Quarternary (Plio-Pleistocene) sediments above (unit 1) from Miocene sediments below.

- Unit 3: 67.5 – 120.5 m. **Middle Miocene to lower Miocene/ middle-upper Oligocene age**, terrigenous mud with sandy mud
  - Upper part consists of terrigenous clay siltstones with admixture of sand-size particles. Generally massive – poorly stratified, olive grey and greyish olive green. Contains small amount of volcanic ash.
  - Middle part contains transitional siliceous mud and minor sandy mud, olive black and olive grey.
  - Lower part consists of dark olive grey terrigenous mud with carbonaceous detritus, scattered volcanic ash and admixture of silty quartz grains.
  - Interpretation: abundance of sponges suggests deposition in cold marine conditions. Bioturbated intervals indicate organic reworking within shallow marine conditions.

- Unit 4: 120.5 – 187 m. **Oligocene – upper Eocene age**, massive terrigenous sandy mudstones.
  - Massive extensively bioturbated terrigenous sandy mudstone locally grades into sandstone and mudstone. Hard and lithified. Olive and dark greenish grey to medium and medium dark grey. Rare and thin layers of volcanic ash and locally calcareous. Thin normally graded units represent turbidites which increase in abundance downward within the unit. Dominated by sandy siltstones with rounded clasts of quartz, feldspars, chert, siltstone and basalt fragments.
  - Interpretation: clay mineralogy suggests re-deposition from the continental platform & mica compositions suggest transformation associated with the alteration and re-deposition of ancient quartz-biotite schists and gneisses from Greenland. However a part of the biotite may have been eroded from alkaline basalts (volcaniclastic/volcanogenic origin from Tertiary lavas of Jan Mayen Ridge)

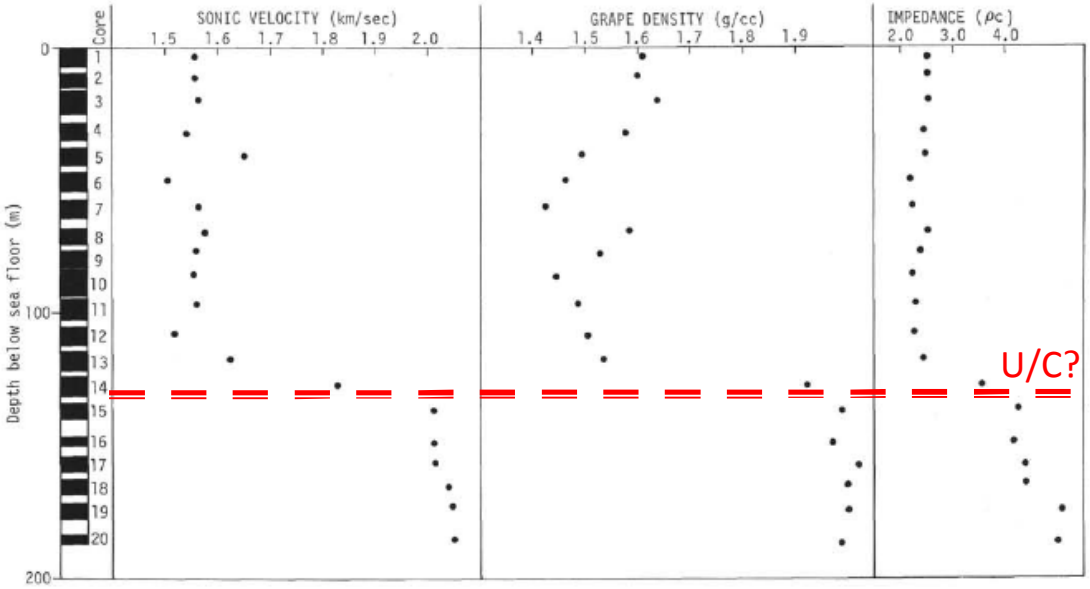

Figure 7. *Density, velocity, impedance, Site 346.*

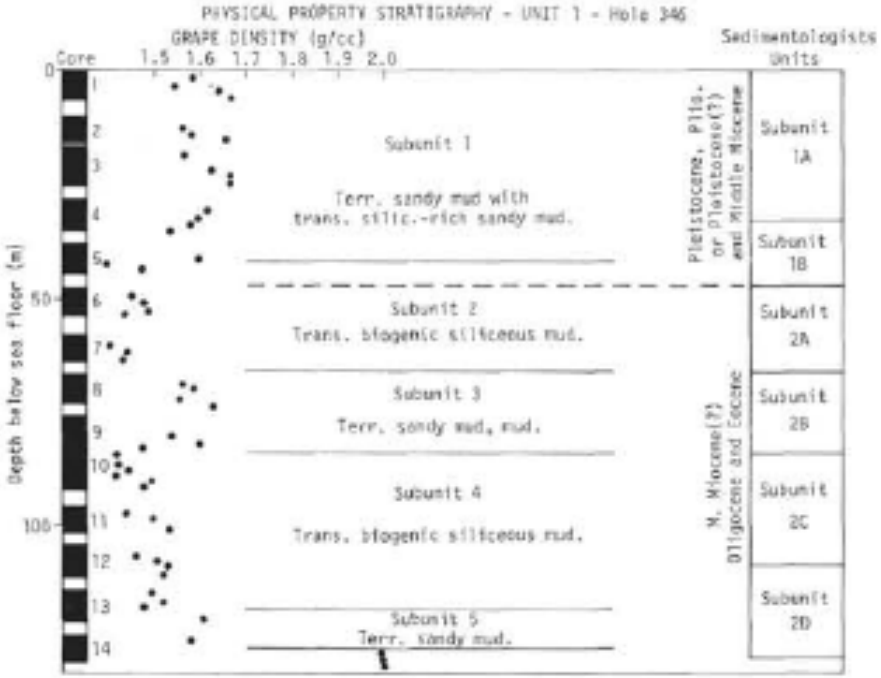

Figure 8. *Density profile – Cores 1-14, Site 346.*

Physical properties of well 347 (same as well 346)

- *The section is differentiated into two distinct units: (1) a lower high density sediment possessing high (>2.0 km/sec) sonic velocity, and (2) an upper unit with low bulk density and low sonic velocity. The abrupt change in acoustic impedance at Core 14, Section 2, indicates the lower unit is a strong reflector of sound, and would be expected to be visible on seismic profile records. (possibly marks the unconformity surface).*
- *The Miocene(?) unit is clearly shown to have high compressive strength, high density and velocity, and high acoustic impedance. It is a significant reflector at 132 meters and should be clearly visible on seismic profiles records =* ***Unconformity on top of Jan Mayen Ridge?***

Biostratigraphy (same as well 346)

- *Sediments from this hole are barren of silicieous microfossils.*
- *Only in sample 1 – a well preserved radiolarian assemblage is present, representing an interglacial.*
- *Core 1 – planktonic foraminifera, arenaceous foraminifera and deep water benthonic species are present. Reworked Cretaceous and Palaeogene species are only rare in this Quaternary sequence*
- *Cores 2- 4 (121 – 190m) arenaceous foraminifera, few nannofossils and dinoflagellates present indicating a late Eocene to Middle Eocene age.*

TABLE 8
Representative Density, Porosity, Velocity, and Impedance Values, Site 347

Core	Depth (m)	ρ (g/cc)	η (%)	c (km/sec)	ρc	Correlation with Site 346
1	0-4.5	1.540	72.79	1.934	2.98	Quaternary
2	121-128	2.054	39.08	2.707	5.56	Unit 2 – late Eocene
3	128-137.5	2.002	42.49	3.082	6.17	Unit 2 – late Eocene
4	187-190	1.951	45.82	–	–	Unit 2 – late Eocene

DSDP Leg 38 - Well 348

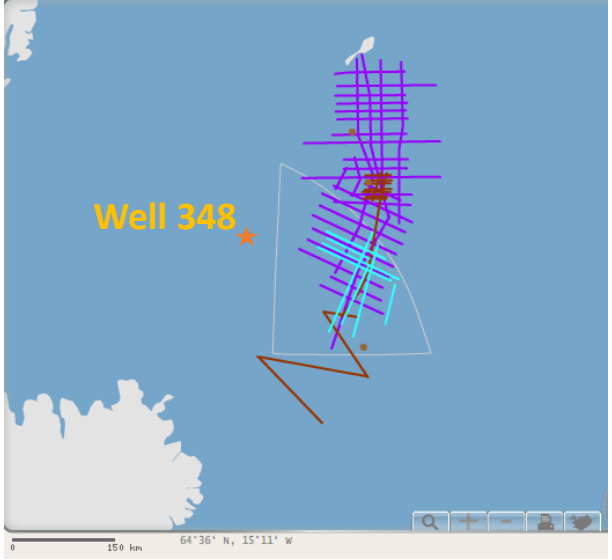

Well Summary
Date: **09/09/1974**
Latitude: **68.503**
Longitude: **-12.462**
Water Depth from sea level (m): **1763**
Bottom Felt at: **1777.0 meters (drill pipe)**
Well penetration (m): **544**
Physiographic feature: **Plateau**
No. of cores: **34**
Interval cored (m): **315.5**
Core recovered (m): **212.51**
Oldest sediment cored depth below sea floor (m): **531.5**
Oldest sediment age: **Oligocene**
Oldest sediment description: **Mud/mudstone**
Basement: **Variolitic basalt**
Depth below sea floor (m): **526.6m (drilled)**
K/AR age: **18-19 m.y. (early Miocene)**

Well lithology

Principal Results:

This site is located in an area of well defined linear magnetic anomalies on the Icelandic Plateau, east of the 10 m.y. isochron of the Iceland-Jan Mayen Ridge. It is west of the magnetically quiet Jan Mayen Ridge. "Glacial" sediments consisting of a mixture of terrigenous mud, sandy mud, and clay, with occasional layers of volcanic ash, extend to 47 meters. Pliocene to lower/middle Miocene, extending from 47 to 256 meters, contains biogenic siliceous sediments which also include terrigenous clay and mud. The underlying Oligocene (?) unit consists almost entirely of terrigenous sediments which lie on basement. Basement is composed of tholeiitic basalt, which varies in texture from fine to medium grained, but contains no pillow lavas. No distinct opaque layer was found. Most likely the "opaque" layer is the basalt itself. Radiometric and palaeontologic age determinations are not inconsistent with an age corresponding to anomaly 6 (21 m.y., early Miocene) for basement.

Site 348 is located on the Icelandic Plateau in the region lying between the presently active Iceland-Jan Mayen Ridge and the presumed "continental" Jan Mayen Ridge. The region of the site contains well defined magnetic lineations symmetrically situated around an extinct spreading axis. Site 348 is located on anomaly 6.
Objectives were 1) To determine the age and nature of basement, especially to ascertain if it is oceanic (in spite of the linear magnetic anomalies, some investigators have maintained that the area may be continental in origin). 2) To determine the nature of the opaque layer which appears to drape basement in this area. Does the opaque layer itself constitute basement? 3) To learn about the history of sedimentation of the Icelandic Plateau.

No available seismic lines intersect this area as of yet

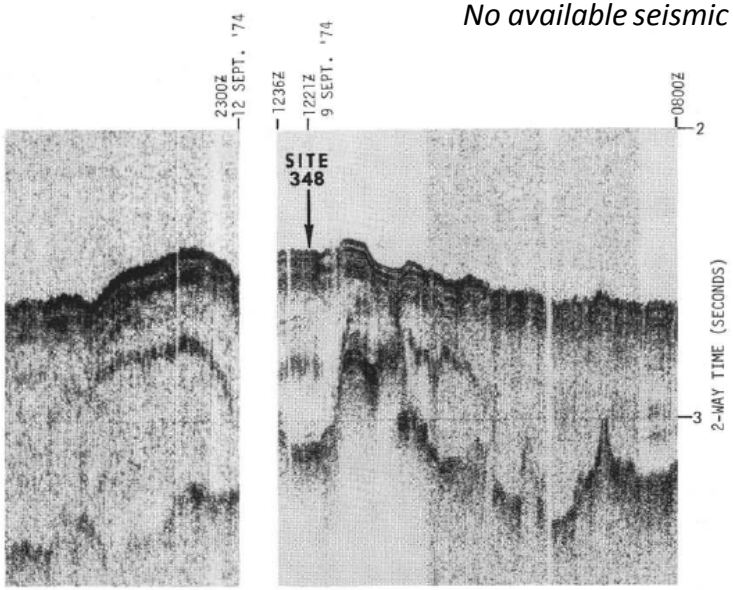

Figure 2. *Profiler record, Site 348.*

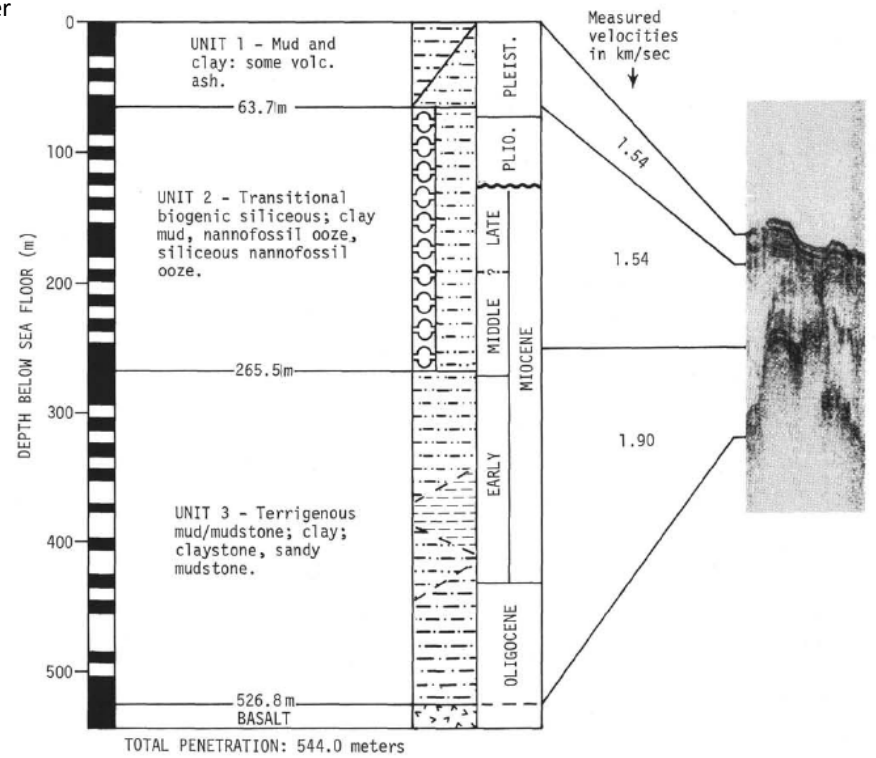

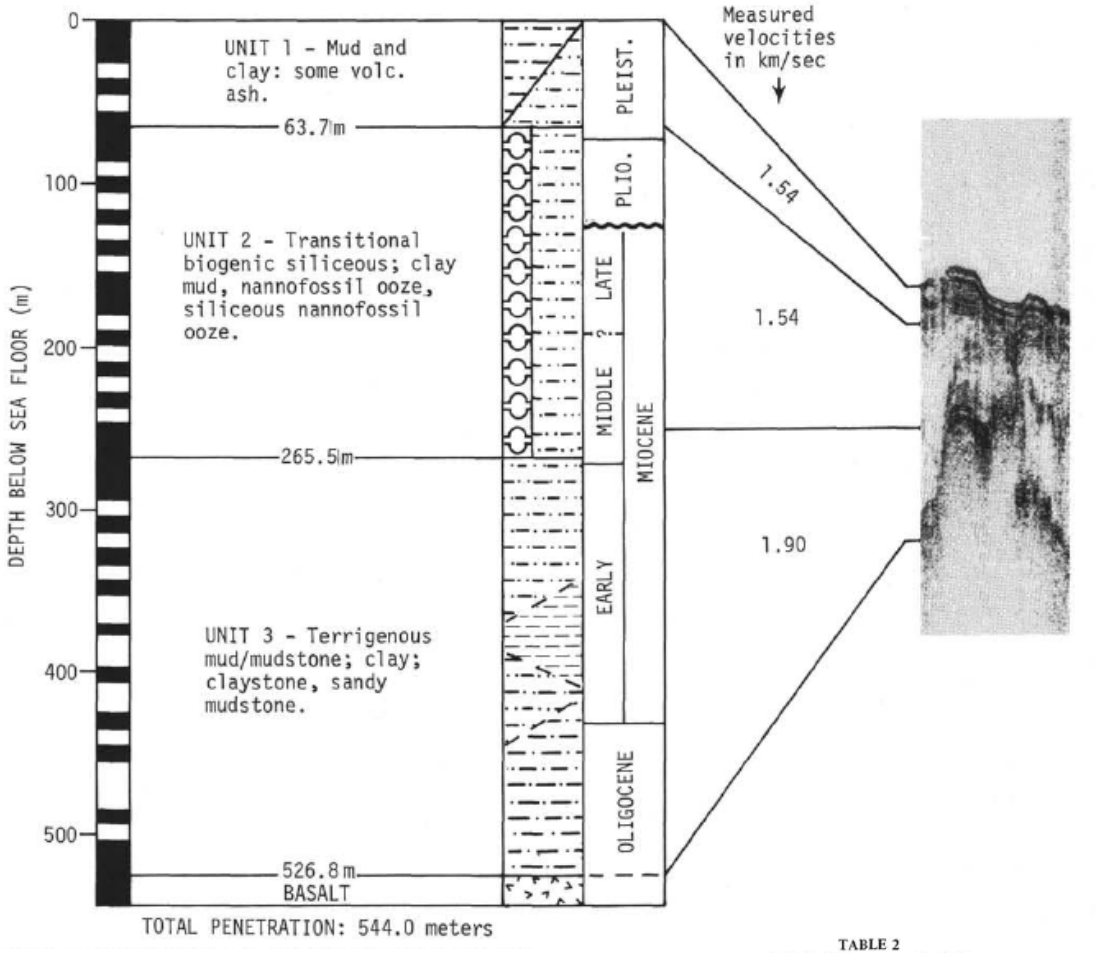

TABLE 2
Lithologic Summary, Site 348

Unit	Depth and Core Numbers[a]	Age	Characteristics
1	0-63.7 (1-1 to 5-4, 120)	Pleistocene	Predominantly mud and clay that generally becomes finer grained downward and contains scattered fine pebbles of various types; minor amounts of scattered volcanic ash, nannofossil-rich mud and calcareous mud
2	63.7-265.5 (5-4, 120 to 18, CC)	Pleistocene to middle Miocene	Predominantly transitional siliceous mud; highly variable in upper part (Cores 6-9), where it includes clay, mud, nannofossil ooze, siliceous-nannofossil ooze, and transitional nannofossil sediment; more uniform in lower part (Cores 10-18); abundant volcanic ash throughout, as discrete units and as volcanic glass mixed with other sediment types; massive, no sedimentary structures
3	265.5-526.8 (19-1 to 32.4, 33 cm)	Early Miocene-Oligocene	Dominantly terrigenous mud/mudstone with clay/claystone in the upper part grading downward into sandy mudstone at base; locally calcareous; no biogenic component visible from smear slides; soft to hard and indurated

Lithology

- Unit 1 – 0 - 63.7 m. Pleistocene age. Terrigenous mud, clay and volcanic ash.
  - Mixture of terrigenous mud, calcareous mud, nannofossil-rich mud and clay.
  - Unit becomes finer grained downward, grading from mud with 10-20% sand (core 1) to mud with 1-10% sand (core 3 & 4) to clay in core 5.
  - No sedimentary structures but mottling is common & volcanic ash units are abundant.
  - Interpretation: deposition of glacial-marine sandy muds and pelagic oozes record both glacial, interglacial and post-glacial sedimentation. Coarse clastic detritus possibly ice-rafted material and progressive downward fining in grainsize indicates gradation into underlying unit 2.

- Unit 2 – 36.7 – 265.5 m. Pleistocene – Middle Miocene age. Transitional siliceous mud/sandy mud.
  - Primarily transitional siliceous mud/sandy mud that typically contain 10%-50% siliceous fossils in various proportions.
  - Also contains 1) terrigenous clay, 2) terrigenous mud, 3) volcanic ash, 4) ash-rich mud, 5) ash-rich transitional siliceous mud, 6) nannofossil ooze, 7) siliceous-nannofossil ooze, 8) transitional nannofossil sediments, and 9) transitional diatomaceous mud.
  - Greatest lithologic variability in upper part (cores 6 – 9). Lower part (cores 10 – 18) consist wholly of transitional siliceous mud with volcanic ash inclusions.
  - Volcanic ash layers (5-10 cm thick) common in cores 6 – 9, 12, 14 & 16.
  - Terrigenous clay and mud common in cores 6 – 13 indicative of the upward gradation into terrigenous sediments of unit 1.
  - Interpretation: slow hemipelagic sedimentation with persistent volcanic ash intervals. Siliceous organisms dominant over calcareous ones.

- Unit 3 – 265.5 – 526.8 m. Lower Miocene – Oligocene age. Terrigenous mudstone.
  - Abundant clay in its upper part (cores 20 - 21) and sandy mudstone in lower part (cores 27 – 32).
  - Intermixed mudstone and sandy mudstone from core 25 downwards to the top of igneous basement rocks
  - Colours vary from dark greenish-grey and greenish-black in upper parts to olive-grey in lower parts.
  - Extensive bioturbation and pyrite nodules increase downwards.
  - Massive with no internal stratification or sedimentary structures.
  - Interpretation: slow rates of terrigenous sediment deposition within (probably) reducing, deep water conditions.

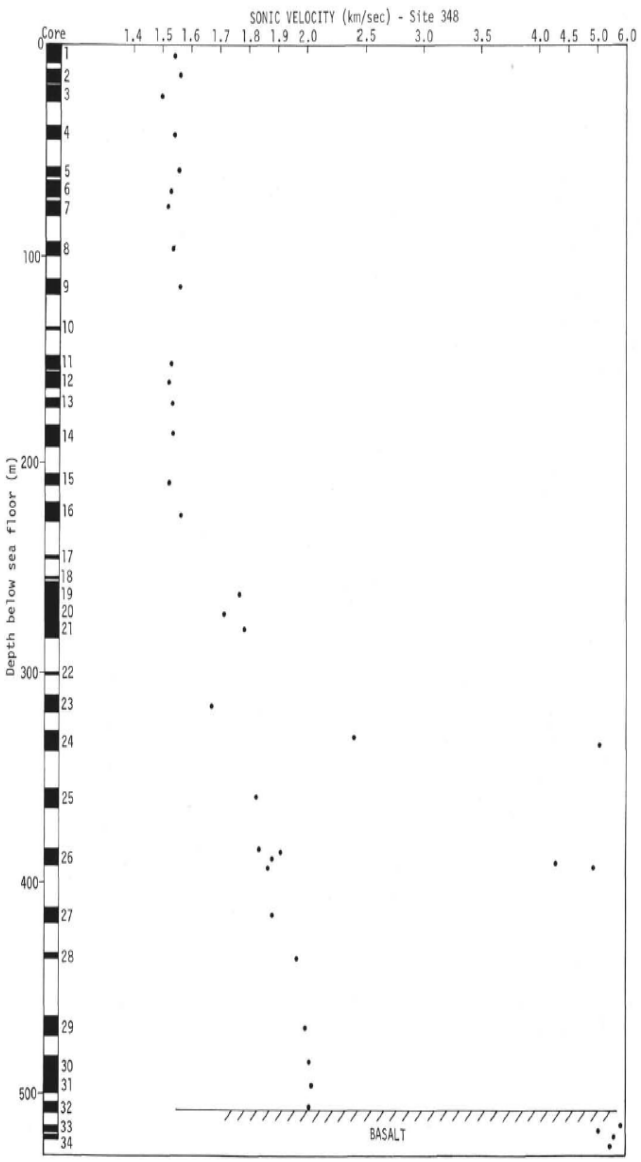

Figure 4. *Velocity profile.*

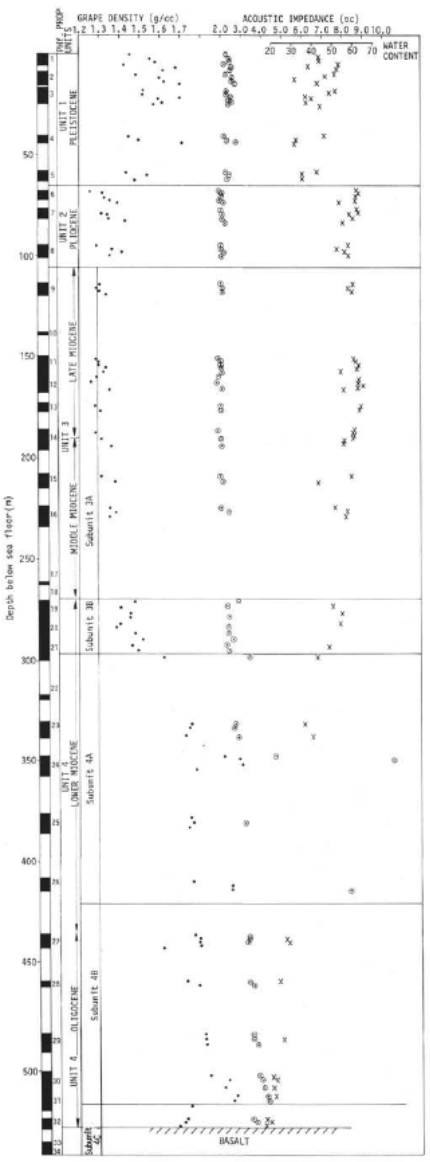

Figure 5. *Density, water content, impedance.*

TABLE 5
Sediment Subdivisions Based on Physical Properties

Unit 1 – surface through Core 5, Section 4 (66 m). Relatively high density, terrigenous sandy muds of Quaternary age. Sonic velocity varies between 1.48-1.56 km/sec. Considerable variation in wet density and water content is seen.
Average bulk (wet) density – 1.56 g/cm^3
Average water content – 41.04%
Average sonic velocity – 1.54 km/sec
Average impedance – 2.40

Unit 2 – Core 5, Section 4 through Core 8, Section 5 (41 m). Sediments form a zone intermediate between terrigenous clastics above and biogenic siliceous oozes below. Density fluctuations are attributed to interbedding of sediments of both types, intermixed with occasional volcanic ash layers. Sonic velocity changes very little.
Average bulk (wet) density – 1.35 g/cm^3
Average water content – 58.89%
Average sonic velocity – 1.53 km/sec
Average impedance – 2.09

Unit 3 – Core 8, Section 5 through Core 17 (165 m). Transitional biogenic siliceous oozes interbedded with minor amounts of terrigenous muds and sandy muds. Density fluctuates within a narrow range, and with depth in section. Little change in sonic velocity or impedance occurs. Sediments are generally noncohesive except where thin clay interbeds are present.
Average bulk (wet) density – 1.32 g/cm^3
Average water content – 59.12%
Average sonic velocity – 1.56 km/sec
Average impedance – 2.03

Unit 4 – Core 19 to Core 21, Section 5 (124 m). Semiconsolidated to well-lithified silt and mudstones, having slightly higher wet density (1.4-1.5 g/cm^3) and considerably higher sonic velocity. Impedance rises slightly above 2.2.
Average bulk (wet) density – 1.45 g/cm^3
Average water content – 50.30%
Average sonic velocity – 1.66 km/sec
Average impedance – 2.42

Unit 5 – Core 21, Section 5 through Core 26 (99.5 m). Well-lithified mudstone, little different from Unit 4 with occasional hard limestone lenses. Toward base of section, increasing amounts of clastic material are present, becoming quite coarse (a muddy sandstone) in Cores 30 and 31. Two high sonic velocity units (>3.5 km/sec), each composed of thin well-lithified limestones overlying a thin (10 cm) interval of lithified mudstones, are present at 342-352 meters and 412-416 meters. Normal velocities (1.8 km/sec) are found in the interval between them.
Average bulk (wet) density – 1.76 g/cm
Average water content – 40.88%
Average sonic velocity – 1.91 km/sec
Average impedance – 3.42

Unit 6 – Core 31, Section 4 to the top of the basalt in Core 32 (11 m). Very fine-grained mudstone showing decreasing density. Velocity continues high (>2.0 km/sec), with sharp discontinuity entering basalt in the lower part of Core 32.
Average bulk (wet) density – 1.810 g/cm
Average water content – 23.61%
Average sonic velocity – 2.05 km/sec
Average Impedance – 3.72

Physical Properties of well 348

- Based on the velocity profile (Figure 4) and the composite density-impedance-water content profile (Figure 5), six subdivisions of the sediments above basement can be made (Table 5).
- Discontinuities in physical properties usually indicate an abrupt change in depositional conditions or an unconformity.
- Lower level of “glacial” sediments (67m) = sharp change in water content and bulk density (downward decrease in density), due to loss of terrigenous material (cohesive clays).
- Pliocene sediments form a transitional sedimentary series – composed of alternating terrigenous clastics and transitional biogenic sediments.
- No obvious discontinuity in physical properties exists across the late Miocene-Pliocene unconformity boundary. Sonic velocity remains constant at 1.55 km/sec through this interval.
- No physical change in properties occur across lower Miocene and middle Miocene palaeontological break – however density increases slightly in cores 19 – 21 and sonic velocity increases in cores 16-22 – interpreted to result from compaction.
- Core 21 (297m) approx. 20m below lower and middle Miocene stratigraphic break = large increase in density and decrease in water content associated with lithological change terrigenous mudstone.
- Density and velocity continue to increase with depth (and decrease in water content) to core 31.
- Below core 31 = abrupt change in lithology and density (Basalt). Density decreases from 2.5 g/cm^3 to 1.7 g/cm^3.

Igneous Petrography

- Basaltic rocks of acoustic basement penetrated at 526.6 – 544 m bsf.
- 5 cores contained 5.75m.
- Basalt at the boundary with between basement and overlying Tertiary sedimentary succession is aphric, aphanitic and very fine grained with no glassy rims typical of pillow lavas. Dark grey to greyish-black coloured.
- Below this boundary, basalt is medium dark grey to dark grey and has a fine-medium grained texture. Glassy surface is not present on these contacts.
- Basalt can be subdivided into 3 types: 1) Variolitic basalt, 2) diabase basalt and 3) Amygdaloidal basalt.
- These basalts are normal tholeiites, although secondary mineral alteration with introduction of pyrite, smectite, chlorite, calcite, amphibole and albite has occurred.
- Probably represent a sill or dyke igneous body – interpretation supported by absence of pillow lava with typical glassy rims and glassy brecciated surfaces.
- Radiometric age dating of basement is 18.8 ± 1.7 m.y. Slightly younger than the 21 m.y age from corresponding magnetic anomaly 6. (Palaeontologically the age of the overlying sediments is early Miocene to Oligocene (from a single foraminifera marker) therefore oldest sediments at this site are early Miocene and basement is indeed 21 m.y. Age of extinct axis gives cessation of spreading at this axis of 18.5 m.y
- seismic profiler record (Figure 2) shows reflectors at about 0.08 sec, 0.22 sec, 0.34 sec, and 0.65 sec. In comparing these times with observed velocities the following units have been chosen:
    - Unit A (corresponding to lithologic unit 1) Cores 1-5, 0-63.7 m; average velocity = 1.54 km/sec; two-way travel time = 0.082 sec.
    - Unit B (corresponding to lithological unit 2, except that the base is at 250 m); average velocity = 1.54 km/sec; two-way travel time = 0.242 sec.
    - Unit C (corresponding to lithological unit 3, except that the top is at 250 m); average velocity (ignoring some streaks of high-velocity limestone—over 4.0 km/sec) = 1.904 km/sec; two-way travel time = 0.291 sec.
    - Hence, calculation values for two-way travel times to major reflectors are 0.08, 0.32, and 0.62 sec.

Biostratigraphy

- Complete section from Pleistocene to Oligocene recovered.
- Pleistocene sediments from core 1-6 from nannoplankton, diatoms and radiolarians.
- Pliocene siliceous ooze (core 6-10) rich in cold water fauna, mainly diatoms, silicoflagellates and radiolarians. Nannoplankton restricted to some thin horizons intercalated with siliceous ooze.
- The late Miocene (core 11 – 18) determined from diatoms, silicoflagellates, dinoflagellates and radiolarians
- Below core 18, sediments are barren of siliceous microfossils
- Early Miocene age determined for cores 19-27 based on few nannofossils and foraminifera.
- Cores 28 – 32 assigned to Oligocene from presence of foraminifera assemblage. Terrestrial plant debris and pollen are dominant in this interval.

Conclusions

- Basement at well site 348 consisting of normal tholeiitic basalt and presence of linear magnetic anomalies = oceanic sea floor (formed by sea floor spreading)
- Basement age is about 21 m.y. Magnetic anomalies give age of about 25 – 18.5 m.y for the intermediate spreading axis between the Iceland-Jan Mayen Ridge (Kolbeinsey Ridge) and Jan Mayen Ridge.
- Change in sediments from terrigenous sediments in Oligocene/Miocene to increased pelagic biogenic siliceous oozes in mid-late Miocene is due to progressive rifting/sea floor spreading away from East Greenland margin.
    - Earliest sediment sourced from Greenland - terrigenous and contain only arenaceous foraminifera (characteristic of Greenland sediments in early opening phase and also earlier in Norway Basin).
    - As spreading axis jumped to new position (Kolbeinsey Ridge) in mid or late Miocene – rate of terrigenous input was reduced and replaced with a dominance of cold water deep marine biogenic oozes
- Lower section of Miocene sediments contain higher proportion of volcanics – deposited when the earlier spreading ridge was located on the Icelandic Plateau
- No distinct opaque layer overlying the basalt was identified – opaque layer is basalt basement?

DSDP Leg 38 - Well 349

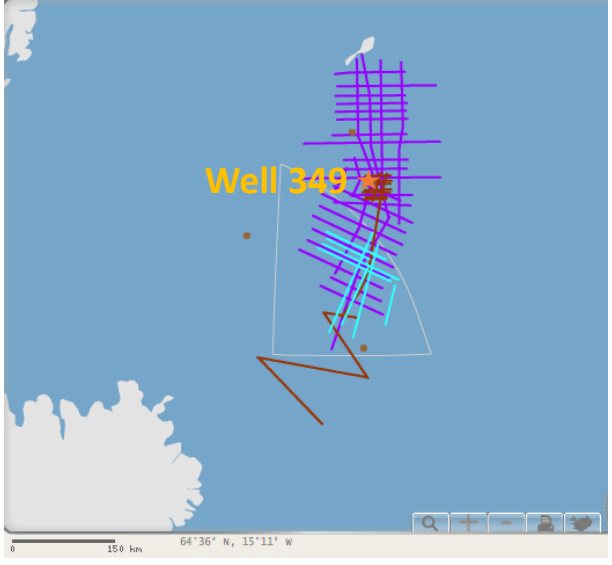

Well Summary

Date: **13/09/1974**
Latitude: **69.207**
Longitude: **-8.097**
Water Depth from sea level (m): **915**
Bottom Felt at: **928.0 meters (drill pipe)**
Well penetration (m): **319.5**
Physiographic feature: **Ridge**
No. of cores: **13**
Interval cored (m): **120**
Core recovered (m): **80.8**
Oldest sediment cored depth below sea floor (m): **319.5**
Oldest sediment age: **Upper Eocene**
Oldest sediment description: **quartz rich clay mineral rich mudstone**

Well lithology

Principal Results:

At this site on the Jan Mayen Ridge, sediments range in age from "glacial" to upper Eocene (as at Sites 346 and 347). The "glacial" sediments consist of muds and sandy muds, with scattered inclusions of volcanic ash. The underlying Oligocene sediments also consist of muds and sandy muds, with volcanic ash in the upper part, and glauconite in the upper and lower parts. Below the unconformity lie mudstones, sandy mudstones, conglomerate sandstone, and breccia with an age of upper Eocene. These beds correspond in the reflection profiler records to the strata with prominent easterly dips. Other than arenaceous foraminifera, these sediments are barren of fossils.

Site 349 was chosen as an additional drill hole on the Jan Mayen Ridge. At this site, the reflection profiler record showed below an unconformity a set of sedimentary strata that dipped to the east. Two possibilities existed; (I) that these beds simply lie stratigraphically above the Eocene sediments encountered at Sites 346 and 347. These sites were drilled close to the eastern edge of the Jan Mayen Ridge, and (2) that these beds had no relationship with the beds in the earlier holes; in particular, they could lie stratigraphically below them, and they might be Mesozoic in age. In any event it was felt that perhaps the hard to penetrate sandstone at Sites 346 and 347 would be absent at this site. If so, the cores taken would help decipher the sedimentary history and origin of the Jan Mayen Ridge.

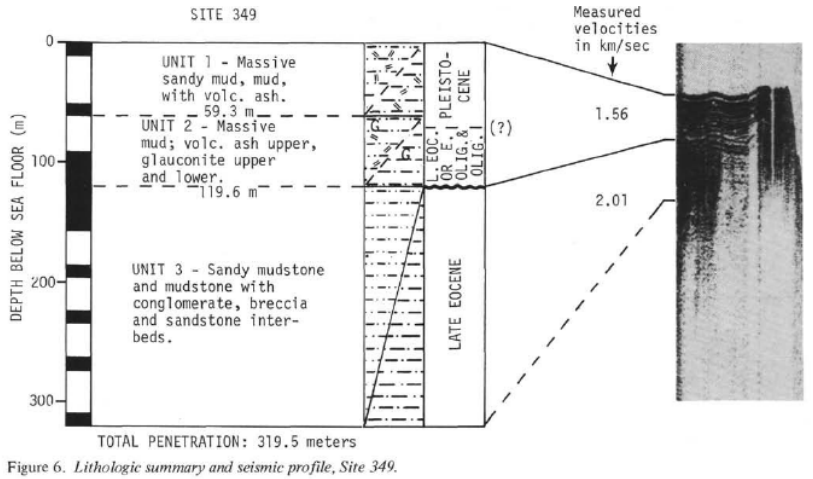

Figure 6. *Lithologic summary and seismic profile, Site 349.*

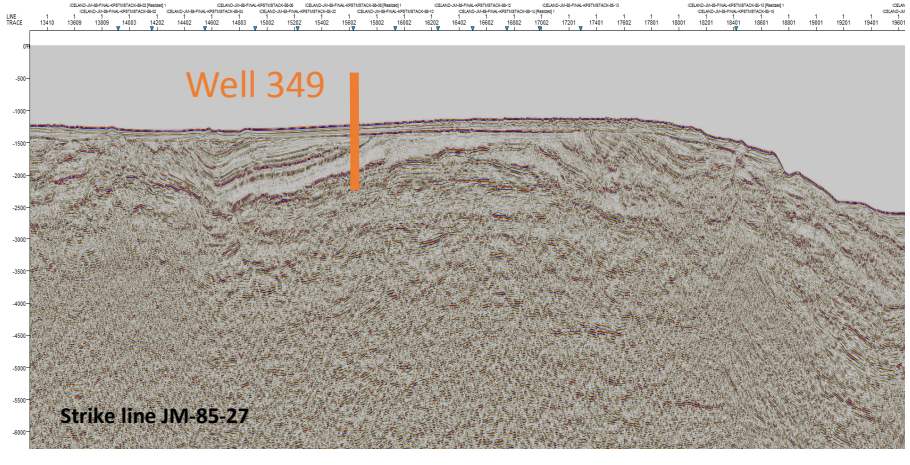

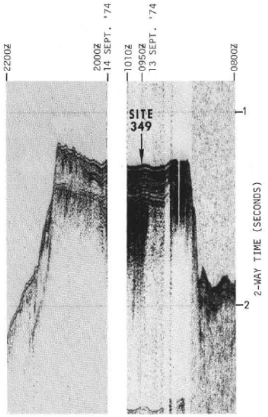

Figure 4. *Profiler record – Site 349.*

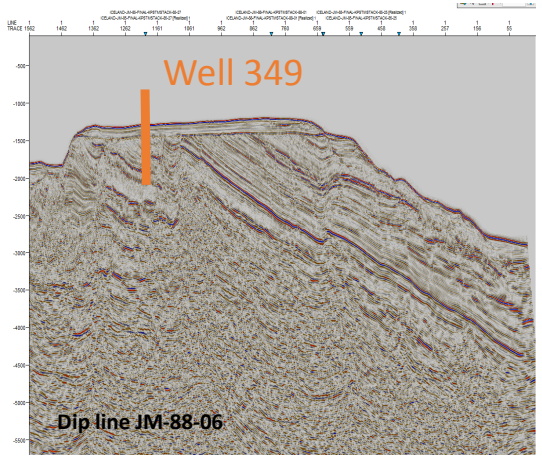

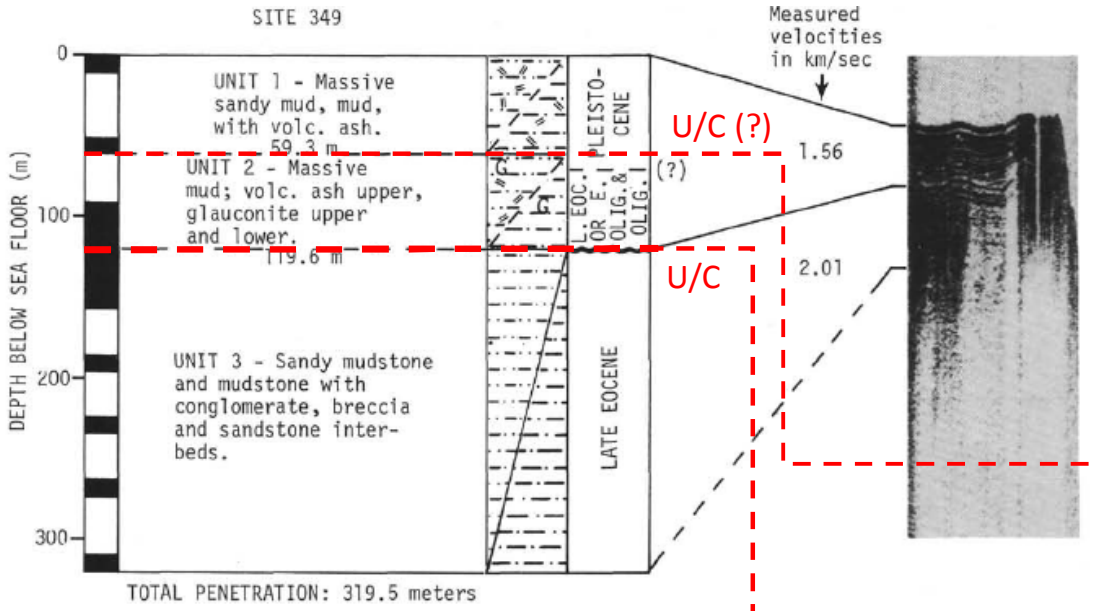

Figure 6. *Lithologic summary and seismic profile, Site 349.*

TABLE 6
Lithologic Summary, Site 349

Unit	Depth (m) and Core Numbers	Age	Characteristics
1	0.0-59.3 (1-0 to 2-4, 100 cm) thickness-59.3 m	Pleistocene	Massive mud and sandy mud with scattered volcanic ash; intensely deformed; soft; locally mottled; locally glauconite-rich
2	59.3-119.6 (2-4, 100 to 5-4, 130 cm) thickness-60.3 m	Pleistocene-Late Eocene	Massive mud with abundant volcanic ash in the upper part and glauconite in the upper and lower part; intensely to moderately deformed; soft to firm; locally mottled
3	119.6-319.5 (5-4, 130 to 13,CC) thickness-199.9 m	Late Eocene-early Oligocene	Sandy mudstone and mudstone with conglomerate, breccia, and sandstone interbeds; indurated and undeformed; locally bioturbated; pyrite nodules and calcareous zones abundant; graded beds common; almost wholly terrigenous; locally zeolite rich

Lithology

- Discontinuous coring means the thickness of sedimentary units and age of stratigraphic boundaries are poorly known and can only be approximated
- Unit 1: 0 – 59.3 m. Pleistocene age. Massive sandy mud with volcanic ash layers
  - Massive, intensely deformed sandy mud, mud and scattered inclusions of volcanic ash.
  - Yellowish-brown coloured with some olive-grey and dark grey colouration in parts
  - Dominantly composed of quartz, feldspar, clay minerals, glauconite and volcanic glass.
  - Minor amounts of detrital minerals, foraminifera, calcareous nannofossils, sponge spicules and radiolarian present
  - Interpretation: represents glacial-marine sedimentation during late Cenozoic but also may include post-glacial Holocene sedimentation.
- Unit 2: 59.3 – 119.6 m. Pleistocene to early Oligocene. Massive mud with volcanic ash and glauconite
  - Boundary between unit 1 and 2 is uncertain, but appears to lie within core 2. Upper part is similar lithology and colour as core 1, but transition into unit 2 is marked by presence of abundant volcanic ash first appearance of significant amounts of glauconite, color change from yellowish-brown to greenish-gray, relatively abundant sponge spicules, changing amounts and types of biogenic constituents, and sharp changes in cohesiveness and other physical properties. The boundary appears to be adjacent to an unconformity separating Pleistocene and Oligocene sediments
  - Significant amounts of volcanic ash in upper part and glauconite in upper and lower parts.
  - Grey to green colouration, intensely to moderately deformed and locally intensely mottled.
  - Sediments consist mostly of clay minerals and quartz and locally mica, volcanic glass, palagonite, glauconite and sponge spicules.
  - Interpretation: unclear process of deposition due to a lack of sedimentary structures – most likely hemipelagic sedimentation.
- Unit 3: 119.6 – 319.5 m. Upper Eocene to lower Oligocene. Intermixed mudstone and sandy mudstone, abundant conglomerate, breccia and sandstone.
  - Boundary between unit 2 & 3 marked by a basal conglomerate separate other lithified strata from overlying soft unconsolidated sediments – no indication of subaerial erosion.
  - Graded sequences are present in lower 2/3rds of the unit. Whole unit is indurated.
  - Bioturbation, pyrite nodules and calcareous layers are locally common.
  - Mudstone/ sandy mudstone composed of quartz and clay minerals, with variable amounts of mica, feldspar, authigenic carbonate and lithic fragments.
  - Graded and ungraded conglomerate and breccia units contain abundant mudstone, siltstone, and sandstone clasts and harder volcanic, limestone and chert clasts. Angular- rounded clasts (up to 8 cm long).
  - Interpretation: large gaps in coring mean depositional environment cannot be constrained. Hemipelagic sediments and turbidites are likely.

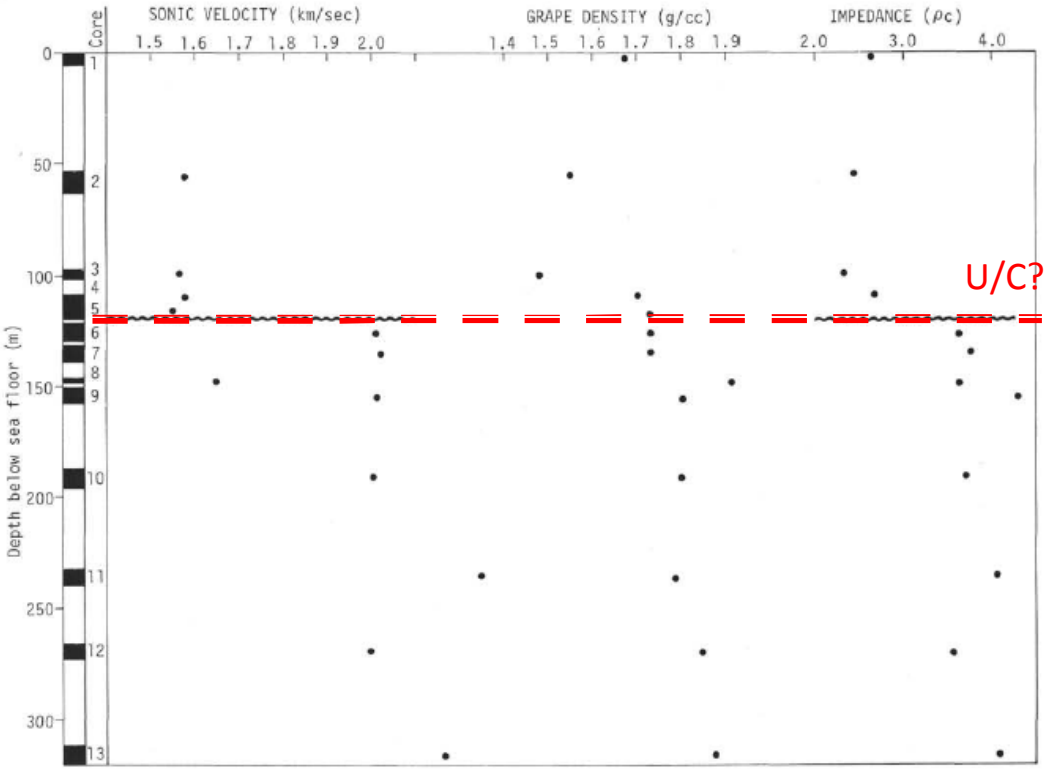

Figure 9. *Velocity, density, impedance, Site 349.*

Physical Properties of well 349

- Sonic velocity, impedance & density identify 2 distinct units.
- The sediments are clearly differentiated by the abrupt change in sonic velocity, beginning in the sediments below the conglomerate in Core 5 an continue at a high level to the base of the hole.
- Sonic velocity above the unconformity is consistent at about 1.57 km/sec (normal Quaternary and late Tertiary sediment velocities).
- Below the unconformity (within the late Eocene section) some extreme velocity values are noted – probably due to lithologic variability.

Biostratigraphy of well 349

- Pleistocene sediments recovered from core 1 and upper part of core 2.
- Core 2, section 4 to Sample 2, CC is rich in sponge spicules indicating a Miocene age (to possible Pliocene age).
- Core 3 and 4 (91.5 – 110.5 m) = Middle Oligocene age based on dinoflagellates and foraminifera.
- Core 5 to 13 (110.5 – 319.5 m) = Late Eocene age based on nannofossils, foraminifera, dinoflagellates and poor radiolarian assemblages.

TABLE 9
Average GRAPE Density, Velocity, Impedance of Sediment Units, Site 349

Unit		GRAPE Density ρ (g/cc)	Sonic Velocity (km/sec)	Impedance
1	$\bar{x}$	1.617	1.570	2.56
	s	0.117	0.015	0.16
2	$\bar{x}$	1.815	2.055	3.72
		0.067	0.192	0.29

Conclusions

- Lithologically similar to well 346/347. “Glacial” beds overly Oligocene units.
- Unconformity at 120 m marked by basal unconformity between unit 2 and 3.
- Early Oligocene or late Eocene units beneath unconformity but lie stratigraphically higher than sediments at site 346/347.
- More work is necessary to establish whether the entire section at Site 349 lies stratigraphically above the section at Site 346, or whether there is an overlap, with a possible facies change between the two sites.
- The cores from Site 349 confirm the Jan Mayen Ridge as a feature with horizontal beds of late middle Oligocene age or younger, overlying an unconformity. Below the unconformity, early Oligocene (and older beds) dip steeply to the east. Data from the youngest beds above the unconformity agree well with the date for the shift of the spreading axis from Norway Basin. The new spreading axis separated Jan Mayen Ridge from Greenland, thereby removing it from the immediate vicinity of a terrigenous sediment source.

DSDP Leg 38 - Well 350

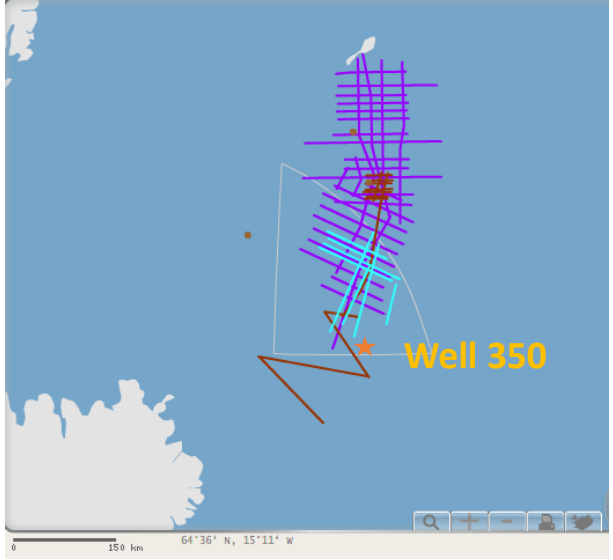

Well Summary

Date: **15/09/1974**
Latitude: **67.055**
Longitude: **-8.295**
Water Depth from sea level (m): **1275**
Bottom Felt at: **1289.0 meters (drill pipe)**
Well penetration (m): **388**
Physiographic feature: **Ridge**
No. of cores: **16**
Interval cored (m): **150.5**
Core recovered (m): **49.5**
Oldest sediment cored depth below sea floor (m): **370**
Oldest sediment age: **Late Eocene**
Oldest sediment description: **mudstone**
Basement: **Basalt breccia/diabase doleritic basalt**
Depth below sea floor (m): **361.7m (drilled)**
K/AR age: **41 m.y. (late Eocene)**

A series of ridges appears to represent the morphologic extension of the Jan Mayen Ridge to the south. Of these ridges, the ones to the west appear to represent the structural continuation of the Jan Mayen Ridge. In particular, they interrupt the otherwise ubiquitous opaque layer of the Icelandic Plateau. The ridges to the east are, however, somewhat different in character. They do not interrupt the opaque layer, but conversely, the opaque layer appears to form the basement of these ridges and is continuous to the east to the extinct axis of the Norway Basin. The ridge on which Site 350 is located is typical of the eastern ridges.
A principal objective of the hole is to try and establish the structural and tectonic relationship of these ridges to:

(a) the main part of the Jan Mayen Ridge to the north and to the west, and
(b) the mid-oceanic type ridge which was active in the Norway Basin in the past, and which lies to the east.
(c) Another objective was to sample the opaque layer which seems to cover or form basement at this site.

No available seismic lines intersect this area as of yet

Well lithology

Principal Results:
A total of 388 meters was penetrated at this site, of which 362 meters was in sediments, and the remainder in basaltic basement. "Glacial" sediments extend from the top to about 36 meters. They consist principally of sandy muds and muds, with admixtures of various amounts of volcanic ash and some foraminiferal oozes. Below the glacial sediments, a lithologic unit has been defined which extends from about 55 to 264 meters. It is middle Miocene in age at the top and extends into the Oligocene at the bottom (264 m). Alternating layers of unconsolidated and indurated to lithified sediments, dominantly terrigenous clays and muds, make up this unit. The underlying lithologic unit extends from 264 meters to the basalt at 362 meters. This unit is dominated by lithified sediments, particularly mudstone, claystone, limestone, breccia, and some sandstone. Turbidites are well developed towards the base of the unit. Near the boundary with the basement, the sediments become highly lithified breccias. Tuff breccias comprise the top portion of the igneous basement (from 362 to 380 m), and overly basalt which extends to the bottom of the hole at 388 meters. The tuff breccia is altered, but the basalt is very fresh compared to that from other sites of Leg 38. The basalts are normal tholeiites. The radiometric date on the basalts as well as the paleontologically determined date on the overlying sediments is late Eocene.

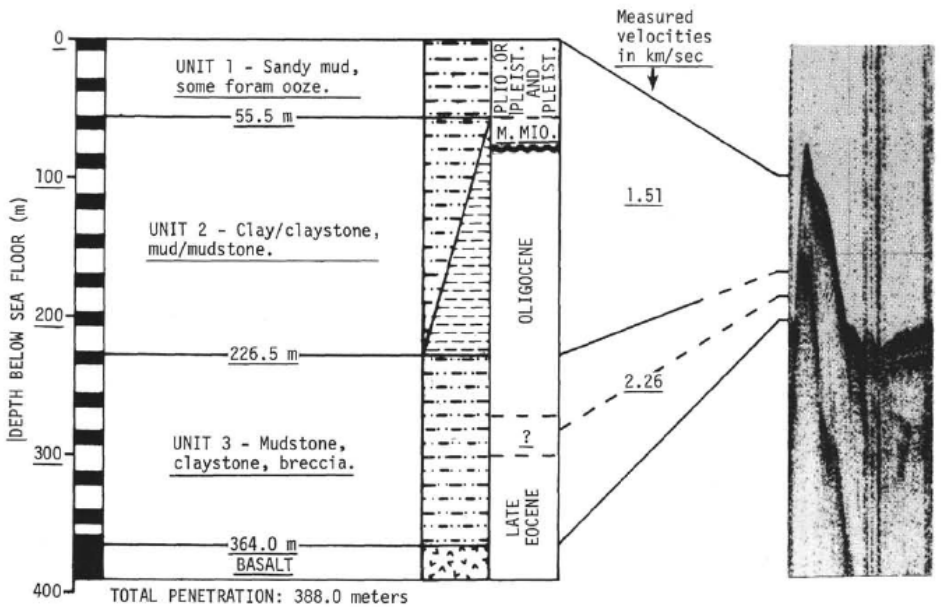

Figure 3. *Lithologic summary and seismic profile – Site 350.*

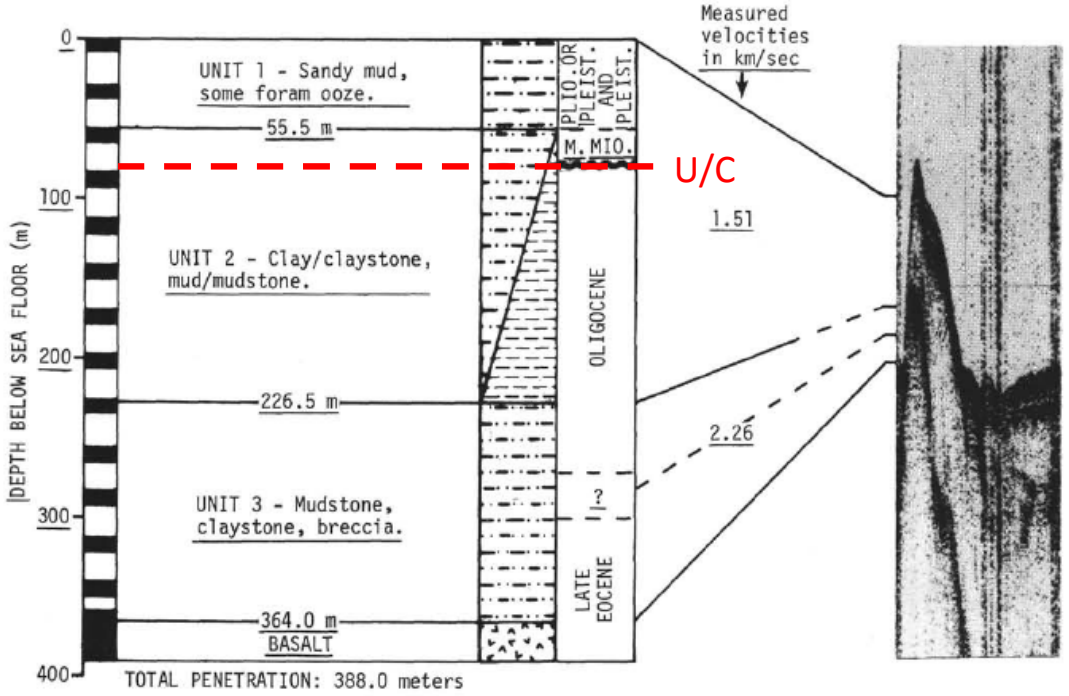

Figure 3. *Lithologic summary and seismic profile – Site 350.*

Biostratigraphy

- Pliocene-Pleistocene sediments (core 1 – 2; 0 - 36.5 m) are poor in nannofossils and foraminifera. Siliceous microfossils are rare.
- Age determination below this sequence is difficult – based mainly on arenaceous foraminifera
    - Middle Miocene (core 3),
    - no age for cores 4 – 6 (84 – 150.5 m),
    - Oligocene (cores 7 – 10; 169.5 – 264.5 m)
- Core 12-14 are late Eocene based on presence of few foraminifera, nannofossils and dinoflagellates. (Diatoms give an Oligocene age for core 12)

Lithology

Unit 1: 0 – 55 m. Pleistocene. Sandy muds and mud with admixtures of volcanic ash and foram oozes.

- Volcanic ash present as specific layers and also in "blebs", streaks and smears.
- Lithified ash is present in core 2.
- Actual Pliocene-Miocene boundary may lie in the uncord interval between cores 2 and 3.
- Interpretation: Strong input of glacial-marine terrigenous material (whilst glacial-periglacial conditions prevailed on land). Intermittent milder conditions indicated by minor Foraminiferal oozes. Volcanism resulted in an important input of sediment.

Unit 2: 55.5 – 226.5 m. Middle Miocene and Oligocene. Alternating claystone and mudstone layers.

- Alternating layers of unconsolidated and hardened to lithified clays and mudstones.
- Volcanic ash exists in conspicuous layers or as admixture to terrigenous, non-volcanic material.
- Lower part of unit 2 (core 5 and below) and upper two cores from unit 3 are finest grained of the entire sediment column.
- Some bioturbation exists in fine grained sediments.
- Turbidites are identified in the lowermost core from this unit and become increasingly important in lower segments of the sediment column
- Interpretation: Upper unit 3 and lower unit 2 terrigenous sediments represent "distal" turbidity currents. Dominance of fine grained material reflects increased water depth, reduced available transport energy and/or reduced sediment supply. Bioturbation & pyrite nodles reflects quiet water, reducing conditions. Upper unit 2 show slighting increasing grain size – Neogene tectonism in source areas & climatic deterioration contributed to increased terrigenous sediment influx into the marine environment.

Unit 3: 226.5 – 364 m. Oligocene to late Eocene. Mudstone, claystone and breccia.

- Predominantly lithified mudstone, claystone, limestone, breccia and some sandstones (as turbidites)
- Turbidites become dominant toward base of the unit (cores 13 and 14) and described as "proximal" turbidites & associated with sediments deposited by grain-boundary flows ("sand falls").
- Near boundary with basalt basement, sediments become breccias and are highly lithified.
- Bioturbation and pyrite concretions associated with fine grained lithologies
- Interpretation: Breccias above basalt represent slump deposits succeeded by "proximal" turbidites and grain-boundary-flow deposits indicating relative proximity to the sediment source along steep submarine slopes (near sub-marine canyons). Limestone oozes originally depositied on the upper parts of a "continental" slope above the CCD and redeposited by turbidity currents, broken during transport and recrystallized after deposition.

Sedimentation History

Lithologic and mineralogical studies of the sedimentary sequence identify 4 major stages in sedimentation history :

1) Late Eocene and Oligocene
2) Oligocene and middle Miocene
3) Plio-Pleistocene
4) Pleistocene

Deposits on the ridge are on the whole mid oceanic-type – dominated by products of basaltic volcanism.

Late Eocene to Oligocene

- Unit 3 accumulated with total thickness of 166m. At the contact between this unit and acoustic basaltic basement is breccia composed of lithified siltstone argillites and altered basalts
- Breccia overlain by tuffitic silty clays (30-40%) admixed with coalified remains and globular pyrite aggregates = product of submarine alteration of the basic hyalopelitic-hyaloaleuritic material.
- At the beginning of this sedimentation stage there were authigenic montmorillonite-hyromicaceous minerals and terrigenous components, later hydromicas, kaolinite and clastic quartz were deposited.
- Eocene-Oligocene deposits are typically turbidites with microbreccia structures of bioturational orign.
- Towards the top of the unit, proportion of terrigenous material and coalified humusified plant detritus increases. No marine fossils.
- These deposits accumulated within the limits of a confined intracontinental basin with associated basic volcanic activity (submarine & on Jan Mayen Island). (*Not a typical open ocean basin*)
- Plant material and fine-sand to silty sediment eroded from acid granitoid rocks were entered the basin from relatively proximal land sources (E. Greenland?).
- Increased organic facilitated diagenesis of pyrite concretions.

Oligocene and Middle Miocene

- Clayey tuffite deposits of basic basaltic composition dominate Unit 2. (Composed of hyalopelitic, hyaloaleurolitic volcaniclastic materials).
- These were altered into ferrous-montmorillonite admixed with hydromicas – sediments are largely microbrecciated by bioturbation and reveal a high degree of zeolitization.
- Upper horizons have a high proportion of manganese hydroxides – cements the microbreccia.
- Siliceous marine diatoms and Radiolaria are only found in top of the interval of unit 2 – core 3
- Volcanic activity (beginning in Eocene) became more intense by upper Miocene.
    - Predominantly fine hyalopelitic and hyaloaleurolitic (basaltic vitroclastic) sediments accumulated in the relatively restricted basin from submarine and island volcanism.
    - Hyaloclastic fragments intercalated with intensive zeolitigation and metal-bearing sediments represent submarine hyrdrothermal activity.
- End Miocene the basin became an open seaway as the ashy basic tuffs contain diatom and radiolarian remains.

Plio-Pliestocene (Unit 1)

- Divided into 2 glacial periods:
    - 1) Subseries 1C (“lower glacial Plio-Pliestocene”) 25.5 m thick, composed of hyalopelitic clays (ferrous montmorillonite developed from basic glass under submarine conditions) admixed with 30-40% terrigenous silts.
    - 2) Subseries 1B (“upper glacial Plio-Pliestocene”) 22 m thick, composed of aleurolitic clays with foraminifera and terrigenous grains of glauconite. Also typically brown basaltic glass fragments are common.
    - Basic volcanism continued until lower Plio-Pleistocene, greatly diminished and replaced by a dominance of terrigenous sediment

Pleistocene (Unit 1)

- 2 members were deposited during this time:
    - 1) Member 1A-II (“lower Pleistocene”) 5 m thick, composed of hyalopelitic ashes (fine detrital basaltic glass with palagonite fragments) and admixtures of terrigenous quartz and foraminifers. Time of sedimentation coincided with period of most intense volcanism on islands of the N. Atlantic
    - 2) Member 1A-I (“upper Pleistocene”) 3 m thick composed of terrigenous clayey, sandy, silty sediments. “Recent” deposits.

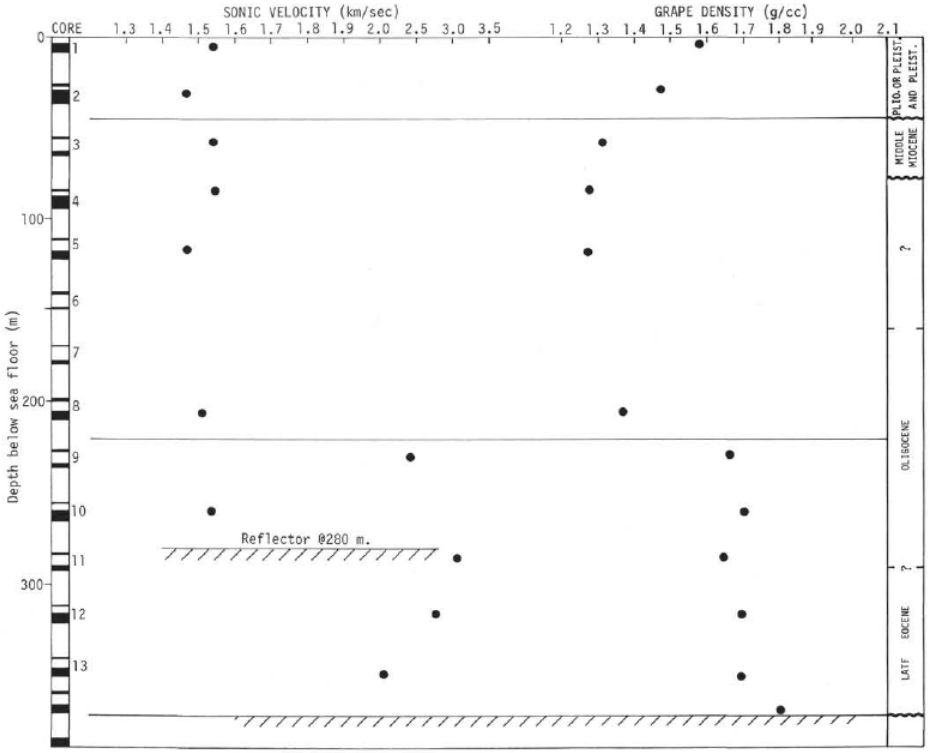

Figure 4. *Velocity, density – Site 350.*

Physical Properties of well 350

- Sonic velocity and density allow generalised subdivision of the sediment; however, incomplete coring mean stratigraphic boundaries are places midway between units where discontinuities exist
- Upper unit of terrigenous sandy muds and muds extending to 45 m. Miocene-Oligocene biogenic siliceous oozes show characteristic low bulk densities extending to 220 m.
- Variable Oligocene-late Eocene unit extents to 361.5 m which overlies brecciated basalt. No evidence of sill intrusion. Normal sedimentary contact with underlying basalts.
- Density increases slightly in the sedimentary unit above the basalt – due to addition of barite (noted as large and small crystals in last few 10's cm of core 13)?
- Acoustic property change between 220 and 280 m. Core 11 and 12 reveal turbidite sandstone sequences alternating with consolidated mudstones and limestones which gave high sonic velocities. Several high velocity limestones had been encountered earlier in the section (core 9) but these did not significantly alter the acoustic characteristics of the unit at that level.

- Lithologic Units 1 and 2; Cores 1-8; 0 to 226.5 meters; Average velocity = 1.516 km/sec; Travel time = 0.3 sec.
- Corresponds to interval 226.5 to 280 meters; Cores 9, 10 defined by physical properties as possessing velocities more akin to Units 1 and 2 than to Unit 3. Representative velocity is 1.55 km/sec (ignoring measurement in narrow limestone block); Travel time = 0.069 sec.
- Including the remainder of Lithologic Unit 3 from 280 to 364 meters; Cores 11-13; Average velocity = 2.666 km/sec; Travel time = 0.063 sec.
- The total travel time = 0.432 sec which compares favorably with data from the reflection record.

TABLE 5
Physical Properties (Averages–Site 350)

Unit		GRAPE ρ(g/cc)	GRAPE η(%)	Sonic Velocity (km/sec)	Impedance (ρc)
1	$\bar{x}$	1.53	73.62	1.50	2.30
	s	0.08	5.58	0.05	0.21
2	$\bar{x}$	1.31	87.75	1.52	1.80
	s	0.04	2.91	0.03	0.40
3	$\bar{x}$	1.70	62.12	2.26	3.44
	s	0.06	3.83	0.59	1.19

Conclusions

- "Glacial" sediments extend from 0 – 36.5 m. Dominantly sandy muds and mud, with admixtures of volcanic ash and some foraminiferal oozes. Fossils are poor in this section with only some planktonic foraminfera, benthonic and arenaceous foraminifera and siliceous fossils. Nannoplankton only found in core 1.
- Lithological unit from 55.5 – 226.5 m is Middle Miocene at top and extends into Oligocene at the bottom. Consists of alternating layers of unconsolidated and indurated-lithified terrigenous clays and muds. Also contains volcanic ash in conspicuous layers. Miocene sediments contain silicoflagellates, ebridians and siliceous foraminifera.
- Underlying lithological unit extends form 226.5 to basalt at 362 m. Dominated by lithified mudstone, claystone, limestone and breccia and some sandstone. Top of this unit there is a sudden downward decrease in density. Overall velocity decreases too but alternates between high and low corresponding to lithified and non-lithified layers in this unit, until uniformly high values are reached below 280 m. Turbidites are well developed at the base of the unit whilst near the boundary with the basement, the sediments are highly lithified. Fauna are poor and arenaceous foraminifera used to assign a tentative late Eocene age.
- Tuff breccias comprise the top of portion of the igneous basement from 362 – 380 m. Tholeiite Basalt (very fresh compared to other Leg 38 sites) extends to the bottom of the hole at 388 m. Radiometric age ranges 40 – 44 m.y – not in conflict with the age of late Eocene determined palaeontologically from overlying sediments.

ODP Leg 151 - Well 907A

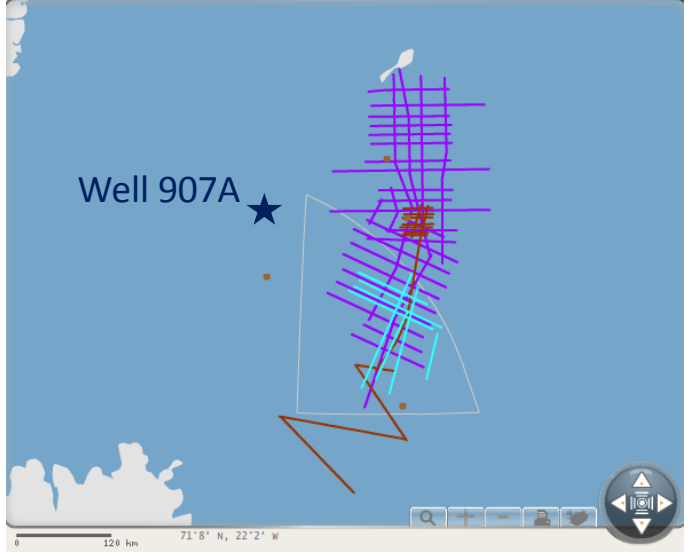

Well Summary
Date: **05/08/1993**
Latitude: **69.25**
Longitude: **-12.698**
Water Depth from sea level (m): **1800.8**
Bottom Felt at: **1811.6 meters (drill pipe from rig floor)**
KB (Distance between rig floor and SL (m): **10.8**
Well penetration (m): **224.1**
Total Depth (m): **2035.7**
Physiographic feature: **Sea floor**
No. of cores: **26**
Interval cored (m): **224.1**
Core recovered (m): **229.98**
Oldest sediment cored depth below sea floor (m): **216.3**
Oldest sediment age: **Miocene**
Oldest sediment description: **silty mud**
Type of crust: **oceanic**
Basement: **Basalt**
Depth below sea floor (m): **216.3 (drilled)**
K/AR age: **18-19 m.y. (early Miocene)**

- An extinct, short-lived spreading axis between magnetic Anomalies 6C and 5D has been suggested to exist on the eastern Iceland Plateau before the present-day Kolbeinsey Ridge came into existence (Johnson et al., 1972; Talwani & Eldholm, 1977)
- According to Talwani and Eldholm (1977), the extinct spreading axis probably represented a period of adjustment associated with the major westward shift of spreading between Anomalies 7 and 5.
- Vogt et al. (1980), however, ruled out the intermediate axis and proposed that spreading from the Kolbeinsey Ridge was symmetrical since post-Anomaly 7 time. If we accept the intermediate axis interpretation, Site 907 has been drilled on Anomaly 6B crust, between 22 and 24 Ma. Using the Vogt et al. (1980) interpretation, Site 907 is on crust of Anomaly 5B age, between 14 and 15 Ma.

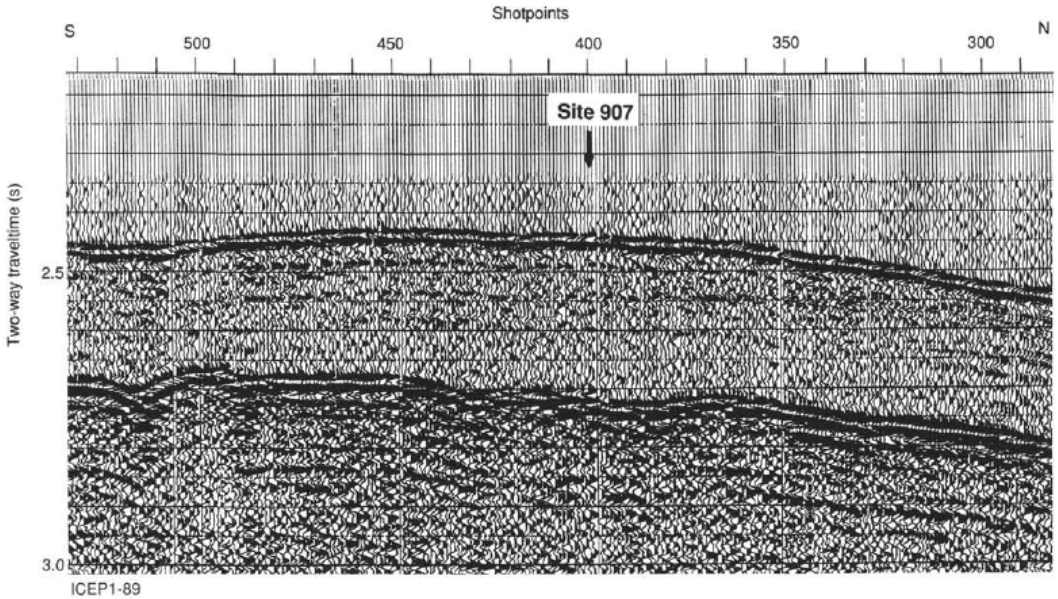

Figure 1. Seismic line ICEP 1-89, Segment A. Site 907 is located at shotpoint 400.

Principal results

- Primary objective of Site 907 was to recover an undisturbed pelagic sedimentary sequence with a content of calcareous pelagic fossils that would make it possible to monitor the formation and variation of oceanic fronts moving back and forth across the Icelandic Plateau.
- The site was planned as a midpoint in an East-West regional transect in the southern part of the Norwegian-Greenland Sea, from the Greenland Margin across the Iceland Plateau and the Norway Basin to the Norwegian Margin. The site was expected to give an open-ocean record of ice-rafted debris (IRD) and carbonate, as it is isolated from local continental influence.
- The site is located on middle Miocene oceanic crust and is overlain by about 360m of sediment allowing high resolution documentation of the last 10 – 12 m.y. The site was also was chosen to find higher concentrations of calcareous pelagic fossils than were obtained at the previous DSDP and ODP sites in the Norwegian-Greenland Sea – location makes it possible to monitor the formation of northern source deep waters through time because the Iceland Plateau is the final station for deep-water production and modification in the Greenland Sea and Arctic Ocean before they are exported into the N Atlantic Ocean.
- Late Cenozoic history of formation and chemistry of northern source deep waters were to be studied through continuously cored sediment sections. Pleistocene pelagic carbonate sequences with pronounced glacial-interglacial cycles and ash layers.
- Strong reflector under the main sedimentary sequence at 2.8 s (TWT) was to be drilled to determine the nature of acoustic basement – real volcanic basement? However, additional reflector segments at ~ 4.3 s TWT have been observed.

- The Iceland Plateau is associated with an opaque, extremely smooth acoustic basement reflector with only short indistinct reflector elements observed below. In some places the opaque reflector is interrupted by peaks appearing to pierce the layer and originate from deeper levels. This led Eldholm and Windisch (1974) to suggest that real oceanic basement was buried beneath the opaque horizon.
- The opaque horizon is associated with a fairly low seismic velocity of 3.3 km/s (Myhre and Eldholm, 1981). Furthermore, the opaque horizon exhibits no obvious age-depth relationship as expected for young oceanic crust.
- The sedimentary sequence in the area can be divided into two major units:
    - the uppermost sequence is characterized by weak, continuous, flat-lying reflectors,
    - the lower sequence is almost transparent.
- At Site 348, 544.0 m was penetrated and spot-cored, with a pelagic Quaternary and Neogene sequence of 526.6 m on top of basalt.
- The K/Ar dating of the tholeiitic basalt provided an age of 18-19 Ma, and its texture varied from fine to medium-grained without any pillow lavas observed. The basalt appeared to be part of a major sill or dike body that could be the opaque seismic layer, and deeper oceanic basement as well as masked sediment layers cannot be ruled out.

- Site 907 located in SW part of the Norwegian-Greenland Sea on eastern Iceland Plateau, west of extinct Iceland Plateau spreading axis on oceanic crust of magnetic anomaly 6B (22-24 Ma).
- Part of a palaeoenvironmental transect from Norwegian to Greenland continental margin & located on shotpoint 400 of a multichannel seismic reflection line collected by University of Bergen.
- Planned to conduct double or triple APC and XCB coring to obtain a complete stratigraphic sequence of Neogene and Quaternary pelagic sediments and to reach basement – 5 lithostratigraphic units were identified ontop of the basalt encountered at 216.3 mbsf.

Well Lithology

Principal results:

Pliocene to Quaternary hemipelagic deposits, upper and middle Miocene biosiliceous oozes and middle Miocene ash-rich muds. 5 sedimentary lithostratigraphic units were recognised:

- Unit 1: (0 - 16.8 mbsf) Quaternary dark grayish brown to grayish brown clayey silts, silty clays, and foraminifer-bearing silty muds with minor amounts of biosilica-bearing silty carbonate ooze. Pervasive bioturbation and distinguished by presence of biogenic calcareous material (foraminiferers). Additionally coarse fractions consist of quartz, feldspar and mica with little volcanic glass. Dropstones (IRD) >1cm are rare.
- Unit 2: (16.8 – 56.3 mbsf) Pliocene to Pleistocene clayey silts and silty clays characterised by the absence of biogenic carbonate and abundance of grey brown to dark grey silt- and sand-sized siliciclastic grains. Volcanic glass is rare increasing slightly towards the bottom of the unit.
- Unit 3: (56.3 – 118.1 mbsf) Upper Miocene to Pliocene clayey silts and silty clays with biogenic silica and more volcanic glass than pervious units and decreased percentage of quartz and feldspars. Primarily dark olive grey, olive grey and very dark grey. Coarse fractions consist of volcanic glass and quartz, feldspar and mica. Lithology and colour boundaries are gradational due to pervasive bioturbation. Dropstones found throughout.
- Unit 4: (118.1 – 197.3 mbsf) Middle to upper Miocene dark greenish grey to dark grey ash- and biosilica bearing silty clays and clayey silts with greenish grey colour bands throughout. Moderate to intense bioturbation giving a mottled appearance. Abundant often graded ash layers ranging from 1 – 15 cm common in upper part of the unit.
- Unit 5: (197 – 216.3 mbsf) Middle Miocene dark olive grey clayey mud and silty clay. Distinguished form unit 4 by its high quartz and clay and low biosilica content. Colour mottling common and burrows are filled with sand-sized volcanic glass.

- Calculated bulk sedimentation rates range from 10-20 m/m.y. in upper Miocene to Quaternary to >80 m/m.y. in middle Miocene.
- Siliceous microfossil assemblages suggest highly productive surface waters during middle Miocene – early Pliocene.
- Subsequent decline of microfossil content and increased presence of IRD since late Pliocene led to deposition of overlying terrigenous sediments typical of glacial depositional environments.
- Up-hole increase in wet-bulk-density and decrease in porosity occurs at approx. 55 mbsf – coincides with onset of major IRD deposition at 2.6 Ma.
- High heat flow values and geochemical anomalies suggest the existence of hydrothermal fluid flow through deeper part of the sequence.
- Sedimentary sequence rests on acoustic basement – nearly aphyric basalts erupted in shallow water (<500m). Homogeneous and massive with glassy tops & bottoms and abundant vesicles = pillow basalts

Table 1. Coring summary, Hole 907A.

Core	Date (Aug. 1993)	Time (UTC)	Depth (mbsf)	Length cored (m)	Length recovered (m)	Recovery (%)
151-907A-						
1H	5	1940	0.0–7.3	7.3	7.27	99.6
2H	5	2015	7.3–16.8	9.5	9.81	103.0
3H	5	2115	16.8–26.3	9.5	9.89	104.0
4H	5	2145	26.3–35.8	9.5	9.88	104.0
5H	5	2220	35.8–45.3	9.5	10.10	106.3
6H	5	2315	45.3–54.8	9.5	10.06	105.9
7H	5	2350	54.8–64.3	9.5	9.90	104.0
8H	6	0030	64.3–73.8	9.5	9.82	103.0
9H	6	0130	73.8–83.3	9.5	10.19	107.2
10H	6	0205	83.3–92.8	9.5	9.92	104.0
11H	6	0240	92.8–102.3	9.5	10.07	106.0
12H	6	0335	102.3–111.8	9.5	9.97	105.0
13H	6	0405	111.8–121.3	9.5	10.00	105.2
14H	6	0435	121.3–130.8	9.5	9.93	104.0
15H	6	0535	130.8–140.3	9.5	9.70	102.0
16H	6	0605	140.3–149.8	9.5	9.92	104.0
17H	6	0640	149.8–159.3	9.5	10.01	105.3
18H	6	0715	159.3–168.8	9.5	9.87	104.0
19H	6	0750	168.8–178.3	9.5	9.99	105.0
20H	6	0825	178.3–187.8	9.5	9.85	103.0
21H	6	0900	187.8–197.3	9.5	9.59	101.0
22H	6	0935	197.3–206.8	9.5	9.58	101.0
23H	6	1015	206.8–216.3	9.5	9.78	103.0
24X	6	1305	216.3–217.3	1.0	0.53	53.0
25X	6	1610	217.3–221.0	3.7	2.41	65.1
26X	6	2100	221.0–224.1	3.1	1.94	62.6
Coring totals				224.1	229.98	102.6

Table 2. Summary of lithologic units, Site 907.

Unit	Dominant lithologies	Interval, mbsf (thickness, m)	Age	Occurrence (core-section)
I	Interbedded silty clay, clayey silt, and foraminifer-bearing silty mud and silty clay.	0–16.8 (16.8)	Quaternary	1H-1 to 2H-CC, 31 cm
II	Silty clay and clayey silt. Defined by the absence of biogenic sediments.	16.8–56.3 (39.5)	Pliocene to Quaternary	3H-1 to 7H-1, 150 cm
IIIA	Interbedded silty clay and clayey silt with thin nannofossil ooze beds. Minor biogenic silica, decrease in % quartz.	56.3–94.1 (37.8)	late Miocene to Pliocene	7H-2, 0 cm, to 11H-2, 30 cm
IIIB	Silty clay and clayey silt, some biogenic silica, no calcareous nannofossils.	94.1–118.1 (24.0)	late Miocene	11H-2, 30 cm, to 13H-6, 30 cm
IV	Biosilica-bearing silty clay and clayey silt. No dropstones, very little quartz.	118.1–197.3 (79.2)	middle to late Miocene	13H-6, 30 cm, to 22H-1, 0 cm
V	Clayey mud and silty clay. Decrease in biosilica, increase in quartz.	197.3–216.3 (19.0)	middle Miocene	22H-1, 0 cm, to 24-1, 0 cm

Lithology

Dominated by unlithified silty clay and clayey silt. Dark grey brown in upper half; olive grey-greenish grey in lower half. Five lithologic units were identified, primarily on the basis of varying amounts of biogenic and siliciclastic material, and volcanic glass.

Unit 1: 0 – 16.8 mbsf. Quaternary. Biogenic clay and silty muds.

- Clayey silt, silty clay, and foraminifer-bearing silty mud with minor amounts of biosilica-bearing silty carbonate ooze, clayey foraminifer ooze, silty mud, foraminifer-bearing clay, foraminifer silty clay, and ash.
- Commonly dark grey brown and dark brown, with thin intervals of olive brown, grey, olive and olive grey.
- Pervasive bioturbation cause colour mottling and gradation between different colour boundaries
- Coarse fraction consists of quartz, feldspar and mica, with little volcanic glass. Dropstones >1cm are rare.
- Three distinct ash layers, 10 to 18 cm thick, have sharp bases, are graded, and have gradational contacts with the overlying lithology.

Interpretation:

- high siliciclastic content (IRD's) and dark coloured sediments reflect glacial conditions. Alternating fossiliferous and fossil-poor sediments and colour changes represent climatic cycles.
- Lower half interglacials represented by foraminifer-bearing sediments & glacials represented by microfossil-barren silty clays.
- Upper half interglacials respresent substantially less of recovered sediment – maybe due to longer glacials, lower interglacial sedimentation rates or higher glacial sedimentation rates.

Unit 2: 16.8 – 56.3 mbsf. Pliocene – Quaternary. Clayey silt.

- dark grey brown, dark grey and grey clayey silt and silty clay comprise >90% of the unit.
- Characterized by the absence of biogenic carbonate and silica and the abundance of silt- and sand-sized siliciclastic grains = clay (5% to 90%), quartz (5% to 40%), feldspar (5% to 35%), mica (<5%), and accessory minerals (<5%).
- Volcanic glass is rare but shows a slight increase toward the base of the unit. Carbonate percentages seldom exceed 1%.
- (1) greyish olive clay – restricted to 26.3 – 26.6 mbsf & included quartz, feldspars and opaques as accessory grains
- (2) dark grey and dark greyish brown ash
- (3) dark grey diatom- and ash-bearing silty clay – 28.52 – 28.8 mbsf overlying one of the indurated greenish grey layers
- (4) grey-ish brown carbonate mud - consists of well-sorted, very fine silt- to clay-sized, rounded particles of carbonate with minor amounts of quartz. There is no evidence for a biogenic origin; hence, the sediment is referred to as detrital.

Interpretation: The dropstones, high quartz and feldspar content, and consistently dark colour indicate an increased glacial regime, beginning as early as 3 Ma.

- The lack of microfossils in general may be attributed to three causes: low productivity, preferential removal by dissolution or bottom currents, and/or dilution by siliciclastic material. However, last explanation is insufficient to explain the unit's barren sediments with no large changes in sedimentation rate from the fossiliferous sediments above and below.
- Productivity may have been negatively affected by Oceanographic changes associated with increased glaciation - expanded sea-ice cover, cooler surface temperatures increased stratification of the water column, and decreased upwelling of nutrients supplied to surface waters.

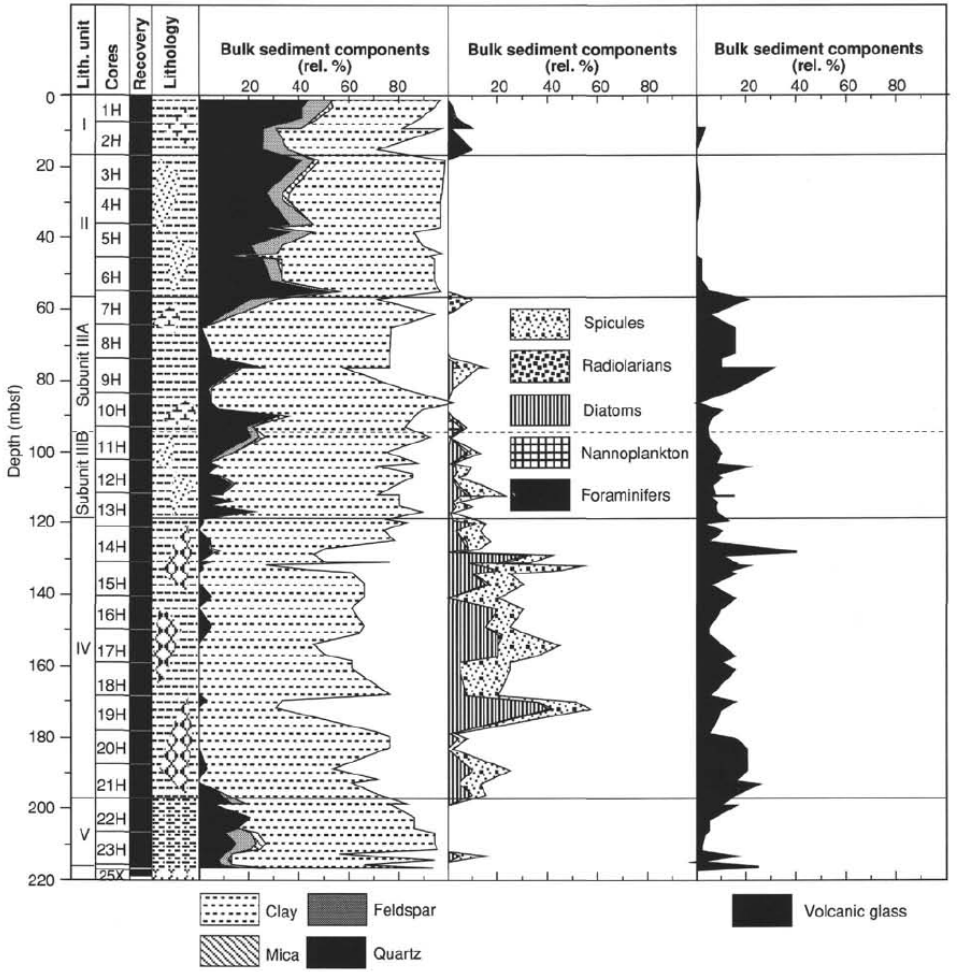

Figure 2. Graphic summary of lithologic units for Hole 907A, and percentages of the three components used to define the lithologic units: dominant siliciclastic components, biogenic content, and volcanic glass.

- Boundary between Units 3 and 4 defined by an increase in quartz & first appearance of dropstones >1cm at 116 mbsf = IRD
- Decrease in sedimentation rate at 135 mbsf within an interval containing a hiatus (11-13 Ma). Biogenic silica decreases at 128 mbsf (10.5 Ma) followed by IRD approx. 12 m higher (9 Ma). Therefore expansion of sea ice/ increased glaciation did not cause decreased biosilica content. Lower biosilica may resulted from decreased productivity due to lower upwelling rates/increased dissolution of biosilica related to greater ventilation of intermediate waters

Lithology (cont.)

Unit 3: 56.3 – 118.1 mbsf. Late Miocene - Pliocene. Olive grey – dark grey clayey silt and silty clay

- Defined by the presence of biogenic silica, an increase in volcanic glass content and a decrease in quartz and feldspar percentage
- Clayey silt and silty clay compose about 40% of the unit - dominant silt- and sand-sized components are, in increasing order: mica, accessory minerals, feldspar, and quartz.
- Dark grey, olive grey, and dark greenish grey, ash-bearing silty clay composes about 30% of the unit.
- Coarse fraction comprises volcanic glass, quartz, feldspar, mica and accessory minerals. Ash layers are common.
- 2 subunits are defined: sub-unit 3A (56.3 – 94.1 mbsf) has interbedded nannofossil ooze and nannofossil silty clay; sub-unit 3B (94.1 – 118.1 mbsf) does not.

Interpretation: represents a transitional phase between Unit 4 sediments (marked by high biosilica and low siliciclastic contents) and Unit 2 sediments (marked by low to absent biosilica and high siliciclastic contents).

- Nannofossil ooze in subunit 3A indicate high productivity and high carbonate production/preservation.
- Distinctive silica-bearing nannofossil layers represent intervals of amplified response of the Norwegian-Greenland Sea to northern hemisphere climate change due to the incursion of warm N.Atlantic surface waters.

Unit 4: 118.1 – 197 mbsf. Middle to late Miocene. Ash- and biosilica-bearing silty clay and clayey silt.

- Definied by high biosilica (10 – 35%) and volcanic glass (10 – 15%) contents and low quartz (<5%) content and lack of dropstones
- dark greenish grey to dark grey ash- and biosilica-bearing silty clay and clayey silt.
- Except for ash layers all colour boundaries are gradational due to bioturbation, causing colur mottling. Green-grey-black burrows are common containing volcanic glass shards
- Ash layers 1-15 cm thick are common in upper part of the unit from 118.1 – 146 mbsf. Thicker layers are usually graded.
- Interpretation: Due to relatively high biogenic component – interpreted as hemipelagic to pelagic.
    - Biosiliceous component suggests high productivity interval.
    - Magnetostratigraphic data supports the inference of high sedimentation rates in the deposition of the lower two-thirds of this unit.

Unit 5: 197.3 – 216.3 mbsf. Middle Miocene. Homogeneous dark olive grey clayey mud and silty clay.

- Distinguished from unit 4 by higher quartz (10-15%) and clay (80 – 90%) content and lower biosilica (<5%). Volcanic glass content is low compared to units 3 and 4.
- Colour mottling due to moderate to extensive bioturbation – burrows commonly filled with sand-sized volcanic glass
- No discrete ash layers observed although volcanic glass abundances range from 5 – 15%.

Interpretation: Origin and transport method of siliciclastic clay and silt fraction is unknown. Possibly from ice-rafting, sediment-gravity flows (turbidity currents) and aeolian transport.

- Ice-rafting unlikely as neaby landmasses were not thought to be glaciated during this time.
- No sedimentary structures were observed (due to moderate - intense bioturbation) that would support a turbidite interpretation, detection may require x-radiographs.

Volcanic ash layers

- Forty-eight distinct ash layers, >l cm thick, were identified in all the lithologic units except lithologic Unit 5.
- The ash also occurs as sand to coarse, silt-sized, fresh glass shards in pocket infillings.
- Thickness of individual ashes ranges from a few mm to 18 cm (6.6 cm average) and commonly show a fining upward trend from a sharp basal contact.
- Ash colour varies from black to grey with more or less brown, olive, or greens. Colourless shards, which may indicate rhyolitic composition, are dominant over brown shards, which are either absent or only present in minor amounts.
- Compared with ODP Sites 642 and 643, the ash layers of Hole 907A are distinctly thicker (7 cm vs. 1 cm) and more abundant. This is consistent with an air-fall origin from eruptions on Iceland leading to thicker deposits at Site 907, closer to the tephra source. If, however, the ashes are as rhyolitic as the light colour indicates, then a non-Icelandic source may be required.
- Using the paleomagnetic age model, ash-layer deposition has been fairly constant throughout the Neogene. Yet, the percentage of ash in the sediments is negligible in the Quaternary and upper Pliocene, and is relatively constant in the rest of the section.
- Therefore difficult to invoke either a constant air fall of ash or bioturbation as mechanisms for distributing/redistributing the ash within these sediments. Bioturbators would have more time and more ash to disperse into the surrounding sediments in the intervals of slower sedimentation rate and higher ash density (e.g, 60-150 mbsf), and this is not seen.

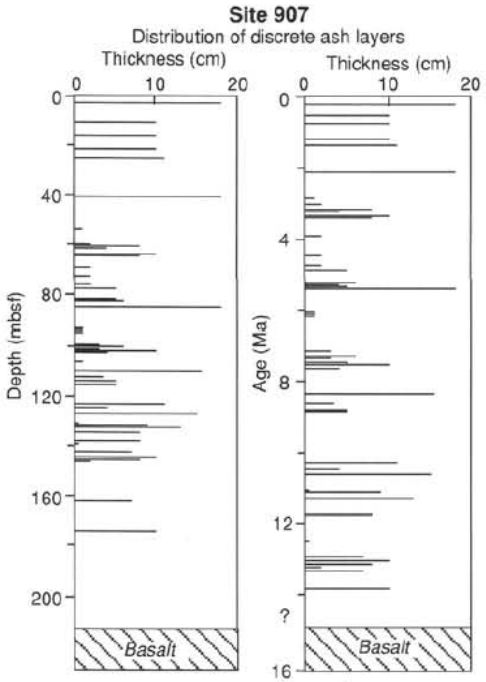

Figure 3. Graphic summary of ash layers >1 cm thick vs. depth in the core and age.

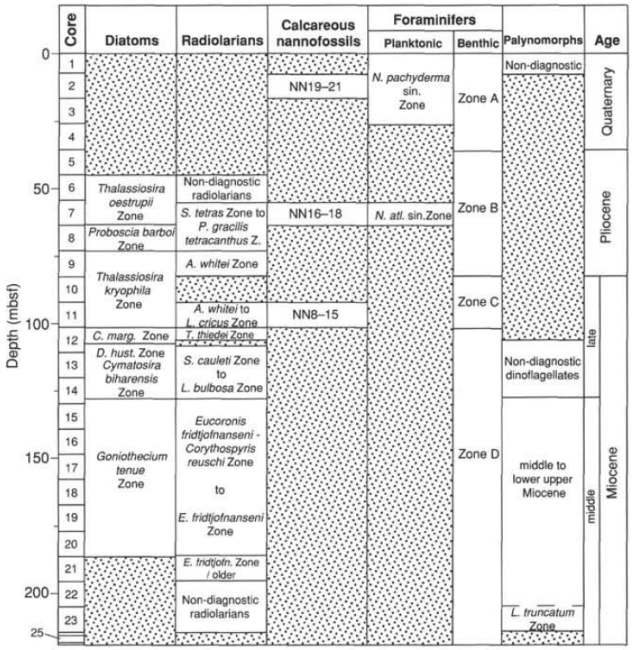

Biostratigraphy

- Pliocene to Pleistocene hemipelagic sediments, upper and middle Miocene biosiliceous oozes, and middle Miocene volcanic ash-rich mud.
- Leg 151 was the third DSDP/ODP leg in the Norwegian- Greenland Sea - some biostratigraphic correlations were made to DSDP Legs 38 and 94 and ODP Legs 104 and 105.
- However, correlation proved difficult for these northern sites because most of the standard planktonic schemes proved insufficient. Biostratigraphic difficulties include the scarceness of calcareous material, high percentage of endemic species, high accumulation of volcanic ash, and variable preservation of siliceous microfossils, particularly in the Pliocene-Quaternary and in middle Miocene ash-rich sediments.
- Site 907 remains useful as a western tie-point for Miocene to Quaternary stratigraphy and paleoceanography of the Norwegian-Greenland Sea.
- Siliceous microfossils indicate an age of 14 Ma in core 21, but age-diagnostic fossils are absent below that level. Dinoflagellate evidence below core 21 indicates the base of the sediment section is no older than about 16 Ma (mid Miocene).
- Upper Miocene/middle Miocene boundary is recognized at 129.5 mbsf by the last occurrence of the diatom *A. ingens,* which marks the top of the *G. tenue* Zone.
- The Pliocene/upper Miocene boundary occurs at 83.3 mbsf according to paleomagnetic evidence - corroborated by the first occurrence of diatoms *T. oestrupü* and *T. jacksonii.* Radiolarians, calcareous nannofossils, and benthic foraminifers from core 11 indicate a Miocene age.
- The Pliocene/Quaternary boundary is recognized at 37 mbsf in the middle of the Olduvai Event. This agrees with the calcareous nannofossils and planktonic and benthic foraminifers, which recognize Pliocene microfossils in core 7.
- Biostratigraphic assignments to the Quaternary are confirmed by calcareous nannofossils, and planktonic and benthic foraminifers found in core 2.

- Middle Miocene sediments are rich in siliceous microfossils, which indicates that surface waters were enriched in nutrients, possibly resulting from upwelling conditions in the Norwegian-Greenland Sea during this time. Upwelling increased the productivity of surface-water species but in turn decreased bottom-water pH, resulting in the dissolution of the calcareous microfossils. This upwelling continued into the late Miocene and early Pliocene.
- However, two brief episodes of carbonate preservation in core cores 11 and 7.
- Increase of ice rafting during the late Pliocene and the return of colder conditions are coeval with a decline in the abundance of siliceous microfossils. An interval spanning the upper Pliocene to lower Quaternary is barren of all microfossils.
- Beginning in the Brunhes, calcareous microfossils become more abundant in the upper two cores of Hole 907A, predominately during the interglacial intervals.

Physical Properties

- The conductivities measured in the upper portion of Hole 907A, from the seafloor to 58 mbsf, range from 0.8 to 1.3 W/m K. The measured conductivities decrease and become relatively constant (0.8- 0.9 W/m K) in the central portion of the hole (58-190 mbsf), which corresponds to lithostratigraphic Units 3 & 4, before beginning to increase again in unit 5 (below ~190 mbsf).
- Decrease in thermal conductivity in the central portion of the hole is associated with high measured values of porosity and water content, especially in lithologic Unit 4. The lower conductivity in Unit 4 is likely associated with the presence of increased amounts of high-porosity, biosiliceous components.

- Significant increase up-core in bulk density, from about 1.5 g/cm3 to about 1.75 g/cm3, over the interval from 55 to 45 mbsf (ca. 2.7-2.5 Ma). The density increase occurs approximately at the base of lithostratigraphic Unit 2, and coincident with the initiation of major Northern Hemisphere glaciation.
- Results of inverse correlation of GRAPE density and Log denisty over the interval from ~83 to 187 mbsf. The records are similar, with a virtual peak-for-peak match over the entire record. The final correlation coefficient was 0.73. On average, the depth of the GRAPE record was shifted upward by -2 m, presumably reflecting the effect of rebound causing a vertical expansion of the sediment core record.

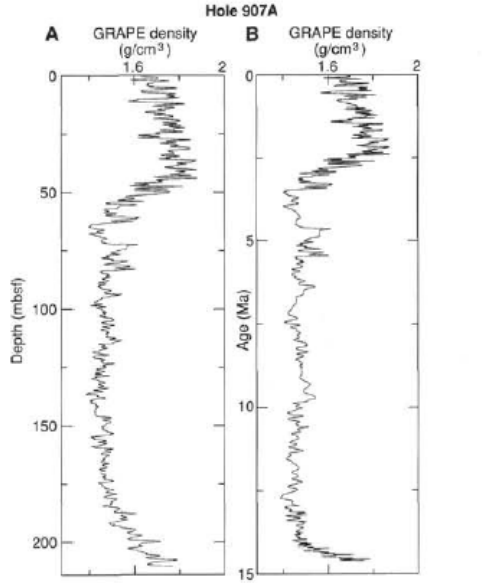

Figure 30. **A.** Downhole GRAPE density, low-pass filtered. **B.** GRAPE density time series.

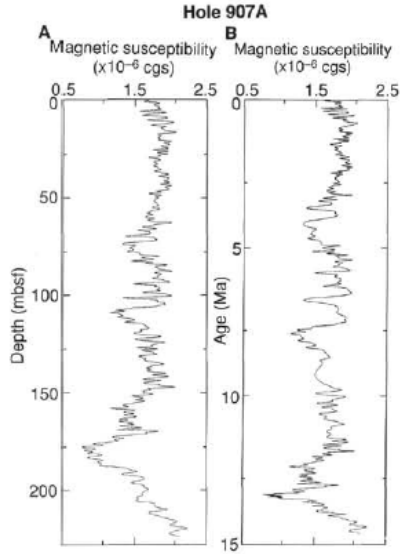

Figure 31. **A.** Downhole magnetic susceptibility, low-pass filtered. Units are logarithmic uncorrected cgs Bartington meter units. **B.** Magnetic susceptibility time series.

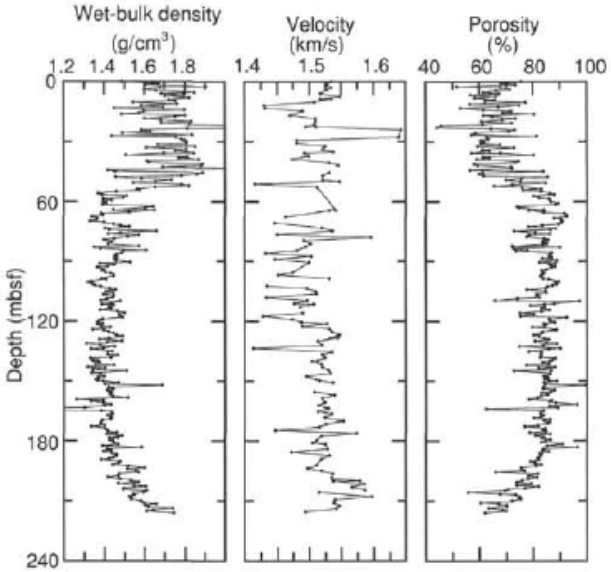

Figure 40. Comparisons among laboratory velocity measurements and measurements of bulk density and porosity vs. depth in Hole 907A.

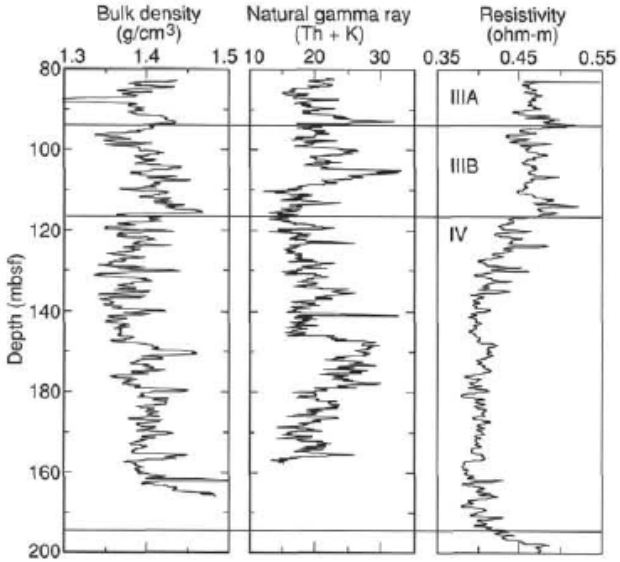

Figure 47. Comparison of the wet-bulk density, computed gamma-ray, and medium induction log data from Hole 907A.

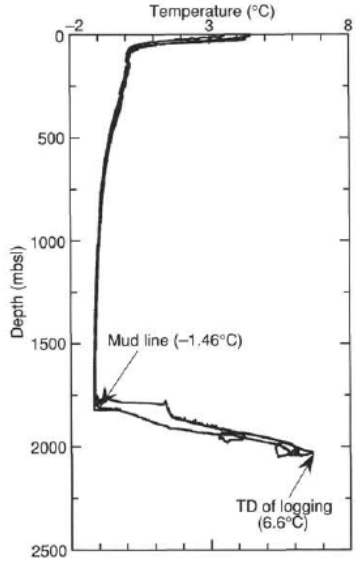

Figure 46. Temperature data recorded by the Lamont-Doherty temperature logging tool (TLT) on the seismic stratigraphy tool string, the first tool string to be run in Hole 907A. TD = total depth in hole.

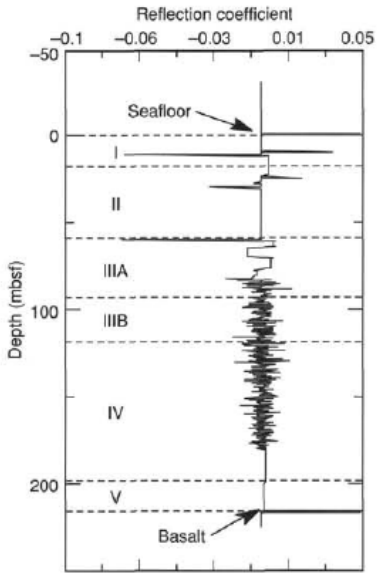

Figure 49. Reflection coefficient vs. depth at Site 907. Also shown are the lithostratigraphic unit boundaries from the "Lithostratigraphy" section (this chapter).

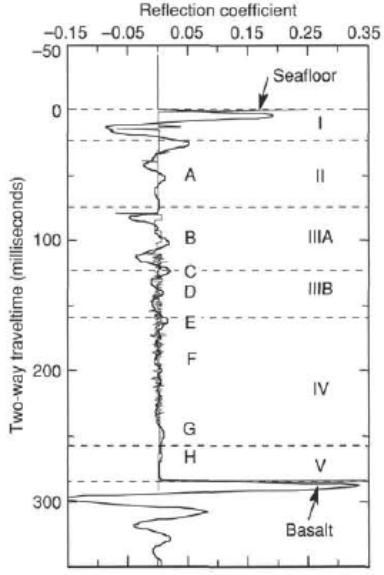

Figure 50. Reflection coefficient and synthetic seismogram shown against two-way traveltime. Locations of lithostratigraphic unit boundaries have been interpolated onto the figure.

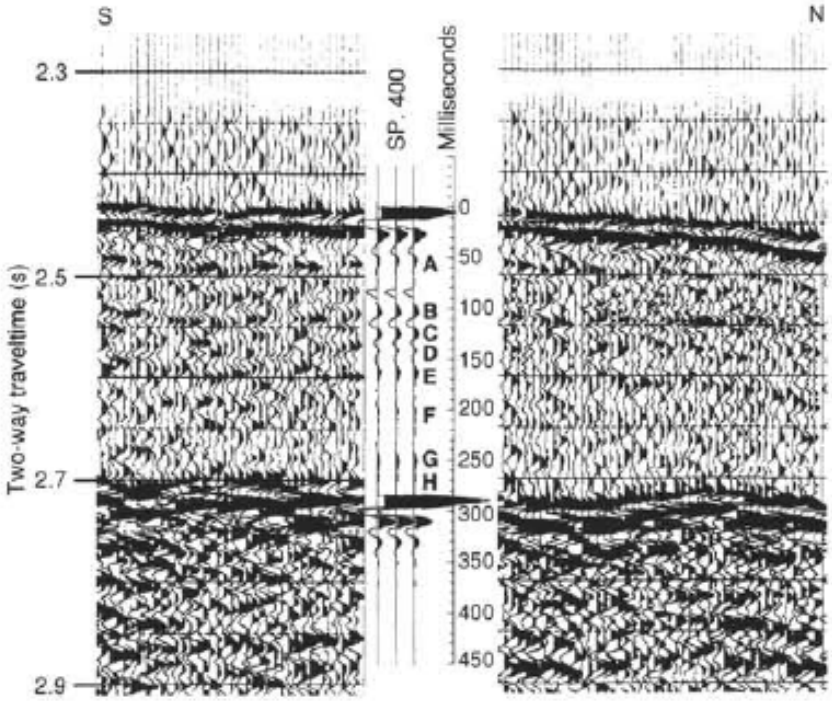

Figure 51. Comparison between synthetic seismogram from Site 907 and equivalent seismic section measured on ICEP1-89 Segment A. Reflector E marks the boundary between the biosiliceous upper/middle Miocene sediments and the detrital upper sediment column (lithostratigraphic Unit III/IV boundary). A–H = potential reflectors.

Synthetic Seismic Tie

- At Site 907 a synthetic seismogram was generated from the velocity and density profiles to correlate reflectors in the seismic section to stratigraphic changes.
- The acoustic impedance profile (the product of density and velocity) and the profile of reflection coefficients (the rate of change of acoustic impedance) were determined both as a function of depth and of two-way acoustic traveltime (TWT). Convolution of the reflection coefficient profile with an assumed source acoustic wavelet resulted in a synthetic seismogram to compare with the measured seismic section.
- By far, the strongest reflection coefficients are found at the seafloor and the basalt, with the basalt reflection coefficient being about 40% stronger than that of the seafloor (Rc = 0.46). The upper part of the sediment section (lithostratigraphic Units I to IIIb), which represents the transition from the Miocene biosiliceous section to sediment accumulation under glacial conditions is marked by several relatively strong reflection coefficients.
- A series of acoustic reflectors is found in the upper sediment section (reflectors A-D) and a reflector (E) roughly at the Unit 3/4 boundary.
- Within Unit IV only subdued seismic reflections are produced, until near the Unit IV/V boundary where the sediment loses its biosiliceous component.
- Comparison of the synthetic seismogram with the seismic section shows that the velocity profile must be nearly correct. The traveltime from seafloor to basalt is predicted well.
- Reflector E proves to be a boundary in the seismic section between an upper sediment column having a number of coherent reflectors and a lower more transparent sediment column. Tracing this horizon should delineate the top of the upper/middle Miocene biosiliceous sediments on the Iceland Plateau.

ODP Leg 162 - Well 907C

Well Summary
Date: **01/08/1995**
Latitude: **69.25**
Longitude: **-12.698**
Water Depth from sea level (m): **1801.2**
Bottom Felt at: **1812.4 meters (drill pipe from rig floor)**
KB (Distance between rig floor and SL) (m): **11.2**
Well penetration (m): **215.1**
Total Depth (m): **2027.5**
Physiographic feature: **Sea floor plateau**
No. of cores: **23**
Interval cored (m): **215.1**
Core recovered (m): **220.23**
Oldest sediment cored depth below sea floor (m): **214.9**
Oldest sediment age: **middle Miocene**
Oldest sediment description: **silty clay**
Type of crust: **oceanic**

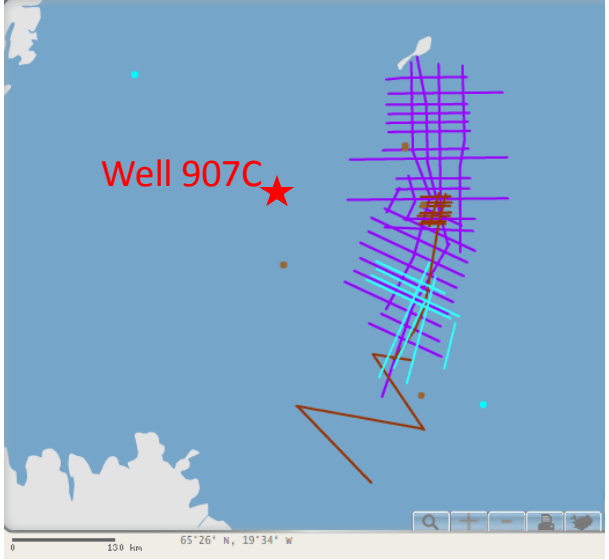

- The drill sites on the Iceland Plateau (Sites 907 and 985) are part of a paleoenvironmental transect from Norway to Greenland designed to study the history of the advection of temperate, saline Atlantic waters into the Norwegian Sea (the "Nordic heat pump"), the position of the mixing front between these warm waters and the cold, partly ice-covered Arctic waters (the Arctic Front), and the position of the front delimiting the less saline, ice-covered Polar Waters of the East Greenland Current farther to the west.
- The transect covers the climatically sensitive and variable thermal gradient between polar areas near east Greenland and temperate areas off Norway. Convection to intermediate depths in the Iceland Sea produces and modifies deep waters in the Nordic Seas, which are then a significant contributor to overflow waters across the Greenland-Scotland Ridge (the Southern Gateway)
- Site 907 located on the Iceland Plateau defined by the 1800-m contour, which gently increases in depth away from the spreading axis, the Kolbeinsey Ridge.
- Site 907 was drilled on what is believed to be Anomaly 6B crust, between 22 and 24 Ma old. The Iceland Plateau is associated with an opaque, extremely smooth acoustic basement reflector, with only short, indistinct reflector elements observed below.
- The primary objective of drilling operations at Site 907 was to recover an undisturbed pelagic sedimentary sequence. The site was expected to give an open-ocean record of IRD and carbonate, as it is isolated from local continental influence.
- Site location also was chosen to find higher concentrations of calcareous pelagic fossils than were obtained at the previous DSDP and ODP sites in the Norwegian-Greenland Sea.
- Leg 162 reoccupied the site of the ODP Leg 151 and drilled the two additional holes (Holes 907B and 907C). Shipboard scientists on Leg 151 described five sedimentary units at Site 907.
- Calcareous material is typically scarce. With the exception of a few thin nannofossil-rich horizons in the Pliocene, biocarbonate is restricted to the last 1 Ma. The site also has a clean magnetic polarity record although there is some uncertainty as to its correlation to the geomagnetic polarity time scale.
- Shore-based studies of the site have since provided a reliable stable isotope record of the last 1 Ma and a record of IRD, showing IRD deposition from surrounding continents back to more than 7 Ma, with major increases occurring at 6 Ma, 2.9 Ma, and 1 Ma.
- The drilling plan for Leg 162 was to core two additional APC holes to construct a complete sediment section and provide additional sampling material.

Principal results

- A complete sediment sequence is documented for almost the entire section to 215 mbsf, and a continuous spliced section was constructed for high resolution paleoclimate studies. It was also possible to establish a spliced composite section
- The scarcity of biogenic material in certain intervals reduce the possibility of biostratigraphic age control, whereas a relatively clean magnetic polarity sequence enables correlation with confidence to the geomagnetic polarity time scale back to the upper Miocene, and with somewhat less confidence further back to approximately 16 Ma.
- Two short hiatuses or condensed intervals are indicated in the middle to late Miocene section. Indications of breaks at these intervals are supported by changes in sediment physical properties.
- Sedimentation rates average 17 m/m.y. over the last 3 Ma, 11 m/m.y. in the 3-5.5-Ma interval, and 22 m/m.y. in the 5.5-11 Ma interval.
- The sediments at Site 907 are dominantly composed of silty clay, clay with silt, and clayey mixed sediment with varying amounts of biogenic material. The biogenic component, which includes calcareous nannofossils, foraminifers, diatoms, and/or spicules, is highly variable with depth.
- Dropstones greater than 1 cm in size are present upward from 62.9 mbsf. Ash layers and ash pods are abundant throughout Site 907 sediments.
- Four distinct lithostratigraphic units are defined with unit boundaries at 16, 63, and 196 mbsf.
- Biogenic material occurs sporadically and intermittently throughout the sequence. It includes both calcareous and siliceous in Unit 1 and predominantly siliceous material in Unit 3. The alternating biogenic-bearing and nonbiogenic sediments may reflect climatically driven changes over the Neogene.
- The boundary of Unit II and III may reflect the most important switch in climatic and oceanic conditions associated with the onset of increased glaciation during the Pliocene = Quartz and feldspar increase markedly upsection at this level, dropstones first occur, and changes in the suite of clay minerals are indicated by changing natural gamma-ray emissions. Decrease in biogenic components subsequent to this boundary may reflect environmental degradation & barren intervals in unit 1 are linked to high-amplitude climatic cycles within the late Pleistocene.
- The geochemistry of the sedimentary sequence is characterized by processes typical of sulfate reduction and processes reflecting alteration of volcanic ash within the sediments and basement basalts below.

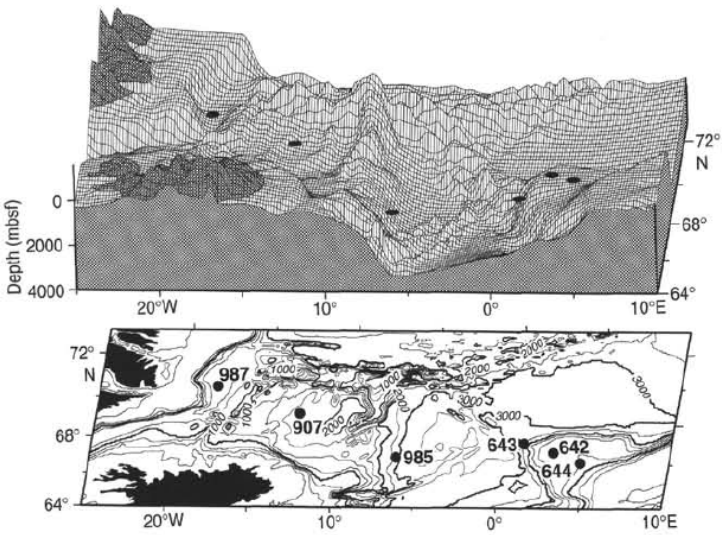

Figure 1. Bathymetry of the Nordic Seas paleoenvironmental transect, showing location of Legs 104, 151, and 162 drill sites. Bathymetric data (in meters) from ETOPO5.

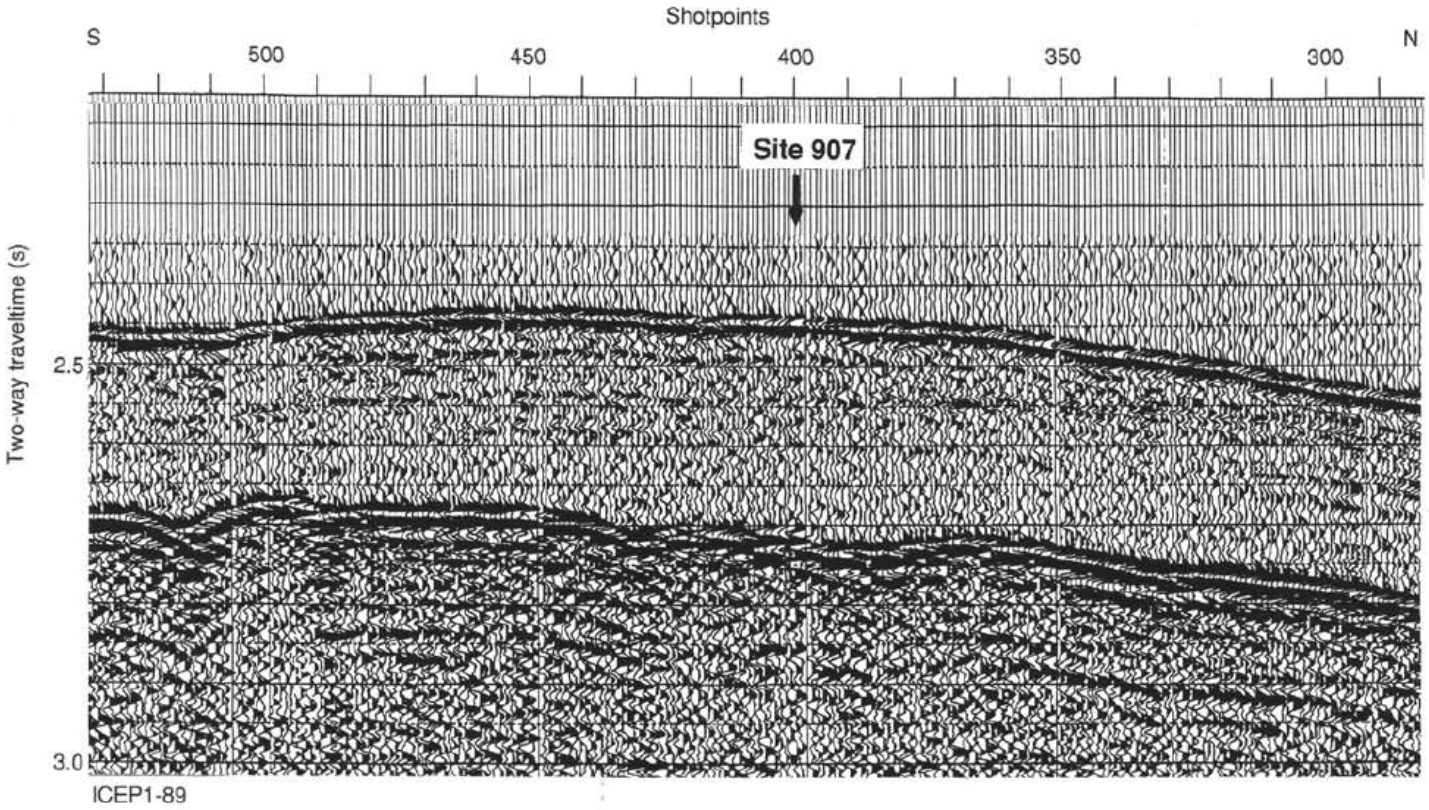

Figure 2. Seismic section through Site 907 (from Myhre, Thiede, Firth, et al., 1995).

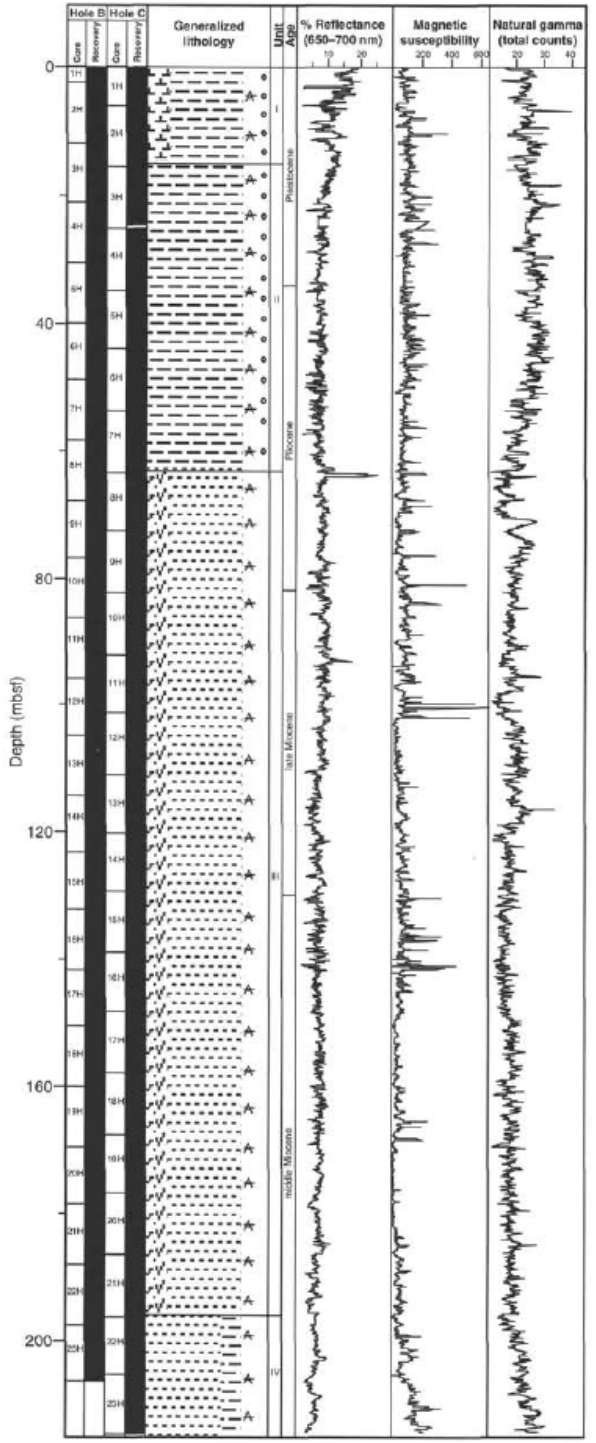

Figure 7. Core recovery, lithostratigraphy, age, percentage reflectance (red band, 650–700 nm), magnetic susceptibility, and natural gamma radiation of sediments recovered in Holes 907B and 907C. (Key to symbols used in the "Generalized Lithology" column can be found in fig. 4, "Explanatory Notes" chapter, this volume.)

Table 6. Summary table of lithostratigraphic units at Site 907.

Unit	Depth (mbsf)	Thickness (m)	Age	Dominant lithologies/criteria
I	0–15.6	15.6	Holocene–"mid." Pleist.	Biogenic microfossil mixed sediment, silty clay, clay with silt, clay. High-amplitude and decreasing trend of reflectance, high amount of quartz and feldspar, color change between Units I and II.
II	15.6–63.1	47.5	"mid." Pleist.–"mid." Plio.	Silty clay, clay with silt and ash, clay. High amount of quartz and feldspar, absence of biogenic sediment, onset of dropstones, downcore increase in natural gamma radiation.
III	63.1–196.1	133.0	"mid." Plio.–mid. Mio.	Dark greenish gray silty clay, clay with silt, clay with diatoms. Reocurrence of siliceous sediment, relatively lower amount of siliciclastic material, no trend in magnetic susceptibility and natural gamma radiation.
IV	196.1–214.9	18.8	middle Miocene	Dark greenish gray silty clay, clay with silt and clay. Downcore increase in magnetic susceptibility and natural gamma radiation, no biogenic sediment, slightly lower amount of siliciclastic material.

- Interpretations are based on alternating biogenic and terrigenous sediment & compositional changes within the siliciclastic component.
- Well 907 is located at the centre of the Iceland Plateau – open ocean conditions likely to have prevailed at this site since the Middle Miocene.
- Low concentration of biogenic material and recurrence of barren intervals cannot be due to near-shore processes (sea-surface turbidity or freshwater input) – therefore accumulation of biogenic intervals must be controlled by sea-surface processes (nutrient limitations. Sea-ice cover; severe climatic conditions) or deep-sea processes (selective removal via dissolution)
- Alternating biogenic-bearing and non-biogenic intervals reflect climatically driven changes over the Neogene.
- Shorter-term changes in oceanographic and/or climatic conditions seem to be superimposed on this long-term variation as reflected by the variations in the abundance of biogenic components that occur within Units 1 and 3.
- Dramatic change in composition and texture of terrigenous sediment is evident between upper units 1 & 2 and lower units 3 & 4.
    - Upsection increase in quartz, feldspar and dropstones suggest onset of increased glaciation during Pliocene (associated changes in natural gamma-ray may be related to a shift on suite of clay minerals.
    - Related to changes associated with
        1. Erosional rates/style
        2. Relative importance of individual source areas
        3. Delivery mechanisms
    - Episodic intervals of course terrigenous material within units 1 & 2 may reflect rare episodes of gravity flows associated with eustatic sea level changes.

Well lithology

The biogenic component/presence is one criterion used to delineate lithostratigraphic units. Two sets of colours occur which are probably related at least partially to carbonate content. Olive brown and olive grey sediments are found only in the uppermost cores (Unit I), whereas dark greenish grey and very dark greenish grey sediments prevail throughout the remaining cores, with many minor gradational variations.

Unit 1: 0-15.6 mbsf. Holocene to Pleistocene.

- Primarily defined by the presence of relatively abundant calcareous microfossils, and high amplitude fluctuations in spectral reflectance. The sediment is predominantly alternating layers of clayey nannofossil mixed sediment with silty clay and clay with silt. Quartz, feldspar, and inorganic calcite are the most common terrigenous silt-sized particles. The pervasive colours of this unit are olive brown and olive grey, broken only by thin, darker volcanic ash layers. Numerous dropstones and volcanic ash layers are scattered throughout.
- Interpretation: barren intervals may be linked to high-amplitude climatic cycles within late Pleistocene

Unit 2: 15.6-63.1 mbsf. Middle Pleistocene to Pliocene.

- Characterized by the absence of biogenic sediment. The dominant lithologies include silty clay, clay with silt and ash, and clay. The sediments are predominantly composed of clay, quartz, feldspar, mica, and accessory minerals. Unit 2, as well as Unit 1, contains higher amounts of quartz, feldspar, and mica than are found in deeper intervals. Dark greenish grey, dark grey, and greenish grey-coloured sediments are pervasive, although minor grey to black volcanic ash layers occur intermittently. Terrigenous components such as quartz and feldspar are relatively invariant across the boundary of Units I and II, in contrast to the down-section disappearance of biogenic material.
- Interpretation: Boundary between unit 2 & 3 may reflect important switch in climatic and oceanic conditions – drop in biogenic content accompanied by onset of dropstones and distinctive change in siliciclastic content.
    - Diminshed accumulation of biogenic material reflects an overall environmental degradation

Unit 3: 63.1-196.1 mbsf. Middle Pliocene to middle Miocene.

- Defined by the re-occurrence of biogenic sediment, in this case, biogenic silica, throughout the unit, with minor calcareous materials occurring within the uppermost section. The primary lithologies of Unit III are dark greenish grey to very dark greenish grey silty clay, clay with silt, clay, and clay with diatoms. With the exception of one small interval containing more than 55% nannofossils, Unit III is characterized by the minor repeated occurrence of biogenic material, primarily siliceous, which increases down-core from less than 5% at the upper boundary, to 5%- 20% in the lower portion of the unit.
- Interpretation:

Unit 4: 196.1-214.9 mbsf. Middle Miocene.

- dark greenish grey to greenish grey silty clay, and clay with silt and clay. No biogenic sediment is found throughout the unit except for trace amounts of siliceous microfossils within the upper portion of the Unit. The coarse fraction of Unit 4is similar to Unit 3, but slightly lower amounts of quartz and higher amounts of sulfides.
- Interpretation:

Biostratigraphy

- Yielded a sedimentary sequence of middle Miocene to Holocene age (-16.0 to 0 Ma). Calcareous nannofossils, planktonic foraminifers, and benthic foraminifers are present down to about 40 mbsf.
- With the exception of two intervals with rare occurrences of calcareous nannofossils, only siliceous microfossils were found from about 40 mbsf to the bottom of the section – diatoms and siliceous flagellates provide the only biostratigraphic information for the deeper part of the hole.

Calcareous nannofossils

- Occur mainly in upper part of cored stratigraphic section
- As coccolithophores are photosynthetic and cannot live under a permanent ice cover, intervals with nannofossils can be interpreted as representing open-water conditions (with no perennial ice cover). Intervals without nannofossils in the presence of planktonic foraminifers may be interpreted as periods with perennial ice cover.
- Reworked Cretaceous nannofossils were ice-rafted from the North Sea area. Their variations may be used to monitor fluctuations in icebergs reaching Site 907 from the North Sea.

Planktonic Foraminifera

- Found only in upper part of the sequence. Assemblages indicate subpolar-polar palaeoenvironmental conditions.

Benthic Foraminifera

- Present through the upper part of the sequence.

Diatoms

- Diatom abundances at Site 907 vary from barren during the Pleistocene, to abundant during the middle to late Miocene.

Siliceous Flagellates

- Below a barren interval at the top of the section, siliceous flagellates (including silicoflagellates, ebridians, and actiniscidians) are continuously present downsection.
- The abundance of these microfossils varies from trace to abundant, the preservation from moderate to poor.

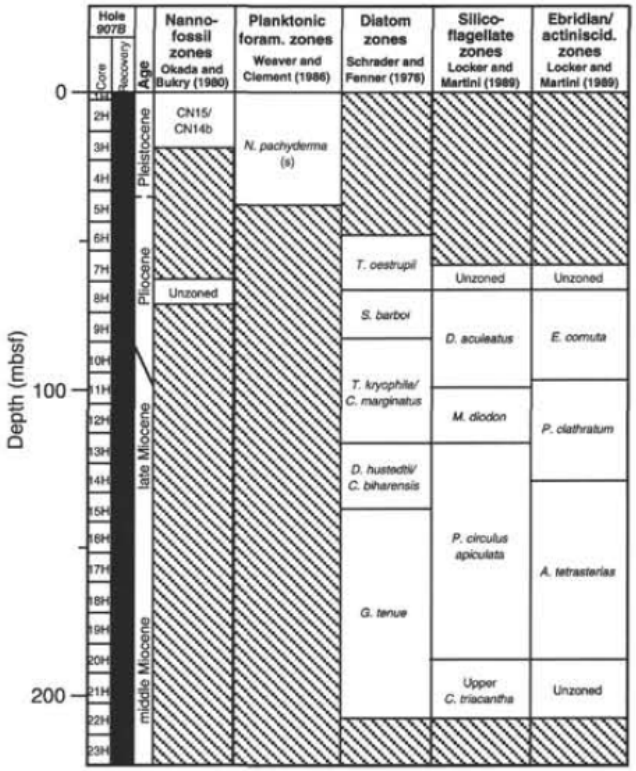

Figure 10. Biostratigraphic summary, Site 907. Hatched intervals indicate absence of fossils. Dashed line at Pliocene/Pleistocene boundary reflects uncertainty in exact placement based on planktonic foraminifer data. Diagonal line separating Miocene/Pliocene indicates inconsistent ages between diatom, silicoflagellate, and ebridian/actiniscidian zones.

Table 7. Depth range of biostratigraphic datums, Site 907.

Datums	Age (Ma)	Core, section, interval (cm)	Depth (mbsf)	Depth (mcd)
		162-907B-		
LO *E. cornuta* (E)	2.61	8H-2, 124 8H-CC, 21–23	62.44 69.47	67.26 74.29
FO *T. zabelinae* (D)	3.90	8H-CC, 21–23 10H-4, 39–41	69.47 83.59	74.29 89.16
FO *T. oestrupii* (D)	5.20	11H-CC, 21–23 13H-1, 39–41	97.91 107.59	104.09 114.71
LO *P. bispinum* (S)	5.23	10H-CC, 20–22 11H-2, 70	88.50 90.40	94.07 96.58
LO *M. diodon* (S)	5.93	11H-2, 70 11H-CC, 21–23	90.40 97.91	96.58 104.09
LO *P. apiculata* (S)	6.59	12H-CC, 21–23 13H-2, 44	107.53 109.14	113.98 116.26
FO *S. barboi* (D)	9.50	13H-2, 39–41 13H-3, 39–41	109.09 110.59	116.21 117.71
LO *D. hustedtii* (D)	10.00	12H-CC, 21–23 13H-CC, 22–24	107.53 117.06	113.98 124.18
LO *C. depressus* (S)	12.39	20H-3, 11 20H-CC, 23–26	176.81 186.97	191.47 201.63

Notes: FO = first occurrence; LO = last occurrence. In parentheses: D = diatom, S = silicoflagellate, and E = ebridian.

Palaeomagnetism

- On Leg 151 the predominantly normal polarity zones in the intervals 110-130 mbsf and 160-180 mbsf were correlated to Chron 5n.2 and Chron 5ABn/5ACn, respectively.
- More likely that the 110-130-mbsf interval correlates to Chron 4n.2 and that the 160-180-mbsf interval correlates to Chron 5ACn/5ADn.
- This modification of the Leg 151 interpretation, is based partly on the different inclination record obtained in the basal 20 m of this recovered section of Leg 162. However, this revised correlation implies changes in sedimentation rate, for which there is no apparent biostratigraphic or sedimentological evidence.
- Four intervals of high bulk density and low water content occur at 63, 100, 132, and 184 mbsf in Hole 907B, coincide with the intervals in which changes in sedimentation rate are implied by the revised magnetostratigraphic interpretation.
    - In this interpretation, the normal-polarity zone in the 100-130-mbsf interval is correlated to Chron 4n.
    - mixed-polarity zone in the 130-140-mbsf interval is correlated to Chron 4r.
    - The 140-160-mbsf interval becomes Chron 4A, and the 160-180-mbsf interval is then Chron 5n.1n/5n.2n.
    - This interpretation may be preferable, as it does not imply large hiatuses in the record, although changes in sedimentation rate are required

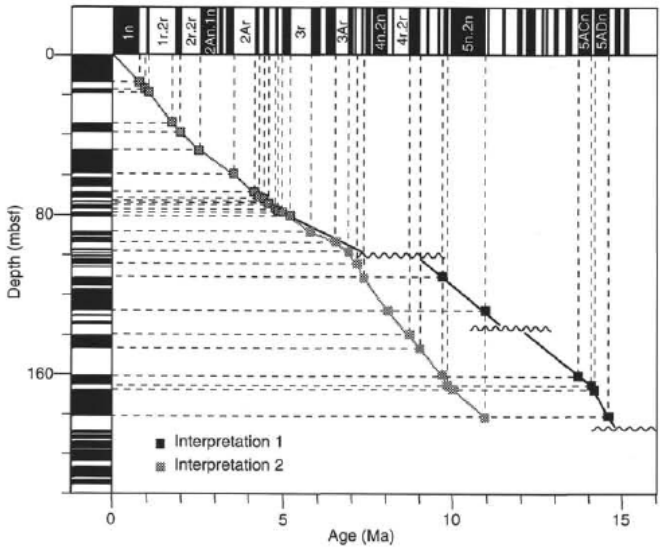

Figure 12. Correlation of Holes 907B and 907C to the geomagnetic polarity time scale (Cande and Kent, 1995). Interpretation 1 is slightly modified after the Hole 907A (Leg 151) interpretation. Interpretation 2 is radically different but does not imply large hiatuses. Wavy lines correspond to levels of high density from physical properties data (see text). The levels of high density correspond to some intervals in which the sedimentation rate is changing, which is implied by the magnetostratigraphic interpretations.

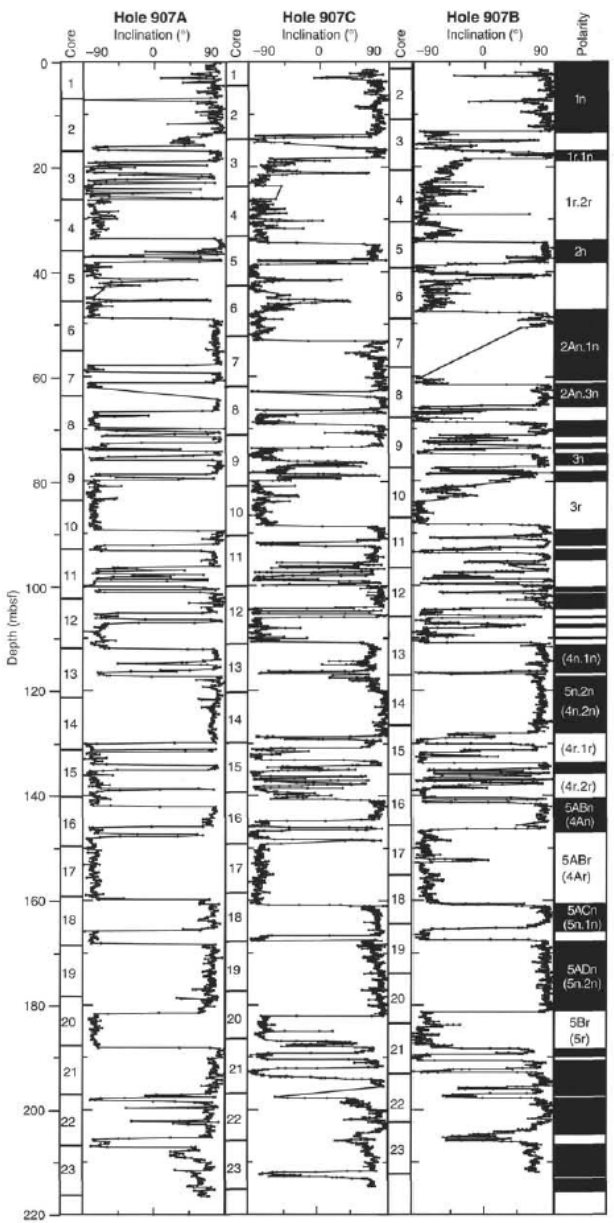

Figure 11. Inclination of the magnetization vector vs. depth (mbsf) after AF demagnetization at a peak field of 30 mT for Hole 907A (Leg 151), and after AF demagnetization at 25 mT for Holes 907B and 907C. For the Miocene, Interpretation 1 (Leg 151) polarity chron assignments are without parentheses; Interpretation 2 (Leg 162) assignments are in parentheses.

Sedimentation rates

- 216 m thick sedimentary section covering the Miocene to Holocene. Sedimentation rate reconstructions were based on magnetic polarity events from all holes.
- Owing to low abundances of calcareous fossils in the section, combined with uncertain calibrations of siliceous fossils, biostratigraphic events were not used for sedimentation rate estimates.
- Site 907 composite depth section was used to relate events recorded in Holes 907A, 907B, and 907C to a common depth scale.
- Sedimentation rates were calculated for both the meters below seafloor (mbsf) depth scale and the meters composite (mcd) scale.
- Below the Gilbert/C3An boundary (5.83 Ma, 94.63 med), two interpretations of the paleomagnetic record at Site 907 are possible. According to the interpretation of the record from Hole 907 A, drilled on Leg 151; hiatuses or intervals of condensed sedimentation may have occurred at approximately 60 mbsf (between the top of Gauss Chron and the top of the Cochiti Subchron), 100 mbsf (between the top of C3An and the top of C5n.2n), and 130 mbsf (between the top of C5r.lr and the top of C5ABr).
- However, Leg 162 sedimentation rate interpretations incorporate data from 907B and 907C and does not invoke any major hiatuses.

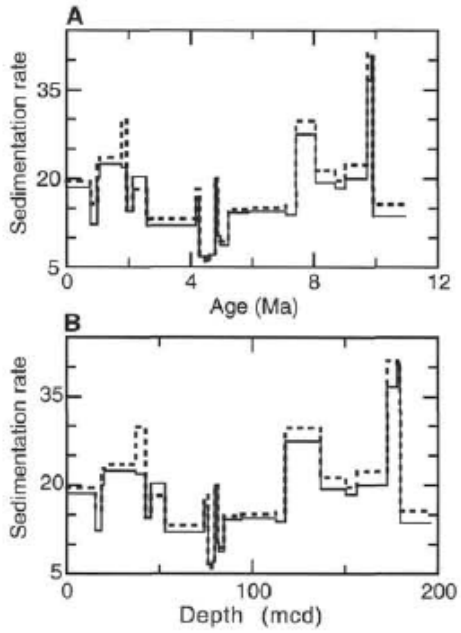

Figure 14. **A.** Average Site 907 sedimentation rates vs. age, based on magnetostratigraphic events listed in Table 10. **B.** Site 907 sedimentation rates vs. composite depth. Solid lines indicate rates in mbsf/m.y.; dashed lines indicate rates in mcd/m.y.

Table 10. Age control points, Site 907.

Event	Age (Ma)	907A (mbsf)	907A (mcd)	907B (mbsf)	907B (mcd)	907C (mbsf)	907C (mcd)	Avg. depth (mbsf)	Avg. depth (mcd)	Rate (mbsf/m.y.)	Rate (mcd/m.y.)
Core top	0.00	0.00	0.00	0.00	0.00	0.00	0.00	0.00	0.00		
Brunhes/Matuyama	0.78	16.15	16.18	13.30	14.87	14.00	14.86	14.48	15.30	18.57	19.62
Jaramillo top	0.99	17.05	18.55	17.10	18.67			17.08	18.61	12.34	15.75
Jaramillo bottom	1.07	19.15	20.65	18.50	20.07	18.40	20.59	18.68	20.44	20.10	22.83
Olduvai top	1.77	33.85	36.58	34.50	37.57	34.80	36.75	34.38	36.97	22.43	23.61
Olduvai bottom	1.95	38.15	43.08	38.50	41.57	37.95	41.13	38.33	41.93	21.90	27.56
Reunion II top	2.14	41.55	46.48	40.60	43.67			41.08	45.08	14.47	16.58
Matuyama/Gauss	2.58	49.05	51.59	47.85	51.92	53.25	55.75	50.05	53.09	20.39	18.20
Cochiti top	4.18	69.95	74.21	68.80	74.07			69.38	74.14	12.08	13.16
Cochiti bottom	4.29	71.15	75.41	71.20	76.88			71.18	76.15	16.36	18.23
Nunivak top	4.48	71.65	75.91	73.25	78.93			72.45	77.42	6.71	6.71
Nunivak bottom	4.62	72.75	77.01	73.85	79.53			73.30	78.27	6.07	6.07
Sidufjall top	4.80	74.25	78.63	74.90	80.58			74.58	79.61	7.08	7.42
Sidufjall bottom	4.89	75.35	79.73	77.40	83.08			76.38	81.41	20.00	20.00
Thvera top	4.98	76.05	80.43	78.55	84.23			77.30	82.33	10.28	10.28
Thvera bottom	5.23	78.75	83.13	80.20	86.22			79.48	84.68	8.72	9.38
Gilbert/C3An	5.89	89.55	94.48	88.35	94.37	88.65	94.42	88.85	94.42	14.21	14.77
C3Bn/C3Br	7.09			106.15	112.71	106.05	112.48	106.10	112.60	14.38	15.14
C3Br.3r/C4n.1n	7.43			110.90	118.13	110.70	117.53	110.80	117.83	13.82	15.40
C4n.2n/C4r.1r	8.07	105.25	111.13	128.15	136.86	128.65	136.85	128.40	136.86	27.50	29.73
C4r/C4An	8.70	111.85	117.73	140.50	149.97	140.60	150.63	140.55	150.30	19.29	21.34
C4An/C4Ar	9.02	114.55	122.27	146.35	156.59	146.55	156.58	146.45	156.59	18.44	19.64
C4Ar.3r/C5n.1n	9.74			160.85	172.77	160.85	172.63	160.85	172.70	20.00	22.38
C5n.1n/C5n.1r	9.88			165.30	178.49	166.65	178.43	165.98	178.46	36.61	41.14
C5n.1r/C5n.2n	9.92	117.05	124.77	167.50	180.69	167.70	179.48	167.60	180.09	40.63	40.63
C5n.2n/C5r.1r	10.95	129.75	137.06	181.30	196.07	182.10	196.30	181.70	196.19	13.69	15.63

Notes: Ages are from Berggren et al. (1995). Depths from Hole 907A below the Gilbert/C3An boundary are not included in the average depths or calculated sedimentation rates.

Physical properties

- Site 907 included non-destructive, near-continuous measurements of bulk density, bulk magnetic susceptibility, compressional wave (P-wave) velocity, and natural gamma radiation on whole-round sections of all cores from each hole using the multisensor track (MST).
- Unit G1: mudline to about 47 mbsf (in Hole 907A, Unit Gl = 0-45 mbsf), which is a zone of variable lithology (e.g., silty clay and clayey silt, with carbonate present in the upper few cores).
    - defined by generally high bulk density and low porosity values relative to the deeper units
- Unit G2: 47-71 mbsf; is considered a transitional geotechnical unit, defined by trends of decreasing bulk density and natural gamma radiation values and increasing water content (also exhibits high-amplitude fluctuations in these properties)
    - Low values of water content (or void ratio) and increased bulk density values at 60—64 mbsf may be associated with a hiatus in sedimentation or a condensed section.
    - Although this horizon (60-64 mbsf) could be interpreted as a geotechnical boundary, by locating the Unit G2 boundary at the base of the second large peak in water content (Fig. 20), our stratigraphy remains consistent between Holes 907 A and 907B.
- Unit G3: is defined from 71 to 193 mbsf, and is further divided in three subunits.
    - There are subtle changes in the trends of all measured properties within Unit G3, but the unit is characterized by generally low values of bulk density (mean = 1.36 g/cm3) and high porosity values (mean = 79.26%) and water content (mean = 60.08%).
    - Subunit G3A (74-102 mbsf) is defined by increasing trends in Pwave (PWL) velocity, porosity, and water content, and by decreasing trends in natural gamma radiation and bulk density towards the base of the unit.
    - Subunit G3B (102-150 mbsf) is defined by less variability and by gentler gradients in most properties than are observed in Subunit G3A. Subunit G3B (102-150 mbsf) is defined by less variability and by gentler gradients in most properties than are observed in Subunit G3A. The Subunit G3B boundary at 150 mbsf is marked by an abrupt increase in shear strength.
    - Subunit G3C (150-193 mbsf), there are lower values of magnetic susceptibility compared to the overlying subunits, and a change to nearly constant or gently increasing values of natural gamma radiation, bulk density, and velocity. There is also higher variability in shear strength values.
- Unit G4 (from 193 mbsf to the limit of recovered sediment in Hole 907B) is defined by increasing trends in bulk density, shear strength, natural gamma radiation, magnetic susceptibility, and velocity, and by decreasing trends in water content and porosity.

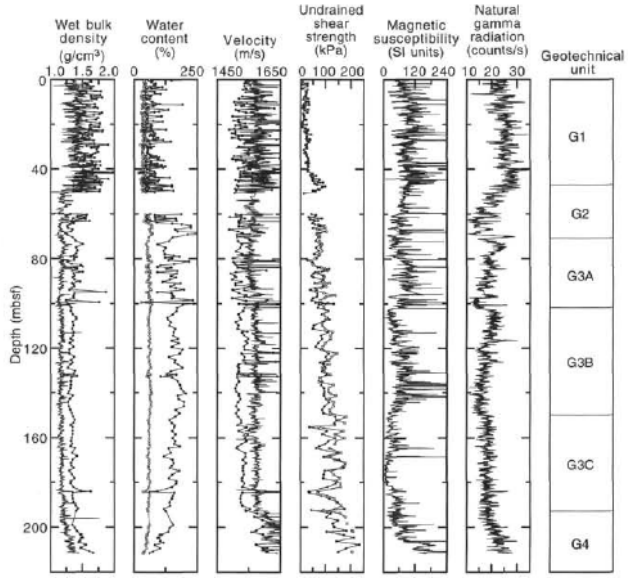

Figure 20. Plots of GRAPE wet bulk density (thin line) superimposed with gravimetric bulk density measurements (line with solid circles), water content (wt% wet sample = open squares; wt% dry sample = solid circles), PWL velocity (thin line) superimposed with split-core velocity (line with solid circles), undrained shear strength measured with the vane (solid circles) or the pocket penetrometer (open squares), magnetic susceptibility, and natural gamma radiation, vs. sub-bottom depth in Hole 907B. Also shown are the boundaries of geotechnical units.

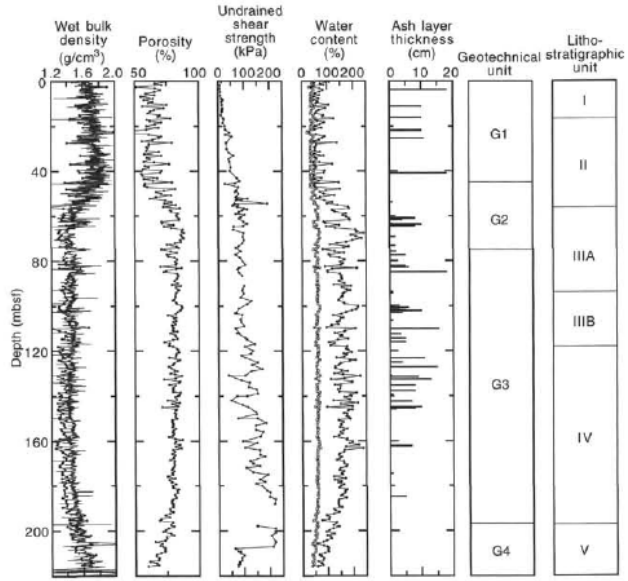

Figure 21. Plots of GRAPE wet bulk density (thin line) superimposed with gravimetric bulk density measurements (line with solid circles), porosity, average undrained shear strength, water content (wt% wet sample = squares; wt% dry sample = circles), and ash layer thickness, vs. sub-bottom depth in Hole 907A. Also shown are the boundaries of geotechnical and lithostratigraphic units (Myhre, Thiede, Firth, et al., 1995).

Table 19. Mean values of physical properties for geotechnical units from Hole 907B.

Geotechnical unit:	G1	G2	G3	G3A	G3B	G3C	G4
Depth range (mbsf):	0–46	46–74	74–193	74–102	102–146	146–193	193–TD
Number of measurements:	110	32	104	35	34	35	14
Water content (% wet wt):	41.60	53.36	60.08	59.11	61.87	59.31	50.90
Water content (% dry wt):	74.77	129.04	154.51	151.04	164.32	148.46	106.47
Wet bulk density (g/cm³):	1.63	1.46	1.36	1.38	1.33	1.36	1.48
Grain density (g/cm³):	2.75	2.73	2.64	2.71	2.59	2.62	2.75
Dry bulk density (g/cm³):	0.97	0.70	0.55	0.57	0.51	0.56	0.73
Porosity (%):	64.85	74.20	79.26	78.92	80.23	78.66	73.29
Void ratio:	2.01	3.44	3.98	4.01	4.15	3.80	2.85
Velocity (m/s):	1548 (106)	1535 (31)	1539 (109)	1546 (33)	1535 (40)	1536 (36)	1595 (13)
Vane shear strength (kPa):	27 (93)	64 (28)	91 (99)	68 (33)	92 (31)	113 (35)	155 (13)
Penetrometer (kPa):	NA	83 (10)	112 (92)	88 (28)	108 (31)	137 (33)	190 (6)
GRAPE density (g/cm³):	1.41 (2512)	1.23 (1534)	1.18 (6505)	1.18 (1418)	1.17 (2369)	1.18 (2717)	1.29 (842)
Difference (WBD – GRAPE)	0.22	0.23	0.18	0.20	0.16	0.18	0.19

Notes: TD = total depth. For parameters other than index properties, the number of measurements used to calculate mean values are enclosed by parentheses. NA = not applicable.

Discussion/ Conclusions

- The interbedded sediment layers between the mudline and about 47 mbsf, which comprise lithostratigraphic Unit I and the upper part of Unit II in Holes 907A and 907B, are nearly indistinguishable in terms of their bulk physical properties; therefore, this interval has been combined into a single geotechnical unit (G1).
- The fluctuations in physical properties within Unit Gl correspond to Pliocene to Quaternary lithologic variability associated with climatic (glacial-interglacial) cycles in the Northern Hemisphere.
- Major changes in sediment texture and composition are suggested by the change in physical properties between geotechnical Units G1 and G3.
- High-amplitude fluctuations in physical properties within Unit G2 are indicated by large increases and decreases in the relative amount of water in the sediment, which may reflect higher and lower abundances of clay minerals and/or increasing and decreasing amounts of biogenic silica in these sediments.
- The significant decrease in bulk density in Unit G2, from about 1.8 g/cm3 to about 1.5 g/cm3 over the interval from 45 to about 60 mbsf, may reflect an increased ice-rafted-debris flux occurring simultaneously with the increased amplitude of oxygen isotope fluctuations from 3.1 to 2.6 Ma.
- The high-amplitude fluctuations in density within this interval may be the expression of changes in the relative accumulation rates and/or composition of ice-rafted debris, clay minerals, and biogenic sediment during glacial or interglacial periods, possibly indicating cold/warm climatic oscillations superimposed on a gradual cooling trend.
- The magnetic susceptibility record is highly variable in Hole 907B, but exhibits distinct minima near the boundaries and in the upper portions of geotechnical Subunits G3 A and G3B, and within Subunit G3C - Similar magnetic susceptibility minima were observed in the record from Hole 907A, where they were attributed to either dilution by high biogenic (siliceous) sedimentation, and/or by a significant proportion of the magnetic material being destroyed by reductive diagenesis.
- Intervals having reduced sedimentation rates or representing hiatuses in sedimentation may be indicated at 60-64 mbsf, 98-100 mbsf (near the boundary between Subunits G3A and G3B), 130-134 mbsf, and at 184-186 mbsf according to the initial interpretation of the geomagnetic polarity reversal stratigraphy in Hole 907B. A relationship between this and the magnetic susceptibility trend is therefore possible.
- Intervals with relatively low natural gamma radiation are also located near the subunit boundaries of geotechnical Unit G3 – these decreases often associated with peaks in water content and changing trend in magnetic susceptibility data. These intervals may be characterized by changes in clay mineralogy, or by changes in the relative accumulation of biosiliceous material.
- Unit G4, is associated with an increase in silt-sized material and by indurated sedimentary layers above igneous rocks recovered in Hole 907A.

ODP Leg 162 - Well 985A & B

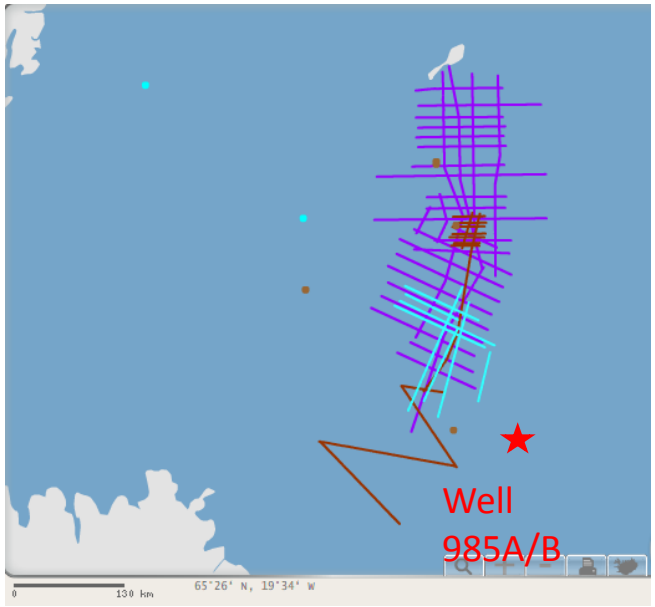

Well 985 A Summary

Date: **03/08/1995**
Latitude: **66.942**
Longitude: **-6.45**
Water Depth from sea level (m): **2787.6**
Bottom Felt at: **2797.8 meters (drill pipe)**
KB (Distance between rig floor and SL) (m): **11.2**
Well penetration (m): **587.9**
Total Depth (m): **3385.7**
Physiographic feature: **ocean floor**
No. of cores: **62**
Interval cored (m): **587.9**
Core recovered (m): **553.42**
Oldest sediment cored depth below sea floor (m): **587.9**
Oldest sediment age: **Early Miocene - Late Oligocene**
Oldest sediment description: **clay and silty clay**

Well 985 B Summary

Date: **07/08/1995**
Latitude: **66.942**
Longitude: **-6.45**
Water Depth from sea level (m): **2787.8**
Bottom Felt at: **2799.1 meters (drill pipe)**
KB (Distance between rig floor and SL) (m): **11.3**
Well penetration (m): **126.9**
Total Depth (m): **2926**
Physiographic feature: **ocean floor**
No. of cores: **14**
Interval cored (m): **126.9**
Core recovered (m): **129.44**
Oldest sediment cored depth below sea floor (m): **155.2**
Oldest sediment age: **Late Miocene**
Oldest sediment description: **clay with silt**

- Located on a gentle slope of the Iceland Plateau into the deeper Norway Basin (~1000m deeper than site 907). Targeted on a University of Bergen seismic line showing an approximately 800-m-thick sediment sequence with little internal seismic structure, the seismic character being quite similar to that of Site 907.
- Site 985 is a part of a paleoenvironmental transect from Norway to Greenland, designed to study the history of advection of temperate, saline Atlantic waters into the Norwegian-Greenland Sea ("the Nordic heat pump"), the position of the mixing front between these warm waters and the cold, partly ice-covered Arctic waters (the Arctic Front) and the position of the front delineating the less saline, ice-covered Polar Waters of the East Greenland Current.
- Aims of site 985:
    1. monitor the history of oceanic and climatic fronts moving east and west across the Norwegian-Greenland Sea
    2. derive an open-ocean record of ice-rafted debris (IRD) and carbonate accumulation
    3. document the history of formation of northern-source deep waters.
- Second objective was to recover a pelagic Paleogene sequence on oceanic crust with an assumed normal subsidence history. The site is located on Eocene Anomaly 22 crust (about 50 Ma). The approximately 800-m sediment cover should contain both Neogene and Paleogene sections from which information on the paleoceanographic evolution of this high-latitude area can be obtained.
    - Prior drilling has documented that carbonate-bearing Oligocene sediments exist in the region, but poor recovery and diagenetic overprinting have precluded stable isotope studies of these sections.
- Predicted that this site is favourable for such studies due to its location on Greenland side of the (now extinct) Aegir Ridge spreading axis, on oceanic crust with assumed normal subsidence history and lack of excessive heat flux associated with strong diagenesis.

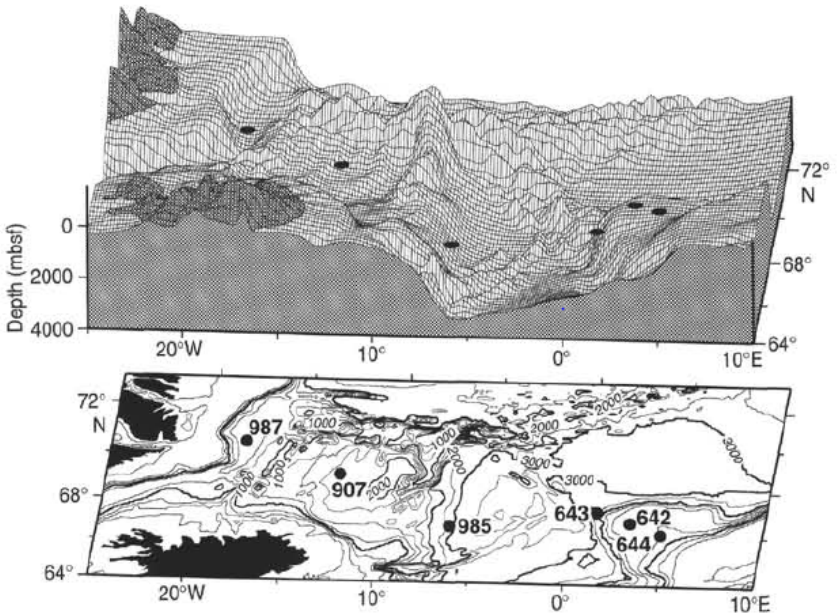

Figure 1. Bathymetry of the Nordic Seas paleoenvironmental transect, showing location of Leg 104, 151, and 162 drill sites. Bathymetric data (in meters) from ETOPO5.

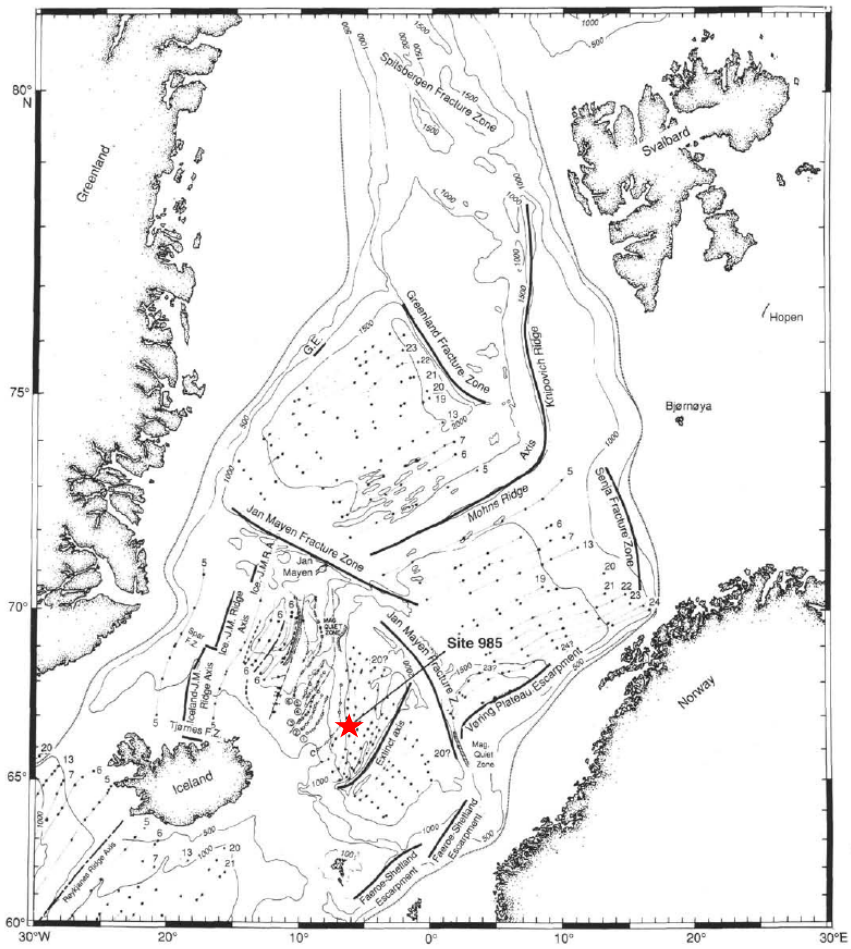

Figure 2. Position of Site 985 on magnetic anomaly map of Talwani and Eldholm (1977). G.E. = Greenland Escarpment (after Talwani and Eldholm, 1977).

Principal results

- The sediments recovered at Site 985 (ICEP-3) are predominantly fine-grained siliciclastics = silty clays, clays with silt and clays.
- Sufficient overlap between the 14 cores drilled in Hole 985B and the upper part of Hole 985A allowed a composite section to be developed for this site.
    - Magnetic susceptibility was the primary parameter used to develop the composite section. Gamma-ray attenuation porosity (GRAPE) density, natural gamma radiation, and percentage spectral reflectance in the 650-700-nm band were used to confirm the hole-to-hole correlations.

- Biocarbonates (>10%) are restricted to the upper parts of the sedimentary sequence and occur in clayey nannofossil ooze with foraminifers and silty clay with nannofossils. Clays and silty clays containing biosilica are encountered only between 240 and 290 mbsf.
- Disseminated volcanic ash, ash pods, and ash layers occur throughout the sedimentary sequence. Discrete ash layers (>1.0 cm thick) are most common in the upper 150 mbsf. individual ash shards generally appear colourless under smear slide examination, but can range in colour from light grey to black – darker ash layers are more common. Much of the ash, particularly in the deeper sediments, is altered and occurs with pyrite, zeolites, and other ash-derived clays.
- Dropstones (>1.0 cm) are confined to the upper sedimentary sequence (0-70 mbsf) and consist primarily of angular to subrounded igneous or metamorphic rock fragments.
- The sequence was dated by means of magnetic polarity records to the latest Miocene, below which it became difficult to correlate to the geomagnetic polarity time scale. The underlying sequence thus has poor age constraints.
- Siliceous microfossils and arenaceous benthic foraminifers provide some age information in the lower section, indicating that the drilled sequence ends in the upper Oligocene.
- Multisensor track (MST) investigations document that a complete section has been recovered over the upper 131 mbsf (Holocene to latest Miocene) with good overlap across core breaks.
- Within the last 7 Ma, sedimentation rates are highest in the last 3 Ma (13-36 m/m.y.) and drop to 10-20 m/m.y. in the middle and early Pliocene (higher sedimentation rates (about 25 m/m.y.) are documented for the latest Miocene).
- The thick early to middle Miocene clay-rich unit precluded significant recovery of Paleogene sediments, and there was a lack of carbonate-bearing Oligocene sediments at the site. Therefore aims of retrieving quantitative Paleogene paleoclimatic information from this site were not fulfilled.
- Five lithostratigraphic units were identified and changes in sediment physical properties appear to be correlated with the few prominent seismic reflectors of the site - some of which appear to reflect erosional surfaces or condensed sections.

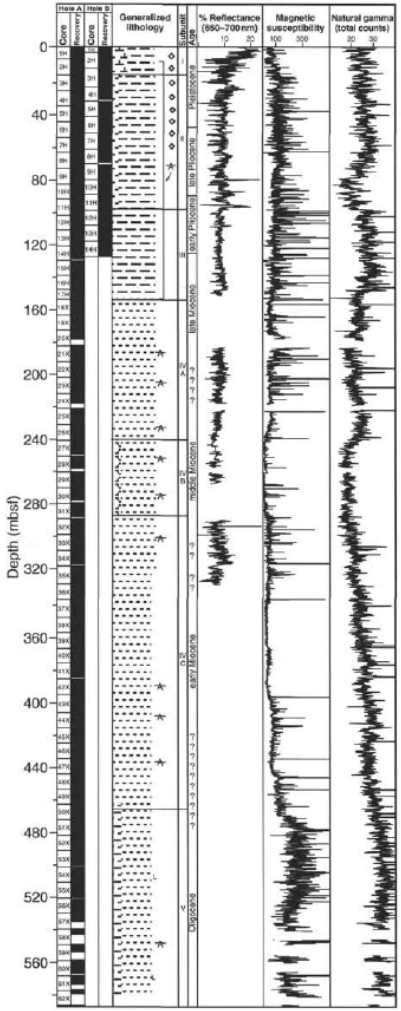

Figure 6. Core recovery, lithostratigraphy, age, spectral reflectance (red band), magnetic susceptibility, and natural gamma radiation of sediments recovered in Holes 985A and 985B. Cores containing ash layers (crossed A's, including bracketed area), dropstones (open diamonds), and limestone layers (letter "L") are shown in column adjacent to the lithostratigraphy. Spectral reflectance, magnetic susceptibility, and natural gamma radiation records are from Hole 985A. (Key to symbols used in the "Generalized Lithology" column can be found in fig. 4, "Explanatory Notes" chapter, this volume.)

Well lithology

Lithostratigraphic units and subunits at Site 985 are defined on the basis of data obtained from seven sources:

(1) visual core descriptions
(2) smear slide examination
(3) bulk calcium carbonate measurements
(4) spectral reflectance measurements,
(5) Magnetic susceptibility measurements
(6) natural gamma-ray measurements
(7) X-ray diffraction analysis of bulk sediments.

Unit 1: 0 - 17.2 mbsf. Holocene – late Pleistocene.

- Defined largely on the basis of relatively abundant biocarbonates (up to 30%) and higher colour spectral reflectance than underlying units (up to 20% for the 650-700 nm range).
- Interbedded layers of grey clayey nannofossil ooze with foraminifers; dark grey nannofossil clay with silt; dark grey silty clay with nannofossils; brown and dark greyish brown clay with silt; and very dark grey to dark greyish brown silty clays.
- Colour changes are gradational and cyclic throughout the unit.
- Bioturbation is slight to moderate in intensity.
- Pyrite is present in small quantities in concretions or pods,.
- Several thin (<l .0 cm) ash layers, ash pods, and a single ash layer 2.0 cm thick are present near the base of the unit.

Interpretation: cyclic, interbedded nature of the sediments testifies to their glacial/ interglacial origin.

Unit 2: 17.2 - 99.2 mbsf. Late Pleistocene to early Pliocene.

- Defined, in part, by the diminished presence of biocarbonate which occurs as a variable sedimentary component, averaging 6.9%.
- Composed of greyish brown to very dark greenish grey silty clay, clay with silt, and clay.
- Biocarbonate-bearing sediments consist of gray to dark greenish gray clayey nannofossil ooze, silty clay with nannofossils, and nannofossil clay.
- X-ray diffraction (XRD) and smear slide analysis both demonstrate an increase in quartz, plagioclase, and pyroxene within Unit 2 relative to the underlying sediments. Both reflectance values and natural gamma-ray counts decrease noticeably at the boundary with the underlying unit.
- Both Unit 1 and 2 contain dropstones, in contrast to the underlying units.
- 16 grey to black ash layers >1.0 cm thick with sharp basal contacts and gradational upper boundaries were identified in Hole 985A.

Unit 3: 99.2 - 155.2 mbsf. Early Pliocene to late Miocene.

- Characterized by the occurrence of clay with silt and by the absence of biogenic sediments & less variation in colour compared to preceding units.
- Isolated spikes of inorganic carbonate are superimposed on a carbonate-free background.
- XRD analysis of the bulk sediments reveals that plagioclase, quartz, and pyroxene are present to a lesser extent than in Units 1 and 2.
- Several types of concretions and discrete lithologic layers occur and seven ash layers, averaging 4.1 cm in thickness, were observed in Hole 985A, and 14 ash layers, averaging 2.8 cm in thickness, were observed in Hole 985B.

Unit 4: 155.2 - 465 mbsf. Late Miocene to late Oligocene

- Distinguished from those of Units III and V by the switch from a lithology above and below Unit IV in which silty clay and clay with silt dominates, to one in which clay with silt is present but indurated clay is dominant.
- ranges from grey to very dark greenish grey in the clay and from dark greenish grey to dark greyish brown in the clay with silt.
- 13 discrete ash layers, averaging 4.1 cm in thickness, were observed
- very low magnetic susceptibility values and the absence of biocarbonates, although isolated inorganic carbonate layers occur
- Subunit 4A: 155.2 - 241.5 mbsf.
    - distinguished from the underlying sediments by higher magnetic susceptibility and natural gamma-ray values and by the absence of biosilica.
    - Two carbonate-rich layers in Subunit 4A that may act as barriers to the diffusion of interstitial waters are noteworthy. XRD analysis of the upper layer indicates that it is composed of poorly crystallized carbonate. These layers yield high velocity measurements and bound sediments with interstitial waters that have anomalously low chloride, sodium, and salinity content, and a hydrocarbon gas content with unusually high proportions of C2+ gases relative to methane. Reduced diversity of arenaceous benthic foraminifers also characterizes this interval. The causes for these anomalies are not known.
- Subunit 4B: 241.5 - 289.6 mbsf
    - Interbedded layers of clay, clay with ash, and clay with biosilica.
- Subunit 4C: 289.6 - 465 mbsf.
    - Distinguished from Subunit 4B by the absence of biosilica and by a gradual increase in natural gamma-ray counts.

Unit 5: 465 - 578.9 mbsf. late Oligocene? to early Miocene?

- Comprised of indurated dark greenish grey to very dark greenish grey clay; olive grey to dark greenish grey silty clay; and very dark greenish grey clay with glauconite and glauconitic clay. These sediments are distinguished from the overlying sediments by a sharp increase in magnetic susceptibility.

Lithostratigraphic Interpretations

Tectonic events that may have influenced sedimentation at Site 985 include:
1. Seafloor spreading and ridge orientation in the Norwegian-Greenland Sea,
2. changes in the Greenland-Scotland Ridge sill depth (Wright and Miller, 1993)
3. initiation of the final closure of the Isthmus of Panama.

Potential climatic events influencing deposition may include:
1. the transition from relatively ice-free conditions in the Miocene, to weak Northern Hemisphere glaciation,
2. Strong Northern Hemisphere glaciation from the late Pliocene to Holocene.

Seafloor spreading in the Norwegian-Greenland Sea was underway by Anomaly 24 time (early Eocene), but may have begun as early as Anomaly 29 time.

- Unit 5 sediments were deposited when the basin was approx. half its modern dimensions and site 985 was shallower and closer to landmasses
- Site of active seafloor spreading was to the east of site 985 – lack of intervening high between Greenland and site 985 allowed for more effecting transport of silt-sized continental material
- Anomaly 7 (Oligocene/early Miocene) spreading shifted from Aegir ridge to Kolbeinsey ridge to the west of site 985 – shift occurred during transition of deposition from unit 5 to 4. Therefore contain fewer silt-sized terrigenous material as site 985 moved further from East Greenland source areas and subsided to greater depths
- Bulk sedimentation rates at Site 985 appear to have remained between 20 and 30 m/m.y. from the Miocene to Holocene – higher rates than at nearby site 907. higher clay content of these Miocene sediments reflect greater clay-fraction sedimentation rates during the Miocene compared to younger succession
- low biocarbonate content of the sediments of Units 5 and 4 implies low production and/or enhanced dissolution during the early Miocene and late Oligocene at Site 985. The presence of a variety of inorganic concretions in sediments of similar age recovered from Site 643 in the Norwegian Sea (opal-CT, calcite, rhodochrosite, manganese-siderite, and fluorapatite concretions). Fluorapatite concretions and pyrite in sediments - Both of these minerals can form during the degradation of organic matter in carbon-rich sediments, suggesting that there was the potential to dissolve biocarbonates from the sediments of Units 4 and 5.
- Biosilica content of Subunit 4B and relatively high sediment organic carbon content suggest enhanced productivity during this time interval.
- Increased silt content of unit 3 (late Miocene and early Pliocene) may mark transition into period of Northern Hemisphere glaciation = increased continental erosion (and thus delivery of silt-sized sediments) via IRD OR via enhanced bottom water production and bottom-current strength linked to either climatic cooling; deepening of the Greenland-Scotland Ridge sill depth or the initiation of the final closure of the Isthmus of Panama.
- Units 2 and 1 record cyclic late Pliocene to Holocene variations between biocarbonate-bearing interglacial sediments and siliciclastic-rich glacial sediments. cycles are presumably related to orbital variations in the Milankovitch frequency bands.
- Paleomagnetic data from Site 985 suggest that the first occurrence of dropstones at the site takes place shortly after the onset of significant Northern Hemisphere glaciation some 2.5 m.y. ago

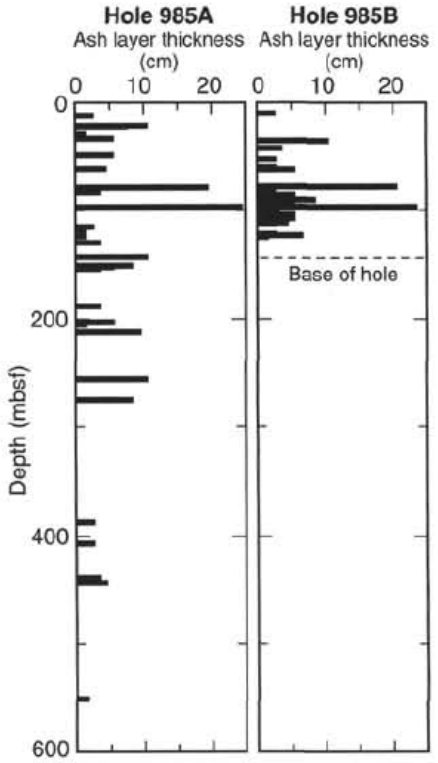

Figure 8. Thickness of ash layers greater than 1 cm plotted against depth at Site 985.

Biostratigraphy

- Sedimentary sequence of Oligocene to Holocene age.
- Calcareous microfossils (i.e., calcareous nannofossils and planktonic and benthic foraminifers) are present down to a depth of about 55 mbsf in Hole 985 A. Calcareous nannofossils are also present through a short interval of about 15 m, centered at 90 mbsf in Hole 985 A.
- Siliceous microfossils are rare at this site and only occur between about 240 and 280 mbsf.
- Agglutinated benthic foraminifers are recorded from about 300 mbsf to the bottom of the section.

Sedimentation rates

- Sedimentation rate reconstructions were based primarily on magnetic polarity events from Holes 985A and 985B.
- Because the sediments at Site 985 were largely barren of microfossils, biostratigraphic events were not used for sedimentation rate estimates in the upper 155 m. Therefore, biostratigraphic information from the rare non-barren intervals provided the only shipboard age control for the lowermost portion of the sequence.
- Sedimentation rates were calculated for both the meters below seafloor (mbsf) depth scale and the meters composite depth (mcd) depth scale.
- Several intervals of relatively high sedimentation rate occur from 1.77 to 1.95 Ma (38 mcd/m.y.), from 3.13 to 3.23 Ma (39 mcd/m.y.), and from 4.78 to 4.88 Ma (43 mcd/m.y.).
- Because the interpretation of the paleomagnetic sequence is not constrained by biostratigraphy, it cannot be ruled out that these "spikes" of less than 200-k.y. duration are artifacts. Likewise, below the C3Ar/C3Bn boundary at 6.79 Ma (154 mbsf or 162 mcd in Hole 985 A), constraints on average sedimentation rates are speculative.
- However, siliceous microfossils and agglutinated benthic foraminifers provide age control over the lower portion of the sequence. In particular, the uppermost *Spongebria miocenica* Zone (14.4 Ma) is at approximately 279 mbsf (287 mcd) in Hole 985A – gives a sedimentation rate of 16 m/m.y. from 6.79 to 14.40 Ma, slightly lower than the sedimentation rates from the late Miocene.
- Given an Oligocene age for the base of Hole 985A (580 mbsf), sedimentation rates over the lowermost portion (bottom 300 m) of Site 985 must be <30 m/m.y.

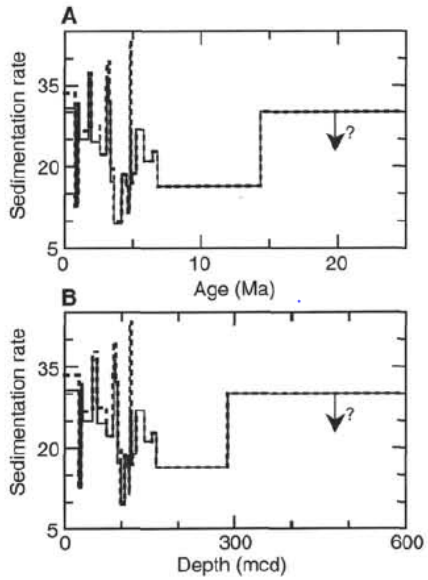

Figure 14. Site 985 sedimentation rates vs. age (**A**) and vs. composite depth (**B**). Solid lines indicate rates in mbsf/m.y.; dashed lines indicate rates in mcd/m.y.

- The physical properties in Hole 985A suggest two periods of reduced sedimentation rate, corresponding with geotechnical Subunit G2C (seismic Reflector Rl) and the contact between geotechnical Units G2 and G3 (seismic Reflector R2).

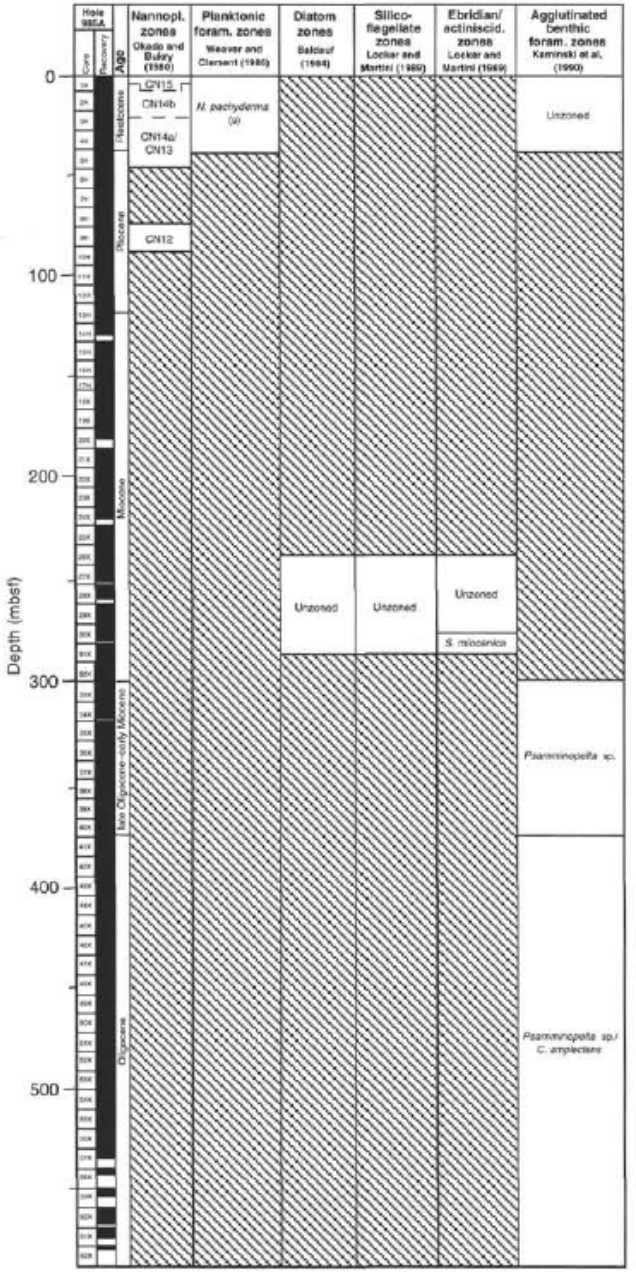

Figure 10. Biostratigraphic summary, Site 985. Hatched intervals indicate absence of fossils. Age boundaries for the Miocene/Pliocene and Pliocene/Pleistocene are based on paleomagnetic data. Other age information is based on agglutinated foraminifers and siliceous microfossil data.

Palaeomagnetism

- The polarity zone records for Holes 985A and 985B can be correlated, although the correlation is hampered by poor definition of reversed- polarity zones.
- The apparent top of the Gauss Chron (Chron 2An) does not correlate in the two holes. The Gilbert Chron (Chron 3n) is better defined in Hole 985B than in Hole 985A. These differences are probably due to differences in the degree of drilling disturbance, partly induced by dropstone occurrence and/or possibly by variable degrees of (magnetic) iron sulfide authigenesis.
- The correlation of the polarity record to the geomagnetic polarity time scale (GPTS) is based entirely on pattern fit of the polarity zones to the GPTS. At this site, the biostratigraphy does not provide useful constraints.
- The correlation of polarity zones to the GPTS implies variations in sedimentation rate, particularly in the upper Gilbert and Gauss Chrons.
- The magnetostratigraphic interpretation below the Gauss/Matuyama boundary remains tentative, although the correlation is strengthened by the correlation of natural gamma radiation between Sites 907 and 985, which indicates that the polarity chron assignments are consistent for the two sites.

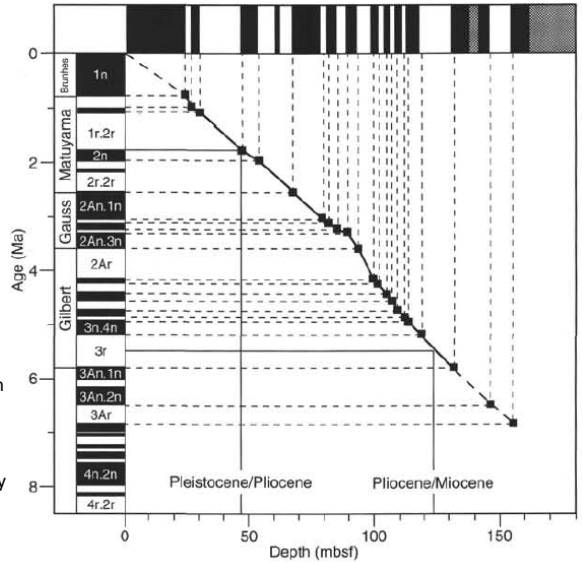

Tentative correlation of polarity zones in Holes 985A and 985B to the geomagnetic polarity time scale. Ages of polarity chrons from Cande and Kent (1995).

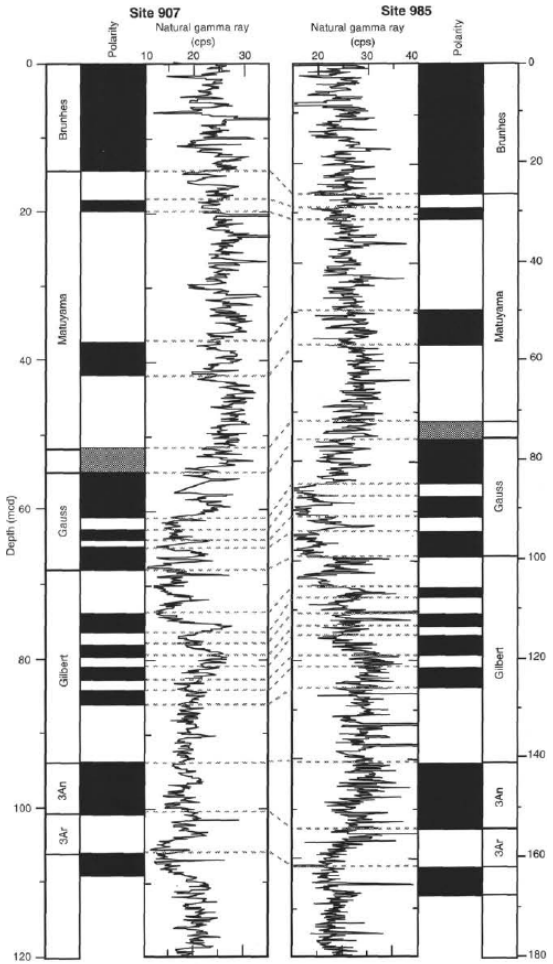

Figure 13. Correlation of natural gamma radiation records (from the shipboard multisensor track) for Sites 907 and 985. The natural gamma-ray correlation supports the Pliocene-Pleistocene polarity chron correlation at the two sites.

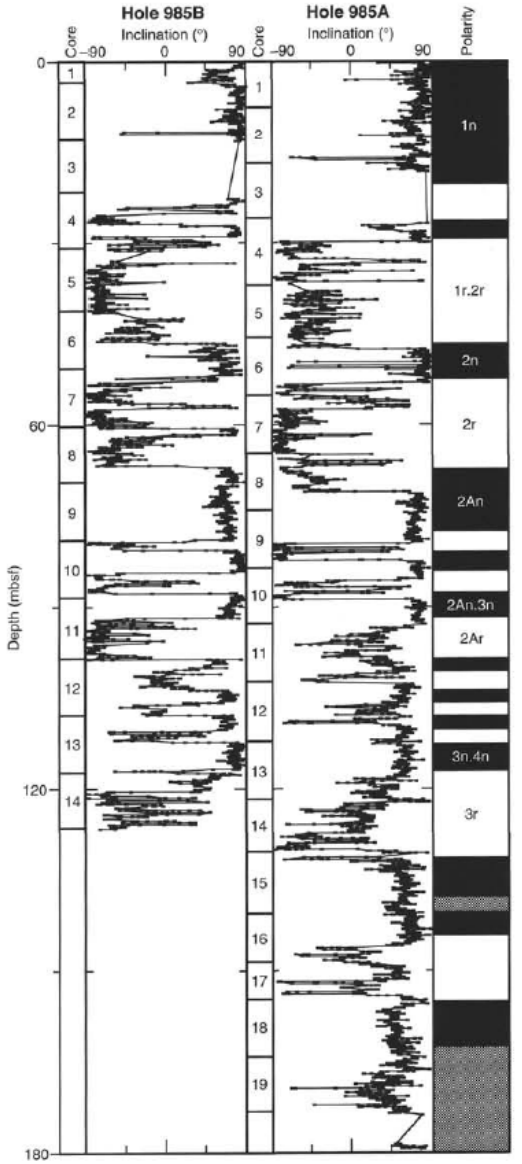

Figure 11. Inclination of the magnetization vector vs. depth (mbsf) for Holes 985A and 985B after AF demagnetization at peak fields of 25 mT. Polarity chron nomenclature after Cande and Kent (1992).

Physical Properties

Aims to:

- Contribute to an understanding of syn- and postdepositional processes on the Iceland Plateau.
- Establish the nature of lithologic/seismic boundaries within the sediments and clarify the geotechnical response of chert and ash layers.
- Examine differences in physical properties due to the presence of hydrocarbons in the sediments

(1) index properties (water content and grain density),
(2) bulk density (GRAPE),
(3) undrained shear strength,
(4) compressional wave velocity,
(5) bulk magnetic susceptibility,
(6) natural gamma radiation.

- Three geotechnical units (Gl to G3) and eight subunits have been defined on the basis of the character and trends of physical properties profiles.

Geotechnical Unit G1 (0-98 mbsf) is divided into two subunits (G1A and G1B).

- Subunit G1A (0-69 mbsf) corresponds to lithostratigraphic Unit 1 and upper part of lithostratigraphic Unit 2 – nannofossil-rich and silt-rich mud with several ash layers, dropstones and dark clay-rich layers.
    - Maximum variability of porosity, P-wave velocity, and natural gamma radiation
    - Average wet bulk density is 1.7 g/cm^3, with values ranging from 1.4 to 2.1 g/cm^3
    - Water content and porosity vary from 21% to 54% and 41% to 75%, respectively.
    - P-wave velocity profiles show large variations as well as a decreasing trend.
    - The highest values correspond to dark, clay-rich layers, carbonate-rich layers, or ash layers that are thicker than 5 cm.
    - Undrained shear strength profiles show a trend of gradual increase from approximately 4 kPa near the seafloor to 40 kPa at the lower boundary of geotechnical Subunit G1A.
    - The magnetic susceptibility record shows increasing values in the upper 20 mbsf and fairly constant values between 20 and 100 mbsf, whereas the natural gamma radiation record exhibits little change in character and gradient.
- Subunit G1B (69-98 mbsf) covers the lower part of lithostratigraphic Unit 2 - silty mud containing nannofossils, ice-rafted debris, and ash layers.
    - High and variable water content (25%-62%), porosity (49%-80%), and shear strength (38-144 kPa) values.
    - Low natural gamma radiation values.
    - The compressional wave velocity profiles show less variability than in Subunit G1 A and a relatively low (1532 m/s) mean value.

Geotechnical Unit G2 (98-290 mbsf) is divided into four subunits (G2A to G2D).

- Subunit G2A (98-155 mbsf) corresponds with lithostratigraphic Unit III which is composed of silty mud.
    - Shows a normal trend with depth to lower water content and porosity, and higher bulk density and P-wave velocity (from 1520 to 1545 m/s).
    - Associated with higher natural gamma radiation values relative to those of Subunit G1B.
    - Undrained shear strength increases with less scatter than in Subunit G1B.
- Subunit G2B (155-217 mbsf) comprises most of lithostratigraphic Subunit IVA, a clay-rich mudstone.
    - Water content and porosity are high and variable (35% to 64% and 61% to 82%, respectively), and bulk density decreases accordingly to 1.31 g/cm^3
    - Compressional wave velocity continues its downhole increase and varies between 1523 and 1673 m/s, and there is a broad velocity peak between 182 and 200 mbsf.
    - Values of undrained shear strength show a sharp increase at the upper boundary of Subunit G2B, indicating a more consolidated or indurated sediment in this subunit.
- Subunit G2C (217-241.5 mbsf) includes the lowermost part of lithostratigraphic Subunit 4A.
    - Shows a change back to low water content and porosity, and higher bulk density, similar to Subunit G2A.
    - The lower boundary is associated with dark sediments and a prominent ash layer having high compressional velocities (up to 1909 m/s), and a clear downward drop in the susceptibility and natural gamma radiation values.
- Subunit G2D (241.5-290 mbsf) corresponds to lithostratigraphic Subunit 4B, which is a clay-rich mudstone containing 10%—15% biosilica.
    - Porosity, grain density, and natural gamm radiation values are similar to those of Subunits G1B and G2B.
    - Grain density shows maximum fluctuation (2.5-3.3) and magnetic susceptibility is at a minimum (mean value of 22 SI units) throughout.

Geotechnical Unit G3 (290-480 mbsf) is divided into two subunits (G3A and G3B)

- Subunit G3A roughly corresponds to lithostratigraphic Subunit 4C, a clay-rich mudstone.
    - Porosity, grain density, and natural gamma radiation values are similar to those of Subunits G1B and G2B.
    - Upper boundary of Unit G3 is distinct and is associated with a high-velocity layer and an abrupt decrease in water content, porosity, and grain density. This boundary also corresponds to the first occurrence of long-chained (>CH4) hydrocarbons in the sediment.
    - Free or adsorbed hydrocarbons were present down to 392 mbsf and may have been the reason why sediment volumes were difficult to measure.
    - Shows a distinctly different trend from the cyclic changes in physical properties observed in the overlying units.
    - Most of the properties display a gentle downcore change, except for the magnetic susceptibility which shows a stepwise increase with highest values in lowermost part of the subunit.
- Subunit G3B (480 mbsf to total depth) includes most of lithostratigraphic Unit 5, a slightly silty, clayey mudstone.
    - Most of the physical properties stay relatively constant throughout the subunit, with averages of 26% water content, 48% porosity, and 1.88 g/cm3 bulk density.
    - Compressional wave velocity shows a decrease just below the upper boundary, followed by an increase, and then fairly constant values below approximately 540 mbsf.
    - Also characterized by high magnetic susceptibility and natural gamma radiation values.

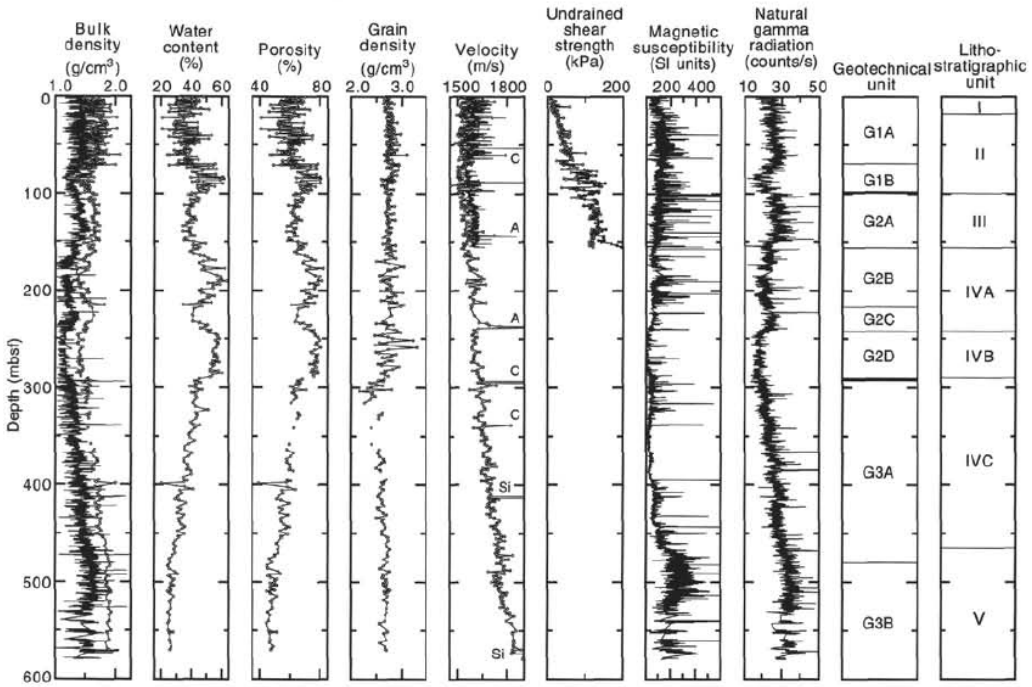

Figure 20. Physical properties data from Hole 985A: bulk density (GRAPE = continuous line; gravimetric = line with open circles), water content, porosity, grain density, compressional wave velocity (PWL = continuous line; split-core measurements = line with open circles; C = carbonate layer; A = ash layer; Si = chert layer), shear strength measured with the vane (open circles) or pocket penetrometer (solid circles), magnetic susceptibility, natural gamma radiation, and geotechnical and lithostratigraphic units.

Discussion

- Variablity is physical properties of Unit G1 likely caused by rapid changes in lithology between carbonate-rich (nannofossil) sediments, ash-layers and dark clay-rich layers – which show up as distinct peaks in velocity profiles
- Distinct boundary between subunits G1A & G!B reflects the change form sediments containing coarser (silt-gravel) associated with glaciations (subunit 1A) to more clay-rich sediments in subunit G1B.
- Contact between units G1 & G2 is well defined in lithology and physical properties – combination of high bulk density and low water content, and porosity in Subunit G2A would suggest that the sediments contain more coarse material (silt) than the overlying unit.
- The boundary between Subunits G2A and G2B is abrupt, and the undrained shear strength measurements (pocket penetrometer) mark the transition into more lithified sediments, characterized as claystones.
- Subunit G2C is probably associated with seismic Reflector Rl, characterised by high-velocity values. Lower boundary is definied by a prominent ash layer and well defined change in physical property profiles.
- Transition related to change in lithology into more silica-rich sediments in subunit G2D – reflected by generally high grain density values
- Contact between units G2 & G3 well defined on physical property profiles & represents a down-hole change in water content, porosity, grain density and natural gamma.
- The upper part of Subunit G3A is associated with free and/or adsorbed long-chained nonbiogenic hydrocarbons (highest concentrations were found in the upper part of the subunit) and low-salinity pore water.
- physical properties in the upper 98 mbsf at Site 985 show values associated with the late Cenozoic climatic cooling (69-98 mbsf) and glacial-interglacial variations (seafloor to 69 mbsf).
- Between 98 and 290 mbsf, the physical properties reflect large-scale changes in accumulation of clastic material (silt) and organic production during the late Miocene to early Pliocene.
- Below 290 mbsf, an abrupt change in all properties marks the transition into a suite of more homogeneous sediments, and the physical properties show a gradual downhole effect of increased overburden.

Seismic Stratigraphy

- Three seismic units, IC-I to ICIII, have been defined, based on changes in seismic character across Reflectors Rl and R2.
- The interval from the seafloor at 3.87 to 4.15 s TWT is defined as seismic Unit IC-I. Using P-wave velocity of 1.58 km/s, the unit is 220 m, thick and characterized by weak, discontinuous reflectors conformable with the seafloor.
    - Reflects the variation in relative proportions of clay, silt, nannofossils, and ash within the unit.
- Reflector R1 = only high-amplitude undulating reflector between basement and the seafloor. Marks a change to the more disturbed character of seismic Unit IC-II. Corresponds to Unit G2C (23 m thick) with lower porosity & P-wave velocity/bulk density than sediments above and below. Potential for erosion at this level.

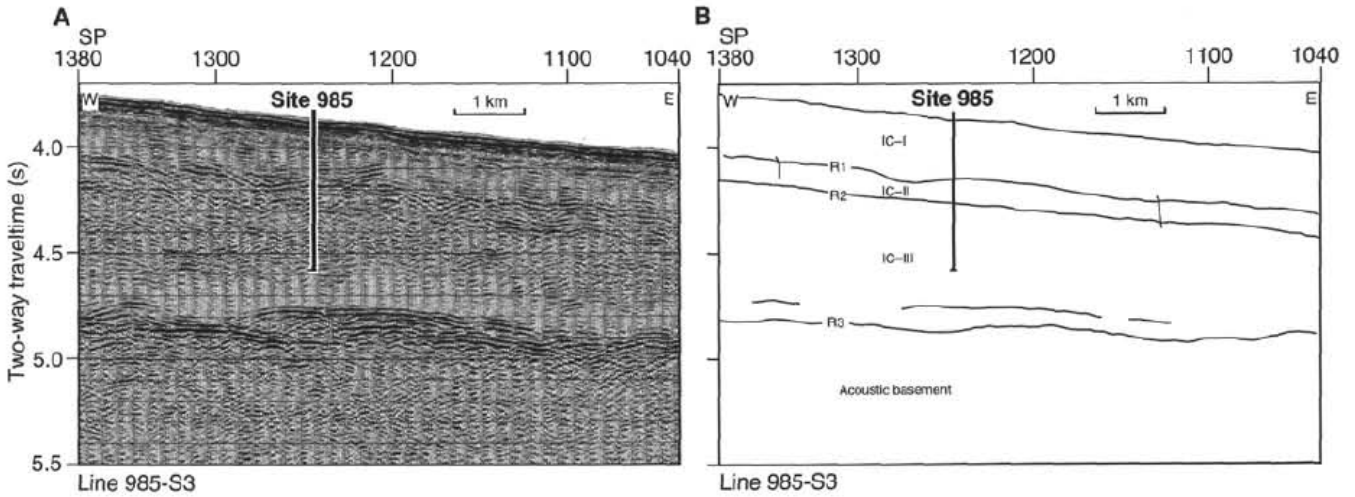

Figure 22. **A.** Seismic Line 985-S3. **B.** Interpretation of Line 985-S3, with seismic units and reflectors shown. Two possible faults are indicated. See Figure 21 for location of the profile. The profile shown is the entire line.

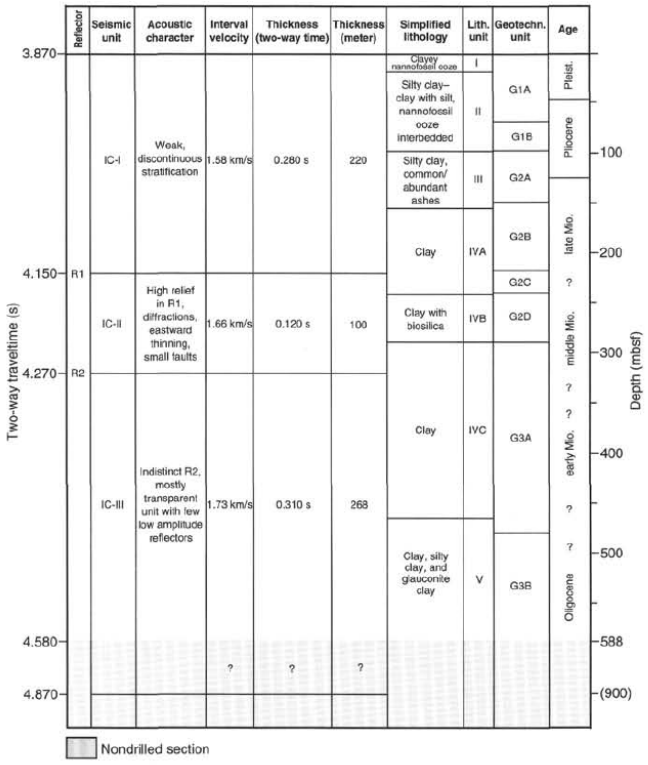

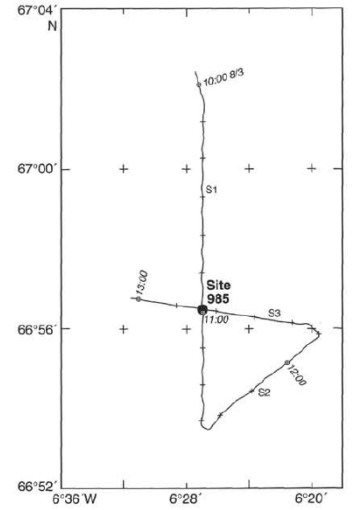

Figure 21. Map showing the site survey track lines near Site 985.

Figure 23. Relationships between seismic stratigraphy, lithostratigraphy, and geotechnical stratigraphy. The depth scale in mbsf is linear within the depths drilled, but note that the figure is not to scale below the drilled depth.

- Unit IC-II = defined from 4.15 to 4.27 s TWT, (100 m thick using an interval velocity of 1.66 km/ s).
    - Disturbed character of the unit due to frequent diffraction hyperbolae resulting from the relief of Reflector R1 (& possibly small faults).
    - Encompass lithostratigraphic Subunit IVB, characterized by an increased content of biosilica, which causes the increased porosity and decreased density and seismic velocity seen in geotechnical Subunit G2D.
- Reflector R2 is based on discontinuous reflector segments forming a coherent zone that parallels Reflector R1 and forms the base of the disturbed character of Unit IC-II.
    - Important change in sediments between 293 and 343 mbsf (upper part of lithostratigraphic Subunit IVC and geotechnical Subunit G3A) that may contribute to the character of Reflector R2..
    - Thin (40-cm) high-velocity (3.8 km/s) carbonate layer is observed at 293 mbsf, below which there is a distinct drop in chloride as well as salinity between approximately 300 and 420 mbsf.
- Unit IC-III = acoustically transparent, with the exception of few, low-amplitude, discontinuous reflectors.
    - Gas-bearing sediments are a possible cause for the homogeneous and nonreflective character of Unit IC-III. However, as no high gas concentrations were noticed below the methane peak at 340 mbsf, the character of Unit IC-III is due to the character of the sediments. The lithologic changes, causing relatively distinct changes in, for example, magnetic susceptibility between lithostratigraphic Subunit 4C and Unit 5, do not produce a seismic response.
- The base of this unit is Reflector R3, which is acoustic basement in the area.
- Bottom of Hole 985A at 588 mbsf corresponds to a two-way traveltime of 4.58 s, using an interval velocity of 1.73 km/s for the drilled part of seismic Unit IC-II.

ODP Leg 162 - Well 987 E

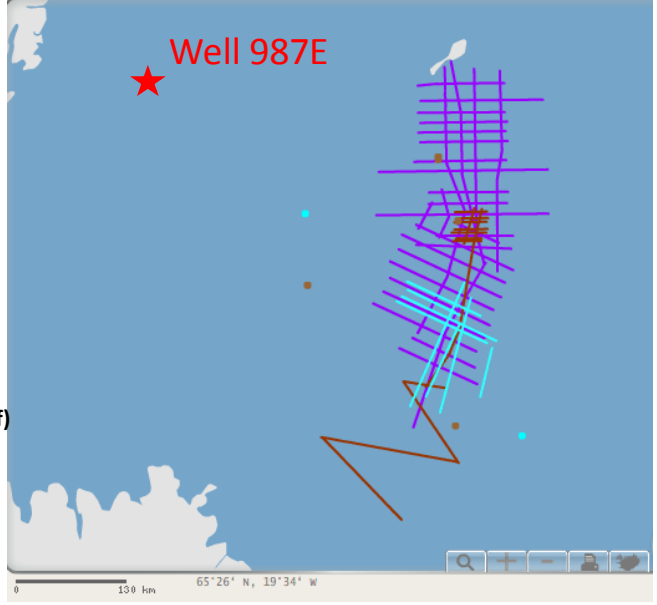

Well 987 E Summary

Date: **26/08/1995**
Latitude: **70.496**
Longitude: **-17.56**
Water Depth from sea level (m): **1672.7**
Bottom Felt at: **1684.2 meters (drill pipe)**
KB (Distance between rig floor and SL) (m): **11.5**
Well penetration (m): **859.4**
Total Depth (m): **2543.6 (drill pipe measurement from rig floor, mbrf)**
Physiographic feature: **ocean floor**
No. of cores: **52**
Interval cored (m): **496.1**
Core recovered (m): **308.82**
Oldest sediment cored depth below sea floor (m): **859.4**
Oldest sediment age: **Early Pliocene – late Miocene**
Oldest sediment description: **silty clay, very indurated, dropstones & dipping/contorted beds**

- Site 987 (EGM-4) was drilled on the Greenland Margin (Fig. 1) to examine the onset and history of glaciation in the North Atlantic region and to establish the history of the Greenland Ice Sheet, its inception, and possible phases of ice extension off the coast.
- Also part of a paleoenvironmental transect from Norway to Greenland, designed to study the history of the advection of temperate, saline Atlantic waters into the Norwegian-Greenland Sea ("the Nordic heat pump").
- By extending the late Pleistocene record available from piston cores back in time, we will be able to obtain a clearer understanding of the relationships between the Nordic heat pump, ocean circulation patterns, and the glaciation history on Milankovitch and longer time scales. This will provide insight into the climatic sensitivity of the Nordic Seas and its possible role as an early responder to orbital climate forcing.
- Site 987 is located on supposed Anomaly 5 crust, about 10 Ma old and hence should enable documentation of the late Miocene to Holocene history of the area.
- The planned drilling to 800 mbsf was intended to penetrate and date the main seismic sequences, defining the phases of fan buildup and shelf progradation, and to date potential ice-rafting events within these units.
- Data from Site 907 on the Iceland Plateau indicate that the western parts of the Nordic Seas experienced a marked intensification of IRD deposition at about 3 Ma, about 200-300 k.y. before the eastern Nordic Seas and the North Atlantic, pointing to Greenland as a possible early responder to the major expansion of ice sheets in the 3-2.5-Ma period.

Principal results

- Five holes were drilled at Site 987 (EGM-4), with a maximum penetration of 859.4 mbsf, estimated to be within a few meters of oceanic basement at this site.
- Despite gas expansion problems in the upper few hundred meters of the section, offsets between holes could be determined for the upper -180 mbsf, and a continuous spliced section was produced for the upper 100 mbsf (approximately the last 1 Ma).
- Paleomagnetic data provided time control, enabling detailed documentation of the glacial history of the Greenland Ice Sheet back to the late Miocene. Biostratigraphic age information is scarce due to predominance of fossil-barren intervals.
- Sediments are mostly fine- to coarse-grained siliciclastics. Evidence for glacial depositional environments prevails throughout the recovered section. Five lithostratigraphic units were defined (2 – 5 in well 987E).
- The seismic stratigraphy, lithostratigraphy, sediment physical properties, and wireline logging results at Site 987 reflect general variations in the frequency and amount of gravity-driven sediment transport from the East Greenland Shelf – related to site's location on NE flank of Scoresby Sund glacial fan.
- Intervals of more frequent debris flows form the most distinct seismic reflectors.
- The main phase of fan construction took place in the late Pliocene to Pleistocene. Although glacial marine deposition and downslope transport is characteristic of most of the drilled sequence, two phases, one in the early Pliocene, and another in the late Pliocene, are particularly pronounced. At these times, thick debris-flow sequences were deposited from an active ice margin presumably positioned at the shelf break.

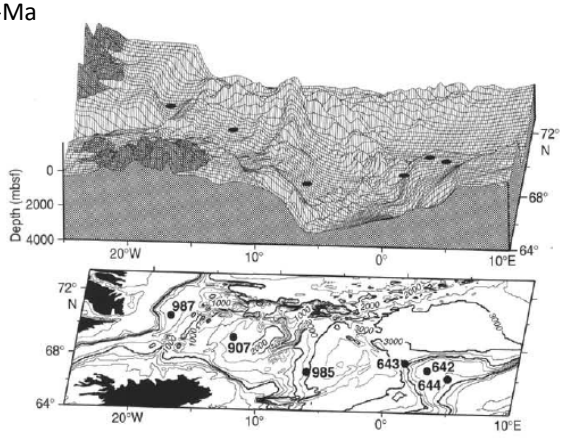

Figure 1. Bathymetry of the East Greenland–Norway transect margin showing the location of Leg 104, 151, and 162 drill sites.

Lithostratigraphy

- The sediments recovered are mostly fine- to coarse grained siliciclastics. The dominant lithologies include silty clay, clayey silt, clay with silt, and silty clay with sand and gravel. More than 500 isolated clasts > 1.0 cm in size are present throughout the section, most of which are interpreted as dropstones.
- 5 lithostratigraphic units and two subunits at Site 987 are defined on the basis of data obtained from seven sources: (1) visual core descriptions; (2) smear slide examination; (3) bulk calcium carbonate measurements; (4) spectral reflectance measurements; (5) magnetic susceptibility measurements; (6) natural gamma-ray measurements; and (7) X-ray diffraction (XRD) of bulk sediments.

Unit 1 - 0 – 305.6 mbsf. Pleistocene – late Pliocene. Silty clay and sand.

- Silty clays interbedded with silt and silt with sand and clay. Thick sandy turbidites are common towards the top of the unit (20-60 cm thick) and are less common and thinner (5-25 cm) in the lower part of the unit.
- Predominantly dark grey to dark greenish grey coloured
- Characterized by low magnetic susceptibility.
- Dropstones (up to 7.3 cm) are also common within this unit
- Sediments containing up to 35% carbonate occur in the inorganic calcite-rich bands, but the average carbonate content for the unit is only 4.9%.
- Quartz, feldspar, and inorganic calcite (up to 56%) are the most common terrigenous silt- to sand-sized components. XRD analysis indicates that amphibole and pyroxene are also common components.
- Interpretation: Turbidites (mm – cm scale) common downslope sediment transport mechanism

Unit 2 – 305.6 – 369.2 mbsf. Late Pliocene. Silty clay with sand and gravel.

- Predominantly silty clay with sand, silty clay with sand and gravel, sand-silt-clay, and clayey silt with sand and gravel.
- The top of Unit 2 is marked by a sharp increase in magnetic susceptibility and sand-sized fraction, as well as a decrease in the clay-sized content.
- Predominantly very dark greenish grey to dark grey coloured sediments
- Quartz and feldspars are the main components of the sand- and silt-sized fraction.
- Carbonate content is very low (0.9%), but some inorganic calcite layers occur at the base of the unit.
- The unit contains numerous isolated crystalline clasts >1.0 cm and randomly oriented gravel.
- Interpretation: increased magnetic susceptibility, bulk density, and compressional velocity, and decreased natural gamma radiation and porosity = debris flows..5

Unit 3 – 369.2 – 575.5 mbsf. late to early Pliocene. silty clay, clayey silt with sand, tilted/contorted beds, dropstones.

- Silty clay with sand, silty clay with sand and gravel, silty clay with gravel, and silty clay.
- Defined by a down core decrease in magnetic susceptibility and sand-sized particles and slight downhole increase in natural gamma radiation.
- Contains a few >l.O-cm clasts, mainly sedimentary and igneous rock fragments, interpreted to be dropstones.
- Distorted and dipping beds and laminations (and rare flaser bedding) occur in various intervals
- Subunit 3A (369.2-65.4 mbsf)
    - very dark grey, dark grey, and very dark greenish grey silty clay.
    - Dark reddish, grey, and dark grey inorganic calcite-clay layers are indurated towards the base of the unit.
    - Tilted beds occur in the middle of the subunit, 417.2 to 446.1 mbsf.
- Subunit 3B (465.4-75.5 mbsf)
    - defined by the downcore increase in the sand-sized fraction of quartz and feldspar.
    - Feldspar and mica are slightly more abundant in this subunit compared with Subunit 3A. Sulfides occur primarily as disseminated pyrite and pyrite concretions.
    - very dark grey, dark grey, very dark greenish grey, and dark greenish grey silty clay interbedded with very dark grey and very dark greenish grey clayey silt with sand, sandy silt with clay, and clayey silt.
    - Crystalline dropstones are scattered throughout
    - Sedimentary layering is common.

Interpretation: similar to Unit 1 (turbidites). Sediments seem to have a high hemipelagic component and seem to be less influenced by turbiditic downslope sediment transport than Units 1, 2, and 4.

Table 5. Description of the lithostratigraphic units at Site 987.

Unit	Subunit	Depth (mbsf)	Thickness (m)	Age	Lithology and characteristic features
I		0–305.6	305.6	Pleist.–late Plio.	Silty clay. Several turbidites and sandy to silty layers. Silty clay with inorganic calcite occurs as a minor lithology.
II		305.6–369.2	63.6	late Pliocene	Silty clay with sand and gravels. This unit is characterized by high magnetic susceptibility, numerous gravels and clasts, and low natural gamma radiation. Debris-flow deposits.
III		369.2–575.5	206.3	early–late Plio.	
	IIIA	369.2–465.4	96.2		Silty clay. Few tilted beds and scattered dropstones occur throughout the unit. Silty clay with inorganic calcite is interbedded as a minor lithology.
	IIIB	465.4–575.5	110.1		Silty clay interbedded with clayey silt with sand, sandy silt with clay, and clayey silt. Contorted beds and scattered dropstones occur throughout the unit.
IV		575.5–657.6	82.1	early Pliocene	Silty clay with sand and gravels. This unit is characterized by high magnetic susceptibility, numerous gravels and clasts, and low natural gamma radiation. Debris-flow deposits.
V		657.6–859.4	201.8		Silty clay. Sediment is very indurated. Scattered dropstones, dipping beds, contorted beds, folding and slumps occur throughout the unit.

Unit 4 – 575.5 – 657.6 mbsf. early Pliocene. silty clay with sand and gravel.

- Similar to unit 2 – composed of very dark grey to greenish grey silty clay with sand, silty clay with gravel and clay.
- Defined by a down-core increase in magnetic susceptibility and sand-sized content and by a decrease in natural gamma radiation and in clay-sized content.
- Bluish grey, greenish grey, and grey carbonate-cemented sandstone and carbonate-cemented silty sandstone intervals small pyrite crystals, rounded quartz, and small rock fragments
- Various igneous, metamorphic, and sedimentary clasts >1.0 cm are present and mica, feldspar, pyroxene, and amphibole are more abundant than in the previous units
- Gravel clasts tend to be aligned parallel to the bedding.
- Interpretation: increased magnetic susceptibility, bulk density, and compressional velocity, and decreased natural gamma radiation and porosity = debris flows.

Unit 5 – 657.6 – 859.4 mbsf. late Pliocene to Miocene. silty clay, very indurated, dropstones, dipping/contorted beds.

- Very dark grey and greenish grey silty clay interbedded with clayey silt, clay with silt and sand, and clayey silt with sand.
- Few graded sandy turbidites are present and sediments are highly indurated. Fine-scale structures, including flaser bedding, dipping beds, wavy laminae, convoluted structures, and folding interpreted to be slumps or water escape structures occur throughout the unit.
- Nonbiogenic carbonate-cemented layers and thin dark clayey laminations are also common.
- Silt filled burrows and benthic foraminifers are more common toward the base of the unit.
- Characterized by low magnetic susceptibility and by a reduced number of sand and gravel clasts and increase in clay-fraction content.
- Interpretation: similar to Unit 1 (turbidites), except that the lowermost part of the unit is more indurated. Sediments seem to have a high hemipelagic component and seem to be less influenced by turbiditic downslope sediment transport than Units 1, 2, and 4.

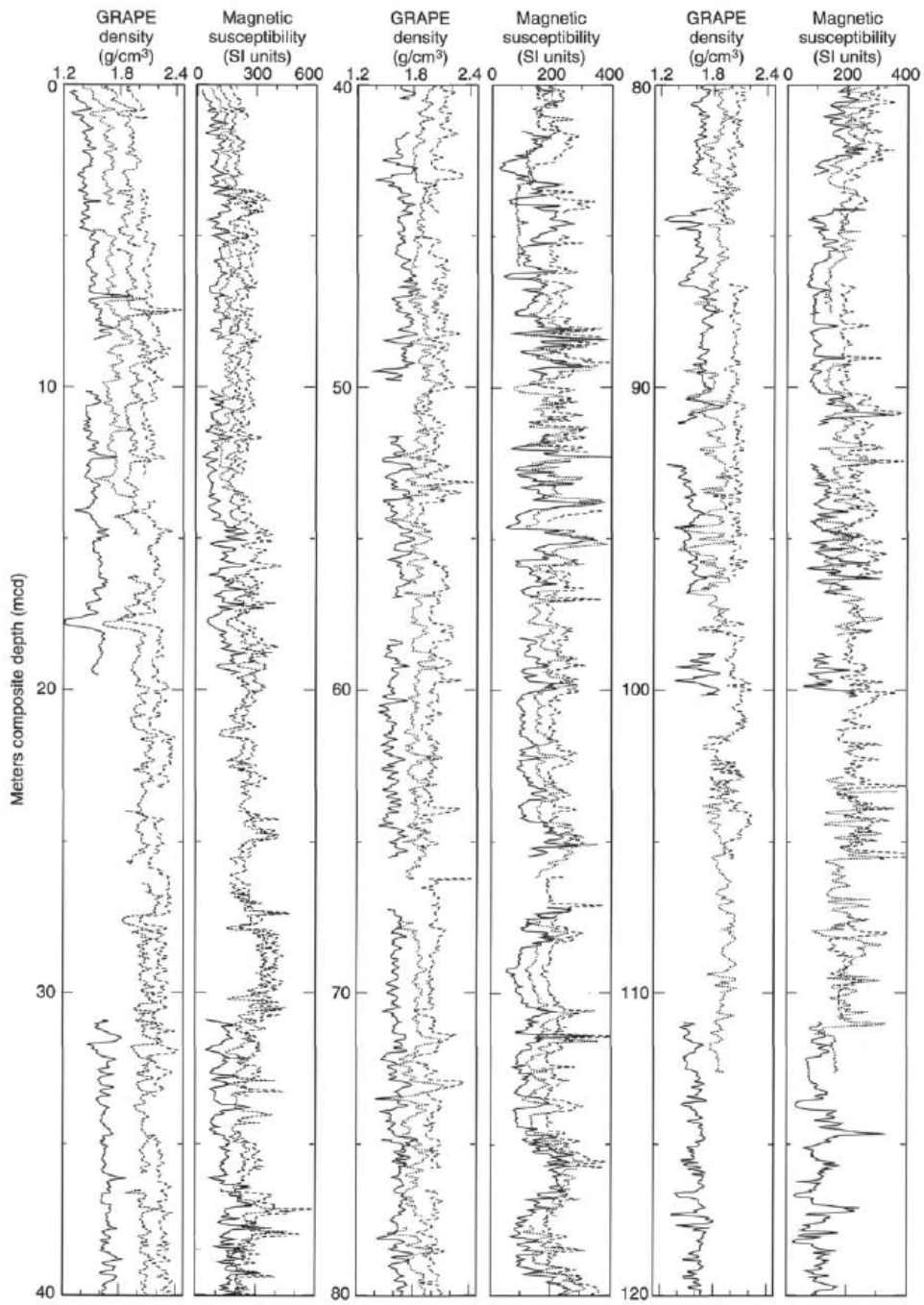

Figure 2. GRAPE density and magnetic susceptibility data from Site 987 on the mcd (meters composite depth) scale. Lines for Holes 987B (dotted), 987C (dashed), and 987D (long dashed) have been horizontally offset from line for Hole 987A (solid) for better display; therefore, values given on horizontal scale are the true values only for Hole 987A. (See also back pocket.)

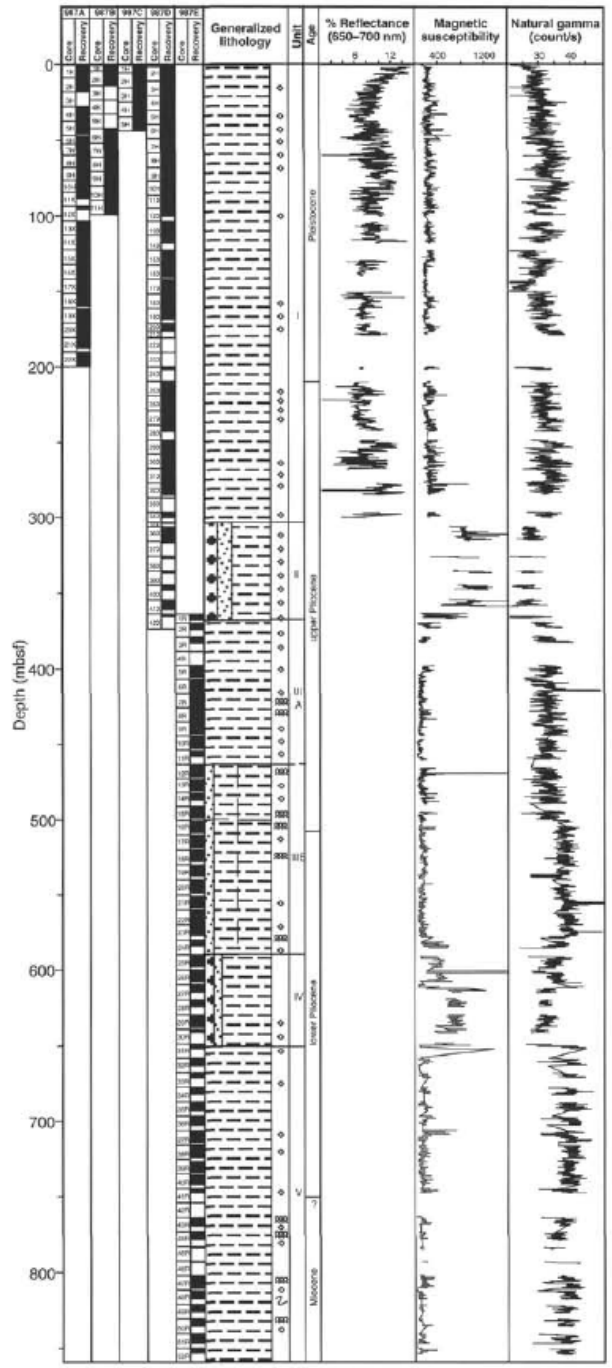

Figure 5. Core recovery, lithostratigraphy, age, spectral reflectance (red band), magnetic susceptibility, and natural gamma-ray intensity of sediments recovered in Holes 987A, 987B, 987C, 987D, and 987E. Cores containing dropstones (open diamonds) are shown in column adjacent to the lithostratigraphy. Spectral reflectance record is from Hole 987D; magnetic susceptibility and natural gamma-ray records are from both Holes 987D and 987E. (Key to symbols used in the "Generalized Lithology" column can be found in fig. 4, "Explanatory Notes" chapter, this volume.)

Biostratigraphy

- The biostratigraphy of Site 987, located on the East Greenland Margin, is incomplete because of the poor preservation of all microfossil groups. Most samples from this site are barren of both siliceous and calcareous microfossils.
- Siliceous microfossils were not observed in any samples, with the exception of rare pyritized diatom fragments in Sample 162-987E-11R-CC.
- Only calcareous microfossil datum could be used to provide age constraints for the sequence.

Sedimentation Rates

- Sedimentation rate reconstructions for Site 987 were based primarily on magnetic polarity events from Holes 987A, 987D, and 987E.
- Because the sediments at Site 987 were largely barren of fossils, biostratigraphic events were not used for sedimentation rate estimates, with the exception of the LO of *Pseudoemiliania lacunosa* at 45 mbsf (50 mcd) in Hole 987°.
- The Site 987 composite depth section was used to relate events recorded in the five holes drilled at Site 987 to a common depth scale.
- To facilitate comparison between sites, sedimentation rates were estimated from age vs. depth plots by drawing straight-line segments (uniform sedimentation rate) between selected datums.
- Sedimentation rates vary from -61 mcd/m.y. from 0.78 to 0.99 Ma, to about 203 mcd/m.y. from 1.77 to 2.58 Ma.

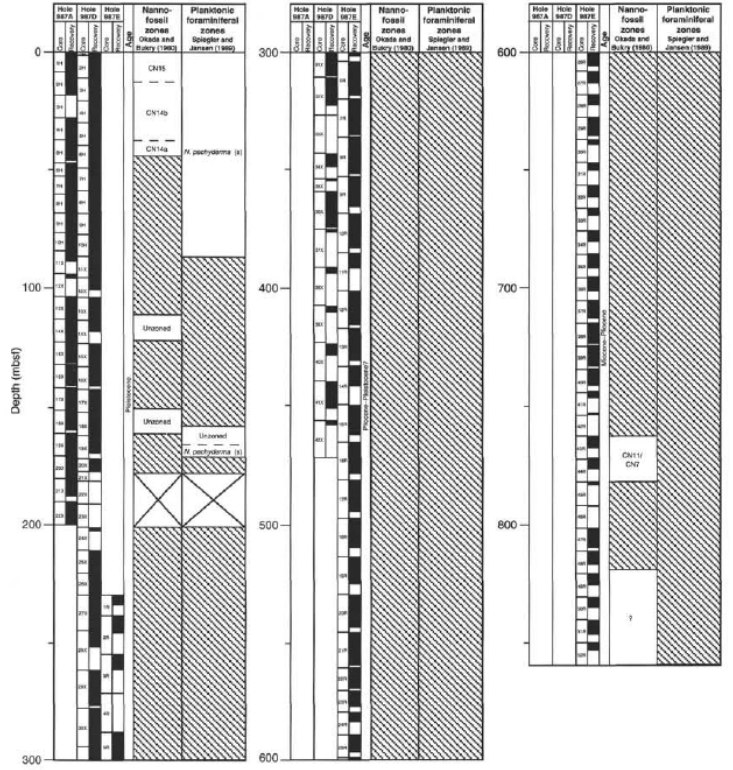

Figure 11. Biostratigraphic summary, Site 987. Hatched intervals indicate absence of fossils. An "X" indicates interval with no recovery. Age information is based on planktonic foraminifer and nannofossil biostratigraphy.

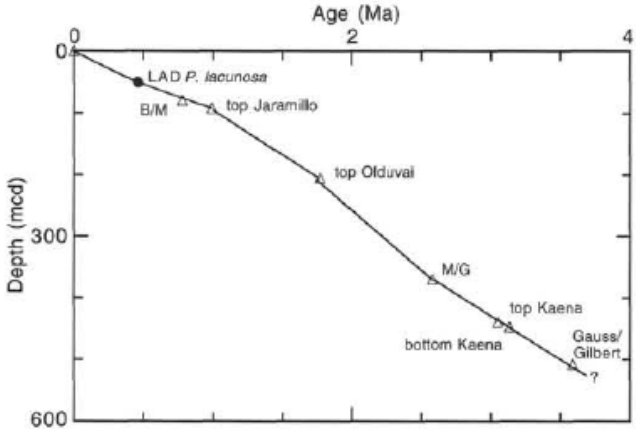

Figure 14. Site 987 age vs. depth (mcd) curve based on biostratigraphic and magnetostratigraphic datums. Solid circle = nannofossil datum; open triangles = magnetostratigraphic datums. M/G = Matuyama/Gauss.

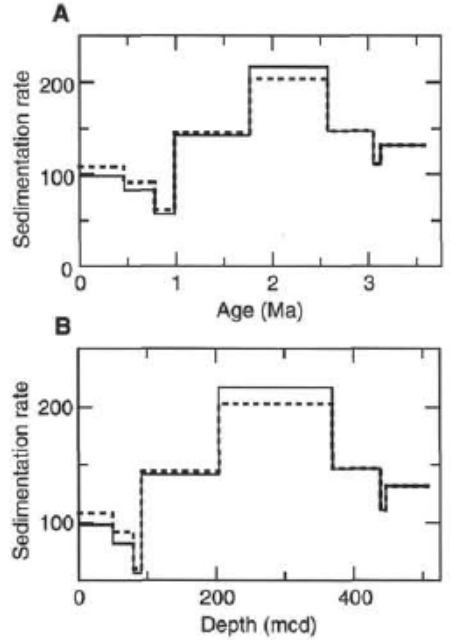

Figure 15. Site 987 sedimentation rates vs. age (A) and vs. composite depth (B). Solid lines indicate rates in mbsf/m.y.; dashed lines indicate rates in mcd/m.y.

Physical Properties

- Physical properties measurements at Site 987 included index properties, bulk density as measured by the GRAPE, P-wave velocity using the PWL and on split cores, undrained shear strength, using both the motorized vane and a fall-cone device, magnetic susceptibility, natural gamma radiation, and thermal conductivity. Downhole temperature measurements were carried out at four depths (32.7, 51.7, 70.7, and 80.2 mbsf) in Hole 987A, using the APC temperature device.

Geotechnical unit G1: 0-304 mbsf.

- Generally show normal increasing or decreasing trends with depth, in response to increased overburden.
- Corresponds to lithostrat unit 1 and seismic units EG-1 and EG2. The reflector separating these seismic units forms a distinct unconformity further upslope, to the west of Site 987, but appears conformable at the site - physical properties do not show any sign of an erosional hiatus at this horizon.
- divided in two subunits at 30 mbsf
- Slightly lower grain density in geotechnical Subunit G1A than in G1B indicates a possible change in mineralogy across the boundary.
- Constant laboratory-measured P-wave velocities between 1500 and 1550 m/s throughout Unit Gl are most likely a result of gas expansion and escape.
- Undrained shear strength shows a steady increase with depth and follows a normal trend for terrigenous sediments.

Geotechnical unit G2: 304-370 mbsf.

- Characterized by a distinct increase in bulk density, grain density, compressional velocity, and magnetic susceptibility, and a corresponding decrease in porosity, as well as in natural gamma-ray counts.
- Grain densities increase from an average of 2.65 g/cm^3 to an average of 2.72 g/cm^3.
- This unit corresponds to lithostrat Unit 2 and the upper part of seismic Unit EG-3, and represents a silty clay with sand and gravel, most likely a series of debris flows.

Geotechnical unit G3: 370-580 mbsf.

- normal, depth-related trends of index properties and *P*wave velocities are the main characteristics of geotechnical Unit G3.
- Unit G3 corresponds to lithostrat Unit 3 (divided in Subunits 3A and 3B), and to seismic stratigraphic Units EG-3 and EG-4.
- The change from lithostrat Subunit 3A to 3B, which marks a slight increase in the amount of interbedded sand layers and corresponds to seismic Reflector R3, shows no apparent response in the physical properties (fig. 20).

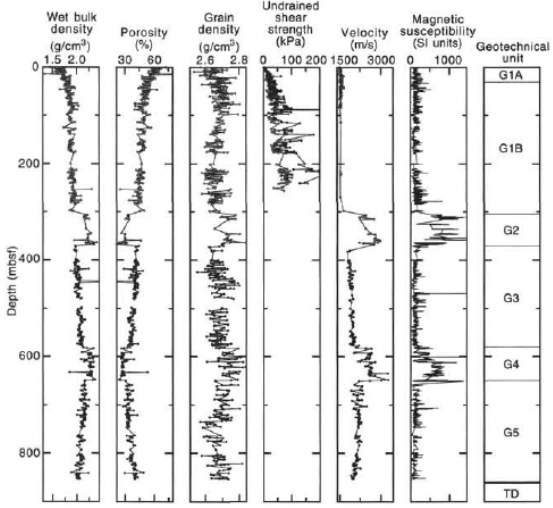

Figure 20. Geotechnical stratigraphy of Site 987, with vertical profiles of wet bulk density, porosity, grain density, *P*-wave velocity, undrained shear strength, and magnetic susceptibility. Open and solid circles represent measurements from Holes 987D and 987E, respectively. Undrained shear strength measurements were made only in Hole 987D, and here the open and solid circles mark motorized vane and fall-cone values, respectively.

Geotechnical unit G4: 580-650 mbsf.

- Similar to geotechnical Unit G2, this unit shows an increase in bulk density, compressional velocity, magnetic susceptibility, and grain density, and a corresponding decrease in porosity and natural gamma radiation values.
- Corresponds to lithostrat Unit 4 and to the upper part of seismic Subunit EG-VA, both having the same characteristics as Unit G2; silty clay with sand and gravel.
- Relates to high amplitude seismic reflectors above a more transparent interval, suggesting that the physical properties reflect debris-flow deposits.

Geotechnical unit G5: 650-859 mbsf, total depth.

- Bulk density, porosity, and compressional velocity show somewhat anomalous trends with depth in this unit, with slightly increasing values of porosity and decreasing velocity and bulk density.
- As both magnetic susceptibility values and natural gamma-ray counts show constant values, the trends most likely reflect predominantly more fine-grained sediments and the increased effect/ frequency of cemented non-biogenic carbonate beds.

Discussion

- Physical properties of the cored sediments at Site 987 reflect variations between hemipelagic deposition of silty clays and downslope, gravity-driven processes forming dense, coarse-grained deposits.
- The variations caused by the probable debris-flow deposits are superimposed on a normal compactional trend with increasing effective overburden. The lowermost part (below 650 mbsf), forms an exception, which may be due to an increased amount of clay-sized grains and cementation.
- Observed variations are most likely a response to changing glacial style between different periods through the Pliocene and Pleistocene.
- Units with increased sand and gravel contents, which we interpret to represent debris-flow deposits, may form when grounded glaciers reach the shelf break. Changes in grain density may indicate a change in sediment source area during such periods.
- Compared to Site 986, on the Svalbard continental margin, the component of debris-flow deposits relative to the total cored sedimentary section appears much less at Site 987 – reflects important differences in the style of glaciation between the two areas?
- Differences between 986 and 987 may also reflect slightly more distal position of Site 987, relative to the base of the slope, and the difference in slope gradient between the two margins.

Heat flow

- The main objective of the downhole temperature measurements at this site was to add to the very sparse heat-flow database for this part of the Norwegian-Greenland Sea.
- A total of 76 measurements of thermal conductivity were carried out in the upper cores of Holes 987 A, 987B, and 987D, to a maximum depth of 109 mbsf.
- Yielded a thermal gradient of 96.5°C/km.
- Extrapolation of the downhole temperatures gives a bottom water temperature of-0.99°C, which is in good correspondence with physical oceanographic data (CTD-casts) from this region.
- Using an average measured thermal conductivity of 1.278 W/(m K) provides a heat-flow estimate of 123.3mW/m2 at Site 987.
- Compared to Site 986, at the Svalbard Margin, the slightly lower heat-flow value measured at Site 987 is consistent with an older crust at the latter site.
- The bottom of Hole 987E, which terminated within a few meters of basement has an age estimate of 6-7 Ma

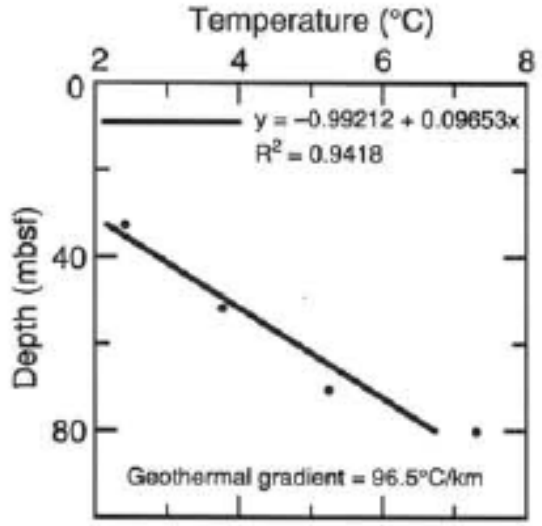

Figure 22. Calculated geothermal gradient for Hole 987B.

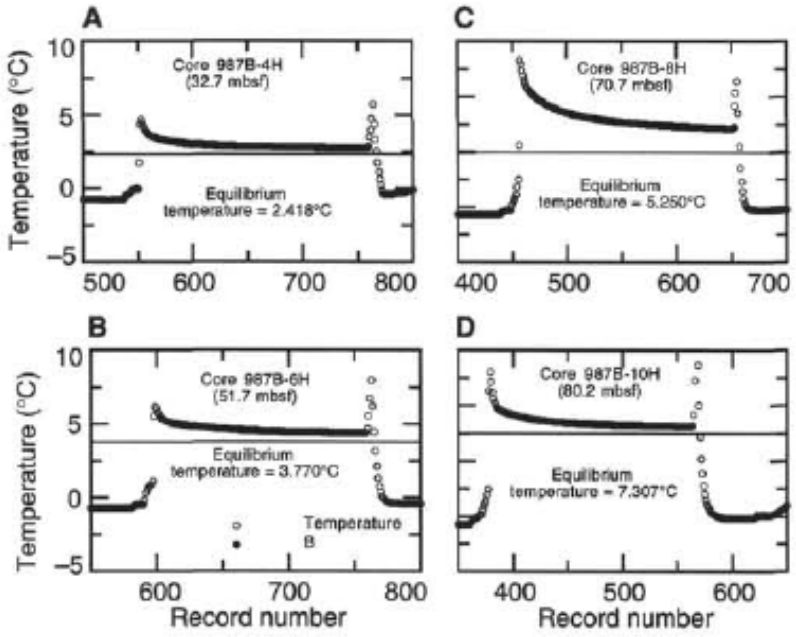

Figure 21. **A–D.** Downhole temperature measurements and calculated equilibrium temperatures from Hole 987B.

Seismic Stratigraphy

- The drilling proposal for EGM-4 (Site 987) was based on a multichannel seismic line (GGU82-12) acquired in 1982 by the Geological Survey of Greenland (GGU).
- East-west-trending dip line across the flank of the Scoresbysund Fan. The proposed site was located near the base of slope, 16 km from the eastern end of the line.
- Hole 987E was logged down to 480 mbsf and compressional velocities taken from the laboratory measurements and used in the time-depth conversions are checked against the velocities from the downhole measurements.

EG-1: 2.375 - 2.590 seconds two-way traveltime (s TWT).

- Characterized by low-amplitude parallel internal reflections, often forming bands of narrow reflectors. Although reflecting bands are continuous over the length of the line, individual reflectors appear discontinuous and may have a slight relief.
- Upslope, however, the seismic character becomes more stratified.
- Characteristic of this unit is westward thinning. It has its maximum thickness (within the surveyed area) at Site 987 and thins rapidly upslope.
- The basal reflector of the unit is R1.
- With an interval velocity of 1.65 km/s, the thickness of seismic Unit EG-1 is 177 m.

Reflector 1 (R1):

- is a distinct unconformity when followed westward, where it shows both erosional truncation of underlying reflectors, and onlap of internal reflectors within Unit EG-1. A lateral change in the character of Reflector R1 is also indicated by the present site survey line (Fig. 27).

EG-2: 2.590 - 2.735 s TWT.

- Seismic character is similar to EG-1 (with exception of at least one strong reflector in the upper part which interferes with the response of Reflector R1).
- Below the strong reflector(s), there are similar low-amplitude, slightly undulating reflectors.
- Internal reflectors downlap on the base of the unit, Reflector R2, but the latter reflector does not appear to truncate underlying reflectors.
- Using an interval velocity of 1.75 km/s, the thickness of seismic Unit EG-2 is 127 m.

EG-3: 2.735 - 2.895 s TWT.

- Lateral variability in seismic character:
  - high-amplitude, conformable reflectors at and west of Site 987
  - Eastward from the site, the unit thins and the deeper internal reflectors, in particular, appear weaker. However, since there were problems with the water guns along this line, and guns had to be changed frequently, an effect of different source signatures cannot be excluded.
- Exhibits the greatest thickening of all drilled seismic units, becoming 0.7 s thick beneath the shelf break.
- Upper 50 ms of Unit EG-3 has a distinctly higher velocity (2.6 km/s) than the lower 110 ms (1.9 km/s) – probably due to seismic interference, but no distinct seismic reflector to define this subdivision.
- Using an average interval velocity of 2.15 km/s, the thickness of this unit is 172 m.
- Basal reflector of this unit is R3.

Reflector 3 (R3)

- A distinct unconformity when followed westward, where it is overlain by downlapping reflectors of Unit EG-3, and shows truncation of underlying reflectors of EG-4.

EG-4: 2.895 - 3.015 s TWT.

- Lateral variability in seismic character:
  - Distinct internal reflectors in the western part of Line 987-S1.
  - East of Site 987, however, the internal reflectors become weak and discontinuous.
- Shows less increase in thickness toward the west compared to the units above.
- Has a thickness of 0.120 s, which equals 120 m using an interval velocity of 2.0 km/s.
- Basal reflector of the unit, Reflector R4.

Reflector 4 (R4)

- Prominent seismic reflector that marks a difference in seismic character above and below, as well as truncating underlying reflectors.

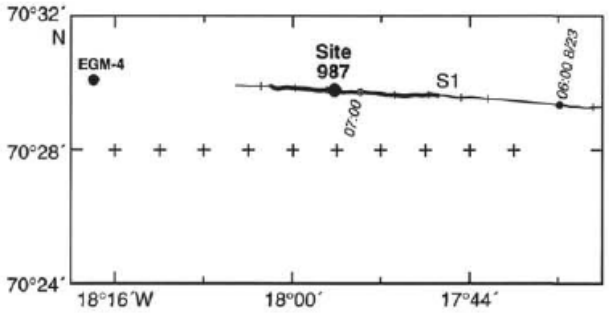

Figure 26. Map showing the proposed site EGM-4 and the site survey near Site 987. Note that the line started farther east at 17°16'E, but only the portion nearest the site is shown here and is discussed in this chapter. Bold line marks profile shown in Figure 27.

EG-5: 3.015 - 3.235 s TWT.

- Divided in two subunits, EG-5A and EG-5B, bounded by Reflector R5.
- Subunit EG-5A is characterized by strong but discontinuous reflections.

Reflector 5 (R5)

- Does not form a distinct, continuous reflector at Site 987, but is defined as the base of Subunit EG-5A.
- Farther west R5 is a prominent reflector as well as an unconformity.
- Subunit EG-5B is displays a structureless and transparent character, which continues to the basement reflector at 3.235 s.
- Average velocity for the rest of seismic Unit EG-5 is 2.4 km/s, giving a total thickness of 264 m of EG-5.

Discussion/conclusions

- Seismic Units EG-I and EG-II correspond to lithostratigraphic Unit 1 and geotechnical Unit G1
- Reflector R1, however, does not appear to be associated with any change in lithology or physical properties. This may explain the lateral, east-west changes observed in the character of both Unit EG-1 and Reflector R1, and could indicate that the changes are caused by varying amounts of downslope, gravity driven sediment transport in the form of turbidites and debris flows.
- Lithostratigraphic Unit 1 consists of hemipelagic silty clay with frequent but relatively thin sand layers interpreted as turbidites. Hence, from the seismic character, an upslope increase in both frequency and thickness of turbidites, possibly also grading into debris flows, would be expected.
- Reflector R2 corresponds to the upper boundary of lithostratigraphic Unit 2, a silty clay with sand and gravel, and geotechnical Unit G2, which are 60 m thick and characterized by high velocities and densities.
- The character of this upper part of seismic Unit EG-3, as well as the physical properties and the lithological character of the sediments, point at debris flows as the likely depositional mechanism.
- The lower part of seismic Unit EG-3 shows low-amplitude reflectors corresponding to lithostratigraphic Subunit 3A and the upper part of geotechnical Unit G3, which are silty clays with normal depth-related trends in physical properties.
- Reflector R3 shows the same lateral changes in character as R1 – more distinct to the west and upslope.
- The transition between seismic Units EG-III and EG-IV, across Reflector R3, does not involve a change in the physical properties but, lithostratigraphically, Reflector R3 corresponds to the boundary between Subunits 3A and 3B marked by an increase of interbedded sandy layers.
- Therefore, Reflector R3 most likely marks the end of a period of increased downslope sediment transport in the form of turbidites and/or debris flows, which had stronger influence on the sediments farther upslope than at Site 987.
- Reflector R4 is most prominent seismic reflector and corresponds to the boundary between lithostratigraphic Subunits 3B and 4 and geotechnical Units G3 and G4.
- Reflector R4 defines the top of an approximately 70-m-thick sandy, gravelly silty clay with distinctly raised densities and seismic velocities.
- Lithostratigraphic Unit 4 is interpreted to represent debris flows and this interval corresponds to the upper part of the reflective upper half of seismic Unit EG-5.
- The debris-flow unit is the main cause for Reflector R4, but the seismic character of seismic Subunit EG-5A continues below the interpreted debris-flow deposit. *P*wave velocity show a larger variation in values above 710 mbsf than below. This may explain the seismic character of Subunit EG-5A, and also indicate a transitional period with increased downslope transport before onset of the main debris-flow activity of lithostratigraphic Unit 5.
- Seismic Subunit EG-5B represents relatively homogeneous silty clays giving rise to the seismically structureless character of this subunit.
- Using P-wave velocities measured in the laboratory for seismic Unit EG-5, acoustic basement is shallower than the bottom of Hole 987E. Therefore, higher velocities than actually measured are used in the time-depth conversion of the lower part of Subunits EG-VA and EG-VB, to result in a basement depth below 860 mbsf.
- An explanation for not having reached basement in Hole 987E is, therefore, a basement relief that is not detected by the seismic data of Line 987-S1 in addition to a possible slight offset of the hole relative to the seismic line, within the range of the dynamic positioning system and the GPS accuracy.
- In summary, the seismic stratigraphy at Site 987 appears to reflect variations in the frequency and amount of gravity-driven sediment transport from the East Greenland Shelf, which is in accordance with the site being located at the northeastern flank of the Scoresbysund glacial fan.
- Intervals of more frequent debris flows form the most distinct seismic reflectors but do not seem to be the volumetrically most important deposits. This differs from Site 986 on the Svalbard Margin, where the greater part of the drilled section apparently consisted of debris flows.
- Palaeomagnetic studies indicate a late Miocene age for the lowermost drilled sediments, immediately above basement.
- A main result of drilling at Site 987 is, therefore, that new and younger ages can be assigned to the main buildup of the Scoresbysund Fan = the main phase of fan construction took place after Reflector R3 time, which we date at approximately lower upper Pliocene.
- The depocenter for the period prior to this is located below the present day middle to inner shelf.

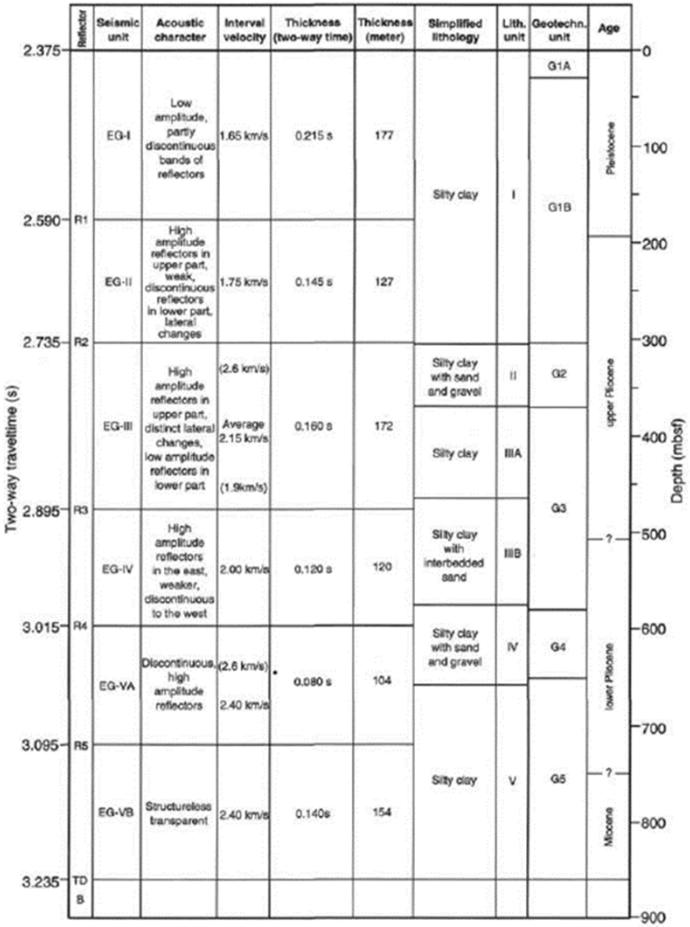

Figure 29. Correlation of the seismic stratigraphy with lithostratigraphy and geotechnical stratigraphy. TD = total depth; B = basement.

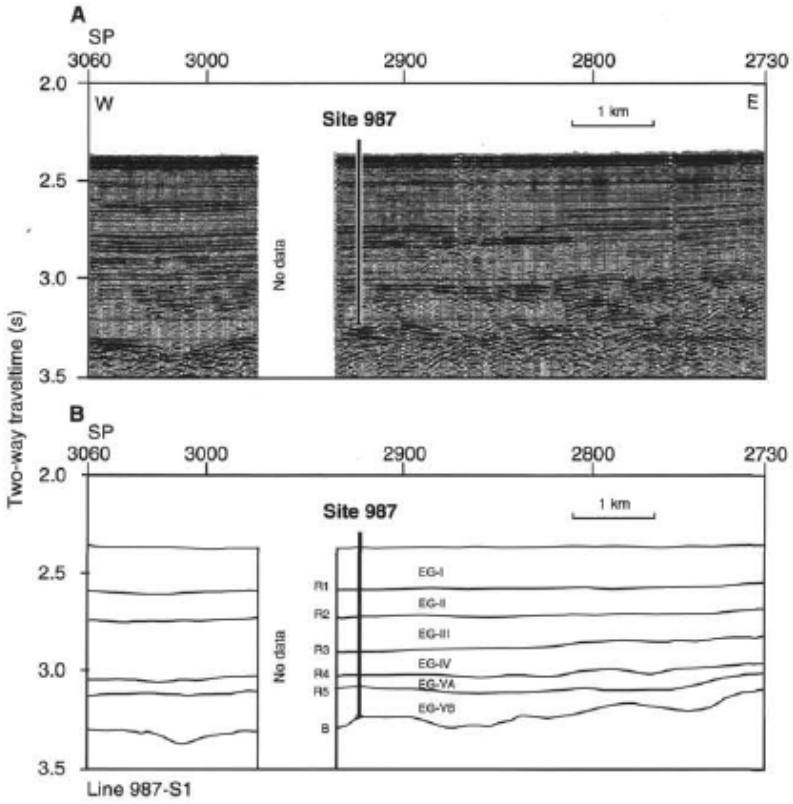

Figure 27. **A.** Part of seismic Line 987-S1, crossing Site 987. **B.** Line interpretation of seismic Line 987-S1. See Figure 26 for location.

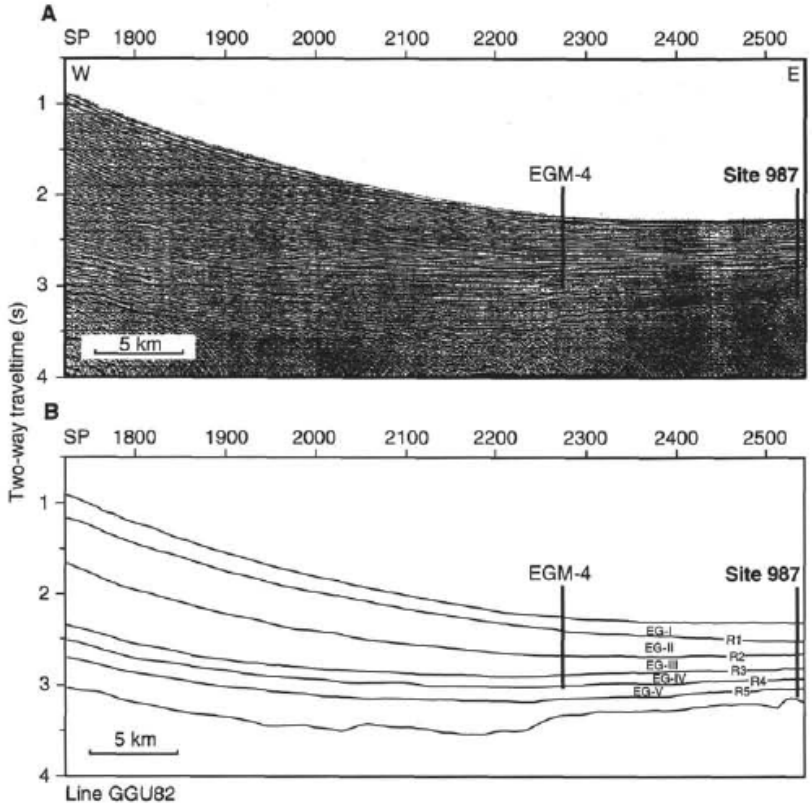

Figure 28. **A.** Portion of pre-cruise seismic Line GGU82-12, showing the proposed site EGM-4 and Site 987. **B.** Line interpretation of seismic Line GGU82-12. See Figure 26 for location of the sites.

Hole 987E: Natural Gamma Ray-Resistivity-Sonic Logging Data

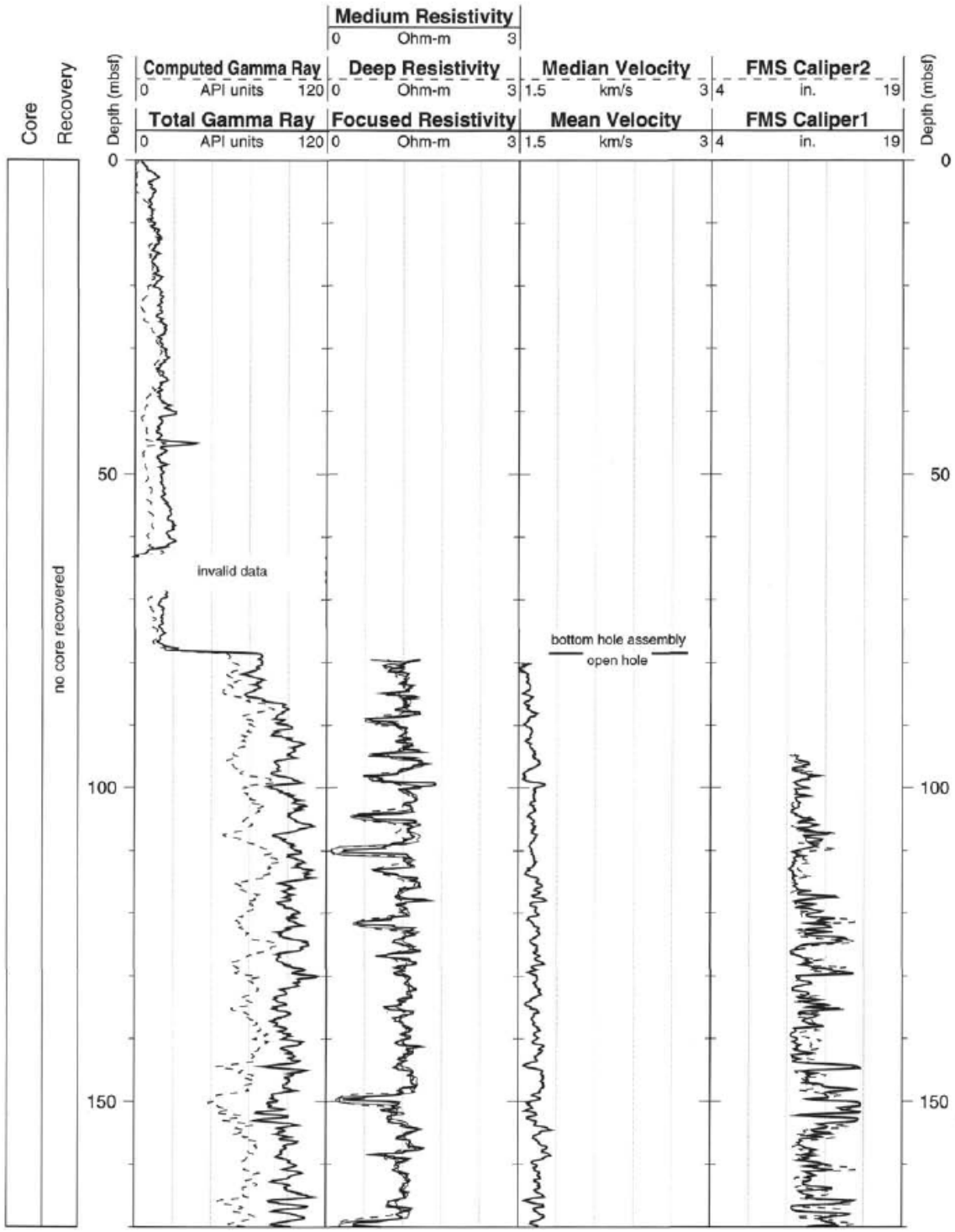

Hole 987E: Natural Gamma Ray-Resistivity-Sonic Logging Data (cont.)

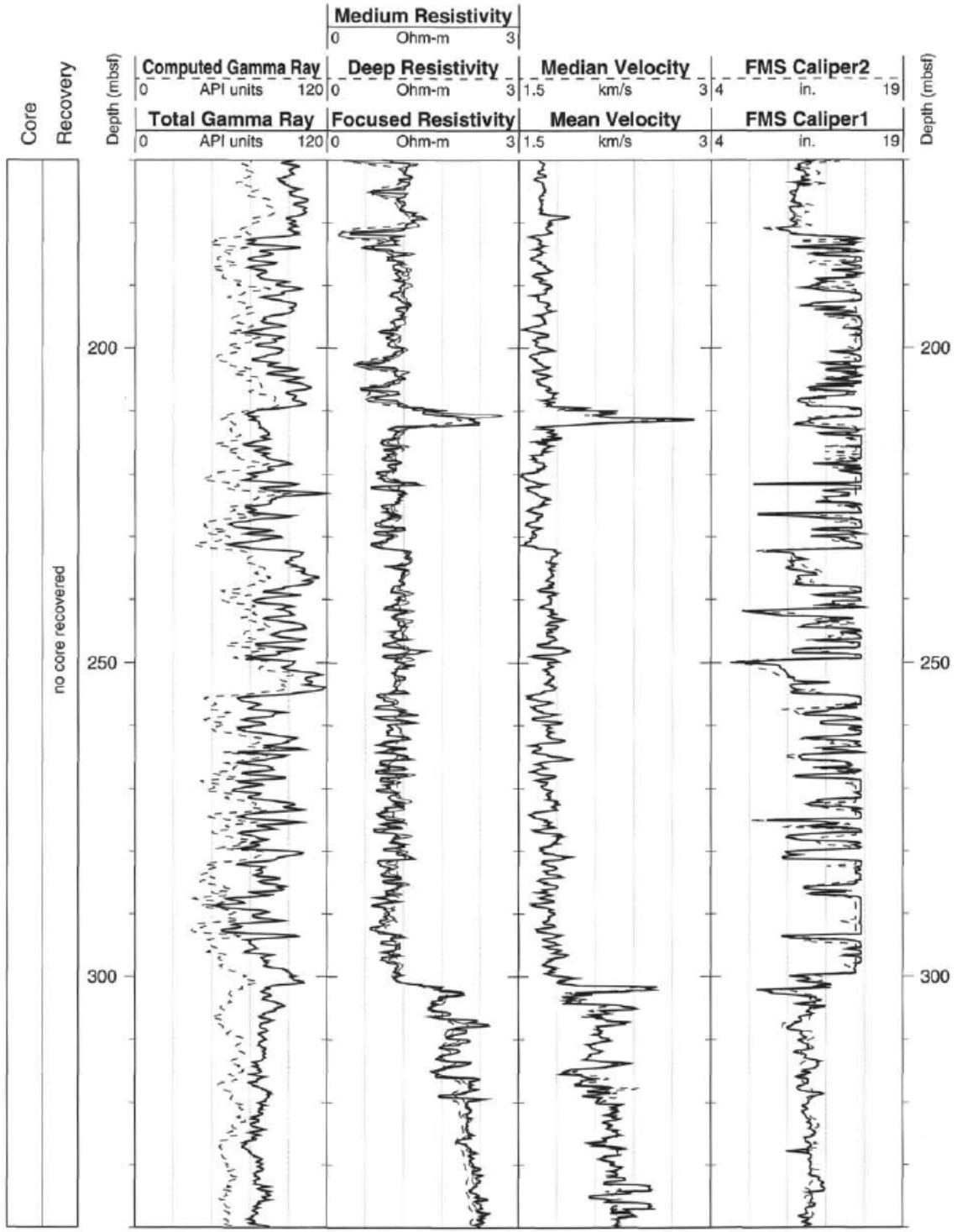

Hole 987E: Natural Gamma Ray-Resistivity-Sonic Logging Data (cont.)

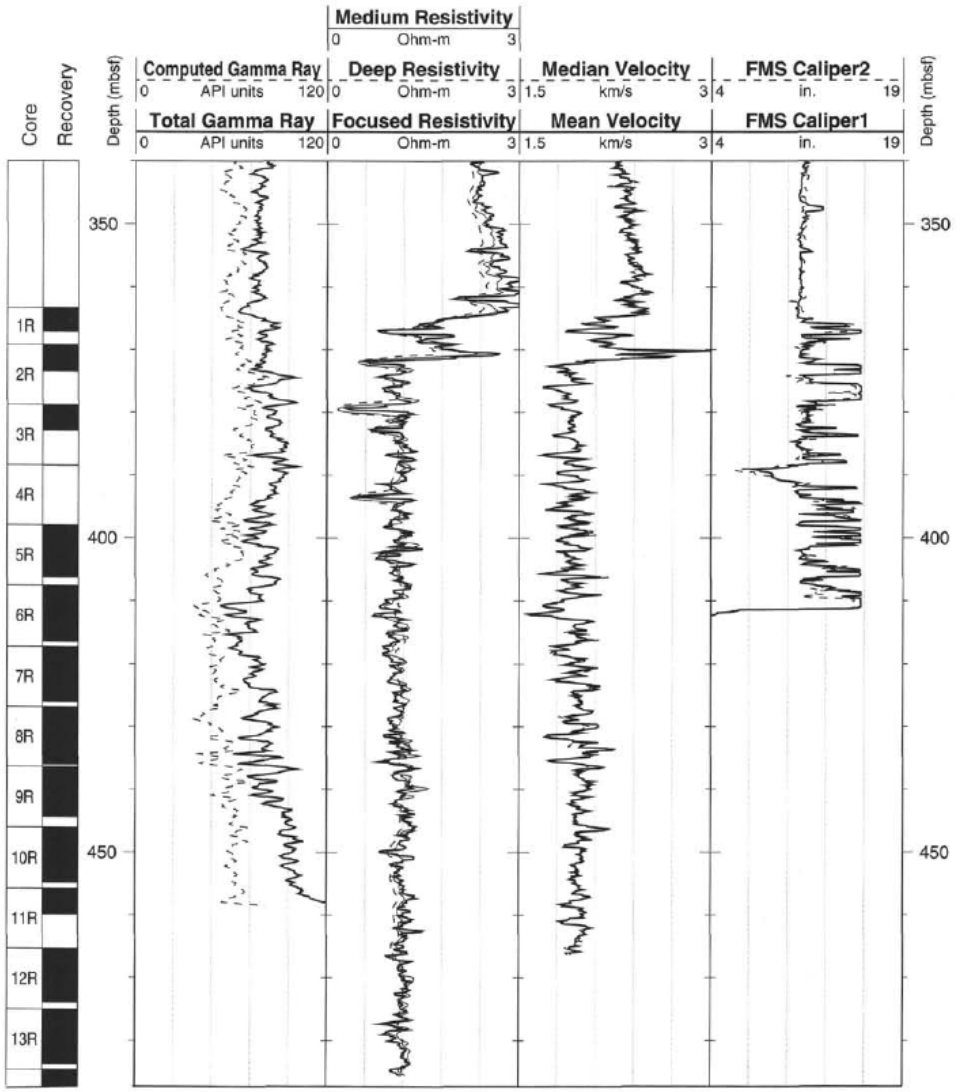

Hole 987E: Natural Gamma Ray-Density-Porosity Logging Data

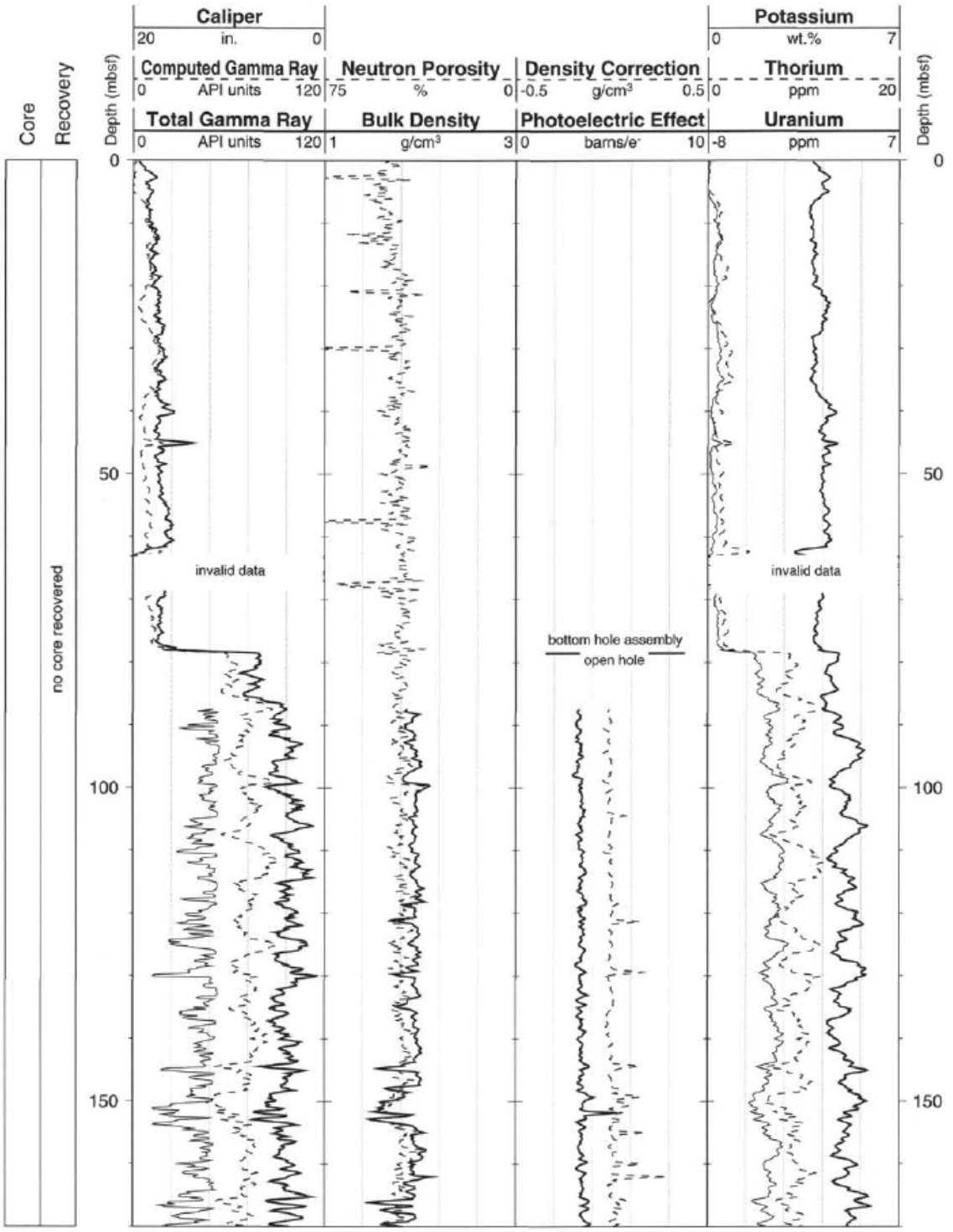

Hole 987E: Natural Gamma Ray-Density-Porosity Logging Data (cont.)

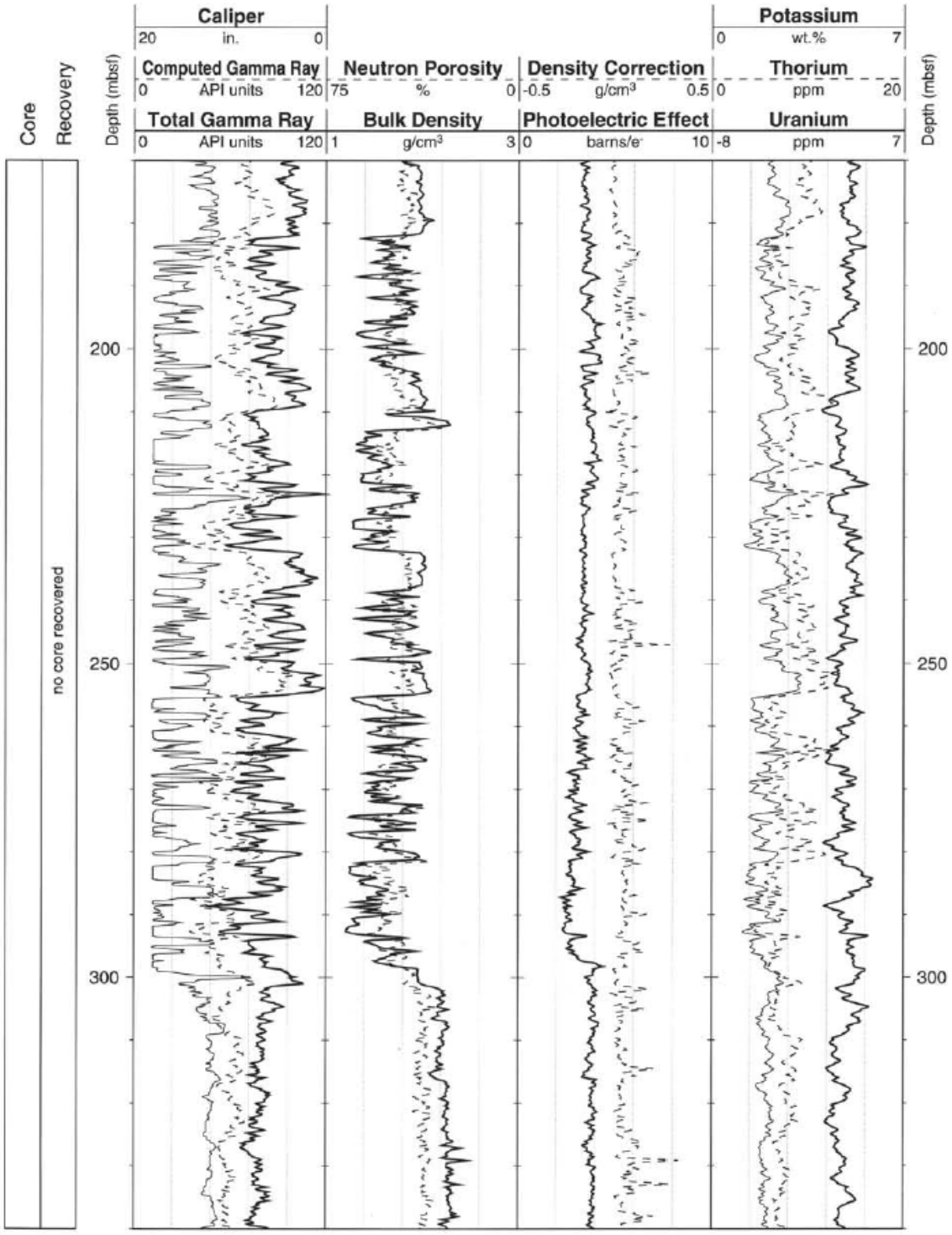

Hole 987E: Natural Gamma Ray-Density-Porosity Logging Data (cont.)

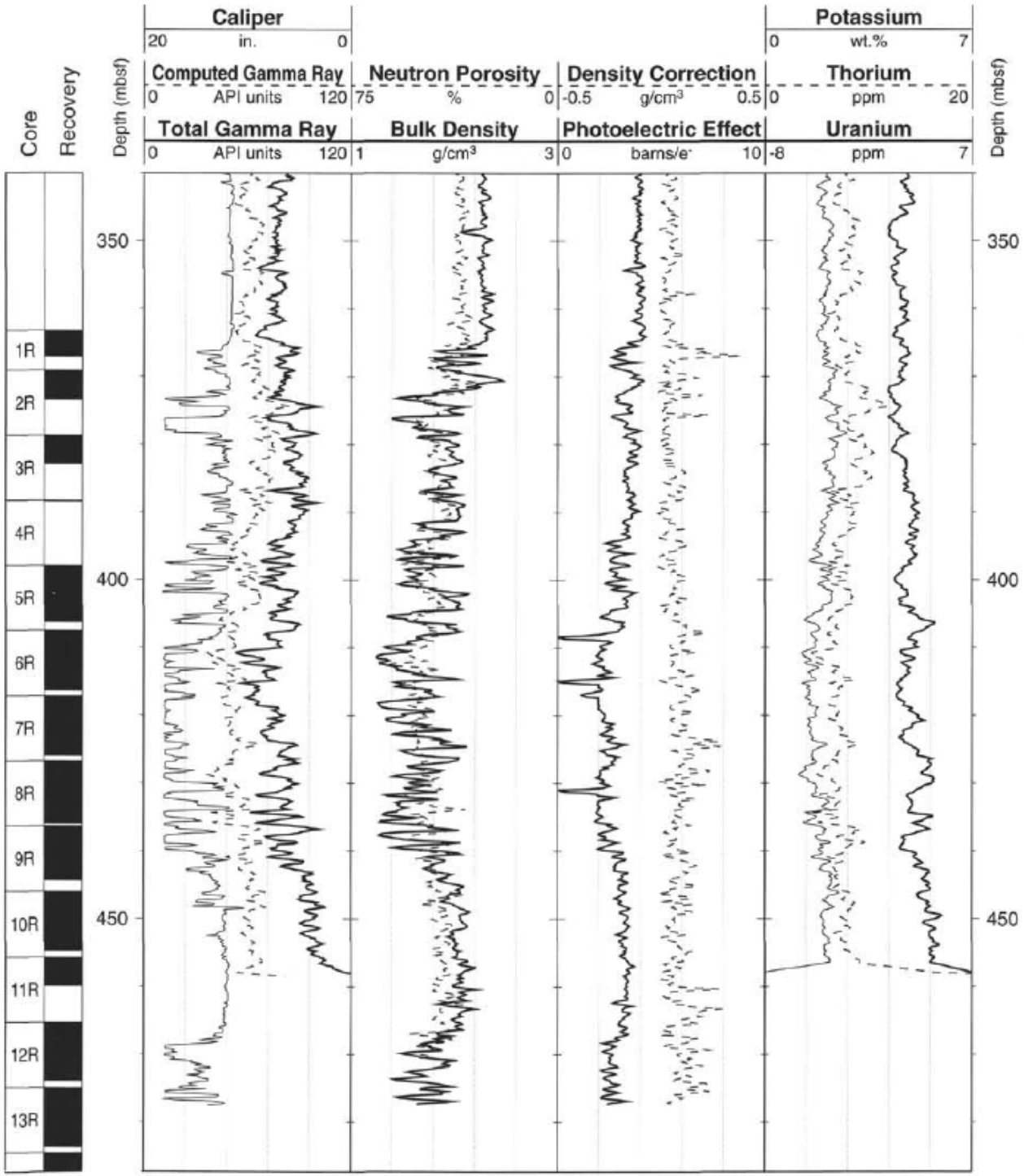

APPENDIX B

Well Correlation Panels

- All Wells Lithologies

- DSDP Well Correlation Panel

Lithological overview of all wells across the Jan Mayen Microcontinent

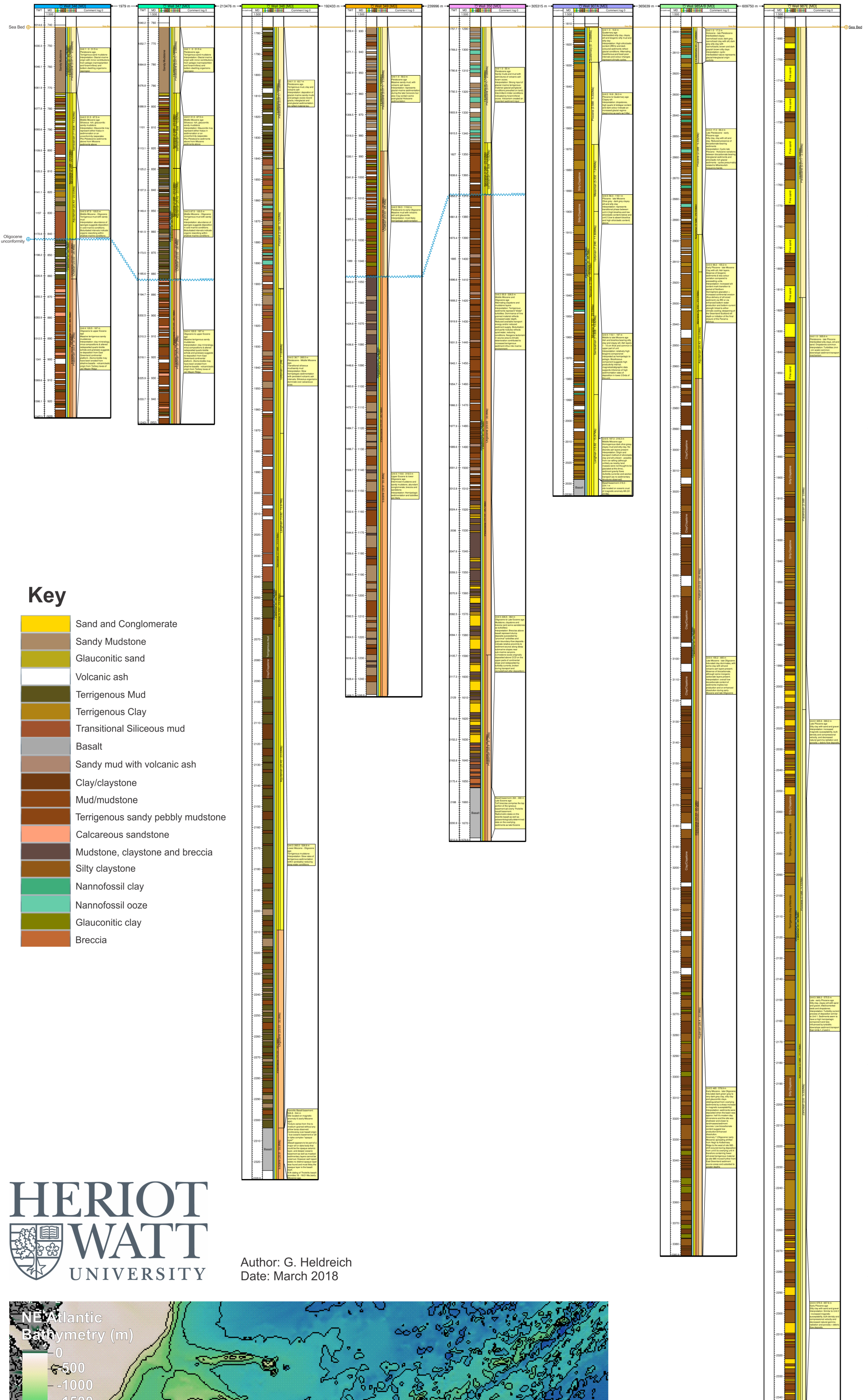

Key

- Sand and Conglomerate
- Sandy Mudstone
- Glauconitic sand
- Volcanic ash
- Terrigenous Mud
- Terrigenous Clay
- Transitional Siliceous mud
- Basalt
- Sandy mud with volcanic ash
- Clay/claystone
- Mud/mudstone
- Terrigenous sandy pebbly mudstone
- Calcareous sandstone
- Mudstone, claystone and breccia
- Silty claystone
- Nannofossil clay
- Nannofossil ooze
- Glauconitic clay
- Breccia

HERIOT WATT UNIVERSITY

Author: G. Heldreich
Date: March 2018

DSDP Leg 38 well correlation panel across the Jan Mayen Microcontinent

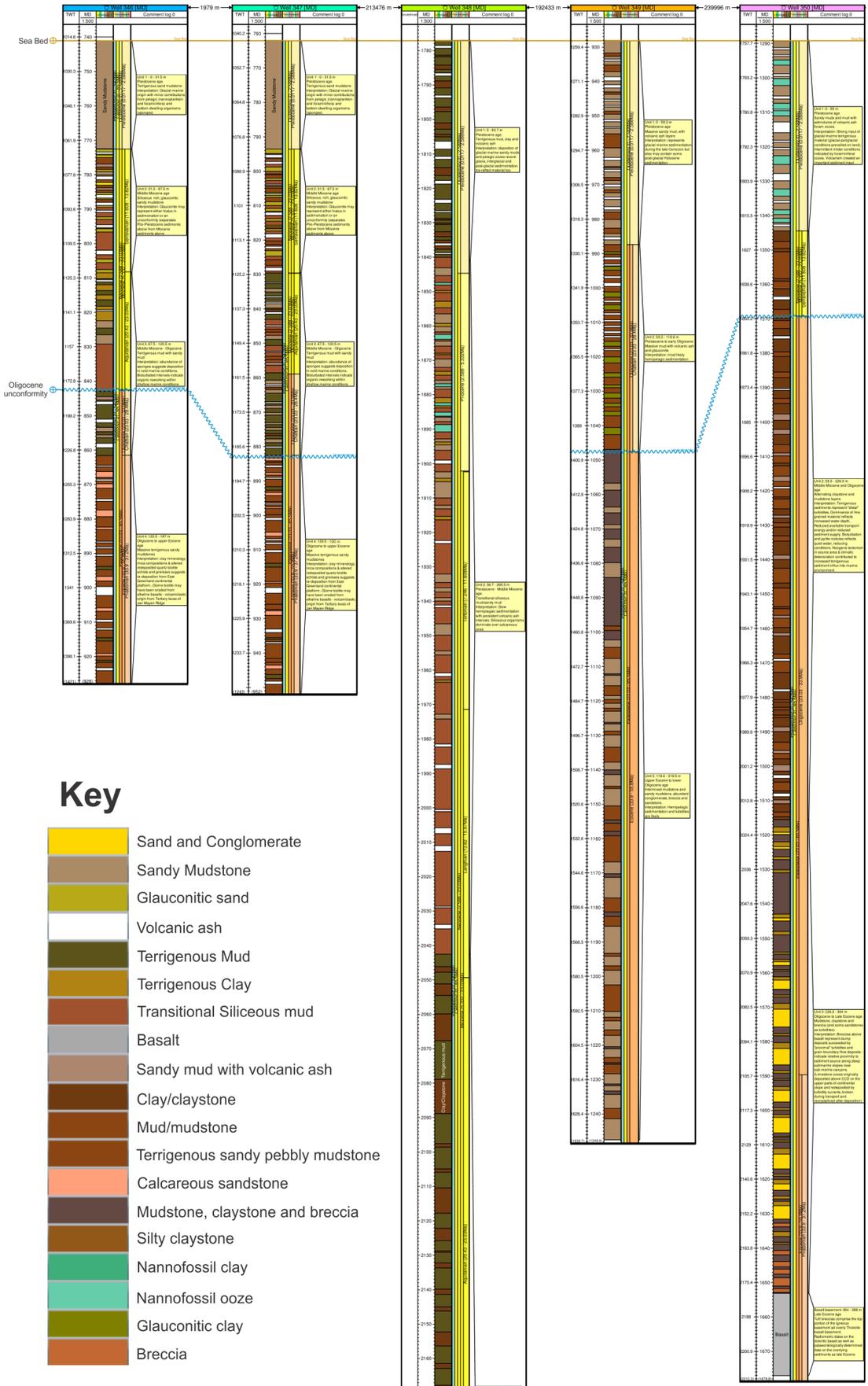

Key

- Sand and Conglomerate
- Sandy Mudstone
- Glauconitic sand
- Volcanic ash
- Terrigenous Mud
- Terrigenous Clay
- Transitional Siliceous mud
- Basalt
- Sandy mud with volcanic ash
- Clay/claystone
- Mud/mudstone
- Terrigenous sandy pebbly mudstone
- Calcareous sandstone
- Mudstone, claystone and breccia
- Silty claystone
- Nannofossil clay
- Nannofossil ooze
- Glauconitic clay
- Breccia

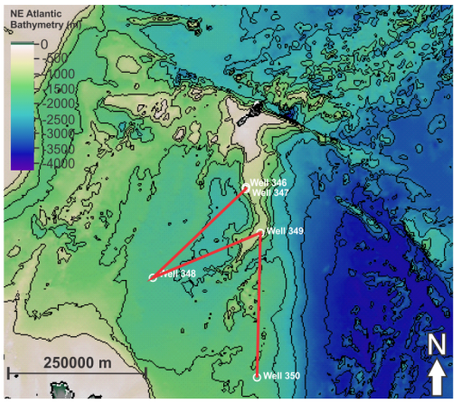

Author: G. Heldreich
Date: March 2018

HERIOT WATT UNIVERSITY

APPENDIX C

Tectonostratigraphic Synthesis Chart for the JMMC

North Atlantic Regional Tectonic Events

Ma | Era | Period | Epoch | Stage | Magnetic Anomaly | Orogeny | Relative Plate Kinematic direction (Greenland relative to Norway) | Rifting/ Extension/ Subsidence | Sea Floor Spreading | Magmatism | Compression/ Uplift/ Inversion

Orogeny

- Late Alpine
- Pyrenean
- Laramide
- Alpine (Austrian)
- Uralian (suturing of West Siberia and Laurasia)
- Pangea
- Variscan (closure of proto-Tethys)
- Caledonian

Relative Plate Kinematic direction (Greenland relative to Norway)

- Continued E-W oriented spreading direction along Kolbeinsey Ridge
- Plate stress vector reorganisation at C13 - ESE relative plate motion between Greenland and NW Europe. WJMFZ orientation (WNW-ESE) reflects the post Eocene change in plate vector. Related to cessation of Labrador seafloor spreading and docking of Greenland with North American plate
- Change in horizontal stress pattern = SE directed compression due to ridge push forces
- Plate stress vector reorganisation (change from E-W in Jurassic to NW-SE in early Cretaceous onwards)
- N-S trending rift systems due to E-W oriented extension direction
- N-S trending rift systems due to E-W oriented extension direction
- Wide variation in extension vector during Permo-Triassic - create mosaic like fragmentation along fused Orogenic belts of Pangea
- Permo-Triassic basins inherit orientation of Caledonian fold belt
- Unstable supercontinent = assembly and rifting/ break up almost simultaneous
- Extensional rift basins preferentially inherit Caledonian structural grain

Rifting/ Extension/ Subsidence

- Increased subsidence/ amplified folding along North Atlantic margins - loading of the shelves by increased rate and flux of sedimentation during glacial-interglacial regime
- Separation of JMMC from East Greenland at C7
- Local renewed rifting & extension in response to Oligocene-Miocene plate reorganisation. Extension in SRC due to onset of westward rift/ spreading ridge propagation
- Break up & opening of Norwegian-Greenland Sea
- Rifting along line of incipient break-up prior to subsequent continental break up ~53 Ma. Extensional faulting on Utrost Ridge, Hel Graben, Nyk High and Gjallar Ridge (outer Voring Basin)
- Broad zone of extension & subsidence from Rockall Trough to western Barents Sea. Cretaceous rifting cross-cuts pre-existing Jurassic rift basin orientations. Considerable crustal extension and thinning created major Cretaceous basins off Mid Norway and East Greenland. Assocaited with considerable syn-rift expansion and coarse clastic depostion in hanging walls of NE trending grabens. More Basin axis - crystalline crust thinned to few kms - almost becoming oceanic before rift cessation.
- NE trending faults cause rift flank footwall uplift on the northern edge of N Atlantic basins (NNS, outer Voring Basin, Trænа Basin, Ribban Basin). These basins underwent rapid differential subsidence and segmentation into sub-basins and highs.
- Intense regional phase of rifting. Associated with stress and opening regime of sea floor spreading in the Tethys. Created Halten Terrace, East Greenland Rift, Viking Graben.
- Break up & opening of Central Atlantic
- Mild extension and thermal subsidence in NE Atlantic (E. Greenland & Mid-Norway margins)
- Permo-Triassic extension poorly dated - mosaic like fragmentation along fused orogenic belts of the Pangea supercontinent. In East Greenland minor rotational block faulting and westwards tilted half-grabens forming terrestrial to shallow marine basins that discordantly cover the older Devonian-Carboniferous basin.
- Rifting in response to post-orogenic collapse and back-sliding of Nappe pile = formation of Carboniferous extensional basins (onshore Mid Norway and East Greenland)

Sea Floor Spreading

- Labrador Sea
- Mohns & Rekyanes Ridges
- Ægir Ridge
- *Proto-Kolbeinsey Ridge? Series of ridge jumps? Extinct spreading axis just west of JMMC*
- Kolbeinsey Ridge
- Atlantic spreading progagate northwards between Iberian margin and Grand Banks
- Central Atlantic
- Tethys

Magmatism

- Oligocene-Miocene sills related with mid-Cenozoic extensional phase.
- Lava flows on western margin of JMMC likely sourced from fissure volcanic complexes due to rifting and break up between JMMC and East Greenland
- SDR formation associated with NAIP. Sills intrude upper Cretaceous and lower Palaeocene successions along the basin marginal highs (Voring, Møre and Faeroe basins).
- Mantle generated melts and underplating/ seamounts beneath thinned hyperextended crust at axis of incipient rifting site (proto-Aegir Ridge).
- Rift flank uplift & flexuring associated with extensional event created regional unconformity against Gjallar Ridge in Lofoten & outer Voring Basin (marginal flanks). Created a core complex (pre-opening underplating).
- Barra Volcanic Ridge system in Rockall Trough. May represent isolated spreading cell.
- NE-SW oriented precursory seafloor intrusions (seamounts) along axis of basement thinning in Møre Basin. Represent a failed rift event.
- Pyroclastic rocks on North Sea and East Greenland, and off Mid Norway.
- Uplift/ thermal doming (possibly hot spot related dome) created severe restriction between the north (Barents Sea, East Greenland, Mid Norway) and south (Southern North Sea, southern UK, southern Europe), caused total marine faunal separation between northern (Boreal) and southern (Tethyan-Atlantic) realms
- Volcaniclastics contemporaneous with rifting (north Porcupine Basin, Erris Trough and Donegal Basin
- Magmatism associated with rifting on East Greenland margin, West Shetland Basin and Møre Margin
- Thermal uplift of Pangea supercontinent (possibly from accumulation of heat under low conductivity continental lithosphere)

Compression/ Uplift/ Inversion

- Uplift & erosion in response to glaciations & isostatic rebound
- Uplift of areas surrounding Norwegian-Greenland Sea due to intra-plate stress regime & ridge push
- Rift flank uplift, erosion and formation of unconformities related to mid-Cenozoic extension.
- N-S / NE-SW trending inversion structures (elongate domes (Helland Hansen Arch, Ormen Lange Dome), reverse faulting and large wavelength bulge of Cretaceous-Palaeocene depocentre axes) on Norway and East Greenland margins in response to NW-SE compressional regime/ ridge-push forces.
- Continued uplift and extensional faulting attributed to pre-opening underplating associated with proto-Iceland plume (Voring & Møre margins and Hatton Bank). Thermally generated uplift.
- Exhumation and rift flank uplift along line of incipient break-up. Caused increased erosion and input of sand into basin flanks (Lange and Lysing Ssts).
- Potential central high between Mid Norway and East Greenland along proto-Ægir Ridge location.

Global Sea Level (metres above present day)

-100 | 0 | 100 | 200 | 300

Present Day Sea-Level

Icehouse / Greenhouse / Icehouse / Greenhouse

Stratigraphic Successions

East Greenland: Onshore (Jameson Land Basin) | Offshore (Liverpool Land Basin)

JMMC: 346 349 350

Mid Norway: Møre Basin | Voring Basin

- Krabbedalen Fm
- Scoresby Land Gp
- Hall Bredning Gp
- Vardekløft Gp
- Neill Klinter Gp
- Jameson Land Gp
- Gipsdalen Fm
- Pingo Dal Fm
- Wordie Creek Fm
- Ravnefjell Fm
- Foldvik Creek Gp
- Celsius Bjerg Gp
- Kap Graah Gp
- Kap Kolthoff Gp
- Vildtal Gp
- Folded Precambrian Basement & Caledonian Orogenic Belt
- Unfolded Precambrian to Ordovician Sediments and Basalts
- Nordland Gp
- Kai Fm
- Hordaland Gp
- Brygge Fm
- Rogaland Gp
- Tare Fm
- Tang Fm
- Springer Fm
- Nise Fm
- Kyrre Fm
- Cromer Knoll Gp
- Lange Fm
- Lysing Fm
- Viking Gp
- Spekk Fm
- Melke Fm
- Garn Fm
- Ile Fm
- Tilje Fm
- Are Fm
- Båt Gp
- Fangst Gp
- Not Fm
- Ror Fm
- Tofte Fm
- Zechstein Gp
- Grey Beds
- Red Beds
- Naust Fm

Potential Hydrocarbon systems

Source Rock | Reservoir | Seal | Trap | Base Model Charge (Permian SR, Jurassic SR) | Hot Model Charge (Permian SR, Jurassic SR) | Potential HC loss

- Possible anoxic marine shales?
- Shallow marine sandstones
- Submarine fan sandstones
- Shallow marine sandstones
- Fluvial
- Hyaloclastites?
- Fluvio-deltaic sandstones
- Shallow marine sandstones
- Syn-rift fault scarp related sandstones (E. Greenland)
- Turbidite sandstones
- Coarse, clastic, (deep water turbidites) input from E. Greenland
- Deep water turbidites (sourced from E. Greenland)
- Syn-rift sandstone & conglomerate submarine gravelly flows (E. Greenland) & Carbonates (Mid Norway)
- Transgressive Marine shales
- Coarse syn-rift conglomerate & sandstone submarine gravity flows (E. Greenland) Carbonates (Mid Norway)
- Deltaic sandstones
- Turbidite sandstones
- Restricted Marine shales
- Deltaic - shallow marine sandstones & deep water turbidies
- Fluvial sandstone?
- Shallow marine tidal & shoreface sandstones
- Lacustrine organic rich shales & coals
- Deltaic & lacustrine sandstones
- Fluvio-lacustrine-aeolian sandstones
- Fluvio-lacustrine sandstones
- Fluvio-deltaic sandstones
- Alluvial-fluvial sandstones
- Shallow marine carbonates & sandstones (E. Greenland) Alluvial-fluvial sandstones (Mid Norway)
- Alluvial sandstones
- Lowstand turbidite fans
- Fully marine carbonates
- Shallow marine carbonates
- Fluvial conglomerate
- Fluvial sandstones
- Organic rich marine shale
- Organic rich marine shale
- Lacustrine shales
- Lacustrine shales
- Potential structural traps formed from 2nd break-up phase
- Potential breaching of Mesozoic/Palaeozoic structural traps from uplift, tilting and Oligocene erosion

HERIOT WATT UNIVERSITY

Author: G. Heldreich

Date: March 2018

This work was carried out as part of a Post Doctoral Research Project based at Heriot Watt University, Edinburgh, UK.

Legend

- Basement
- Conglomerate
- Sandstone
- Floodplain and delta plain mudstones
- Shallow - Marginal Marine Shales
- Deep Marine Shales
- Evaporites
- Limestones
- Siliceous Ooze
- Hyaloclastites
- Lavas/ volcanic intrusions
- Unconformity
- Organic-rich shales
- Deep-water fans
- Ice-rafted dropstones